A SPECTROSCOPIC STUDY OF SOME PHOTOCROSSLINKING RESINS

A thesis submitted for the degree of Doctor of Philosophy in The City University.

by

Christopher Lowe.

The City University,

March, 1985

INDEX

ACKNOWLEDGEMENTS

I am grateful to Professor R.S.Davidson, without whose foresight and tenacity I would not have had the opportunity to do this Ph.D. I would also like to thank him for the many discussions we have had, which have stimulated my own thoughts.

Many thanks to the SERC and to Ciba Geigy Plastics and Additives Division at Duxford who funded my research through a CASE award. In particular I would like to thank [redacted] and [redacted] who gave me helpful advice and gave up their time to listen to me. I would like to make a special mention of [redacted] supertech., of Ciba Geigy, Duxford who helped a great deal along the way.

I would like to express my appreciation to Nicolet who allowed me to use a 60 SX in their laboratories at Warwick.

I am obliged to [redacted] who pointed me in the right direction during the derivation of the statistical model and the kinetic model. Thanks also to [redacted] who helped solve other mathematical problems that have cropped up.

Many thanks to: [redacted] who helped with the interpretation of N.M.R. spectra, [redacted] for obtaining the mass spectral data, and [redacted] for obtaining the G.P.C. data.

Many, many thanks to [redacted], who whilst typing my thesis, has patiently deciphered my hieroglyphics and transformed them into a readable form.

Finally thanks to, [redacted] for being there.

ABSTRACT

Polymers containing chromophores based on 1,3-diphenyl-prop-2-en-1-one (chalcone) undergo photocrosslinking when irradiated with UV light. This photocrosslinking reaction was followed using four different spectroscopic techniques.

UV/visible photoacoustic spectroscopy was used to try and assess the degree of cure in the polymer film. Some changes in the spectra of the polymers were observed. However it was shown that this technique cannot be used for quantitative work since the PA signals exhibit saturation. The highly absorbing nature of the polymers and the limited modulation frequency range of the instrument, meant that this problem of saturation was insurmountable.

Depth profiling of some samples was achieved by variation of modulation frequency.

A signal occurring 90^{o} out of phase with the main signal was attributed to reflection of heat from the sample - substrate boundary.

A simple statistical model was derived, which indicates that polymers based on chalcone should have the same number of unreactive sites as polymers containing the photoreactive cinnamate group. However polymers based on 1,5-diphenyl-pent-1,4-dien-3-one should have fewer unreactive sites.

The use of IR transmission spectroscopy proved useful for comparing rates of reaction of polymers containing different concentrations of the same chromophore and of polymers containing different chromophores. Irradiation generated a concentration gradient, this made it impossible to determine absolute rates. A kinetic model was devised in which attempts were made to account for concentration of unreactive sites and for the development of concentration gradients.

The IR spectra indicate that the statistical model predictions of unreactive sites are too high.

More information about the absorption bands of the polymers, in the UV/visible region was obtained by diffuse reflectance spectroscopy, particularly at low wavelengths. The polymers exhibit a short wavelength absorption band which was not found in solution spectra. This band disappears on irradiation and was tentatively assigned to an intermolecular interaction in the solid phase.

Well resolved IR spectra of small samples were obtained using FT-IR-PAS, powders gave even better spectra than films. However band intensities in the FT-IR-PA spectra were found to be different to those in transmission IR spectroscopy. These differencies were attributed to the thermal diffusion depth varying with frequency in FT-IR-PAS.

An attempt was made to use FT-IR-PAS to depth profile polymer films, but this was found to be a difficult process due to it not being clear as to whether operating under saturation conditions or not.

CHAPTER ONE

INTRODUCTION

1.1 General Comments.

Nature has used a photochemical reaction since life began i.e. photosynthesis. However man has only recently begun to recognise the added versatility that photochemistry brings. Although photography has now been in use for well over a century, organic photochemistry has only been extensively investigated since 1950. Photochemistry is now well established and in many cases synthesis of compounds that was once difficult can now be achieved[1].

Perhaps the area that has been affected more than most is the synthetic coating industry. Before the advent of photopolymers, coatings needed to be baked on, in a high temperature, energy intensive, oven, thus precluding some materials from being coated. Now UV curing can often achieve the desired excellent finishes in less time and at lower cost.

The advantages of using photosensitive systems are as follows[2].

1) They undergo rapid reaction and thus lend themselves to high speed automation.

2) In many cases they can be formulated into solventless systems saving on cost and environmental pollution.

3) Reaction can be carried out at room temperature. Thus inflammable materials can be coated and if required thermal cure can be effected subsequently in suitable systems.

4) Compared to thermally cured systems there is low energy consumption.

Problems occur with thick and highly pigmented layers as both these factors limit photocuring. Oxygen inhibition may occur in certain

systems, reducing cure efficiency and thereby increasing running costs. The design of all UV cure systems must take these factors into account as well as the cost of the basic resin which in some cases can be quite high.

1.2 Applications of Photosensitive Polymers

Photopolymers are used in the wood coatings industry where they are used as fillers, sealers and coats. Both unsaturated polyester/styrene systems and acrylate systems are used in this case[2].

Coatings for vinyl flooring are another usage. These are normally based on urethane acrylate formulations which have excellent abrasion resistance[2].

Acrylates have also been used as paper coatings and can be used to cover metals[3]. In the latter case epoxy acrylate/reactive diluent blends have been used. However due to poor adhesion and poor rates of cure in pigmented coats, a 'thermal bake' is also required.

Epoxymethacrylates have been used as solder masks and in a variety of dental applications[4].

Irradiation through a photographic negative of polymers containing for example cinnamate or chalcone groups followed by 'development', i.e. washing with a suitable solvent, yields a relief pattern where the parts that were exposed remain, as they have become solvent resistant[5]. Those parts that were not exposed remain soluble. This process is used in the manufacture of printed circuits, integrated circuits, and printing plates. The polymers are known as photo-resists because they are photo-sensitive polymers which resist the etchant that is used to etch the uncovered metal surface.

Positive resists can also be used in which the polymer becomes soluble on irradiation.

Thus it can be seen that organic photochemistry has also affected the efficiency of the printing industry and has had considerable impact on the electronics industry.

1.3 Basic Photochemical Principles.

1.3.1 Selection Rules

In order to understand how photochemical reactions occur, it is necessary to look at some elementary chemistry.

As chemical bonds are broken and formed during a chemical reaction, only light with sufficient energy to break these bonds will cause photochemical reactions to occur. Hence the use of the UV/visible region to initiate these reactions.

Light interacts with an electron in the ground state of a molecule and causes it to be promoted to a higher level, the photon is absorbed in the process. The transitions can occur between a π bonding orbital and a π^* antibonding orbital, or a nonbonding orbital and a π^* antibonding orbital, or a nonbonding orbital and a σ^* antibonding orbital. Not all transitions are allowed and those which are not can be determined using selection rules.

Firstly the electron may only be promoted between orbitals of the same symmetry. If the symmetry changes the transition is not allowed. Secondly there are many vibrational and rotational levels associated with each electronic configuration. However only those transitions which involve no change in interatomic distance and no change in nuclear kinetic energy will be allowed, as it is assumed that the transition takes place so quickly that the goemetry is unchanged. This is the Franck-Condon Principle[6]. Thirdly the spin of the electrons must be considered. Pauli's exclusion principle states that when two electrons occupy the same orbital their spins must be paired, i.e. one must have the opposite spin of the other. This is termed the singlet state as the multiplicity, as defined in Russel-

Saunders coupling is equal to 1. For most molecules in the ground state, this is the normal state of affairs because all the electrons are spin paired. Oxygen is an exception because it has two unpaired electrons in 2 different π^* antibonding orbitals. This is termed the triplet state as this has a multiplicity of three i.e. there are three closely spaced energy levels †. Transitions between singlet and triplet states are forbidden under the selection rules as the spin overlap is zero.

A triplet state is lower in energy than the corresponding singlet state in the same molecule. This is because in the triplet state the electrons in the highest occupied orbitals occupy different regions of space, or exhibit the avoidance tendancy to a greater extent than in the singlet state. The singlet state will thus be higher in energy than the triplet state because of electrostatic repulsion between the electrons

Fourthly a transition will be forbidden if the overlap between initial and final orbitals is small. This arises in the case of a transition between a nonbonding orbital and a π^* antibonding orbital in a carbonyl group.

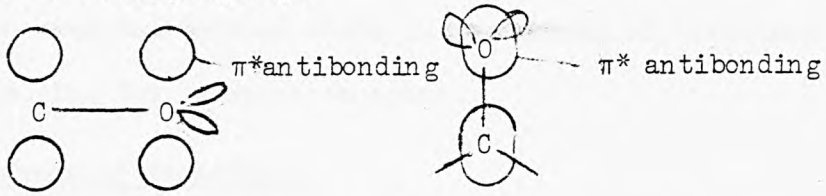

Figure 1.1 Antibonding orbital of carbonyl group.

The selection rules are determined under the Born-Oppenheimer approximation. As with other approximations it cannot cover all cases. Thus even forbidden transitions may be possible, however the intensity of the absorption will be small. The actual magnitude

† N.B. The Russel Saunders coupling theory considers the total angular momentum of a system containing several electrons i.e. it is a combination of the orbital angular momentum and the spin angular momentum.

depends upon how forbidden the transition is i.e. whether it is spin forbidden, overlap forbidden, symmetry forbidden, vibrationally forbidden or a combination of some or all of these.

1.3.2 Exceptions to the Selection Rules

Perhaps the most important exception is the singlet-triplet case. Here the transition between the singlet state and the triplet state is made possible by spin/orbit coupling. That is although the total angular momentum of a molecule must remain constant for a given energy content, the spin angular momentum and the orbital angular momentum (gained by an electron orbiting a nucleus) can vary as the angular momentum is switched between the two. Thus all singlet states have some triplet character and vice versa.

The fact that singlet-triplet transitions and the converse are difficult (forbidden), means that if a triplet state is formed it will not decay to a singlet state quickly. As most ground states exist in the singlet state, excited triplet states will be relatively long lived, compared to excited singlet states, which can decay back to the ground state very easily. This longevity accounts for the importance of the triplet state in photochemical reactions i.e. there is time for reaction to occur.

1.3.3 Types of Transition

In general $\pi \rightarrow \pi^*$ transitions are the strongest, although if the transition is forbidden then the absorption will be weak. The position of the peak absorption is dependant upon the degree of conjugation. The more conjugated a system the longer the wave length of the transition.

$n \rightarrow \pi^*$ Transitions are symmetry and/or overlap forbidden and so are of low intensity. They are normally the bands which occur at longest wave lengths and are considered characteristic of molecules possessing chromophores with multiply bonded hetroatoms.

$n \rightarrow \sigma^*$ Transitions occur in the alkyl halides. A nonbonding halide electron is promoted to the σ^* antibonding orbital, which effectively breaks the bond and hence produces two radicals. These transitions are normally partially forbidden.

1.3.4 Geometry of the Excited State

On excitation the electronic configuration changes, which will give rise to changes in the geometry of the molecule. This is best demonstrated by ethene. On excitation of a π electron to the π^* antibonding orbital, the π bond in ethene is effectively broken and the two CH_2 groups are joined by a single bond only. Thus the excited state will relax, as the electrons now occupy p like orbitals on the respective carbon atoms. The most stable conformation occurs when the p like orbitals are at right angles to each other minimizing repulsion. This rotation is thought to be the basis for cis-trans isomerization.

1.3.5 De-excitation of Excited States

Fluorescence is a very fast process ($k_f \simeq 10^6 - 10^9\ s^{-1}$) because it occurs when an excited state relaxes to a lower state of the same multiplicity via a radiative transition. Thus it is spin allowed. In most cases the transition is usually $S_1 \rightarrow S_0$ although $S_n \rightarrow S_m$ and $T_n \rightarrow T_m$ have been observed . If the absorption and fluorescence spectra are taken of a compound they are not superimposed. This is explained by the Franck-Condon principle. On excitation the higher vibrational levels of the excited states are populated because of the necessity that interatomic distance and nuclear kinetic energy do not change. Vibrational relaxation then occurs so that the lower vibrational levels of the excited states are populated. Emission occurs from these levels to the various vibrational levels in the ground state. Thus the energy of the emitted photons is less than the energy of the absorbed photons. In fact the fluorescence spectrum is a mirror image of the absorption spectrum.

Phosphorescence is a much slower process ($k_p \approx 10^2 - 10^4\ s^{-1}$) because it occurs when an excited state relaxes to a lower state of different multiplicity via a radiative transition. Thus it is spin forbidden. In most cases it is the $T_1 \rightarrow S_0$ transition that is observed as vibrational relaxation from the higher states occurs so fast that phosphorescence cannot compete. Because the triplet state is so long lived it is susceptible to quenching collisions and thus plays a big part in photochemical reactions.

As with fluorescence spectra, phosphorescence spectra are mirror images of the $S_0 \rightarrow T_1$, absorption spectra for the same reasons.

Radiationless Transitions have been used to explain: Why emission invariably occurs from the S_1 and T_1 states, why the quantum yield of fluorescence (ϕ_f) is less than 1 and why ϕ_f is independant of which state (S_1 S_2 S_3 etc) is initially excited.

There are three types of radiationless relaxation these are:

i) Vibrational relaxation i.e. energy is lost by collision with other molecules.

ii) Inter-system crossing i.e. one state of a certain multiplicity converts into another of different multiplicity (e.g. $S_1 \rightarrow T_1$).

iii) Internal conversion i.e. one state relaxes to another of the same multiplicity.

Intersystem crossing and internal conversion occur via a similar mechanism.

The rate of a non-radiative transition is dependant upon the square of the electronic matrix element $\{\int (\phi_1 H^1 \phi_2 d\tau)^2\}$ and the square of the vibrational overlap integral $\{\theta_{1_i}/\theta_{2_j}\}^2$. This latter term is self-evident, the former term is a measure of the overlap between the orbitals of the initial and final states multiplied by a perturbation operator which brings in the time dependant nature of the transition.

Thus the rate constant can be expressed as:-

$$k_{nr} \propto (\phi_1 \mid H^1 \mid \phi_2)^2 \sum_i \sum_j (\rho\, \theta_{1_i} \mid \theta_{2_j})^2$$

ϕ_1 and ϕ_2 are the electronic wave functions of the initial and final states. H^1 is a perturbation Hamiltonian operator.

θ_{1_i} and θ_{2_j} are the ith and jth vibrational components of the initial and final states.

ρ is the state density factor which describes the number of vibrational states in state 2 isoenergetic with the levels in state 1 from which the transition occurs.

For a transition to be allowed the intergrals must be non zero. If the electronic matrix element is considered then the first criteria is that the wave functions should overlap. The second criteria is that they must be of the same phase, otherwise destructive interference will occur. Symmetry can be used to determine whether or not this second condition is fulfilled.

If the integral is to be non zero the product must be an even function. Thus the product of the characters of the representations of the wave functions ($\Gamma\, \phi_1 \times \Gamma\, \phi_2 \times \Gamma\, H^1$) must belong to the totally symmetric irreducible representation A_1. If $\Gamma\, \phi_1 \times \Gamma\, \phi_1$ does not belong to the A_1 representation then $\Gamma\, H^1$ must not.

This is the basis of El Sayeds' selection rules for intersystem crossing. The Hamiltonian for intersystem crossing is the spin-orbit coupling operator which does not belong to the A_1 representation. Thus the $^1(n\, \pi^*) \leftrightarrow {}^3(n\, \pi^*)$ and $^1(\pi\, \pi^*) \leftrightarrow {}^3(\pi\, \pi^*)$ transitions are forbidden where as the $^1(n\, \pi^*) \leftrightarrow {}^3(\pi\, \pi^*)$ and $^3(n\, \pi^*) \leftrightarrow {}^1(\pi\, \pi^*)$ transitions are allowed.

In the same way, because the internal conversion operator H_{ic} is totally symmetric, only states which belong to the same irreducible representation will give a non zero integral. That is only states of

the same symmetry will undergo internal conversion. Thus $S_1 \rightarrow S_0$ will be forbidden because S_1 and S_0 will have different symmetries.

Forbidden transitions can be predicted to occur if rigorous symmetry restraints are relaxed. This is done by considering vibronic coupling (i.e. including vibrational terms). Thus $S_1 \rightarrow T_1$, forbidden in aromatics by El Sayeds rules can occur via vibronic coupling as can $S_1 \rightarrow S_0$.

The vibration overlap integral is a measure of the overlap between the vibrational sublevels associated with the initial and final states. That is if degeneracy occurs between one sublevel of one excited state and a sublevel of another excited state of the same molecule, then a transition may take place if the vibrational overlap is large. If it is small or zero then the transition is forbidden.

Another way of looking at this is by considering energy versus internuclear distance diagrams. If the internuclear distance and energy content are similar (e.g. point X) then the only difference is in electronic configuration. Thus the transition will be easy as internuclear distance will not need to change and kinetic energy will be zero for both sides i.e. X is the turning point for both the

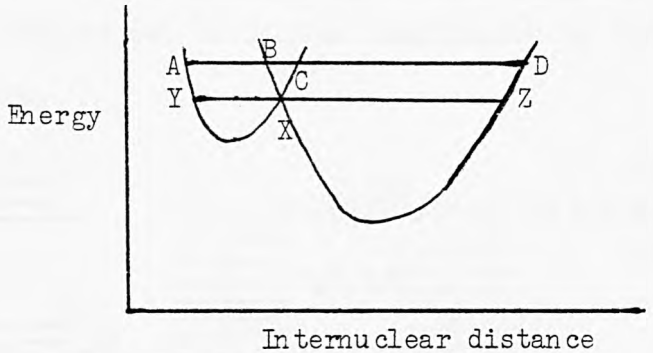

Figure 1.2 Diagram of Internuclear distance vs Energy for two different excited states in a molecule.

YX level and the ZX level. This means that the Franck Condon principle is obeyed.

If the AC and BD are now considered then any transition will need a

change in internuclear distance or an abrupt change in kinetic energy. Both are contrary to the Franck - Condon principle.

These phenomenon result in rapid conversion between the upper levels, but in the lower levels energy differences and internuclear distances are greater, thus conversion is more difficult and emission (fluorescence or phosphorescence) can compete.

1.3.6 The Jablonski Diagram

It is possible to represent all the states of a molecule in one diagram. On the same diagram the various transitions mentioned above can be represented. This type of diagram is a Jablonski diagram[7].

The y axis is an energy axis, the x axis has no significance. The various states are ranged in order of increasing energy and numbered S_0, S_1, S_2 etc and T_1, T_2 etc depending upon whether they are singlets or triplets. The singlets and triplets are separated horizontally for clarity.

Transitions are represented by lines between the states, different lines representing different processes. i.e → absorption of a photon, ---→ radiative decay as in fluorescence or phosphorescence and ⇝ non-radiative decay as in intersystem crossing and internal conversion. The diagram can be further complicated by the inclusion of vibrational levels.

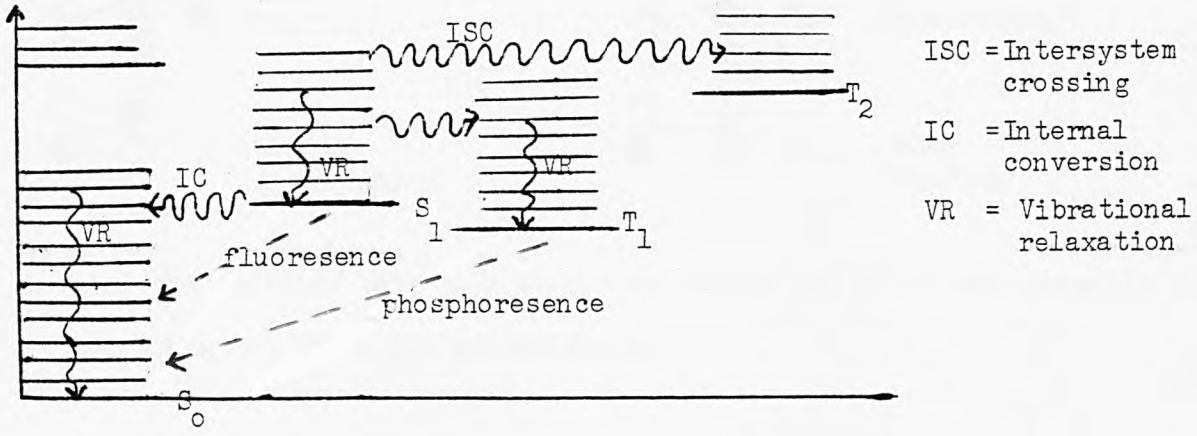

Figure 1.3 A simplified Jablonski diagram.

1.3.7 (2 + 2) Cycloaddition Reactions

Cycloaddition reactions occur between two independant unsaturated systems and are examples of concerted reactions going by a cyclic transition state. Thus they obey the Woodward-Hoffman rules of **conservation of orbital symmetry.**

For unsaturated systems the higher molecular orbitals can be visualised as sets of p orbitals, the phases of which are dependant upon the energy. That is in the lowest orbital the p orbitals will be arranged so that lobes of the same phase will have the same orientation. In the highest orbital they will be arranged so that the lobes alternate phase. Only orbitals of the same phase will overlap to form a bonding orbital. Those of different phase, overlap to form an antibonding orbital.

The simplest model of this theory is the frontier orbital approach. In this model the electrons in the highest occupied molecular orbital (HOMO) on one molecule are 'looking for' a vacant orbital which is the lowest unoccupied molecular orbital (LUMO) on another molecule. If the symmetry of the two orbitals is the same then reaction will occur, if it is not then no reaction will take place.

Take for example the Diels-Alder reaction. This takes place between a diene and a monoene. The HOMOs and LUMOs are drawn below, the shaded areas are of the same phase as are the unshaded areas.

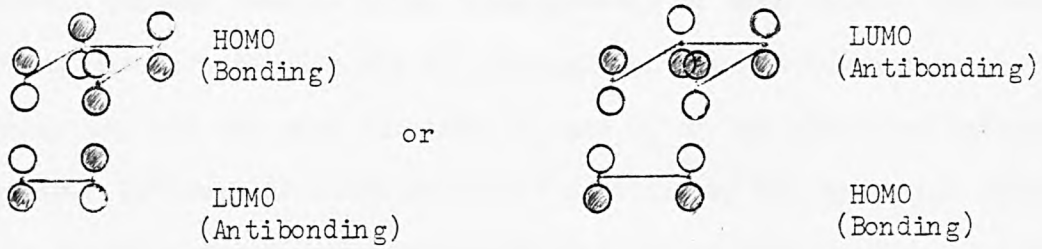

However the reaction between 2 ethene molecules will not occur themally as the HOMOs and LUMOs are incompatible.

i.e.

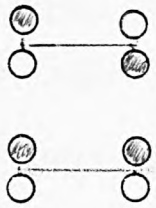

On irradiation an electron is promoted from the π bonding orbital to the π^* antibonding orbital. The HOMOs and LUMOs are now compatible.

i.e.

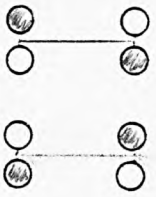

Thus bond formation takes place and cyclo-butane is formed.

In the above systems, reactions must occur on the same face (i.e. bond formation) as the strain of twisting, which is required if bonds are to be formed on opposite faces, is too great. The above systems, are suprafacial - suprafacial cyclo-addition. However if the system were flexible enough suprafacial - antara-facial reactions could occur.

1.3.8 Photo-organic Reactions Going Via a Biradical Transition State

The ultimate biradical would be a bifunctional system in which the two radical centres behaved quite independantly of each other. The most common case occurs when the two radical centres are degenerate, or nearly so, and the wave functions ϕ_A and ϕ_B of the electrons interact weakly. Although distinct molecular orbitals ψ_1 and ψ_2, which embrace both centres, develop, the energy difference is small and the electrons can be distributed over the two orbitals as shown below.

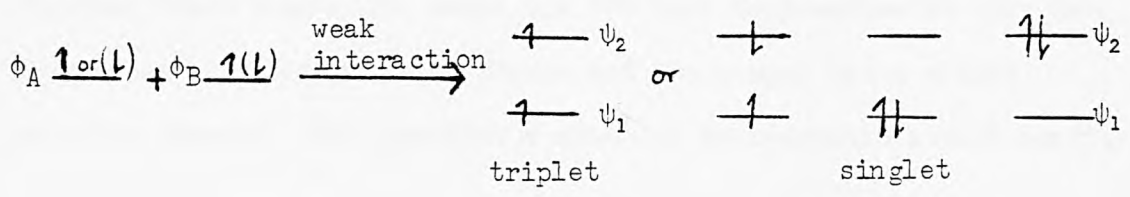

The singlet biradical state can only be properly described by a mixture of all three singlet configurations.

If ϕ_A and ϕ_B interact more strongly by increasing the amount of overlap, the energy difference between ψ_1 and ψ_2 increases. In this case the electrons tend to pair off in ψ_1 alone for energetic reasons and the singlet state becomes more stable than the triplet state. As can be seen from the diagram the singlet state approximates to a covalent bond between radical centres ϕ_A and ϕ_B.

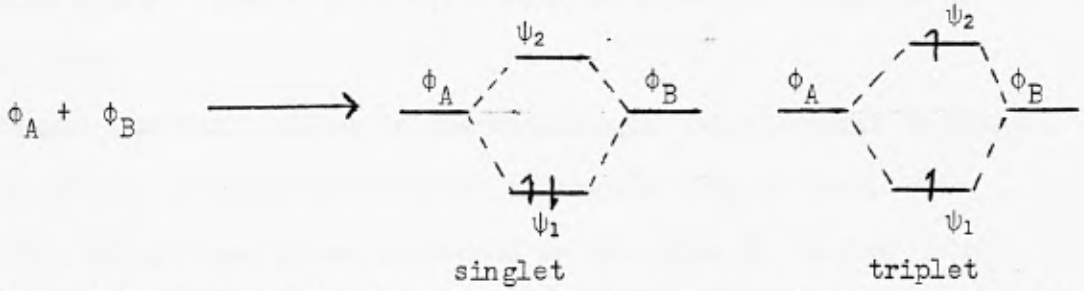

If ϕ_A and ϕ_B cease to be degenerate ψ_1 approximates to ϕ_A and ψ_2 to ϕ_B. In this case the singlet state is again the most stable configuration but it corresponds to a Zwitter ionic state with both electrons in ϕ_A

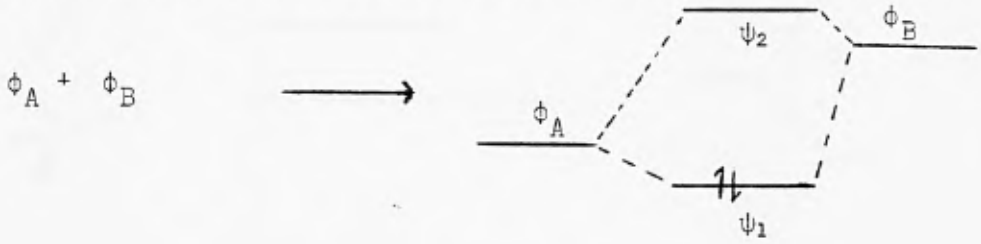

Thus biradical character occurs only when overlap between the two radical centres is small.

1.4 The Chemistry of the Carbonyl Group.

1.4.1 The C = O Double Bond and Acidic α Hydrogens

The chemistry of carbonyl compounds is dominated by the electronegativity of the oxygen atom and the polarizability of the π bond. Together these phenomena cause the C=O bond to polarise so that the carbon has a slight positive charge and the oxygen has a slight negative charge. This provides a site for nucleophilic attack leading

to addition across the C=O double bond.

Addition of acids to the reaction mixture causes the bond to polarise further.

This increases the susceptibility of the carbonyl carbon to nucleophilic attack. Addition of acids also promotes the formation of the enol form.

A second important effect of the mobility of the electrons in the π bond and the electronegativity of the oxygen atom is that, the acidity of hydrogen atoms connected to the alpha (α) carbon is increased. This is due to the fact that the anion produced is stabilised by delocalization of the negative charge.

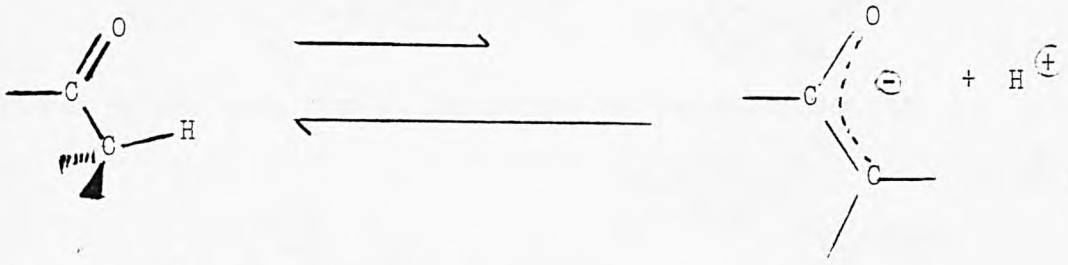

1.4.2 The Aldol Condensation Reaction

The aldol condensation reaction takes place between two molecules of an aldehyde or ketone, to form a β-hydroxyaldehyde or a β-hydroxyketone. At least one of the molecules must have an α-hydrogen and the reaction will only take place in the presence of a dilute acid or base. Essentially the α-carbon of one molecule becomes attached to the carbonyl carbon of the other. The base catalysed mechanism is shown below, taking ethanal as an example.

Scheme 1.1

1) $CH_3CHO + OH^{\ominus} \rightleftharpoons H_2O + [CH_2CHO]^{\ominus}$

Abstraction of α-H

2) 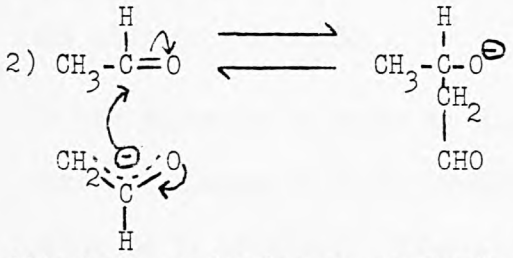

Attack by carbanion on carbonyl carbon.

3) 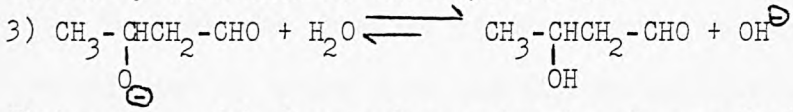

Abstraction of hydrogen from water to give product and regenerate OH^- catalyst.

Scheme 1.2

a) 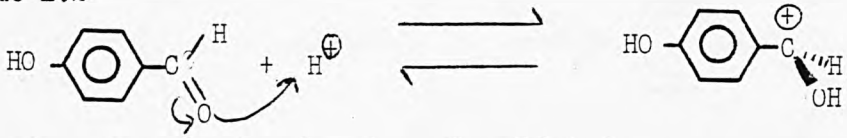

Formation of carbonium ion from the aldehyde.

b) 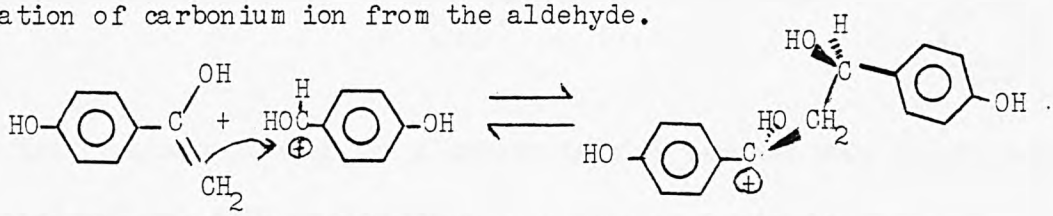

Attack by the enol form of the ketone on the carbonium ion.

c) 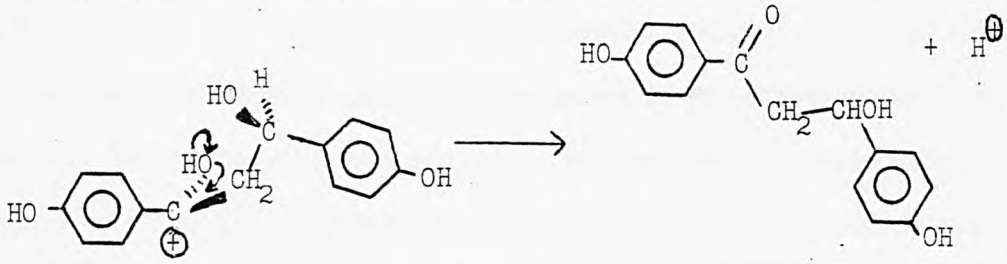

Reformation of catalytic proton and formation of β-hydroxy ketone.

d) 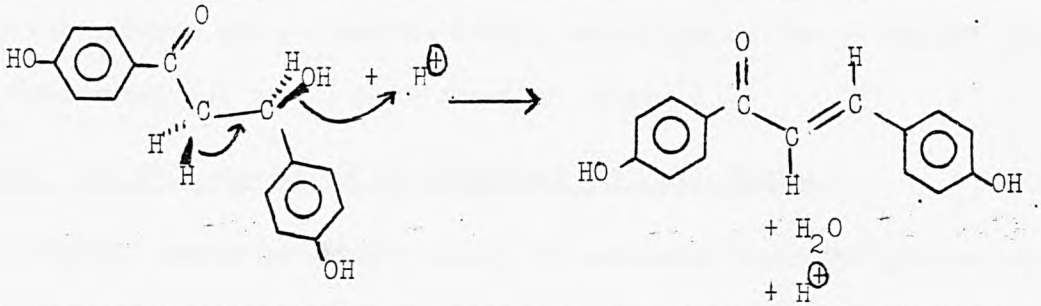

Acid catalysed elimination of water to form α,β-unsaturated ketone.

Elimination of water by addition of dilute acid will yield an α, β-unsaturated aldehyde or ketone. When the C = C bond can conjugate with an aromatic system the unsaturated ketone is isolated, without the addition of acid.

In the majority of cases an aldol condensation between two different carbonyl compounds is not feasible since a mixture of 4 possible products is obtained. However if one reactant contains no α-hydrogens and the carbanion from the other reactant is formed slowly, (this can be effected by either slow addition of catalyst or slow addition of reactant) then good yields can be obtained. An example is the Claisen-Schmidt condensation of aromatic aldehydes with methly ketones.

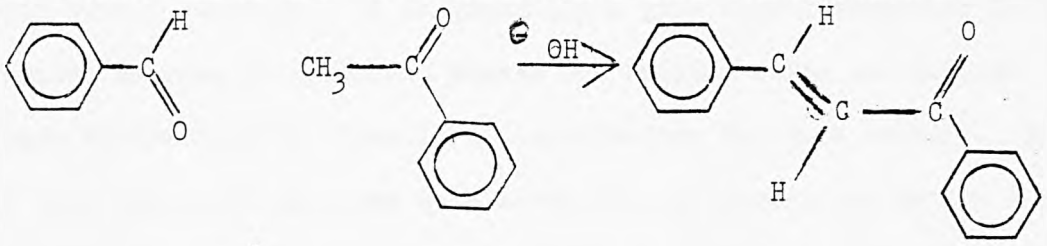

The self condensation of the aldehyde is slow because only dilute base is used and can thus be ignored.

Acid catalysis can be used when acid conditions are[8] required or when the reverse reaction of step 1 competes with the forward reaction of step 2. In the case of the reaction between 1-(4- hydroxyphenyl) ethan-1-one and 1-(4- hydroxyphenyl) methanal, acid catalysis is used for both reasons, i.e. poor yields are obtained with base catalysis and the hydroxy groups require acidic conditions. The mechanism for an acid catalysed reaction is shown in Scheme 1.2.

1.4.3 The Photochemistry of Saturated Carbonyl Groups.

The excited states of lowest energy in saturated carbonyl groups are the singlet and triplet ($n\pi^*$) states. In general intersystem crossing in aromatic ketones is so efficient that the singlet state is very short lived. In aldehydes and aliphatic ketones the life time of the singlet state is comparatively much longer. The electron density in

the π^* antibonding orbital on the carbonyl group is greatest near to the carbon atom. (Exactly the opposite to the π bonding orbital). Thus not only is the π bond effectively broken in the excited state, but the site for nucleophilic attack is also essentially neutralised.[9]

The chemistry of the ($n\pi^*$) excited state of the carbonyl group is dominated by the unpaired electron in a p orbital on the oxygen. The three major types of reaction that saturated carbonyl compounds in the excited state undergo are i) α-cleavage ii) hydrogen abstraction and iii) addition to alkenes.

Cleavage of the α-bond to give two radical fragments is called a Norrish type I reaction. It is generally a more common occurance in the gas phase, because in condensed phases the excited state can undergo hydrogen abstraction or vibrational deactivation far more readily. In order that the α C-C bond can be cleaved the electronic excitation energy must be converted into vibrational energy. The bond strength of the α C-C bond is about 325 kJM^{-1}. Most excited state energies of simple aliphatic ketones are of the same magnitude. Thus the other mechanisms of deactivation will compete with α-cleavage.

α-Cleavage can occur in condensed phases if there is a particularly weak α-bond in a compound. This is true for aryl t-butyl ketones and benzoin ethers amongst others. See Scheme 1.3

Hydrogen abstraction is caused by the half occupied nonbonding orbital on the oxygen of the carbonyl excited state taking a hydrogen atom from a donor molecule, which may be solvent, an added reagent or a ground state molecule of reactant. Here the ($n\pi^*$) excited state is behaving in a similar way to the alkoxy radical. The products of hydrogen abstraction are two radicals which then undergo secondary radical reactions. See Scheme 1.4.

Intramolecular hydrogen abstraction is called a Norrish type II reaction.

Scheme 1.3

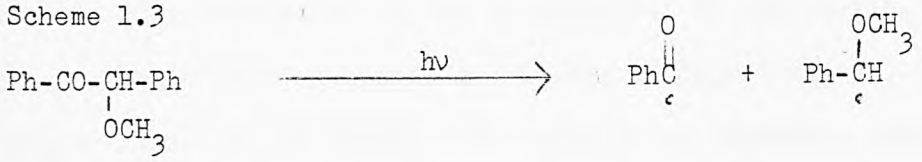

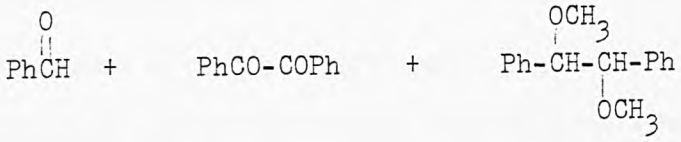

Scheme 1.4

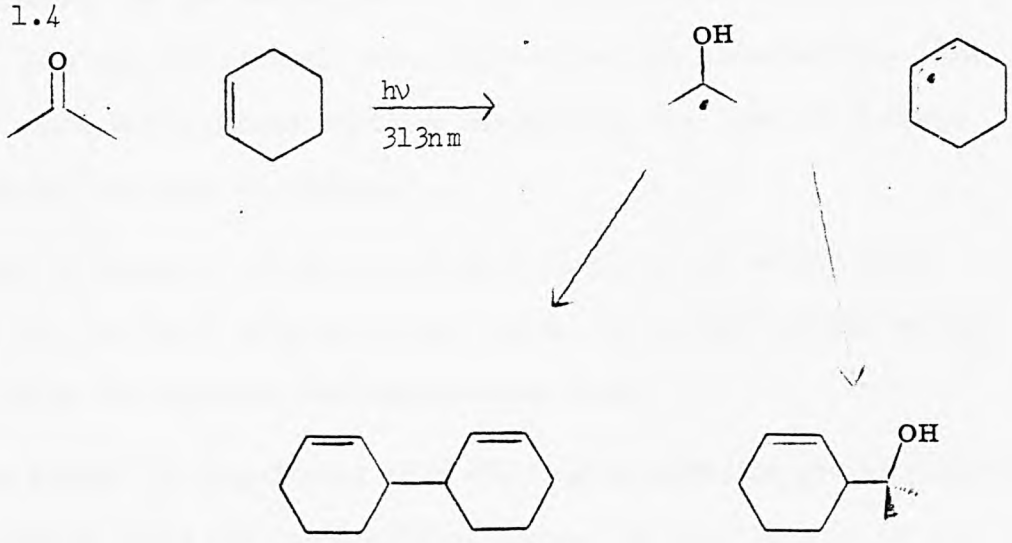

Generally hydrogen abstraction reactions of ketones take place from the ($n\pi^*$) triplet state as the singlet state is too short lived to undergo efficient intermolecular reaction. If the lowest excited state of a compound is the ($\pi\pi^*$) triplet state then the rate of hydrogen abstraction is low. The difference can be rationalised by considering the spatial orientation of the electrons in the two different states. The ($n\pi^*$) triplet state has an unpaired electron in an exposed p type orbital on the electron deficient oxygen atom. The ($\pi\pi^*$) triplet state has no such unpaired electron and the oxygen atom is electron rich.

If alkenes are present during the photolysis of carbonyl compounds, cyclo-addition occurs across the double bond to give 4 membered oxygen heterocycles.[10] These are called oxetanes.

The reactions are non stereospecific i.e. all stereoisomers are produced. This can be rationalised using a biradical intermediate. The excited state which causes reaction varies with the type of carbonyl compound and the type of alkene.

Aliphatic or aromatic ketones react with simple alkyl substituted ethenes via the ($n\pi^*$) triplet state. Again the initial attack on the alkene is by the electron deficient oxygen atom.

When the alkene is substituted with electron withdrawing groups aliphatic ketones react using the ($n\pi^*$) singlet state. In this case it is the electron in the π^* antibonding orbital that is responsible.[11] Aromatic ketones do not react due to the efficiency of intersystem crossing to the triplet state. Presumably this difference is because the singlet state is of much higher energy than the triplet state.

As mentioned previously the triplet state has a long life time as deactivation to the product ground state requires spin inversion. This allows the bond in the biradical intermediate to rotate. Thus the reactions that go through the triplet state are nonstereospecific.

Reactions that go through the singlet state are stereospecific because the singlet state has a short lifetime and rotations cannot occur before deactivation.

1.4.4 The Photochemistry of α,β-Unsaturated Carbonyl Groups

The photochemistry of α,β-unsaturated carbonyl groups is substantially different from their saturated counterparts. This is due to a re-ordering of the molecular orbitals caused by conjugation of the alkene double bond. i.e. the energy of the π bond is brought closer to that of the nonbonding orbital on the oxygen which is unperturbed by conjugation. If aryl groups are attached to the other end of the alkene further stabilisation occurs and inversion of the π and n orbitals is obtained[12].

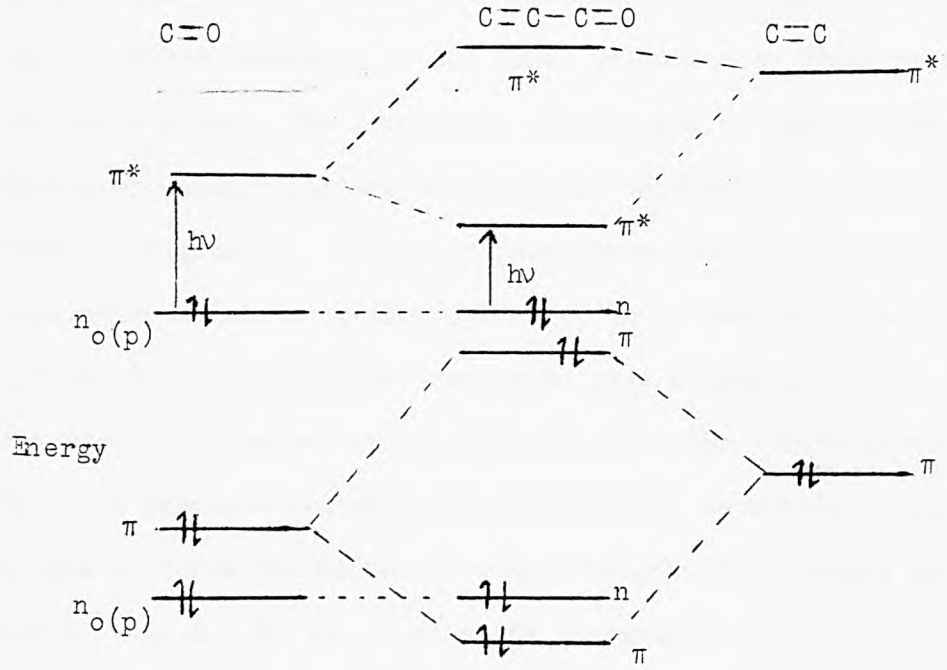

Figure 1.4
Energy level diagram of molecular orbitals in α,β-unsaturated carbonyl systems.

Thus the absorption spectrum of unsaturated carbonyls shifts significantly towards the red, as compared to saturated carbonyls, and the triplet energy is reduced from around 350 kJM^{-1} ($84kcalM^{-1}$) to around 250 kJM^{-1} ($60kcalM^{-1}$).

Thus the photochemistry of these compounds is dominated by the $\pi\pi^*$ excited state which explains why they undergo cyclo-addition to give substituted cyclobutanes and not oxetanes.

There are 2 important systems containing aryl α,β-unsaturated carbonyl groups used in the UV curing industry. These are:-

i) Cinnamate based resins.

ii) 1,3- diphenylprop-2-en-1-one (chalcone) based resins.

i) The photochemistry of cinnamic acid(PhCH: CHCOOH) and its derivatives has been extensively studied since Stobbe and Bremer[13] first considered it amongst the α,β-unsaturated carbonyl compounds that they investigated. Schmidt and Cohen[14] showed how topochemical factors affect the reactivity and the stereochemistry of the final product when dimerization occurs in the solid phase. The hypothesis put forward is that in the solid phase molecules undergo minimal movement and that reaction takes place between nearest neighbours. This also means that above a certain distance of separation molecules will not react. Their results showed that the α-form of the trans isomer reacts to give α-truxillic acid, the β-form dimerizes to give β-truxinic acid and that the γ-form does not react. This has been attributed to the distance of separation, i.e. in the α- and β- forms the distance between neighbouring double bonds is 3.9 Å ± 0.2 Å. In the γ- form the distance is 4.7Å ± 0.2Å. The stereo-specifity is explained by the fact that the molecules are arranged head to tail in the α- form and head to head in the β- form.

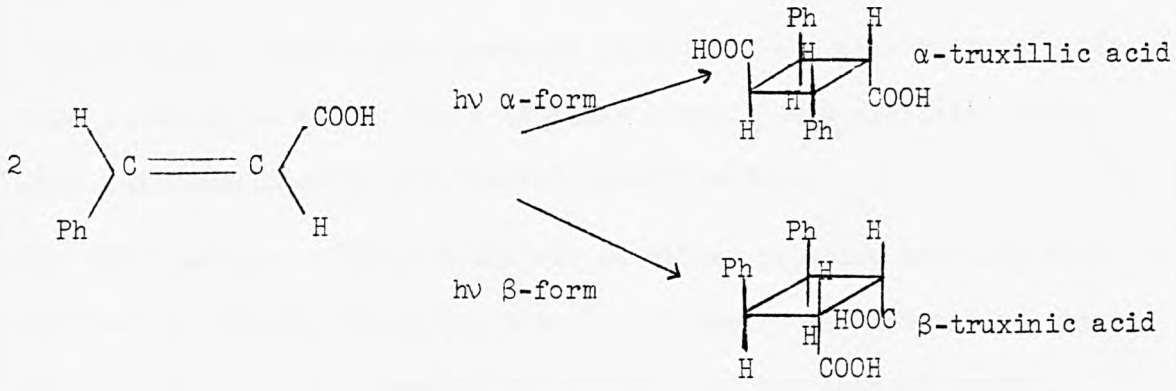

The cis isomer [15] has a separation distance of 4.4 Å. In this case a metastable dimer is formed which prefers to relax to two trans molecules rather than continue to the ground state dimer. This again is attributed to the distance between neighbouring double bonds.

Cinnamic acid and its derivatives are sensitive to light below 320nm. The range can be extended towards the red by using sensitisers[16], such as Michlers ketone, p-nitroaniline and picramide. When these compounds are mixed into polystyrene they still show phosphorescence. However when they are mixed into polyvinyl-cinnamate no phosphorescence is observed because the polyvinyl-cinnamate is acting as a triplet quencher by being excited into its own triplet state.

Recently it has been shown [17] that ethyl cinnamate dimerises in the liquid phase. In fact 90% of the double bonds react. It was found that both cis and trans isomers contributed to the dimerization, although the trans isomer seemed to be more important. The head - head arrangement predominated over the head - tail arrangement. This was demonstrated by the products being in a ratio of 9 : 1. The major product of dimerization in the liquid phase was the δ-truxinic ester.

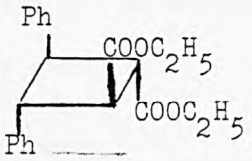

δ-truxinic ester

As can be seen from the diagram this product is the least sterically hindered product and so steric hinderance is very important in the liquid phase. Other minor products included: the neo-truxinic ester, the μ -truxinic ester, the β-truxinic ester, the α-truxillic ester, the ε-truxillic ester and the γ-truxillic ester.

The dimerization of ethyl cinnamate in dilute solution has also been studied by Shindo, Horie and Mila[18]. It was shown that the reaction proceeds even in the presence of triplet quenches such as oxygen,

demonstrating that the reaction can also go via the singlet state. These workers also showed that the dimerization is a second order reaction.

The triplet energy of cinnamates has been deduced to be 343 kJM^{-1} (57 kcal M^{-1})[2].

Baltrop and Coyle[19] have suggested a biradical mechanism for the dimerization of cinnamates consistent with other α, β-unsaturated carbonyl groups such as 2-cyclohexenone.[20, 21]

Azuma, Samui and Ogata[22] have developed a kinetic model for dimerization in polymers based on a scheme developed by Tsuda[23]. This involves four basic reaction paths which are:

1) Excitation $C^{So} \xrightarrow{h\nu\ k_1} C^*$

2) Dimerization $C^* + C^{So} \xrightarrow{k_2} C\text{-}C^* \rightarrow C\text{-}C$

3) Isomerization $C^* \xrightarrow{k_3} C$ isomer

4) Deactivation $C^* \xrightarrow{k_4} C$

C^{So} denotes the cinnamate group in the ground singlet state.

C^* denotes lowest excited state consisting of singlet or triplet state.

In a solid $k_3 \simeq 0$ [16] as molecular movement is restricted. Thus assuming a steady state of the excited species the concentration of excited molecules is given by:

$$[C^*] = \frac{k_1 [C]}{k_2 [C] + k_4} \quad 1.4.1$$

but as the photodimerization is assumed to be slower than deactivation $k_4 >> k_2 [C.]$

$$[C^*] = \frac{k_1 [C]}{k_4} \quad 1.4.2$$

The rate of production of the excited state is equal to $k_1 [C]$ which in the Azuma, Sanui, Ogata model is expressed by

$$k_1 [C] = \frac{\alpha\ I_{abs}}{\ell} \quad 1.4.3$$

where I_{abs} = Absorbed intensity, $\alpha = 1/Ah\nu$ and ℓ = film thickness

A= Avagadro's number, h= Plank's constant, ν= wavenumber of incident light

The rate of photodimerization is given by:

$$\frac{-d[C]}{dt} = k_1[C] - k_4[C^*] + 2k_2[C^*][C] \qquad 1.4.4$$

substitution of 1.4.2 and 1.4.3 in 1.4.4 gives:

$$-\frac{d[C]}{dt} = 2\alpha I_{abs}\frac{k_2[C]}{\ell\ k_4} \qquad 1.4.5$$

as $k_1[C] = k_4[C^*]$

For a sample in which all the incident intensity is absorbed $I_{abs} = I_o$

$$-\frac{d[C]}{dt} = 2\alpha I_o\frac{k_2[C]}{\ell\ k_4} \qquad 1.4.6$$

Thus the observed rate constant $k_{obs} = 2\alpha I_o \frac{k_2}{\ell\ k_4}$ and first order characteristics should be observed.

$$\text{i.e. } \ln\frac{[C_o]}{[C]} = k_{obs}t \qquad 1.4.7$$

For a sample in which only a small fraction of the light is absorbed

$I_{abs} = 2.303\varepsilon[C]\ I_o$ where ε = extinction coefficient. Substitution of this in 1.4.5 gives;

$$-\frac{d[C]}{dt} = 4.606\alpha\varepsilon I_o\frac{k_2[C]^2}{k_4} \qquad 1.4.8$$

$$k_{obs} = 4.606\alpha\varepsilon I_o\frac{k_2}{k_4}$$

$$\text{and } \frac{1}{[C]} - \frac{1}{[C_o]} = k_{obs}\ t \qquad 1.4.9$$

i.e. for thick, highly absorbing films there is a dependence on thickness, where as for optically thin films the reaction rate is independent on thickness and second order rather than first order kinetics apply. These workers found deviations from the theory and suggested that this was due to reduced mobility of the cinnamate groups. However this model applies only to irradiation with monochromatic light and no allowances have been made for a concentration gradient.

ii) As with most other aromatic ketones 1,3-diphenyl-prop-2-en-1-one (chalcone) undergoes efficient intersystem crossing in the excited state,

from the singlet state to the triplet state. Recently[24] it has been argued that the triplet state is orthogonal in geometry and that it is responsible for the dimerization reaction. The reasoning was based on the lifetime of the triplet state (<20ns) and on the fact that the rate of quenching by isoprene is almost independent of polar para substituents. Increased planarity is associated with longer lifetimes. As styrene has a twisted structure in the excited state but has a lifetime greater than 20ns, then it reasonable to assume a twisted structure for chalcone in the excited state. In a twisted structure orbital overlap with the aromatic ring will be poor and hence the independence of polar para substituents.

The products of quenching are best rationalised as involving a stable allylic/benzylic biradical.

Scheme 1.5

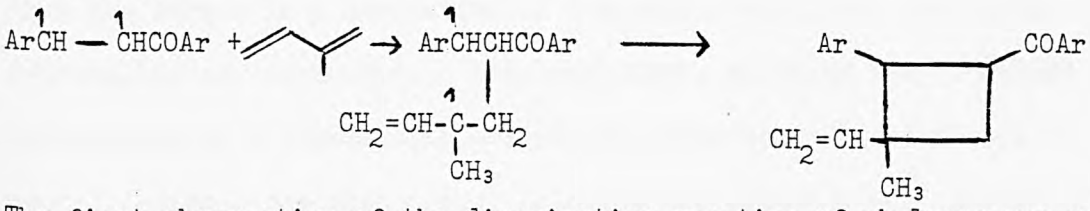

The first observation of the dimerization reaction of chalcone was again noted by Stobbe and Bremmer.

Irradiation of the 4 ,4' — diglycidylether of 4,4' —dihydroxy chalcone

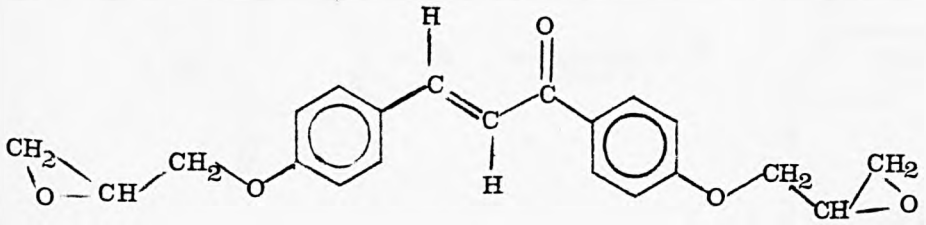

has been followed by Zahir[25] and Panda[26]. Zahir showed that both truxillic and truxinic cyclo-adducts are formed in both the solid and the solution phase. A second order reaction has been postulated,

N.B. Chalcone will be used for the sake of brevity instead of 1,3- diphenyl-prop — 2 — en — 1— one in the rest of this thesis.

however this breaks down after a short period of time possibly because no account of dependence upon light intensity has been included.

The trans isomer of the 4,4'-diglycidylether of 4,4'-dihydroxy-chalcone also undergoes trans-cis isomerization, the cis isomer undergoes cis-trans isomerization. A photostationary state is obtained very quickly, the actual concentrations of cis and trans isomers is wavelength dependent.

One of the first examples of photo dimerization of an α,β-unsaturated carbonyl was that of 1,5-diphenyl-pent-1,4-dien-3-one. (dibenzal-acetone).[27] When this compound was irradiated in ethanol a colourless dimer (m.p.135°C) was obtained. Praetorius and Korn[28] irradiated it with sunlight in acetic acid in the presence of uranyl chloride as a sensitiser. This yielded a colourless dimer (m.p.245°C).

Shoppee et al[29] have demonstrated by oxidation to the acid and by NMR that the former is a derivative of δ-truxinic acid, and the latter is an α-truxillic and derivative. This derivative has also been obtained by irradiation of a crystalline complex of trans-trans 1,5-diphenyl pent-1,4-dien-3-one with uranyl chloride and acetic acid,[30] X-ray crystallography has confirmed[31] the α-truxillic acid structure.

Scheme 1.6

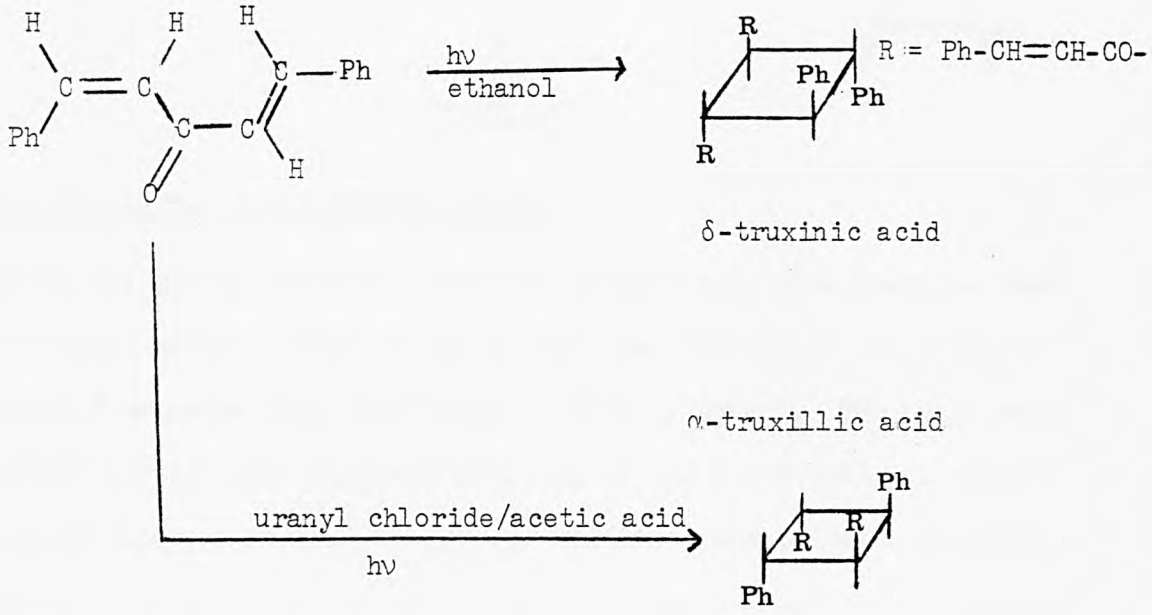

This suggests that the former is formed from the excited singlet state and the latter from the lowest triplet state. 1,5-Diphenyl-pent-1,4-dien-3-one in the pure solid state does not photodimerize.

1.5 The Chemistry of the Epoxide Group.

1.5.1 Preparation of Epoxides

Epoxides are prepared by two major methods:-

1) from halohydrins and 2) by peroxidation of carbon-carbon double bonds.

Scheme 1.7

1) $CH_3-CH=CH_2 \xrightarrow[H_2O]{Cl_2} CH_3-\underset{OH}{CH}-\underset{Cl}{CH_2} \xrightarrow{Conc\ OH^{\ominus}} CH_3-\underset{O}{CH}-CH_2$

2) 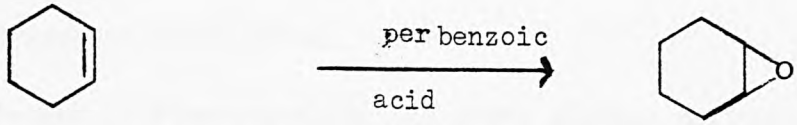

Essentially 1) is an adaptation of Williams ether synthesis. The base abstracts the hydroxyl proton which promotes the elimination of chlorine.

The mechanism of the second method is as follows:-

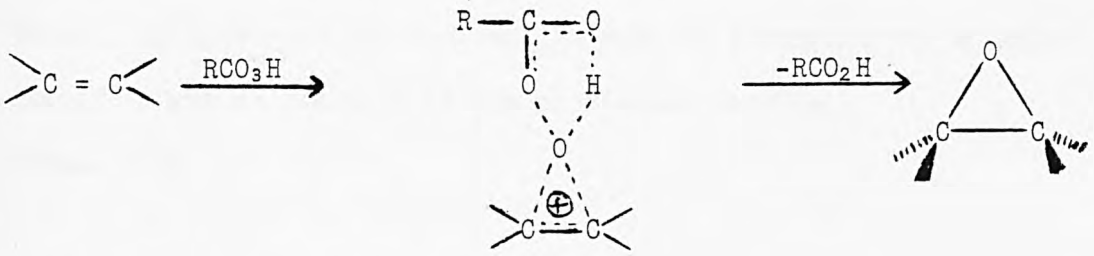

1.5.2 Reactions of the Epoxide Group.

Epoxides are highly reactive, terminal groups being more reactive than non-terminal groups. This is due to the ease with which the highly strained 3 membered ring (bond angle $\simeq 60^{o}$) is opened. The three major reactions are i) acid catalysed cleavage of the C - O bond, ii) base catalysed cleavage of the C - O bond and iii) reaction with Grignard reagents.

i) Acid Cleavage

Reaction of epoxides with acids leads to the protonated epoxide, which can then react with numerous nucleophilic reagents to form compounds possessing two functional groups. e.g. reaction with water yields a glycol, reaction with an alcohol yields a hydroxy ether.

Scheme 1.9

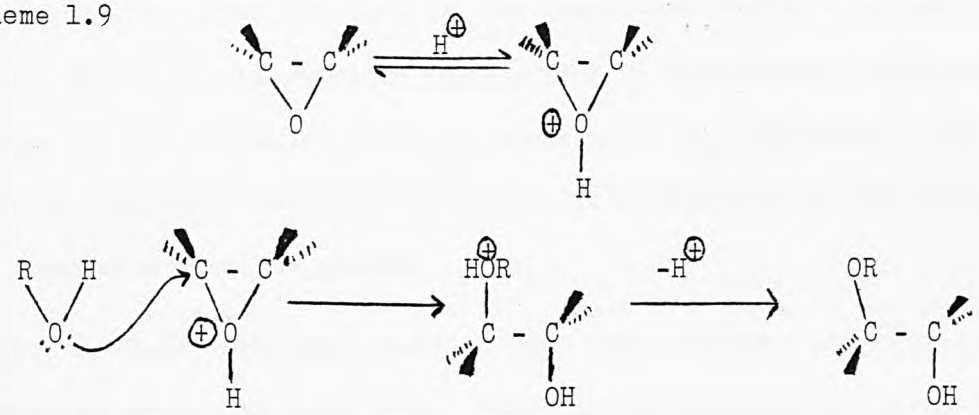

R = hydrogen or alkyl group.

This process is stereospecific and gives glycols corrsponding to antiaddition across the C - C double bond.

ii) Base Cleavage

Epoxides differ from ordinary ethers in that they can be cleaved with bases. In this case the nucleophile must be strong,as the epoxide itself is not as reactive as the protonated epoxide.

Scheme 1.10

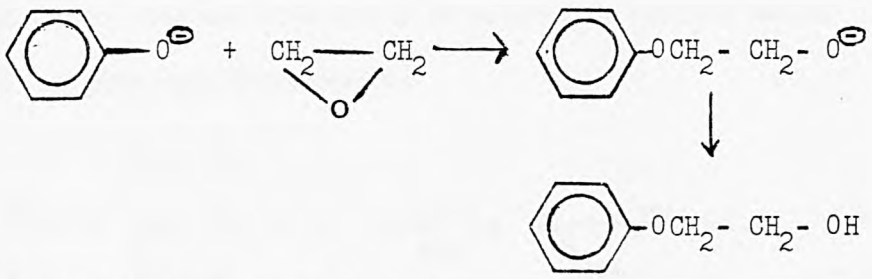

iii) Reaction with Grignard reagents

This is made possible by the nucleophilic nature of the alkyl or aryl group of these reagents. In this case the magnesium attaches itself to the oxygen atom. Hydrolosis then leads to the primary alcohol.

Stereochemistry

The attack of the nucleophile and the cleavage of the C - O bond occurs at the same time, i.e. via an S_N2 mechanism, in both the acid and base catalysed reactions[32]. During the acid catalysed reaction the breaking of the epoxide C-O bond is considered to have proceeded further than the forming of the other C-O bond in the transition state. The carbon atom at the centre of the reaction has aquired an appreciable positive charge and the mechanism takes on appreciable S_N1 character. Thus in the acid catalysed reaction the carbon atom attacked is that which can support a positive charge.

During the base catalysed reaction both bond breaking and bond forming proceed at about the same rate. Thus the controlling factor is steric hinderance and the carbon atom attacked is that which is least crowded. Hence acid and base catalysis lead to different isomers, thus effecting regioselectivity.

1.5.3 Epoxy Resins

Industrially, propylene oxide, ethylene oxide and epichlorohydrin are the most important epoxy compounds. The latter is the compound used in the synthesis of epoxy resins. Epichlorohydrin is produced from propan-1,2,3-triol by treating it with hydrogen chloride at 100°C. This results in two of the hydroxyl groups being replaced with chlorine. The resulting product is treated with solid potassium hydroxide which eliminates HCl to give epichlorohydrin.

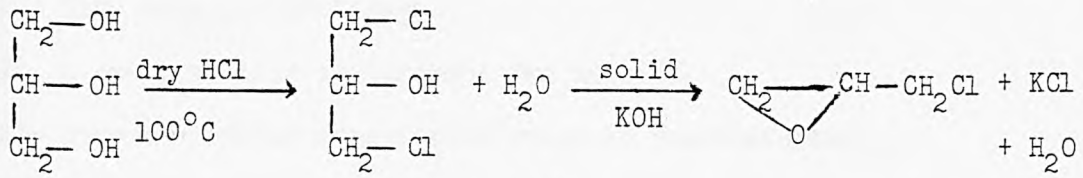

Scheme 1.11

Epoxy resins with terminal epoxide groups (glycidyl compounds) are prepared from epichlorohydrin by reacting them with compounds con-

taining at least 2 acidic hydrogens in the presence of a base. (2 acidic hydrogens are required so that 2 epoxide groups per molecule are introduced). The reaction steps are as follows:-

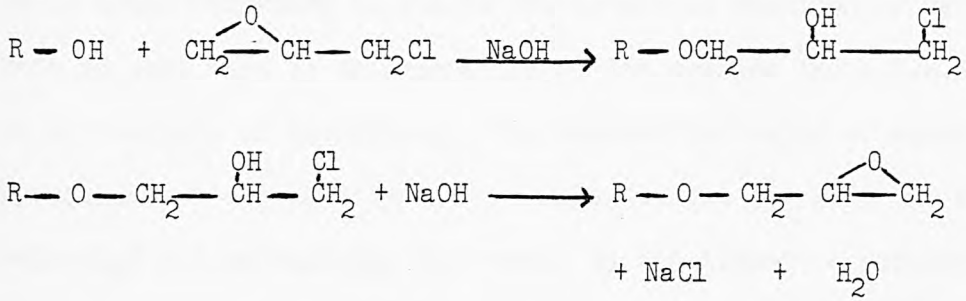

Scheme 1.12

If excess NaOH is added another molecule will react with the epoxide group causing polymerization.

Scheme 1.13

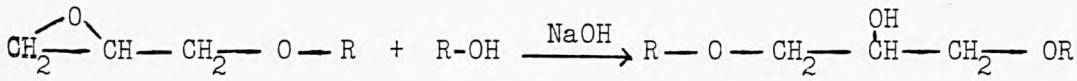

R is normally aryl but can be alkyl.

The low molecular weight resins are crosslinked using hardners. These must be anionic or cationic reagents as epoxides will not undergo free radical reactions. However nucleophiles such as amines and electrophiles such as alkyl halides will react.

Other epoxy resins with epoxy groups in the middle of the chain are prepared from unsaturated compounds treated with peracids.

The advantages of epoxy resins are that:-

1) They produce no volatiles.
2) They have low shrinkage.
3) A great variety of hardners can be used.
4) They are stable over a wide range of temperatures.

The disadvantages are:-

a) They are expensive.
b) They may exotherm i.e. overheat, due to production of energy by the reaction.

c) Some epoxy compounds are toxic.

1.5.4 Determination of Epoxide Groups

It is often necessary to follow the extent of reaction of epoxy resins. This is best done by determination of the epoxide value i.e. the number of equivalents of epoxide/kg. The theoretical value of which is found by dividing a thousand by the molecular weight (to find the number of moles/kg) and multiplying the result by the number of epoxide groups in the compound.

The determination uses the ability of epoxide rings to undergo quantitative acid catalysed ring opening. Care must be taken when choosing the conditions, otherwise the results obtained will be inaccurate. The conditions are:-

i) anhydrous, non-alcoholic (to avoid serious side reactions).

ii) terminal epoxide groups give best results (i.e. those that cannot support a carbonium ion too well).

The best method has been found[33] to be the use of perchloric acid titrated against anionic halide salt, in glacial acetic acid. Hydrochloric acid was used for many years but the reaction was slow, the reagents unpleasant, back titration was necessary and accuracy in many cases left something to be desired. Thus HCl was superseded by HBr. This in turn was superseded by the production of HBr in situ from a quaternary ammonium salt and perchloric acid.

Scheme 1.14

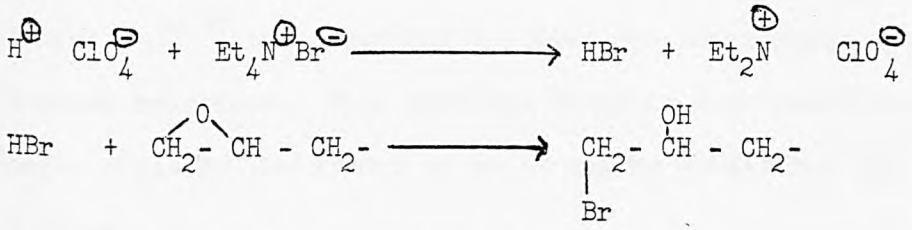

Thus if all the HBr reacts and all the $HClO_4$ reacts to produce HBr then the number of moles of $HClO_4$ reacted is equal to the number of moles of epoxide present.

Thus if the concentration of the $HClO_4$ is 0.1M then the number of moles $HClO_4$ = $\frac{0.1 \times \text{titre in mls.}}{1000}$.

$\therefore$ No. of moles of epoxide groups in X grams of sample. = $\frac{0.1 \times \text{titre in mls.}}{1000}$

No. of moles of epoxide groups in 1 gram of sample. = $\frac{0.1 \times \text{titre in mls.}}{1000 \times X}$

No. of moles of epoxide groups in 1 kg of sample. = $\frac{0.1 \times \text{titre in mls.} \times 1000}{1000 \times X}$

= $\frac{\text{titre in mls.}}{10 \times X}$

The end point can be detected using a potentiometric method or if the resin does not affect the colour change, then methyl violet can be used, the end point occurs when the solution turns an apple green colour. The usual sequence being: purple, blue, turquoise, green and yellow. Hence a quantitative measurement is obtained.

1.6 The Chemistry of Photopolymerization.

1.6.1 General View

Polymerization involves the reactions of small molecules with either:- molecules of the same compound (homopolymerization) or molecules of a different compound (copolymerization). These reactions can be induced thermally by a catalyst or photochemically. It is this latter option that will be considered here.

Delzene [34,35] has suggested a scheme for classifying photopolymerization reactions. This involves dividing such reactions into two major classes, the second of which can be subdivided into a further 2 types.

Type 1 Each increase in molecular weight requires its own photochemical activation. This type usually involves the formation of cross links

between pre-existing polymer chains.

Type 2A A photoinitiator absorbs a photon to give an excited state which forms radicals and thus free radical polymerization occurs.

Type 2B A photoinitiator absorbs a photon to give an excited state which forms cations and thus cationic polymerization occurs.
Type 1 is true photopolymerization as polymerization involves the excited states of the monomer. Type 2 is photoinitiated polymerization as additives which cause the monomer to polymerize are the species which absorb the incident light.

1.6.2 Photoinitiated free radical Polymerization (Type 2A)

The monomers to be polymerized contain either multiple bonds or strained rings. Alkenes are by far the most important. During polymerization the π bonds are destroyed and two new σ bonds are formed. The mechanism of free radical polymerization of acrylate monomers serves as as example. Scheme 1.15

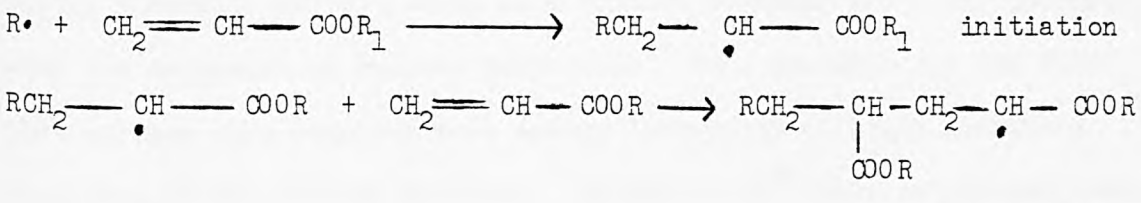

initiation

Propagation.

Both termination and chain transfer reactions compete with initiation and propagation, and thus limit the molecular weight which can be achieved. Chain transfer occurs when a polymer radical abstracts hydrogen or another atom from another compound in the system. Termination occurs when two radicals are destroyed by mutual interaction.

It[36] can be shown that the rate of free radical polymerization is given by:-

$$R_p = k_p \left[\frac{I_o \, \phi \, (1 - \exp^{-\varepsilon [PI] \, b})}{k_t} \right]^{\frac{1}{2}} [M]$$

k_p = rate constant. k_t = termination rate constant.

ϕ = Quantum yield for production of primary radical pair.

I_o = Intensity of incident light ε = extinction coefficient

$[PI]$ = Concentration of photoinitiator b = film thickness.

$[M]$ = Monomer concentration.

Thus the rate of polymerization is dependant upon $k_p/k_t^{\frac{1}{2}}$. As termination reactions require little activation energy and are thus diffusion controlled, k_t is inversly proportional to viscosity. Thus $k_p/k_t^{\frac{1}{2}}$ increases as viscosity increases. This gives rise to the Trommsdorf effect[37]. i.e. the rate of polymerization increases in the early stages until depletion of monomer takes control.

Because the rate is dependant on the square root of the intensity, a greater degree of polymerization is achieved by using a low intensity of light for a long period rather than a higher intensity for a correspondingly shorter period.

Oxygen is known to inhibit free radical polymerization both by combining with free radicals in the polymerizing system to produce unreactive peroxy radicals, and by acting as a triplet quencher which can interfere with the mechanism of radical production. This accounts for the fact that surface cure requires more energy (intensity of light absorbed) than cure at the bottom of a film. Holman et al[38] have calculated that, for a 12.5 μm thick film of an acrylate resin containing benzoin n-butyl ether, the ratio of absorbed energy between the surface 1μm layer and the bottom 1μm layer is 20:1. Clarke and Shanks[39] have shown that in the absence of oxygen the curing of a film of butyl acrylate containing benzoin is greatest when the sample thickness is least. They have also shown that there is a maximum in the curve of extent of polymerization versus initiator concentration which has been attributed to an uneven distribution of radicals at high concentrations.

The effects of oxygen can be reduced by i) increasing the intensity of the light thus increasing the rate of reaction[40]. ii) using amines to regenerate active radicals by chain reaction. iii) use of wax barrier

coats. iv) conversion of triplet oxygen to singlet oxygen by dye sensitization followed by scavenging of singlet oxygen. and v) carrying out polymerization in an inert atmosphere.

Oxygen is in fact the major problem of free radical polymerization. It is difficult and expensive to eliminate and it detracts from the properties of the cured surface even when measures have been taken to eliminate it. Termination is also caused by the radicals that initiate polymerization and as the excited states are short lived reactions cease soon after irradiation has ceased.

Another major drawback is the rapid shrinkage which occurs, This will detract from the adhesion of the coating to the substrate.

1.6.3 Types of Prepolymer used in Free Radical Polymerization.

Unsaturated polyesters made by the esterification of maleic anhydride or fumaric acid with bifunctional or polyfunctional alcohols, are used in conjunction with a reactive diluent such as styrene in a wide variety of industrial applications.

Prepolymers possessing (meth)-acrylate or meth-acrylamido end groups comprise another major type of UV curable resin. These compounds are made by the reaction of diglycidyl derivatives of bis-phenol A with acrylic or (meth)-acrylic acid. These polymers have better mechanical and adhesive properties than the unsaturated polyester resins. Pendant vinyl urethane groups can be introduced via the hydroxyl groups formed. These groups improve adhesion to metal surfaces together with elastic and impact properties.

1.6.4 The Chemistry of Some Major Free Radical Photoinitiators.

There are two types of radical initiators :- i) Those that produce radicals via a unimolecular reaction, ii) Those that produce radicals via a bimolecular reaction.

i) Most unimolecular processes involve α - or Norrish type I cleavage.

The most well known of this type are the benzoin ethers (Ph-C(=O)-CH(OR)-Ph) the most effective being those where R in an alkyl group from a secondary alcohol[41,42]. The rate constant for α cleavage for alkyl ethers is $>10^{10}s^{-1}$ whereas for benzoin itself it is $\simeq 10^{9}s^{-1}$.[43] The difference is attributed to the ability of the benzylic substituent to stabilize an adjacent positive charge.

It has been shown by N.M.R.(CIDNP) and ESR that the radicals produced by α-cleavage are a benzoyl radical and an α alkoxy benzyl radical:-

Scheme 1.16

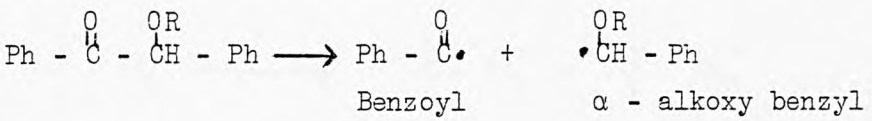

The effectiveness of these radicals seems to be dependent on the system. In acrylates and (meth)acrylates both are equally effective[45], whereas when styrene is present the benzoyl radical is more effective[43,44]. The explanation could lie in the difference between experimental conditions used[46].

Because benzoin ethers work in the presence of styrene, a powerful triplet quencher and yet can be sensitized by a triplet sensitizer it would seem that splitting can take place from either excited state.

Another derivative of benzoin, 2,2-dimethoxy 1,2-diphenyl ethanone (Ph - C(=O) - $C(OCH_3)_2$Ph) also undergoes Norrish type I cleavage. This compound has been found to give better can stability than benzoin ethers[47], due to the lack of an α-benzylic hydrogen. It also shows enhanced reactivity due to the extra electron donating group and to the fact that a methyl radical is produced via a secondary fragmentation of the benzyl radical. One of the drawbacks of the system is that the methyl benzoate produced from this secondary fragmentation may leave the coating with a residual odour.

Scheme 1.17

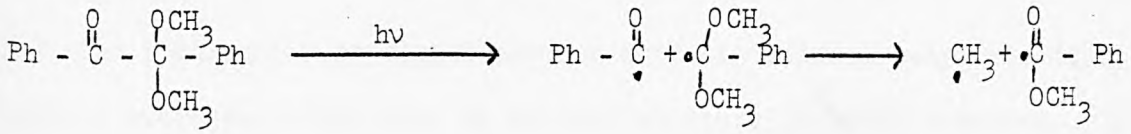

This process has also been followed by CIDNP and found to be very temperature dependent[48].

Surface cure can be improved by addition of tertiary aliphatic amines[47]. This is due to the suppression of oxygen inhibition by a chain reaction which allows the amine to consume oxygen[49].

Scheme 1.18

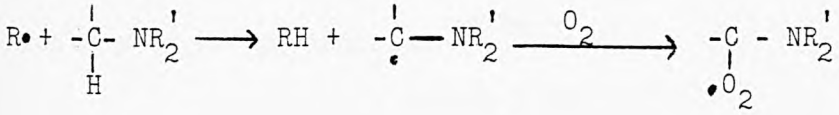

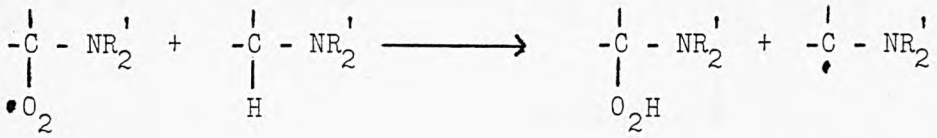

2,2 - Diethoxy-1-phenyl ethanone is an efficient photoinitiator for unpigmented coatings. This compound undergoes both Norrish type 1 and Norrish type 2 cleavage. As no benzylic radical is produced there is less yellowing, hence the suitability for unpigmented coatings.

Scheme 1.19

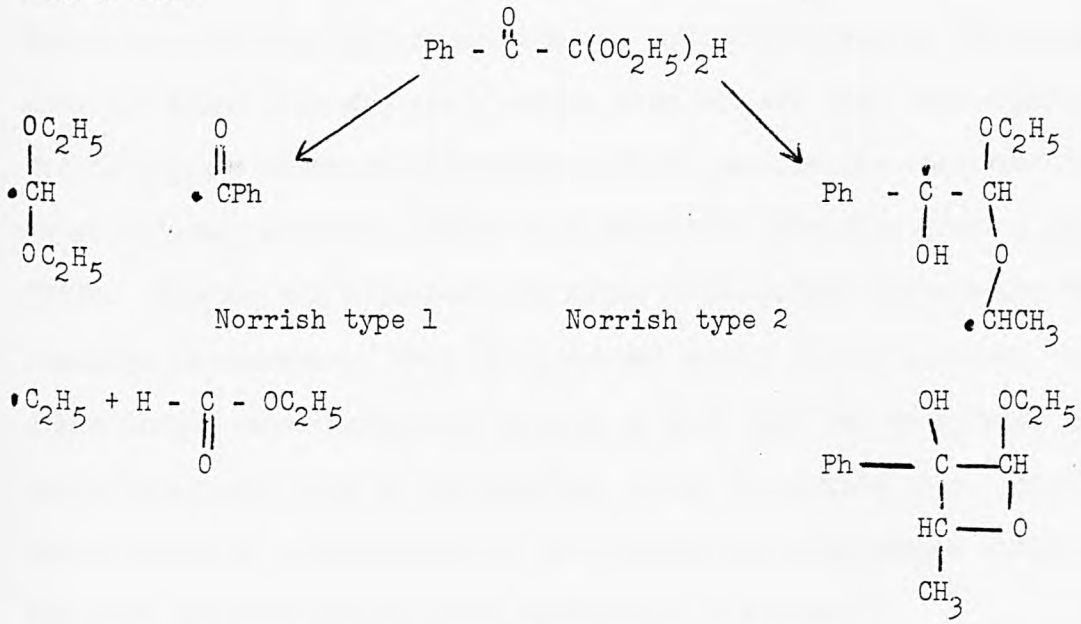

Green, Stark and Zahir state both processes give rise to radicals which can initiate polymerization[2].

ii) The bimolecular processes used to initiate radical polymerization involve hydrogen abstraction by an excited state carbonyl compound. In

this type of system a suitable hydrogen donor is also required, these are generally thiols, alkyl ethers, alcohols and particularly amines, (e.g.triethanolamine). The ketones used include benzophenone, Michlers ketone, derivatives of thioxanthone and anthraquinone.

The mechanism for hydrogen abstraction from amines by ketones involves the formation of an excited charge transfer complex which splits into radicals by proton transfer [50,51].

Scheme 1.20

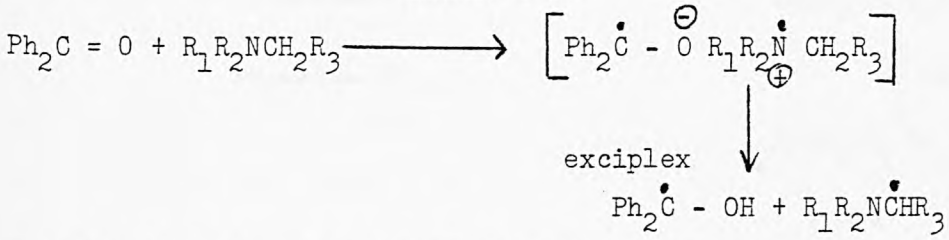

Exciplex formation is possible because of the low ionization potentials of amines. For commercial formulations derivatives of the parent compound are used because of superior solubility and more favourable absorption characteristics and possibly better absorption characteristics. Ketone amine systems produce only 1 radical per molecule, whereas unimolecular cleaving systems produce two radicals/molecule. Furthermore although amine radicals are electron rich and are thus very efficient in initiating the electron deficient acrylate groups, the corresponding ketyl radicals are more likely to dimerise or terminate growing polymer films. However the advantages in using ketone/amine systems are that no cleavage is necessary, thus the absorbed energy can be lowered. This means longer wavelengths can be used, a fact that may be helpful in pigmented coatings, such as the acrylate based UV curable inks. Another factor which is advantageous is that amines minimize oxygen inhibition and thus the need for an inert atmosphere is avoided.

The thiol-ene system, developed by W.R.Grace and Co.[52,53] is another variation of this type of system. In this case a polythiol and a polyene undergo free radical initiated crosslinking. Benzophenone is used as a hydrogen abstractor. The proposed mechanism[52,53,54] is as

follows:- Scheme 1.21

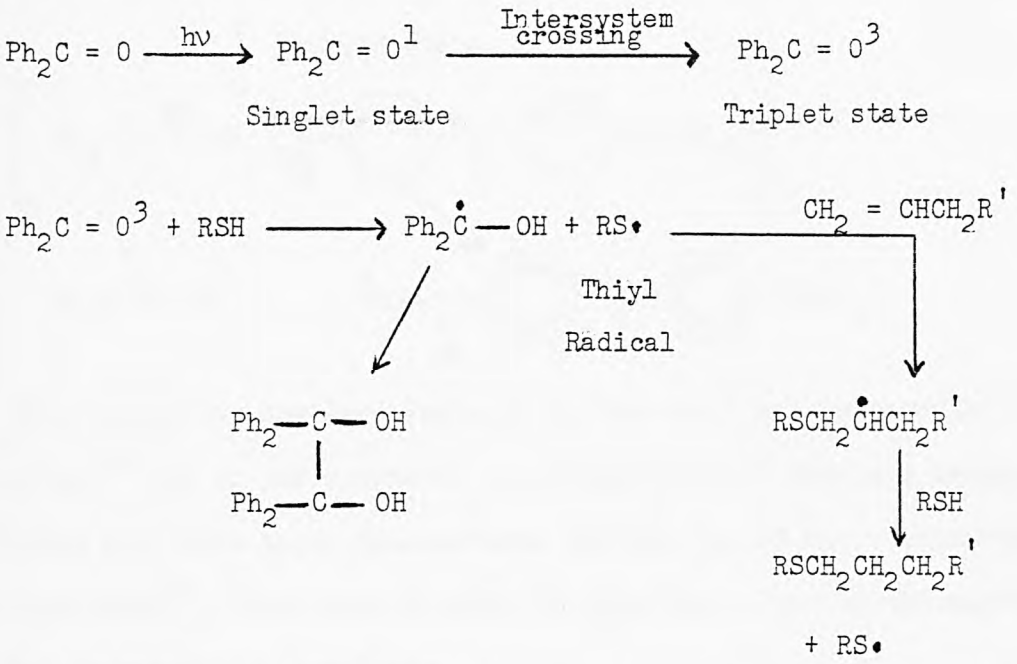

Triaryl phosphines have been found to improve the rate of crosslinking and the mechanical properties[55]. This is because they scavenge traces of sulphur which can cause inhibition. Thus the crosslinking density is improved which in turn improves the mechanical strength.

Benzoin ethers have also been used as initiators for thiol-ene systems, the mechanism involves both hydrogen abstraction and unimolecular cleavage. These systems have been used for printing plates, UV screen inks solder masks and other coatings.

Michlers ketone 4,4'-bis(N,N'-dimethylamino)benzophenone contains both amine and ketone groups, and thus in theory could be used as both the hydrogen donner and the hydrogen abstractor. Unfortunatly it is a poor initiator on its own[56]. This is due to the amino group pushing electrons onto the oxygen so that the alkoxy radical nature of the $n\pi^*$ state is severely reduced. However Michlers ketone has been used in conjunction with benzophenone as a synergistic mixture in pigmented inks[57]. The mechanism is thought to involve a triplet exciplex which splits into radicals. See scheme 1.22

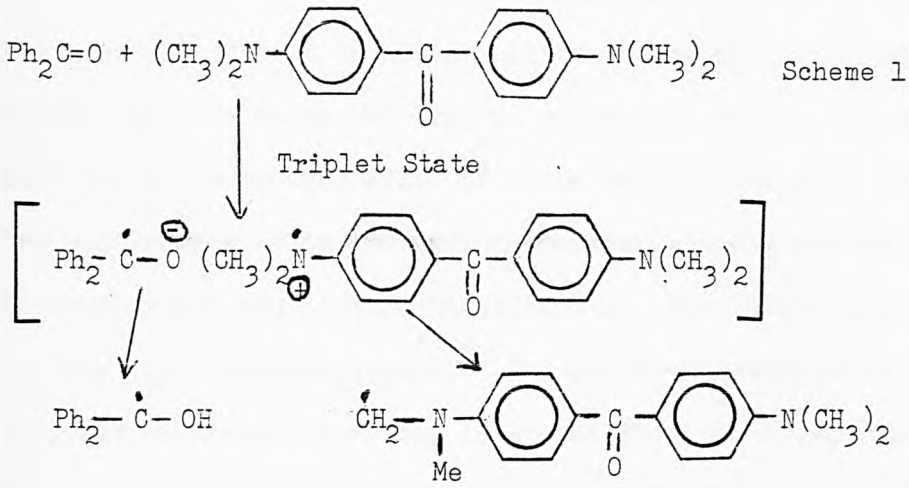

This system has now been replaced by the ethyl homologue of Michlers ketone[58] due to the suspected carcinogenicity of Michlers ketone. There are three major thioxanthone derivatives of major commercial importance[59], these are: 2-chlorothioxanthone, 2-methylthioxanthone and 2-isopropylthioxanthone.

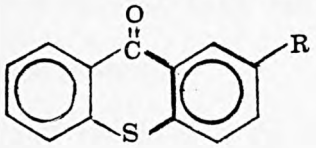

R = -Cl or $-CH_3$ or $-CH(CH_3)_2$

Aminobenzoates such as ethyl 2,4-dimethylbenzoate are used in conjunction with thioxanthones. Thioxanthones have a maximum absorption at 385nm although the range is 360-400nm. Thus the lamps used for curing are mercury lamps[47] dosed with iron iodide, so as the output between 360-400nm is increased. Because of this range of absorption thioxanthones can be used with organic pigments which transmit in this region.

1.6.5 Photoinitiated Cationic Polymerization(Type 2B)

The resins that are generally used in this system are epoxy resins based upon either bisphenol A diglycidyl ether or cycloaliphatic epoxy resins made by peracid epoxidation.

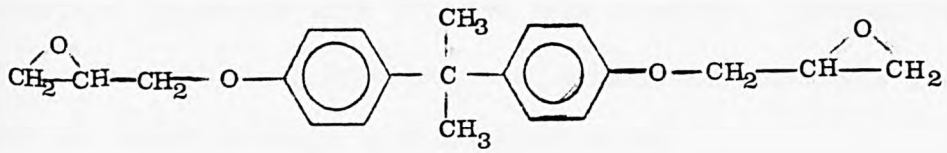

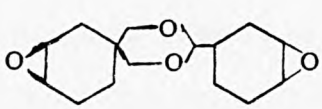

The most significant cationic initiators are aryl diazonium salts, diaryl iodonium salts and triaryl sulphomium salts. It is essential that the corresponding anion of these salts is of poor nucleophilicity, the most common being: tetrafluoroborate, hexafluorophosphate, hexafluoroarsenate and hexafluoroantimonate. The larger anions are better as they are less nucleophilic. The actual polymerization is initiated by Lewis or Broensted acids, liberated from the above salts by photolysis. These cationic polymerizations are not affected by molecular oxygen.

1.6.6 The Chemistry of Some Major Cationic Photoinitiators

i)Aryl diazonium salts were the first systems to be used[60,61,62]. On photolysis a Lewis acid, nitrogen and a benzene derivative are formed[3].

Scheme 1.23 $ArN_2^{\oplus}MX_n^{\ominus} \xrightarrow{h\nu} ArX + MX_{n-1} + N_2$

A Broensted acid can be formed from the Lewis acid if traces of water are present.

Scheme 1.24 $PF_5 + H_2O \longrightarrow H^{\oplus}PF_5OH^{\ominus}$

The nitrogen can cause bubbles if the films are too thick, which detracts from the film properties.

A second disadvantage is the low thermal stability of diazonium salts, a fact that affects the pot life of the system. Storage stability can be improved by the addition of cyclic amides, nitriles, substituted ureas and sulphoxides[64]. Thermal stability can also be extended by introducing electron releasing substituents in the para position, which allows delocalization of the positive charge. The wavelength of absorption is also increased as is the quantum yield for photolysis. In fact the absorption range can be varied to suit requirements by varying the substituent on the benzene ring[62]. Thus the curing of coatings, pigmented with TiO_2 are made possible. Although pale yellow-brown when wet, loss of nitrogen on irradiation, destroys the chromophore and the cured coatings is a brilliant white.

On irradiation with no resin present no change is observed in the infra-red spectrum of the diazonium salt, whereas irradiation in the resin

gives rise to complete loss of the diazonium group. This suggests that the evolution of nitrogen occurs subsequent to some initiator/monomer interaction.

ii) Iodonium and sulphonium salts, with the same corresponding anions as above, have been developed to overcome the low thermal stability of diazonium salts and the evolution of nitrogen on their photolysis.

The photosensitivity of iodonium and sulphonium tetrafluoroborates was investigated in the early seventies[65,66]. By studying the effects of radical scavengers together with the products of photolysis (e.g. diphenyl iodonium tetrafluoroborates yields benzene, iodobenzene, a Broensted acid $H^{\oplus}$ and acetone[66], similar results were obtained from the photolysis of 4,4' - di- tert-butyldiphenyl iodonium tetrafluoroborate in acetonitrile, ethanol-water and acetone[67]) the following mechanism has been proposed.

Scheme 1.25

$$Ar_2I^{\oplus}X^{\ominus} \xrightarrow{h\nu} (Ar_2I^{\oplus}X^{\ominus})^*$$

$$(Ar_2I^{\oplus}X^{\ominus})^* \longrightarrow ArI^{\oplus}\bullet + Ar\bullet + X^{\ominus}$$

$$ArI^{\oplus}\bullet + SH \longrightarrow ArI^{\oplus}H + S\bullet$$

$$ArI^{\oplus}H \longrightarrow ArI + H^{\oplus}$$

SH = monomer or solvent

Triaryl sulphonium salts photolyse the same way[68] i.e.homolytic bond cleavage of the excited state generates radical cations which abstract hydrogen from a donor. Subsequent loss of a proton yields the Broensted acid which is responsible for the initiation of polymerization when the salts are included in a formulation.

The absorption spectra of the 'onium salts are affected only slightly by simple substituents on the aromatic rings. Thus they all absorb in the 230-260 nm region, with little absorption above 300 nm. A second drawback is that the products of photolysis (aryl iodide or diaryl sulphide) have almost identical absorption spectra to the parent compounds, and therefore compete for radiation. Thus simple diaryl iodonium salts and

triaryl sulphonium salts are not used for curing of thick or pigmented sections.

To overcome the second problem complex triaryl sulphonium salts such as these below are used.

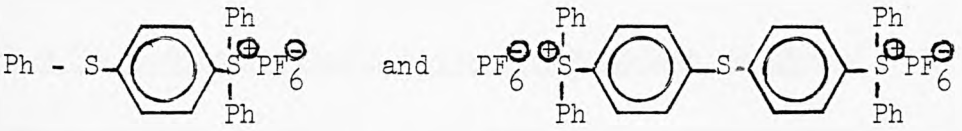

These compounds have significant absorption above 300 nm and thus improve performance as the photolysis products do not compete for the radiation[69,70,71].

A different approach is required with iodonium salts. In this case a photosensitizer is used. Dyes such as acridine orange and benzoflavin have been used[72]. The mechanism of photosensitization involves electron transfer from the photosensitizer to the 'onium salt[73].

Sulphonium salts can also be sensitized in this way with perylene[74]. However because of their more favourable reduction potentials, iodonium salts can be sensitized with a larger range of compounds.

Diazonium salts, supplied as a two part system to be mixed prior to use, are still the most commonly used cationic photoinitiator. Use of iodonium and sulphonium salts has been restricted by their lack of availability, a confused patent situation and a need for expensive cycloaliphatic epoxides for rapid cure.

Anions of low nucleophilicity have very little effect on the absorption spectrum and rate of photolysis[68]. However the rate of polymerization is heavily dependent upon the size and thus nucleophilicity of the anion. (i.e. the larger the less nucleophilic). The order of merit is $SbF_6^- > AsF_6^- > PF_6^- >> BF_4^-$

There are two major problems associated with cationic photoinitiation, they are i) they cure much slower than free radical initiated acrylate

systems[75], ii) minute quantities of certain types of adventitious impurity i.e. nucleophiles can inhibit cure either partly or totally. Amines are the most common example. Thus pigmented systems based on cationic polymerization present a great problem. However not all pigments affect the rate of polymerization.

1.6.7 Photopolymerization via Cycloaddition Reactions

These systems require no initiator as the excited state produced by absorption of the incident radiation, undergoes reaction with another chromophore of the same type in the ground state. Most of these systems are based on unsaturated aromatic carbonyl compounds. Some do require sensitization[76] as their absorption spectra do not correspond with the emission spectra of the lamps used in UV curing.

The rate of polymerization is dependant upon the intensity of the incident radiation and the square of the concentration of the chromophore[18,25] amongst other things.

Because polymerization is solely dependant upon a photochemical process and not secondary thermal reactions the Stark-Einstein law whould be obeyed i.e. each reaction requires the absorption of 1 photon.

Another law is the Bunsen-Roscoe law or the law of reciprocity[77,78]. This states that the quantity of the reaction products of a photochemical reaction is proportional to the product of the intensity of the incident radiation and the time of exposure. Thus a high intensity of radiation for a short period gives the same result as a lower intensity of radiation for a longer period. Continuous irradiation should give the same result as intermittent irradiation if all other factors are kept constant. (c.f. section 1.6.2)

These systems are not free radical initiated but generally react via the triplet state, (although there is evidence to suggest that the singlet state can play a part[18]. Thus oxygen will have a much less pronounced effect on the rate of reaction. Photo-oxidation may also occur.

1.6.8. Types of Polymer used in Photopolymerization by Cycloaddition

The polymers can contain the active group either pendant to the chain or in the backbone of the chain. The first system to be investigated[76] and patented[79] was poly vinyl cinnamate, prepared by the esterification of polyvinyl alcohol with cinnamoyl chloride. The product was a photocross-linkable polymer with the active groups pendant to the chain.

Use of chalcone as a pendant group has been investigated by Unruh[80]. This polymer was made by the condensation of polyvinyl acetophenone with benzaldehyde. He showed by comparison with 4-ethyl-1,3-diphenyl-prop-2-en-1-one, that the polymer behaves in a similar fashion to a monomer of the same structure. Initially trans-cis isomerization occurs, further irradiation causes cycloaddition to take place, forming insoluble products in the case of the polymers.

Other methods of preparing polymers with pendant active groups are:- addition of p-isocyanato benzalaceto-phenone, to polyvinyl alcohol and by a Friedel-Craft reaction between polystyrene and cinnamoyl chloride.

The chalcone unit can also be introduced into a polymer backbone by reacting 4,4'-dihydroxy chalcone with epichlorohydrin[25,26]. Chain extension is achieved with bifunctional 'advancing' agents such as bisphenol A, or by reacting the chalcone type bisphenol with a low molecular weight diepoxide. Zahir[25] has shown that trans-cis isomerization is wavelength dependent and that dimerization occurs from a photo-stationary state between the two isomers.

1.6.9. The Chemistry of Cycloadding Systems

Cinnamate systems generally contain a sensitiser to extend the range of sensitivity towards the visible. However as mentioned in 1.4.4 the dimerization of cinnamate systems can take place via either the singlet or triplet state depending upon the presence of sensitizers. It has been found that the quantum yield of dimerization is higher for the unsensitised

polymer.

Photosensitisers must have high extinction coefficients at the wavelengths used for irradiation so that low concentrations can be used. They must also have a high quantum yield of intersystem crossing (ϕisc) and the lifetime must be long. Finally they must have triplet energies of similar magnitude to the acceptor. Some typical sensitisers and their triplet energies are given below:-

Naphthalene	61 kcal M^{-1}
Benzophenone	68.5 kcal M^{-1}
Michlers ketone	61 kcal M^{-1}
N-methyl 2-benzoyl β-naphthothiazoline	54 kcal M^{-1}

The fourth in this series has been found to give the best results for speed of crosslinking. It has also been found that ϕisc is greater in a polymer matrix than in solution[81].

There has been no attempt to sensitize chalcone systems. This is due to their absorption spectra extending further into the visible than cinnamate systems.

Zahir[25] has suggested that photodimerization is a second order process. This can be rationalized by assuming that the rate limiting step is dependent upon the concentration of molecules in the excited state and the concentration of ground state molecules surrounding them. However the concentration of molecules in the excited state is dependent upon the initial concentration, and on the intensity of the light a fact Zahir has chosen to ignore. The mechanism proposed by Cadwell and Singh[24] involves a biradical intermediate rather than a concerted 2 + 2 cycloaddition. The picture is complicated by the suggestion that photocleavage of the cyclobutane dimer[25] can occur slowly, again via a biradical mechanism. Further complications arise from the fact that free radicals can initiate polymerization[84] and dihydromers can be formed under certain

conditions[85].

As mentioned in 1.4.4 cyclodimerization in the solid phase is dependent upon the distance of separation between adjacent chromophores. In amorphous solids such as polymers other factors such as average site reactivity and extent of energy delocalization in the matrix also play a part.

It has been shown for polyvinyl cinnamate[82] that not all chromophores are suitably orientated to effect dimerization, i.e. the quantum yield dropped from an initial value of 0.18 to zero after a conversion of about 50%. A similar effect has been seen with polymers containing chalcone groups[83]. This gives rise to the concept of reactive and non-reactive sites.

In order to obtain gel formation and hence insolubility, intermolecular processes rather than intramolecular processes are required. The former will occur if the polymer coils interpenetrate freely. If the polymer molecules remain isolated intramolecular interactions will occur leading to no increase in molecular weight and hence no gel formation. The quantum yields of intermolecular crosslinking and total crosslinking have been estimated[86] for polymers containing chalcone like chromophores. The ratios of ϕinter to ϕtotal were found to be in the 0.22 - 0.25 range, indicating a high degree of chain inter-penetration in the solid polymer matrix.

Other types of systems that undergo cyclo-crosslinking include those containing coumarins, derivatives of maleic acid, anthracenes and stilbenes.

1.6.10 Positive Resists

Positive resists work in exactly the opposite way to those discussed above. On irradiation the polymer becomes soluble. The resists depend upon dissolution inhibitors undergoing chemical change on irradiation.

One system involves[87] derivatives of 2-diazo-1,2-naphthoquinone, mixed in relatively large amounts into phenolic novolacs, which act as dissolution inhibitors. On photolysis the diazo compound rearranges to an indene carboxylic acid derivative. Aqueous alkali can now leach out the phenolic resin and the indene carboxylate from the exposed areas.

Scheme 1.26

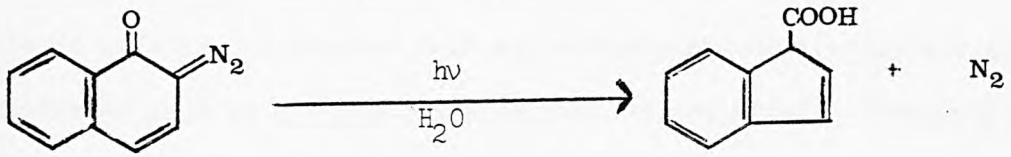

The advantages of negative resists are:-

i) Good resistance to etching

ii) Generally quite cheap

iii) Quality is easily reproduced.

iv) Adhere well to substrate

v) Developing conditions need not be too rigerous

The main disadvantage of negative resists is that the polymer must swell so that uncrosslinked material can be leached out by the developer. Swelling can be to as much as four to five times, thus reducing resolution. A second drawback is the sensitivity of negative resists to oxygen.

The advantages of positive resists are:-

i) Less swelling on development

ii) Insensitive to oxygen

iii) Can be imaged by projection rather than contact with resist pattern

The disadvantages are:-

i) expensive ii) less sensitive iii) poorer adherance to substitute iv) less forgiving during development v) quality is difficult to reproduce.

1.6.11 Commercial Photoresists.

There are three types of resist used in the electronics industry. Selection of the type to be used depends upon the demands to be made on the resist. For printed circuits requiring only low resolution (250-1000μm)

a UV curable screen inks are used. For higher resolution (50-400μm)such as in computors and telecommunication devices, dry film resists have dominated the market until recently. These consist of a photoactive resin sandwiched in between a polyethylene film and a polyethyleneterephthalate film. The resin is thought to be a resin of methyl methacrylate copolymerised with methacrylic acid or itaconic acid to render it alkali soluble. A monomer such as pentaerythritol triacrylate and an initiator such as anthraquinone derivative are added. Irradiation causes the monomer to polymerize around the base resin affecting resistance to aqueous alkali.

Before irradiation the polyethylene film is removed and the bare resin is laminated onto the board. Irradiation takes place through a photographic film master and the polyester film. This latter is peeled off after irradiation and development is effected by an organic solvent or an aqueous based alkaline developer. After the plate is etched the resist is stripped off with stronger organic solvents or alkaline solutions.

Over the past four to five years liquid resists have been competing for the market. It is claimed that the material costs for liquid resists are about $\frac{1}{3}$ of those for dry film resists. There are two types of liquid resist. The first is based on epoxy resins containing a light sensitive group which undergoes photocycloaddition. The resin is stored as a solution, the solvent being removed by heating before use. The system is developed with cyclo-hexanone and then a latent amidine hardener is activated with a thermal bake. This resist remains with the board. If the board is faulty the resist can be removed before the thermal bake with 2-ethoxy ethanol.

The second type is based on a thiol-ene system, it is stored as a neat liquid resin. Thus the photographic master cannot be brought into contact during cure which reduces resolution. After development a second treatment with UV hardens the resist. This system is aqueous developable.

For resolutions of 1μm and less which are required for producing features on silicon chips three approaches are being tried. These are:- using mid UV radiation, using Xrays and using electron beams.

In the first case a positive resist has been developed[88] based on a phenolic-resin novolac containing 4 and 5-sulphonate diester derivatives of 2-diazo 1,2-naphthoquinone. Another type of positive resist has been developed whereby irradiation causes reduction of molecular weight by breaking polymer chains. This system is based on acrylic resists co-polymerised with 3-methacryloximino 2-butanone and methacrylonitrile.

Poly (2,3-dichloro-1-propyl acrylate) copolymerised with glycidyl meth-acrylate and ethyl acrylate have been developed for use with Xrays from palladium sources. Similar polymers have been used with electron beams.

1.7 Photoacoustic Spectroscopy

1.7.1 Introduction to Photoacoustic Spectroscopy

The photoacoustic effect was originally discovered[89] and investigated[90] by Alexander Graham Bell in the early 1880s. However after a flurry of activity[91,92] it was discarded as an interesting phenomenon of no practical use. This was until Viengerov[93] used it to evaluate concentrations of gaseous species in gas mixtures. Improvements by Luft[94] led to commercial instruments having sensitivities that permitted measurements of concentrations as low as a few parts per million.

It was not until the early 1970s that condensed phases were considered[95] since then there has been an explosion in the number of papers published on the subject.

The effect relies upon the non-radiative de-excitation processes that occur when a molecule is excited by an external energy source, such as a beam of light. The generation of thermal energy causes heating of the sample which, in the case of a solid sample, then heats a layer of gas in contact with the surface of the sample. This will of course expand

according to Charles law.

If the incident light is modulated (flashed on and off) then the generation of thermal energy will be periodic. The time taken for energy transfer to occur is small compared to the time between individual bursts of light, thus it can be considered instantaneous. This periodic generation of thermal energy will give rise to a thermal wave of the same modulation frequency as the incident light. The thermal wave will cause air in a closed cell to expand and contract, that is a compression wave will be set up which can be detected with a microphone.

1.7.2 The Rosencwaig-Gersho Theory (R.G.Theory)

The Rosencwaig-Gersho theory[96,97] was the first general theory for the photoacoustic effect. It is a one dimensional analysis of the production of a photoacoustic signal in a simple cylindrical cell.

Essentially it consists of an exercise in unsteady state heat transfer which sets up an equation for the periodic temperature at the gas solid boundary. The complex ampltude of this periodic temperature variation is used to develop an equation which describes the expansion and contraction of a layer of gas in contact with the sample surface. The pressure variation generated by this expansion and contraction is calculated using the adiabatic gas law on the assumption that the boundary layer is acting like a piston. A parameter Q is used to describe the envelope of this sinusoidal pressure variation, which is the actual signal picked up by the microphone.

One of the most important parameters to come out of the solution of the thermal diffusion equations besides the variable temperature function is, $a = \left(\frac{\omega}{2\alpha}\right)^{\frac{1}{2}}$. Where ω is the modulation frequency and α is the thermal diffusivity. The units of a are cm^{-1} and it is termed the thermal diffusion coefficient. The inverse is μ, the thermal diffusion length and this gives the maximum depth from which generated heat will contribute to the heating of the gas layer in contact with the sample. It has been

shown that the thickness of the layer of gas acting as the piston is dependent upon the thermal diffusion depth of the gas and is given by

$$x = 2\pi\mu'$$

The explicit formula of Q the sinusoidal pressure variation is:-

$$Q = \frac{\beta I_o \gamma P_o}{2\sqrt{2}(T_o \kappa \ell' a'(\beta^2-\sigma^2))} \left[\frac{(r-1)(b+1)e^{\sigma\ell} - (r+1)(b-1)e^{-\sigma\ell} + 2(b-r)e^{-\beta\ell}}{(g+1)(b+1)e^{\sigma\ell} - (g-1)(b-1)e^{-\sigma\ell}} \right]$$

1.7.1

β = optical absorption coefficient.

Io = Incident Intensity.

γ = Ratio of the specific heats of gas.

Po = Ambient Pressure.

To = Ambient Temperature.

a = Thermal diffusion coefficient for sample

a' = " " " " gas.

a" = " " " " backing

κ = Thermal conductivity for sample.

κ' = " " " gas

κ'' = " " " backing

$\sigma = (1 + i)a$

$b = \kappa''a''/\kappa a \qquad g = \kappa'a'/\kappa a \qquad r = \frac{(1-i)\beta}{2a}$

In order to simplify the above equation special cases are considered where many of the terms are simplified. There are two groups considered, optically transparent and optically opaque. For each category three cases are considered according to the relative magnitude of μ and the thickness ℓ.

In these cases $\kappa''a'' > \kappa'a' \qquad \kappa''a'' \simeq \kappa a$ thus $b > g$ and $b \simeq 1$

also putting $Y = \frac{\gamma P_o I_o}{2\sqrt{2}\, T_o \ell'}$

For transparent solids $(\ell_\beta > \ell)$

i) $\mu >> \ell$ and $\mu > \ell_\beta$ i.e. thermally thin samples

$$Q \simeq \frac{(1-i)\beta\ell}{2a'}\left(\frac{\mu''}{\kappa''}\right)^{Y} \qquad 1.7.2$$

ii) $\mu>\ell \quad \mu<\ell_\beta \quad Q \simeq \frac{(1-i)\beta\ell}{2a'}\left(\frac{\mu''}{\kappa''}\right)^{Y}$ 1.7.3

iii) $\mu<\ell \quad \mu<<\ell_\beta$ i.e. thermally thick samples

$$Q \simeq \frac{-i\beta\mu}{2a'}\left(\frac{\mu}{\kappa}\right)^{Y} \qquad 1.7.4$$

In the first two cases the equation is the same, i.e. the signal is proportional to $\beta\ell$ and has a ω^{-1} dependance due to μ''/a' being proportional to $1/\omega$. An important result is that the thermal properties of the backing material come into play. In the last case the signal is proportional to $\beta\mu$, i.e. only light absorbed in the first thermal diffusion length contributes to the signal and the thermal properties of the backing are no longer significant. In this case the frequency dependance varies as $\omega^{-3/2}$. Thus by varying μ a depth profile can be obtained in theory. For opaque solids $\ell_\beta<<\ell$

i) $\mu>>\ell \quad \mu>>\ell_\beta$ i.e. thermally thin solids.

$$Q \simeq \frac{(1-i)}{2a'}\left(\frac{\mu''}{\kappa''}\right)^{Y} \qquad 1.7.5$$

ii) $\mu<\ell \quad \mu>\ell_\beta$ i.e. thermally thick solids.

$$Q \simeq \frac{(1-i)}{2a'}\left(\frac{\mu}{\kappa}\right)^{Y} \qquad 1.7.6$$

iii) $\mu<<\ell \quad \mu<\ell_\beta$

$$Q \simeq \frac{-i\beta\mu}{2a'}\left(\frac{\mu}{\kappa}\right)^{Y} \qquad 1.7.7$$

The first two equations describe the independance of the signal from β the absorption coefficient, and thus is the mathematical description of photoacoustic saturation. The signal is again proportional to ω^{-1}. The third case shows a dependance upon $\beta\mu$ and thus if $\mu<\ell_\beta$ an unsaturated spectrum can be obtained. This equation demonstrates the value of the photoacoustic technique when looking at opaque solids. Again there is a change in dependance on modulation frequency to $\omega^{-3/2}$.

Many workers have shown the validity of these equations such as the independance of the signal from β for opaque samples[95], the dependance of signal magnitude on thickness[98], saturation effects[99] and the change in dependance on modulation frequency from ω^{-1} to $\omega^{-3/2}$ when going to thermallys thick solids from thermally thin solids[100].

The R.G. theory has been refined to explain observed derivations at very low frequencies [101,102,103] and to include contributions to the signal from thermally induced vibrations of the sample[103].

1.7.3 Depth Profiling using Photoacoustic Spectroscopy

As mentioned above an inhomogenous sample may be depth profiled by variation of the modulation frequency. This was done on a piece of apple peel[104]. A spectrum at modulation frequency of 220Hz showed only the essentially non-absorbing waxy layer on the surface, on changing to a modulation frequency of 33Hz the chlorophyll and carotenoid compounds contributed to the signal and an absorption band well into into the visible region was observed. Depth profiling can also be effected by varying the phase angle between the PA signal and the incident radiation[105]. In this case the in phase spectrum recorded the waxy cuticle layer of a spinach leaf. A spectrum recorded 90° out of phase should have given no signal as the in phase component is zero. A spectrum of the chlorophyll was observed.

It has been shown that for a two layer system, where the first layer is transparent and the second layer absorbing, that there is an increase in phase lag given by[106]:-

$$\psi = \frac{x}{\mu_2} \qquad 1.7.8$$

ψ = phase lag x = thickness of non-absorbing layer.

μ_2 = thermal diffusion length of non-absorbing layer.

This fact has been used to measure polymer film thicknesses.

An equation has been formulated for a signal from two layers and the dependance on the relative values of ℓ_β ℓ and μ is demonstrated with

computer generated plots[107]. These show that the signal magnitude is largely unaffected by differences in the thermal properties. However the phase angle changes by 45^{o} when the modulation frequency is such that only the first layer contributes to the signal. For transparent and absorbing ($\ell_{\beta} = \ell$) samples this change is abrupt. For opaque samples the change is more gradual.

An extension to this technique is thermal wave[108,109] imaging. In this case radiant energy from a laser is modulated in order to produce a photoacoustic signal. Detection from different depths depends upon the phase lag caused by thermal diffusion from various depths taking varying periods of time to reach the surface. This phase lag between incident radiation and signal is described by:-

$$\psi = \frac{d}{\mu} + \theta \qquad 1.7.9$$

where θ = a phase lag introduced by instrumental response.
The rest of the equation is as before. Kirkbright and Miller[109] have shown how ink on two opposite sides of a polymer film can be detected at different phase settings and thus indicate that a depth profile may be obtained. It is hoped that information on flaws in the crystal lattice etc. can be detected using this technique.

1.7.4 Some Applications of Photoacoustic Spectroscopy.

This section deals only with UV visible and near IR application for FT-IR-PAS see separate section.

Photoacoustic spectroscopy has been used over the past 11 years to obtain absorption spectra of many types of solid samples, especially those that are opaque or in such a form that conventional spectroscopy cannot be used without a great deal of sample preparation which may, in some cases, destroy the moiety under study.

Biological studies of blood smears, previously restricted by light scattering, and intact plant matter together with marine phytoplankton

have been reviewed by Rosencwaig[107]. He has also demonstrated the uses to medicinal science. Photochemical studies, particularly deexcitation processes in condensed media, are yet another application.

Following Rosencwaigs initial study[110], quantitative methods of analysis of T.L.C. plate materials have been established over the past few years[111,112,113]. One of the most interesting inventions is that of a mobile PAS cell that can be placed over a T.L.C. spot[113]. This general technique has been used to determine the amount of food dyestuffs in colouring material extracted from fruit gums[115].

Another avenue of research is the application to pharmaceutical preparations[114]. Quantitative analysis of active agents in tablets has been performed[115] and the UV band edge of suncream lotions has been determined.

Yet another use has been the study of dyes and fluorescent whitening agents (FWA) already in situ on the wool[116,117]. In the latter case it has been shown that the F.W.A. can be detected and how it is destroyed on irradiation.

The near IR has been used to determine the amounts of polyvinyl acetate in PVA/PVC copolymers by monitoring the 2.1μm carbonyl peaks relative to the 1.75μm C-H peak.[118]

Another recent application to polymers is the study of the thermal degradation of polyurethanes[122], quininoneimides were detected as was the monomer and diamines formed by the reaction of the monomer with water.

Determination of moisture content in various materials such as milk substitutes, paper[119], single cell proteins[118] and starch[120] is another use of the near infra-red region. The photoacoustic response was found to be linear over low concentrations but nonlinear over high concentrations. This has been rationalised with the R.G.theory[120].

Thermal wave imaging mentioned above is now stimulating great interest, detection of flaws in integrated circuits, and cracks in metals together with examination of adhesive bond were recently reported[121].

1.8 Infra-red Spectroscopy

1.8.1 Introduction.

Infra-red spectroscopy has developed over the past 35 years, into a well established technique of polymer analysis. Infra-red rays were discovered by William Herschel[123] in 1800, when he directed a spectrum of the suns rays onto a thermometer and found that some visible rays had a heating effect. It was not until the early 1900s however, that Coblenz built the first IR spectrometer and obtained the spectra of over 100 organic compounds[124].

In 1951 Hausdorff[125] presented a collection of IR spectra of polymers and since then many more collections have been published[126].

Photons of the mid infra-red region possess energy of the same order of magnitude as the energy difference between vibrational energy levels in a molecule. The absorption of infra-red radiation leads to transitions between these different vibrational levels.

The basis for the use of IR spectroscopy is the fact that many chemical groups absorb in a relatively narrow frequency range irrespective of the nature of the other functional groups present. Tables of these characteristic frequencies have been constructed from the immense amount of data collected. The exact frequency is dependent on the precise nature of the functional group, e.g. the carbonyl group in saturated ketones absorbs at 1725 cm^{-1} - 1705 cm^{-1}, in unsaturated ketones the range is 1685 - 1665 cm^{-1}. In saturated aldehydes the group absorbs at 1740 - 1720 cm^{-1} and in unsaturated aldehydes the range is 1705 - 1680 cm^{-1}. Esters give a band between 1750 - 1735 cm^{-1}.

1.8.2 Theory.

The bond between 2 atoms in a molecule can be regarded as a spring that obeys Hookes law. That is, its vibrational motion can be described by the following equation:-

$$F = -kX$$

F = Restoring force.

k = Force Constant.

X = Distance removed from equilibrium position.

The force constant k is usually a measure of the strength of the spring, thus in this case it is a direct measure of bond strength (this is different to the dissociation energy). Another property of k, is that it is dependent upon electronic configuration.

A vibrating diatomic molecule can be treated using S.H.M. theory. Thus the classical equations can be applied.

The frequency of vibration $\nu = (1/2\pi)\sqrt{k/\mu}$ 1.8.1

μ = reduced mass = $\frac{1}{m_a} + \frac{1}{m_b}$

m_a = mass of atom a in the molecule

m_b = mass of atom b in the molecule

μ is used to simplify the mathematics, i.e. quantum mechanics shows that the vibrating diatomic molecule can be treated as just one particle moving. This particle moves such that its movement is equal to the change in interatomic distance, and it has a mass of μ.

The potential energy is given by:-

$$V = \tfrac{1}{2}kq^2 \qquad 1.8.2$$

q = displacement i.e. change in interatomic distance

At q max total energy = potential energy as there is no movement at this point.

If the above value is substituted in the Schrödinger wave equation, an expression for the total energy is obtained.

Thus $E = (n+\frac{1}{2})(h/2\pi)\sqrt{k/\mu} = (n+\frac{1}{2})h\nu$ 1.8.3

$\Delta E = (n+1+\frac{1}{2})h\nu-(n+\frac{1}{2})h\nu = h\nu$ 1.8.4

n = vibrational quantum number, h = Plank's constant, c = speed of light, ν = wave number

Unfortunatly a diatomic molecule does not execute pure S.H.M., this is in part due to the fact that as the interatomic distance changes, so does the electronic configuration and hence k.

In an attempt to correct for this non-ideal behavior, anharmonicity constants have been introduced. (These are in fact empirically determined parameters.) The new energy equation is as follows:

$E = h\nu_e(n+\frac{1}{2})-h\nu_e x_e(n+\frac{1}{2})^2$ 1.8.5

ν_e = frequency if molecule exhibited ideal behavior

x_e = anharmonicity constant

Various selection rules are also required so that the theoretical number of absorptions is equal to the observed number of absorptions. These selection rules are determined using quantum mechanical and symmetry techniques. The basic selection rule is that $\Delta n = \pm 1$ if a transition is to occur, but this selection rule breaks down when applied to real systems because of anharmonicity. Hence Δn can equal ± 2 and higher, this gives rise to overtones which, although weak are usually clearly visible. (These overtones will not appear at exactly double or half frequencies due to equation 1.8.5.)

In an attempt to extend the diatomic molecule model, the concept of the normal vibration must be introduced. This vibration is one in which all the atoms of a molecule vibrate with the same frequency and in the same phase.

e.g. H_2O

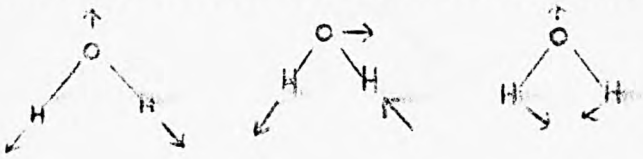

(the arrows show the direction in which the atoms move.)

There are 3N-6 normal vibrations in a non-linear molecule of N atoms and 3N-5 in a linear system.

Normal vibrations are described by normal coordinates which in turn can be found from matrices. (For a comprehensive discussion of the theory see reference 127.)

The complex vibrations of the molecule can now be described by using the superposition principle to combine any number of normal vibrations.

1.8.3 Types of Vibration

For every symmetry type there are a number of standard vibrations. These are as follows:

Stretching

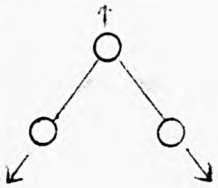

Symmetric
(given the symbol ν_s)

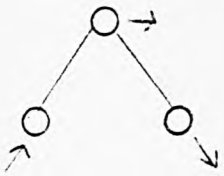

Antisymmetric
(given the symmbol ν_{as})

Angle Bending and Rocking

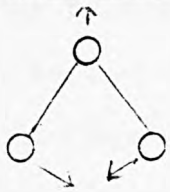

Bending
(given the symbol δ)

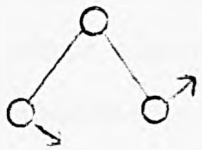

Rocking
(given the symbol ρ_r)

Wagging- defined as a change in the angle between bond and a plane.

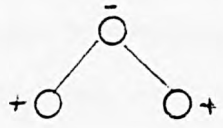

(given the symbol ρ_w)

Twisting - defined as a change in the angle between 2 planes

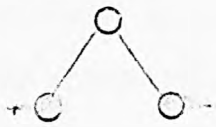

(given the symbol τ)

Out of Plane Deformation

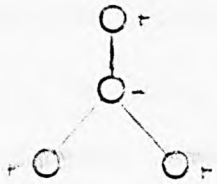

(given the symbol π)

In the above vibration the central atom oscillates in the vertical plane.

Group Frequencies

One of the fundamental principles used in the interpretation of infra-red spectra, is that of group frequencies. Certain groups absorb at characteristic frequencies or over a narrow range of frequencies, regardless of the rest of the molecule. These frequencies are known as group frequencies, and have been, for the most part, obtained empirically. This information is usually collated and put on group frequency charts.

One may justifiably ask the question, how can a single group in a molecule, which vibrates as a whole (normal vibration), absorb at an isolated frequency? The answer lies in, the relative masses of the atoms in the group, and on the type of bonding. Thus groups containing light atoms e.g. hydrogen (OH, NH_2, CH_3 etc), or heavy atoms e.g. halogens (CCl, CBr, CI etc), have amplitudes and velocities of vibration which are either, very much larger or very much smaller, than in the rest of the molecule. Thus it seems very likely that these vibrations will have a strong controlling influence on the normal vibration. The rest of the

molecule acting as the mechanism, through which the frequency of the group vibration is broadened into a narrow band. If a group contains a multiple bond, similar effects operate. Hence most, are to a certain extent, independent of the rest of the molecule.

If the system is conjugated however, or atoms of similar masses are connected by bonds of similar strength (which is basically the same thing), isolation of group frequencies is impossible.

1.8.4 Methods of Obtaining Vibrational Spectra

There are two methods of obtaining vibrational spectra, these are:-
Using absorption of infra-red light.
Using emission of light via Raman Spectroscopy

Infra-red Spectra are obtained by simply irradiating a sample with infra-red light and measuring transmission or absorbance. When a vibration absorbs light at a certain frequency, transmission decreases. Hence, scanning over a wide range of infra-red frequencies, will yield a spectrum. For the most part, transmission will be relatively constant but at certain frequencies a decrease will be observed. Thus the positions of the frequencies of the vibrations, are readily observed.

Raman Spectra are obtained by irradiating a sample with visible or UV monochromatic radiation, of frequency ν, (this light is absorbed by excitation of electrons). Most of the light is emitted with the same frequency as the incident radiation (Rayleigh scattering). However, a little of the emitted radiation has frequencies different to that of the incident radiation. This is due to molecules not falling back to the initial state, (usually electronic and vibrational ground states) but a different state (electronic ground state, first vibrational level). Hence some scattered light will have frequency $\nu - \nu_i$ (Raman scattering), ν_i = vibrational frequency. Thus vibrational frequencies are observed as Raman shifts.

The above conditions give rise to Stokes line, if however a molecule

already in an excited state, absorbs, the resulting emission may have a frequency $\nu + \nu_i$. This condition will give rise to anti-Stokes lines.

A molecular vibration will exhibit infra-red activity, if the dipole moment changes with the vibration e.g.

$\leftarrow O = C = O \rightarrow$ is not infra-red active because of no dipole change

$\leftarrow O = C = O \leftarrow$ is infra-red active because there is a dipole change

To exhibit Raman activity, a molecular vibration must change the polaritability. In most cases where infra-red activity is absent, Raman activity is present. This does not mean to say that Raman and infra-red activities, operate exclusively. Indeed in many cases both are present.

1.8.5 Applications

Qualitative Analysis

There are two major areas in polymer chemistry where infra-red spectroscopy is used. Historically the first is qualitative analysis in which polymers are identified. This can be done by comparison with spectra of known polymers collected into catalogues. A second approach uses the fact that bands can be attributed to various groups e.g.

$\diagdown C = O$ $\quad$ $\diagdown\!\!\!\!\blacktriangle C - O$ $\quad$ $\diagdown N - H$ $\quad$ $-OH$

The position of the bands is dependent on factors such as intra and inter molecular forces, steric hinderance, high electronegativity of adjacent atoms, conjugation effects, tacticity and crystallinity.

Model compounds are often synthesised so that an accurate interpretation of the more complicated polymer spectrum can be achieved. If hydrogen or carbon isotopes are used as substitutes for atoms in the polymer, a shift in the fundemental frequency is observed according to 1.8.6.

$$\frac{\nu'}{\nu} = \left(\frac{\mu}{\mu'}\right)^{\frac{1}{2}} \qquad 1.8.6$$

ν = fundemental frequency before isotopic substitution

ν' = " " after " "

μ = reduced mass of atoms before isotope substitution

μ' = " " " " after " "

In this way the 1100-1400 cm^{-1} region of the spectrum of polystyrene (which is used as an infra-red standard) was accurately assigned to the C-H bonds in the chain or from the ring[128]. Other polymers which have been deuterated for this type of analysis include:- polybutadiene,[129] polyvinyl chloride[130] and polymethyl methacrylate[131].

If one monomer of a copolymer possesses an absorption band in a region where the second monomer does not absorb, e.g. styrene - acrylonitrile then the IR spectrum can be used to differentiate between the copolymer and the homopolymer.

Quantitative Analysis

Quantitative analysis by infra-red spectroscopy has been used to determine the composition of copolymers, determine quantities of additives, study polymerisation, isomerization and cyclisation reactions, study curing of epoxy resins, follow ageing processes in polymers and to study tacticity and crystallinity.

The position and intensity of the bands is dependent on the number of atoms in a group, the strength and nature of the bonds and on the geometry of the molecule as a whole. This last factor means that the chain length can affect the position of the band. Thus calibration must be performed using standard polymers in which the concentrations of the functional groups is known.

If the spectra are obtained in transmittance then 1.8.7 is required to convert to absorbance.

i.e. $$A = \log \frac{T \text{ base}}{T \text{ band}} \qquad 1.8.7$$

T base = the transmittance of the baseline

T band = " " " " band.

For nonlinear backgrounds the construction of a base line is not

standardised, a selection of the different methods used is illustrated in figure 1.5.

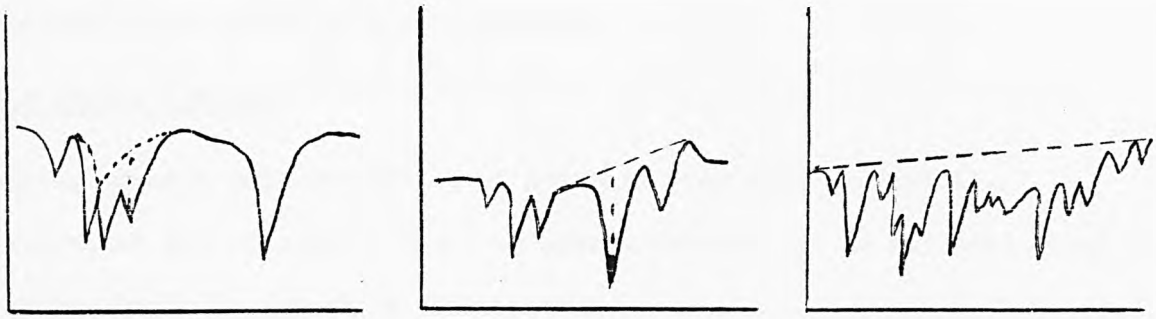

Figure 1.5 Examples of different methods used to construct base lines in infra-red spectra.

The decision of which method to use is left to the experimenter. Thus results from the same study will be self consistent but comparison of the results with other studies must be performed with care.

Polymer samples are generally prepared by casting a film from a solution onto a KBr disc. The film thickness can vary considerably, affected by non-uniformity of substrate and in some cases the method used to cast the film. This problem can be overcome by using an internal standard which should have an absorbance band in a region free from polymer absorbances. This band is then ratioed to a band in the spectra of the polymer. If the concentration of the standard is known then the following equation will apply.

$$\frac{A \text{ polymer}}{A \text{ standard}} = \frac{k_p \ell C_p}{k_s \ell C_s} = \frac{k_p C_p}{k_s C_s} \qquad 1.8.8$$

A suitable absorption band in the spectrum of the polymer can also serve as an internal standard and is referred to as the reference band. For example in the determination of the composition of vinyl chloride - vinyl acetate copolymer the CH_2 deformation band at 1435 cm^{-1} common to both monomers is used as the internal standard. The ratio of the carbonyl band absorbance at 1730cm^{-1} to that of the reference band at 1435cm^{-1} determines the composition[132]. In a more recent example of the use of IR spectroscopy for quantitative analysis of 'mixed' polymers,

Takayanagi and Goto[133] studied how the spectrum of poly (p-phenylene terephalamide) changed as more polybutadiene was introduced to produce either graft or block polymers.

The Ageing Process

Ageing changes many properties of polymers including mechanical, dielectric and spectral. Thus the ageing process can be followed using various bands in the infra-red spectrum.

The major reactions of the ageing process are oxidations of the polymers with the resultant formation of carbonyl groups. Thus polymers such as polyethene in which there are no original carbonyl groups, the identification of these groups is simple. Luongo[134] showed that thermally aged polyethene produced bands at 1705 cm^{-1}, 1718 cm^{-1}, 1730 cm^{-1} and 1740 cm^{-1}, which were assigned to acidic, ketonoic, aldehydic and ester carbonyl groups[135]. The amount of carbonyl group is dependent on the conditions and time of ageing. E.g. thermal ageing of polyethene yields ketonoic groups where as exposure to UV light produces mainly aldehydic groups.

Because of the many different types of carbonyl group formed quantitative estimation of carbonyl content is difficult. When this is the case the increase in absorbance is plotted against time to give a kinetic curve, which can be useful in the study of the ageing process.

Unsaturated bonds are formed on ageing. It was shown[135] for polyethene, by using the bands between 850-1000 cm^{-1} caused by vinyl (CH_2=CH) and vinylidene (CH=CH) groups, that the thermal ageing process occurs via a different mechanism than U.V. ageing. The oxidation of a $>C=C<_{C}$ system to a $C=C-\overset{O}{\overset{\|}{C}}$ system was followed by the appearance of a band at 1685cm^{-1}.

Scheme 1.26

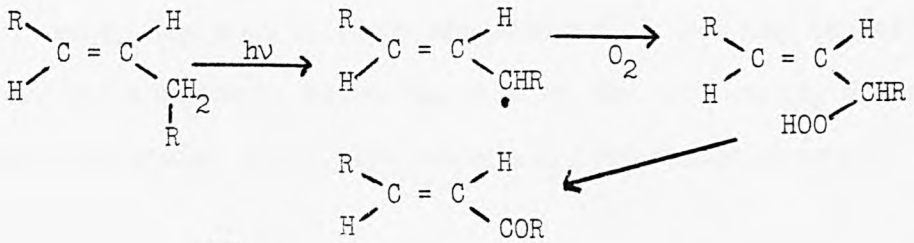

Photochemical ageing at the surface of polymer blends containing styrene acrylonitrile and butadiene was studied[136] by cutting the weathered samples into thin strips and obtaining IR spectra of the top and middle slices. Hydroxyl, aldehyde, ketonic groups were formed in the surface layer together with peroxides and acidic groups. The diene part of the blend was the most susceptible to attack. Bendaikha and Decker[137] have studied the photodegradation of epoxy-acrylate films using IR in conjunction with G.C. and UV spectroscopy. Irradiation of the films under an oxygen atmosphere with light of a wavelength greater than 250nm apparently completely destroyed the phenyl rings in the bisphenolic epoxy system. Ester and ether linkages were slightly less readily destroyed and the hydroxyl band showed an initial increase due to the formation of peroxides. Photolysis of the film under a nitrogen atmosphere reduced the susceptibility to photodegradation. However the yellowing of the epoxy-acrylate increased under nitrogen, showing that the discolouration is not due to photooxidation of photodegradation products.

Quantitative Study of UV Curable Systems

The first use of IR spectroscopy in this context was reported by Nishikabo et al[138] in 1974. They followed the curing of epoxy-acrylates using the $1640cm^{-1}$ band. Quite independantly in 1976 Collins et al[139] studied the photopolymerization of trimethylolpropane triacrylate with various concentrations of benzoin isobutyl ether as the photoinitiator, using the $1630cm^{-1}$ band. Absorptions in this region, which are due to C = C stretching, were also used by Van Neerbos[140] to study the photo-polymerization of a system comprising of an acrylic ester epoxy resin, poly(ethyleneglycoldiacrylate) and the dimethylketal of benzil as the photoinitiator. The films were $30x10^{-6}m$ thick. He showed that cure to 98% was very quick but the surface cured more slowly than the bulk. Infra-red spectroscopy was used by Plews and Philips[141] to study the effect of film thickness and atmosphere above the film on the photocuring of an aliphatic urethane acrylate, which also contained trimethylpropanetri-

acrylate and a photoinitiator. The amount of cure was measured as a function of the percentage of the residual double bonds left in the coating which was obtained from the 808 cm^{-1} band (caused by CH_2 twist of the acrylate group). These workers demonstrated how oxygen drastically affected the cure of thin films and also how cure under nitrogen is independent of photon flux density.

The 808 cm^{-1} band had been used previously[142] to study an acrylate resin film on a sodium chloride disc, when it was subjected to a 500 μs flash from a Xenon flash tube. The transmission was monitored with a fast running chart recorder. The polymerization initiated by 1 flash was complete in a fraction of a second. After 3 flashes only 42% of the double bonds remained.

More recently Azuma, Sanui and Ogata[22,143] have studied photosensitive rubbers containing pendant cinnamate groups using IR spectroscopy. The cinnamate group gives rise to a band at 1637 cm^{-1} caused by C = C stretch. On irradiation the adjacent C = C bonds cyclize during a photocrosslinking reaction and thus the 1637 cm^{-1} band decreases in intensity. The workers have used their results to develop a kinetic model for these systems. They have also shown a dependance of rate on the glass transition temperature.

The photocrosslinking[144] of unsaturated polymethacrylic esters has been followed using the 1640 cm^{-1} band in conjunction with D.S.C. Activation energies were determined from the results of both methods. The wildly different values were partially attributed to the different film thicknesses used for the different techniques.

Attenuated Total Internal Reflectance (ATR) Spectroscopy and Polymer Surfaces.

Attenuated Total Reflectance is a technique used for studying polymer surfaces. It depends upon reflection of IR radiation from a sample in contact with a material of refractive index greater than air (the

optical element). E.g. thallium bromo-iodide KRS-5, refractive index 2.4 or germanium, refractive index 4.0. The detected spectrum is very similar to an absorption spectrum. This form of spectroscopy was suggested almost simultaneously by Fahrenfort[145] and Harrick[146].

The effective depth of penetration of the radiation is given by[147]:-

$$d_p = \frac{\lambda_o}{2\pi n_1(\sin^2\theta - n_{21}^2)^{\frac{1}{2}}} \qquad 1.8.9$$

λ_o = Wavelength

θ = angle of incidence from the normal to the surface.

$n_{21} = \frac{n_2}{n_1} = \frac{\text{refractive index of sample}}{\text{refractive index of optical element.}}$

Thus depth of penetration is dependent on wavelength, and bands become stronger with increasing wavelength (decreasing frequency). It is also proportional to the refractive index of the sample. However the depth of penetration is inversly proportioned to the angle of incidence and the refractive index of the optical element. The refractive index of the sample falls below the mean level on the high frequency side of an absorption band and rises above the mean level on the low frequency side. Increasing the angle of incidence and increasing n_1 will reduce changes in $\sin^2\theta - n_{21}^2$ when n_2 changes. Thus high angles of incidence and optical elements of high refractive index improve spectrum quality and at the same time limit the spectrum to that of the surface. However intensity suffers. To combat this Multiple Internal Reflectance (MIR) is used. The effective penetration is about 1×10^{-6}.

A.T.R. has been used to follow photodegredation of the surface of polyethene terephalate films[148], to study the effects of fluorine gas on polymer surfaces[149]. The effects of surface oxidation on the adhesion of polythene to aluminium foil were reported by Willis and Zichy[147] who also followed the surface curing reactions of epoxy resins and polyurethane based laquers. Varying the depth of penetration was

demonstrated by Blias et al[150]. These workers studied the photooxidation of polypropene at various depths using different optical elements. They showed that the formation of hydroxyl groups by UV light > 320nm is predominantly at the surface.

Other Applications

IR spectroscopy has also been used in conjunction with x-ray spectroscopy, sodium fusion, and N.M.R. to analyse paints[151]. FT-IR spectroscopy was used to study weathered pigmented acrylamide crosslinked to acrylic coatings[152]. Palpacuer et al[153] used infra-red spectroscopy to follow the effects of increasing the amount of dopant in polyacetylene films doped with iodine. They concluded that the cis-trans isomerization initiated by doping was irreversible although doping was not. Some cis character remained however even at high dopant concentrations. It can be seen from the above discussion that IR spectroscopy is used extensivly in the field of polymer science for many different applications.

1.9 Objectives of the Project

The aims of this project were:-

i) To study photocrosslinking reactions of some photosensitive resins using a variety of spectroscopic techniques, including:- UV/Vis Photoacoustic dispersive IR, UV Diffuse Reflectance and FT-IR-PA. and thus establish which method could be best applied.

ii) To find the residual double bond content.

iii) To follow the reaction and obtain evidence for kinetic and if possible mechanistic models.

iv) To investigate the depth profiling capability of the photoacoustic technique.

CHAPTER TWO

U.V.- VISIBLE PHOTOACOUSTIC SPECTROSCOPY.

2.1 General Comments

Polyvinyl Cinnamates have been known to undergo photocrosslinking for the past 25 years. They have been used as photoresists and the mechanism and kinetics of their reactions have recently been investigated. As 1,3-diphenyl-prop-2-en-1-one (chalcone) is similar in structure, is also known to undergo photocrosslinking and has been largely neglected in the literature, it was proposed to use photoacoustic spectroscopy to study polymer films containing these compounds. On curing the chromophore is destroyed and hence changes in the UV absorption spectrum will be observed.

The polymers used in this study are based on two related systems, these are:- 1,3- diphenyl-prop-2-en-1-one (chalcone) and 1,5-diphenyl-penta-1,4-dien-3-one (dibenzalacetone).* These chromophores are introduced into

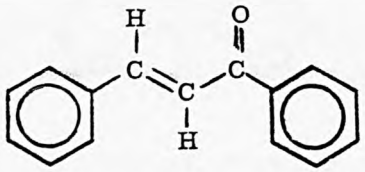

chalcone

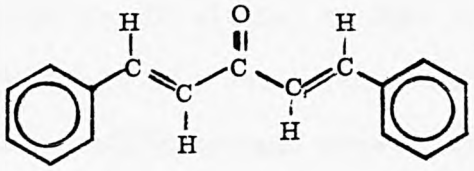

dibenzalacetone

*. Dibenzalacetone will be used instead of 1,5-diphenyl-penta-1,4-diene-3-one in this thesis for the sake of brevity.

the polymer backbone by first preparing the 4,4'-diglycidyl ethers from the 4,4'-dihydroxy compounds. The epoxy resins were then advanced into low molecular weight polymers using 5,5-dimethyl hydantoin as the link molecule. This was chosen because it has two acidic hydrogens and two distinct carbonyl groups which can be used as internal standards during studies using infra-red spectroscopy.

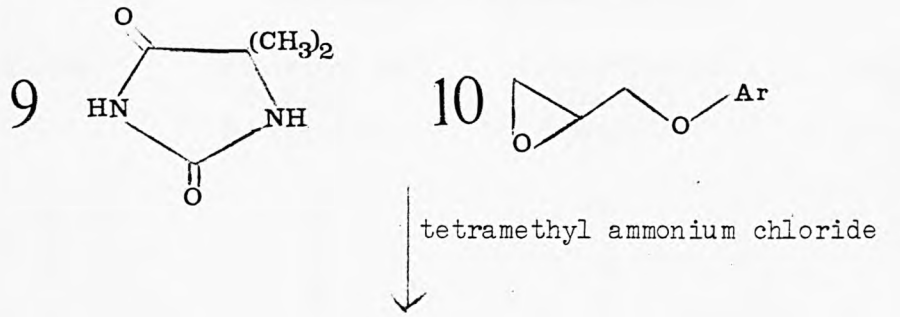

polymer 1

In order to reduce the concentration of chromophore but keep the other properties the same, bisphenol A diglycidyl ether (BADGE) was used in

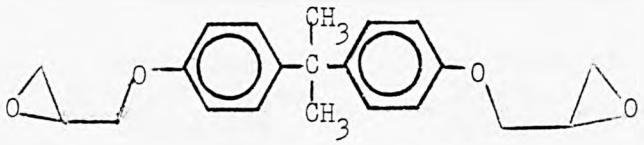

proportions such that the molar ratio of chromophore+ BADGE : dimethyl hydantoin remained at 10:9. BADGE was chosen because it has two aryl rings, a molecular weight similar to that of the molecules containing the chromophore and it is a lot cheaper than the chromophoric systems which may be important in certain commercial applications. The polymers and the molar ratio of their components are shown in tables 2.1a and 2.1b.

Two other polymer systems have been prepared. These are:-

i) 3,4-diglycidyl ether of 3,4-dihydroxy chalcone which was advanced with dimethyl hydantoin to produce a chain with pendant groups.

ii) 4,4-diglycidyl ether of 4,4-dihydroxy dibenzalacetone which was advanced with pentan-1,5-diol to monitor the effects of reducing the rigidity of the polymer chain.

Table 2.1a

Molar Ratios of Chalcone to Dimethyl Hydantoin to BADGE in Chalcone Series of Polymers

Polymer	Proportion of Chalcone Derivative	Proportion of Dimethyl Hydantoin	Proportion of BADGE
1	10	9	0
2	9	9	1
3	8	9	2
4	7	9	3
5	5	9	5
6	3	9	7
7	1	9	9
8	0	9	10

Table 2.1b

Molar Ratios of Dibenzal Acetone to Dimethyl Hydantoin to BADGE in the Dibenzal Acetone Series.

Polymer	Proportion of Dibenzal Acetone Derivative	Proportion of Dimethyl Hydantoin	Proportion of BADGE
A	10	9	0
B	9	9	1
C	8	9	2
D	7	9	3
E	5	9	5
F	3	9	7

2.2 Initial Experiments

2.2.1 Experimental Method

The polymers were kept as a solution, the solvent being 2-ethoxyethanol. Films were initially deposited by drawing a glass rod horizontally through a sample of the solution placed at one end of the substrate. Teflon paper was used as a substrate because: it is non-absorbing in the

spectral region of interest, samples for the photoacoustic spectrometer are easy to obtain, it is non-adhesive and non-adsorbing. The film was then placed in an oven at 80°C for 10 minutes in order to ensure all the solvent was evaporated.

Polymer A was used for these initial experiments and a 500W water cooled medium pressure mercury lamp was used for irradiating the samples.

2.2.2 Results and Discussion

Two sampling techniques were attempted i) samples were cut from films irradiated for different lengths of time and the spectrum run.
ii) a sample was cut from an unirradiated film and placed in the photo-acoustic cell. The film was irradiated in situ and spectra obtained of the same sample at different irradiation times. The spectra that were obtained are shown in figures 2.1 and 2.2.

A comparison of figures 2.1 and 2.2 shows that the P.A. signal is critically dependent upon sample size. This has led to a standardisation of the sampling technique (see 2.3).

Both examples show the same three interesting features. These features are most clearly demonstrated in figure 2.2.
a) The spectrum below 450nm is demonstrating photoacoustic saturation.
b) Loss of the chromophore on irradiation is observed. This is indicated by the large reduction in signal amplitude above 400nm. i.e. the shoulder is smoothed and moves towards the blue end of the spectrum. No further reduction is seen after 30 minutes indicating that cure is complete even though there are some chromophores remaining which cannot be photo-dimerized because of unfavourable spacial orientation.
c) The signal magnitude at the bottom of the band edge increases with irradiation, and continues to rise after cure can proceed no further. This is consistent with the film turning bright orange on prolonged irradiation. This observation indicates that a secondary reaction is taking place. It has been postulated by Zahir that the cyclo-butane

Figure 2.1
PAS of samples cut from different films of polymer A irradiated for various lengths of time.

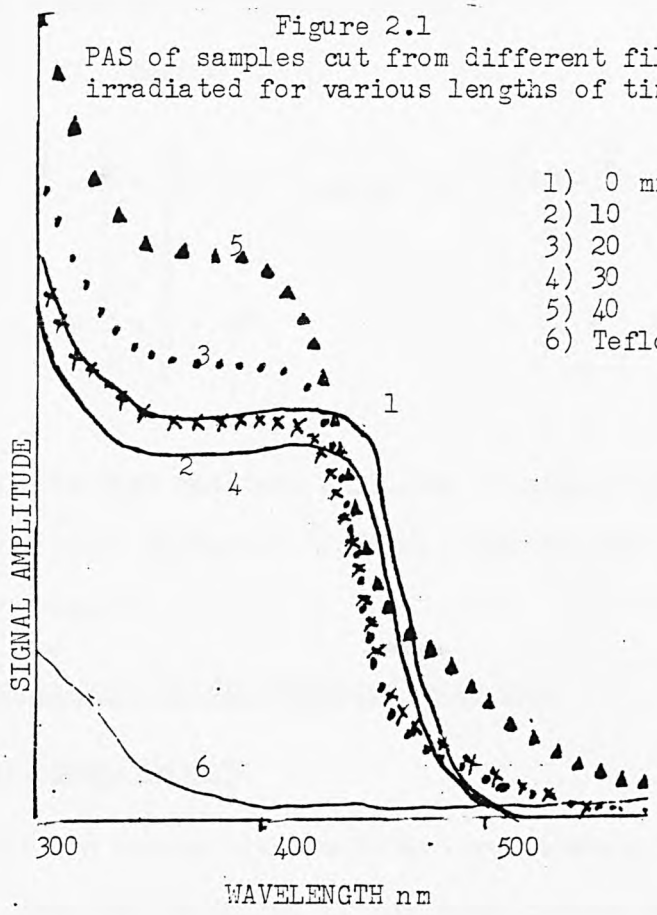

Figure 2.2
PAS of the same sample of polymer A irradiated for various lengths of time in the sample cell.

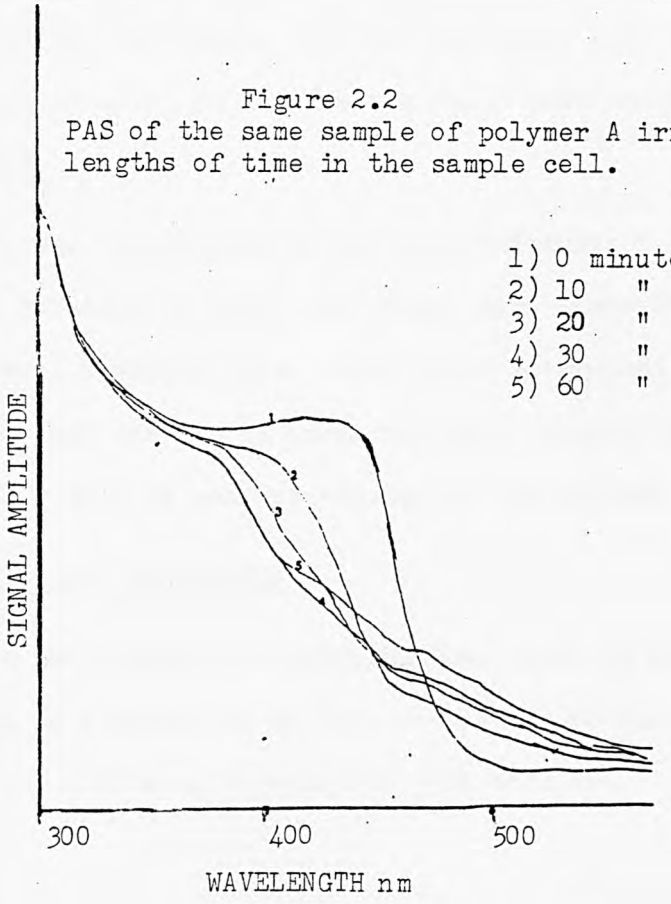

ring can be opened by UV light as follows.

Scheme 2.1

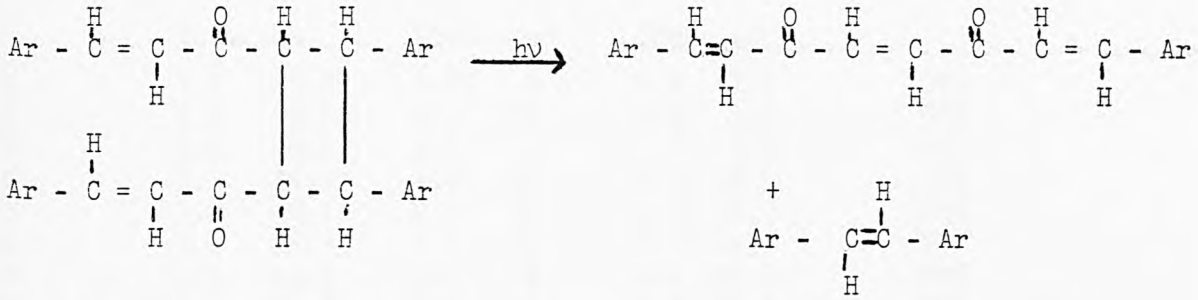

This type of cleavage reaction will lead to highly coloured compounds. Alternatively photo-oxidation could be occurring and producing highly coloured by products.

2.3 Standardization of The Sampling Technique

2.3.1 Experimental Method

In order that the sample size could be kept constant two cutting tools were made. Each one consisted of two razor blades seperated by a distance of 5mm or 15mm using a wooden spacer. The method was based on the punch and die technique. The cutting tools were used as the punches and a length of wood was used as the die. Best results were obtained with hardwood.

To eliminate the variability of the film thickness a K hand coater was used. This consists of eight wire wound bars numbered 1-8. Each one has a different diameter wire. Thus a pre-determined wet film thickness is deposited when the bar is drawn through a liquid sample. An impression bed with a clip at one end ensures an immobilized substrate.

2.3.2 Results and Discussion

Use of the K hand coater demonstrated that there is an enormous amount of shrinkage on evaporation of the solvent as one would expect. Using a micrometer the following thicknesses were obtained.

Table 2.2 Thicknesses of Films of Polymer A Deposited by K Bars 1-8

K Bar	Substrate Thickness		Wet Film Thickness		Dry Film Thickness		% Shrinkage
	Thou	µm	Thou	µm*	Thou	µm	
1	1.1	26.5	0.25	6	0.1	2.5	58%
2	1.1	26.5	0.5	12	0.2	5.0	58%
3	1.1	26.5	1.0	24	0.3	7.5	68%
4	1.1	26.5	1.5	36	0.4	10.0	72%
5	1.1	26.5	2.0	50	0.5	12.5	75%
6	1.1	26.5	2.5	60	0.7	18.0	70%
7	1.1	26.5	3.0	75	0.9	21.6	72%
8	1.1	26.5	4.0	100	1.2	28.5	72%

*As predicted by R.K.Print Coat Instruments.

The shrinkage is about 70-75% in most cases. The low values for the first two cases may be due to large inaccuracies inherent when measuring very thin films.

A film was deposited using a No.1 K bar and different samples were taken. The spectra that were obtained at different modulation frequencies are shown in figure 2.3

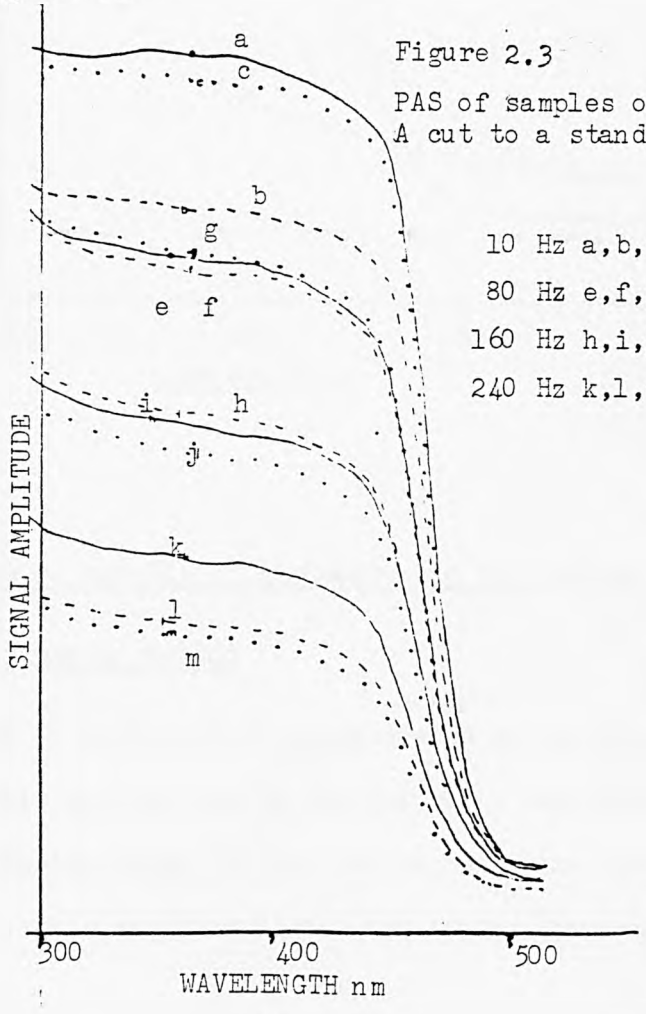

Figure 2.3

PAS of samples of films of polymer A cut to a standard size.

10 Hz a,b,c

80 Hz e,f,g

160 Hz h,i,j

240 Hz k,l,m

These spectra show a greatly improved consistency. Further experiments demonstrated how the sensitivity often had to be increased for samples that had been irradiated for longer periods. This was attributed to sample curling which is caused by expansion of the polymer on irradiation. This problem was solved using a commercial adhesive in the bottom of the cell. The improvement in results can be seen in figure 2.4

Figure 2.4

PAS of irradiated film of polymer A.

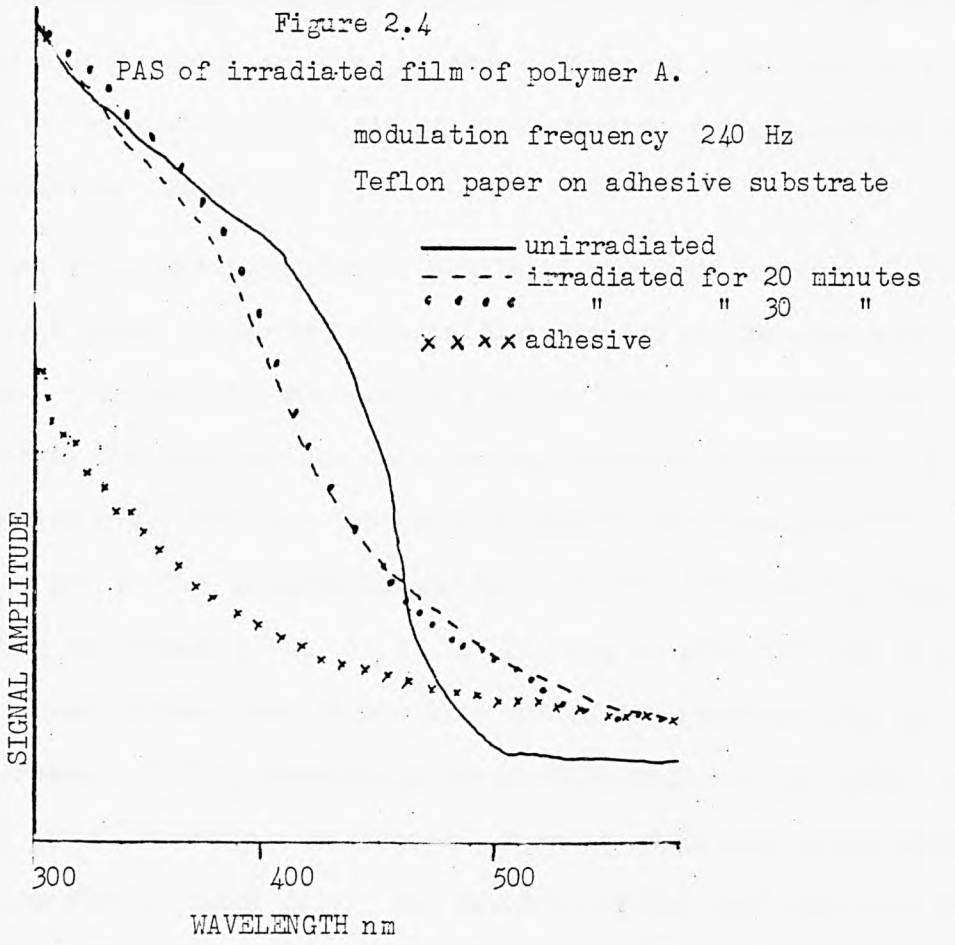

2.4 Efforts to Get Out of Photoacoustic Saturation

2.4.1 Experimental Method

As mentioned in section 2.2 photoacoustic saturation proved to be a problem. This problem can be theoretically overcome by reducing the thermal diffusion depth (μ) to a value less than the optical absorption depth (ℓ_β). This requires higher modulation frequencies. A second

option would be to reduce the thickness of the sample to a value lower than ℓ_β. This was effected by diluting the polymer solution with cyclohexanone. A third option would be to reduce the chromophore concentration thus effectively increasing ℓ_β. This last option was effected by using the polymers 1-8 and A-F.

2.4.2 Results and Discussion

The maximum modulation frequency attainable with the OAS 400 is 240Hz. As can be seen from the previous spectra (figures 2.3 and 2.4) it is not possible to bring the spectra out of photoacoustic saturation with such a low modulation frequency.

The spectra of a very thin film of polymer A are shown in figure 2.5.a, figure 2.5.b shows spectra of a thicker sample, at the same modulation frequency. The lack of structure is still evident in the very thin film. Unfortunately the film was too thin for any accurate measurements to be made on thickness. The fact that cure is almost complete after 30 seconds is due to the thinness of the film and the 1800w curing lamp used during the irradiation. It is interesting to note that the band edge has moved further towards the blue end of the spectrum than in previous cases. This is because in thick films only the top cures, the bottom of the film remains unaffected. This is reflected in the photoacoustic spectra of thick film. The movement of the band edge occurs because the film becomes transparent at lower wavelengths due to the removal of some chromophore. In the thin film cure is achieved throughout the film, up to about 85%(see later), and thus with chromophore nearly completely removed the band edge recedes further.

The spectra of polymers A-F and 1-4 are shown in figures 2.6a- 2.6d. They all demonstrate the increase in signal amplitude below 350nm (even the substrate shows this), thus effectively masking photoacoustic saturation. The high signal amplitude below 350nm is attributed to the optics of the instrument absorbing the light combined with a low source

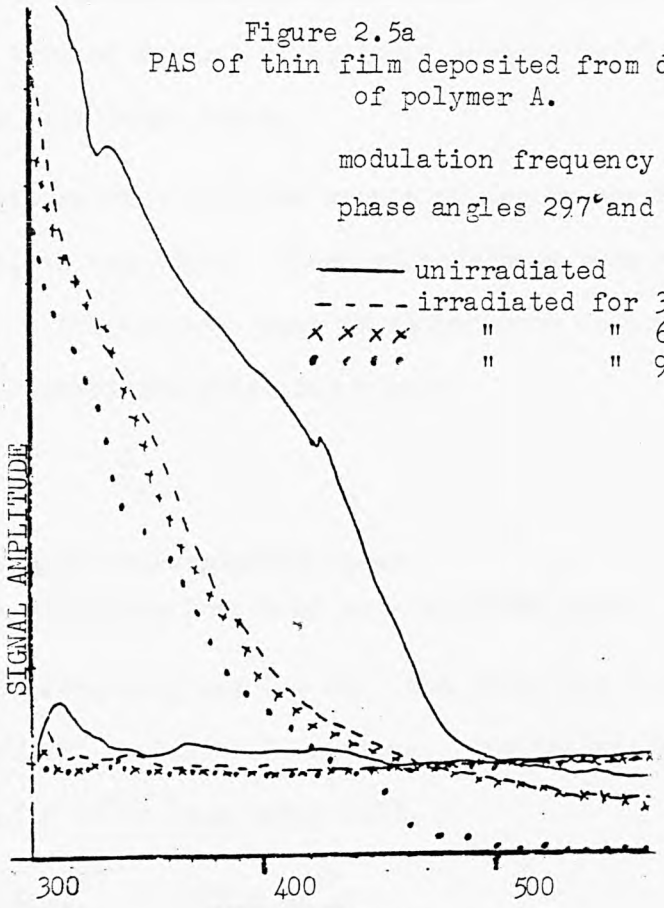

Figure 2.5a
PAS of thin film deposited from diluted solution of polymer A.

modulation frequency 240 Hz
phase angles 297° and 207°.

——— unirradiated
- - - - irradiated for 30 seconds
× × × × " " 60 "
• • • • " " 90 "

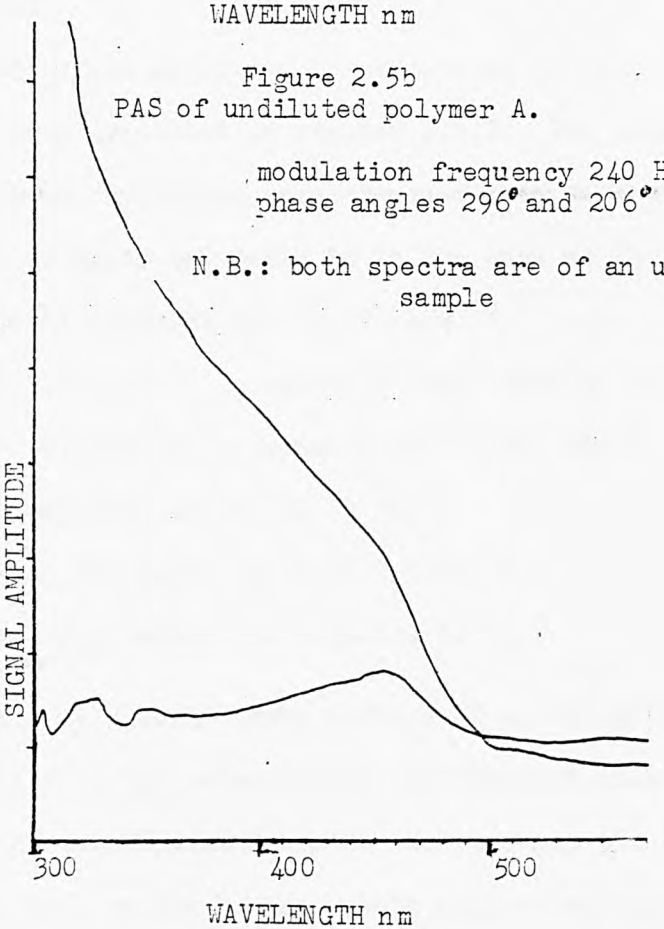

Figure 2.5b
PAS of undiluted polymer A.

modulation frequency 240 Hz
phase angles 296° and 206°

N.B.: both spectra are of an unirradiated sample

output. Thus very little light is reflected onto the pyrolytic detector (which is used as a reference) and any signal coming from the cell will be ratioed against effectively nothing which gives the impression of a very large signal.

The spectra of the reverse sides show a change in phase angle and a reduction in signal magnitude. These effects have been previously[106] observed when a transparent layer is placed over an absorbing layer. Equation 1.7.8 gives the phase lag ψ as:-

$$\psi = \frac{x}{\mu_2}$$

x = thickness of non-absorbing layer
μ_2 = thermal diffusion length of non-absorbing layer

The modulation frequency was 240 Hz. The phase lag difference varied between 9° and 12° or 0.16-0.21 radians. The thickness of the teflon paper was 26.5×10^{-6}m (see table 2.2).

$$\therefore \mu_2 = \frac{26.5 \times 10^{-6}}{0.21} = \underline{126 \times 10^{-6}\text{m}}$$

The density of teflon paper can be calculated to be 1380 kg m^{-3} from experimental data presented in chapter 2.8.2. The thermal conductivities and specific heat capacities were obtained from Kaye and Laby[154]. The specific heat of paper was taken to be the same as that of cellulose.

For paper thermal conductivity (κ) $0.06 Wm^{-1}K^{-1}$
density (ρ) = 1380 kgm^{-3} specific heat capacity (c) = $1.3 Jg^{-1}K^{-1}$
For teflon $\kappa = 0.25 Wm^{-1}K^{-1}$ density (ρ) = 1380 kgm^{-3}
specific heat capacity (c) = 1.0 $Jg^{-1}K^{-1}$
Using the values for paper $\mu_2 = 16.7 \times 10^{-6}$m
Using the value for teflon $\mu_2 = 38.7 \times 10^{-6}$m.

The first value is clearly wrong because if μ_2 was only 16.7×10^{-6}m then no signal from the polymer would be observed when the substrate was uppermost. The second value is much smaller than the experimental value. This could in part be due to inaccurate measurement of the phase lag.

Figure 2.6a
PAS of polymers A and B on a Teflon paper substrate

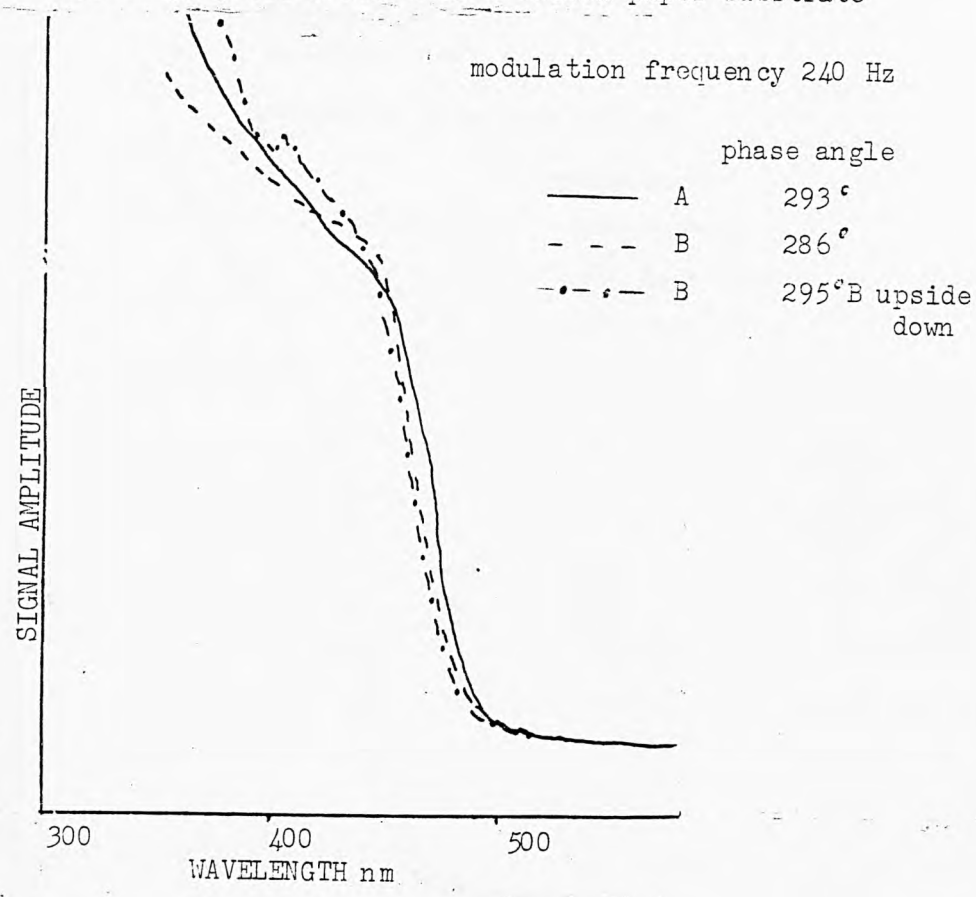

Figure 2.6b
PAS of polymers A, C and D

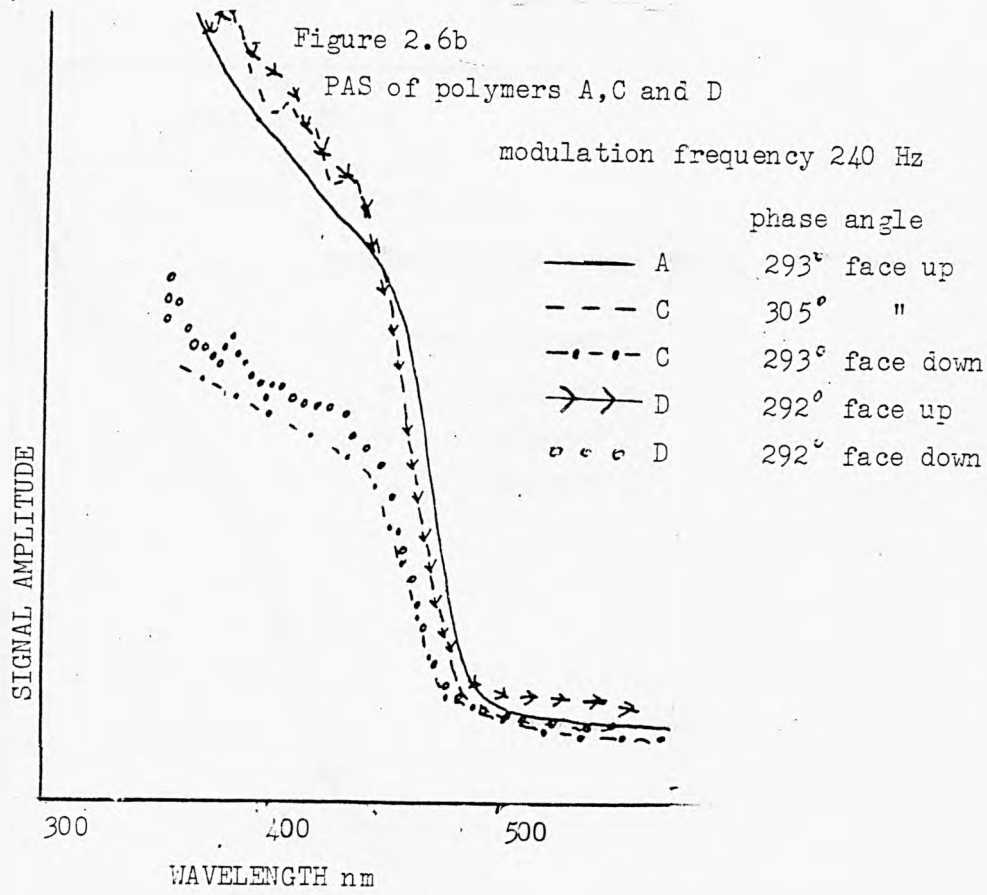

Figure 2.6c
PAS of polymers E and F

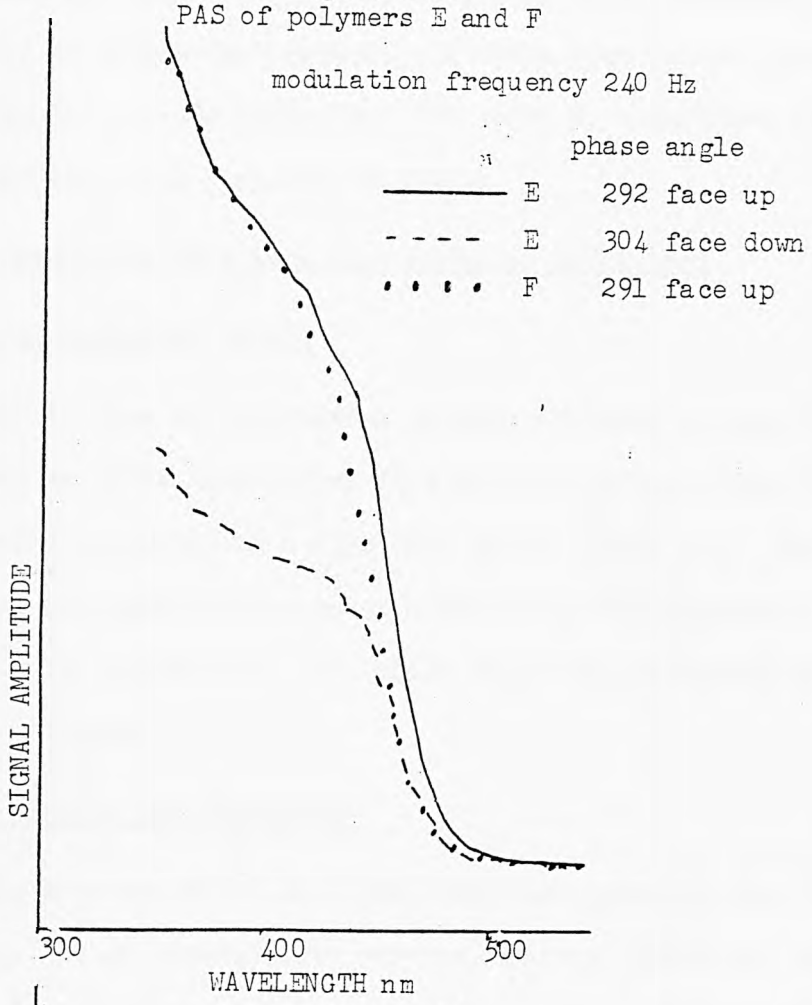

Figure 2.6d
PAS of polymers 1-4

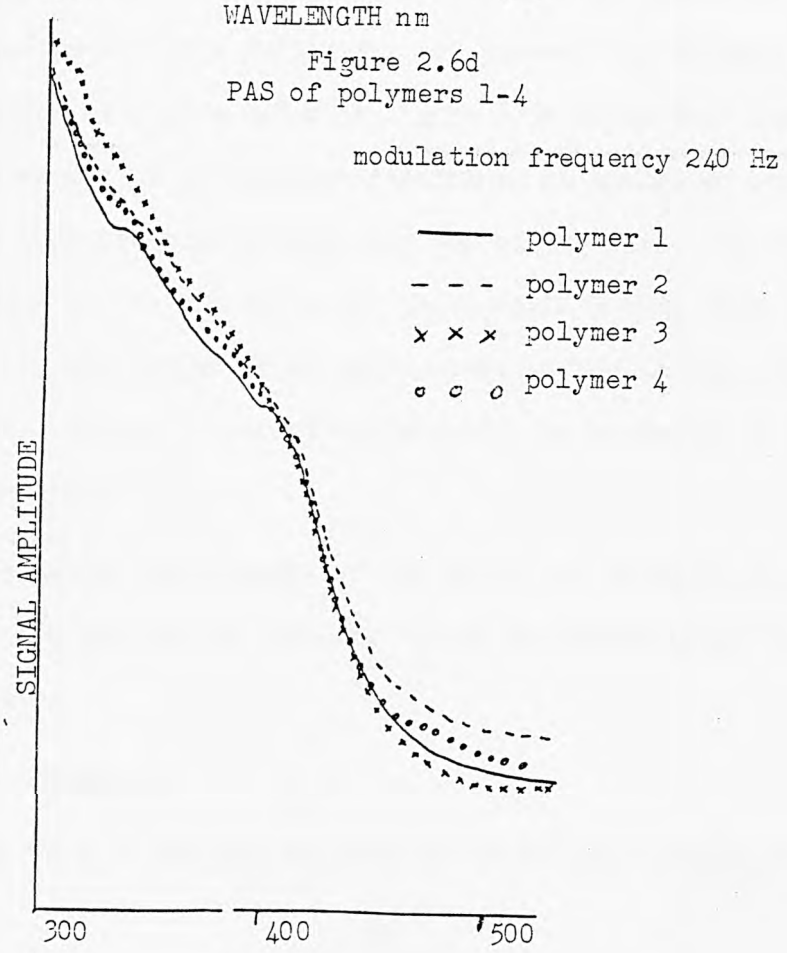

However in order to test the theory further the values of thermal conductivity and specific heat capacity need to be obtained for teflon paper by an independent method. If these gave better agreement with the experimental results above then PAS could be considered as a technique for measuring such physical constants.

2.5 Irradiation of a 10μm Film under an 1800W Lamp

2.5.1 Experimental Method

In order to show the difference between the rate of cure under a 500W lamp and an 1800W lamp a 10μm film was cast using K bar 4 as this was of comparable thickness to a film cast with a glass rod. The film was irradiated and samples were taken after 1,2,3 and 10minutes. The results are shown in figure 2.7. The phase angle was optimised to give maximum signal at 440nm.

2.5.2 Results and Discussion

There is some variation in signal magnitude possibly due to sample curling. It is obvious that cure is reaching completion after 3 minutes irradiation and will definately not proceed any further after 10 minutes. Comparison of figure 2.7 with figure 2.5a shows that there is a considerable amount of chromophore remaining, as explained previously this is due to cure occuring in only the top of the film. An interesting observation is the change in the phase angle during cure, a fact that was initially attributed to an improvement in the thermal properties of the polymer. However a second explanation is presented in the following sections (2.6, 2.7).

A quantitative measurement of the amount of chromophore remaining is impossible because the shoulder gives no identifiable feature which disappears.

2.5.3 Conclusion

The top of a 10 μm film is cured in 10 minutes irradiation23cm from an

1800W curing lamp when the temperature of the apparatus is 100°C. Whereas a similar film irradiated 8cm from a 500W lamp needs 30 minutes of irradiation before a similar degree of cure is obtained. Thus the effect of light intensity is clearly demonstrated.

Figure 2.7
10μm film of polymer A irradiated under 1800W lamp.

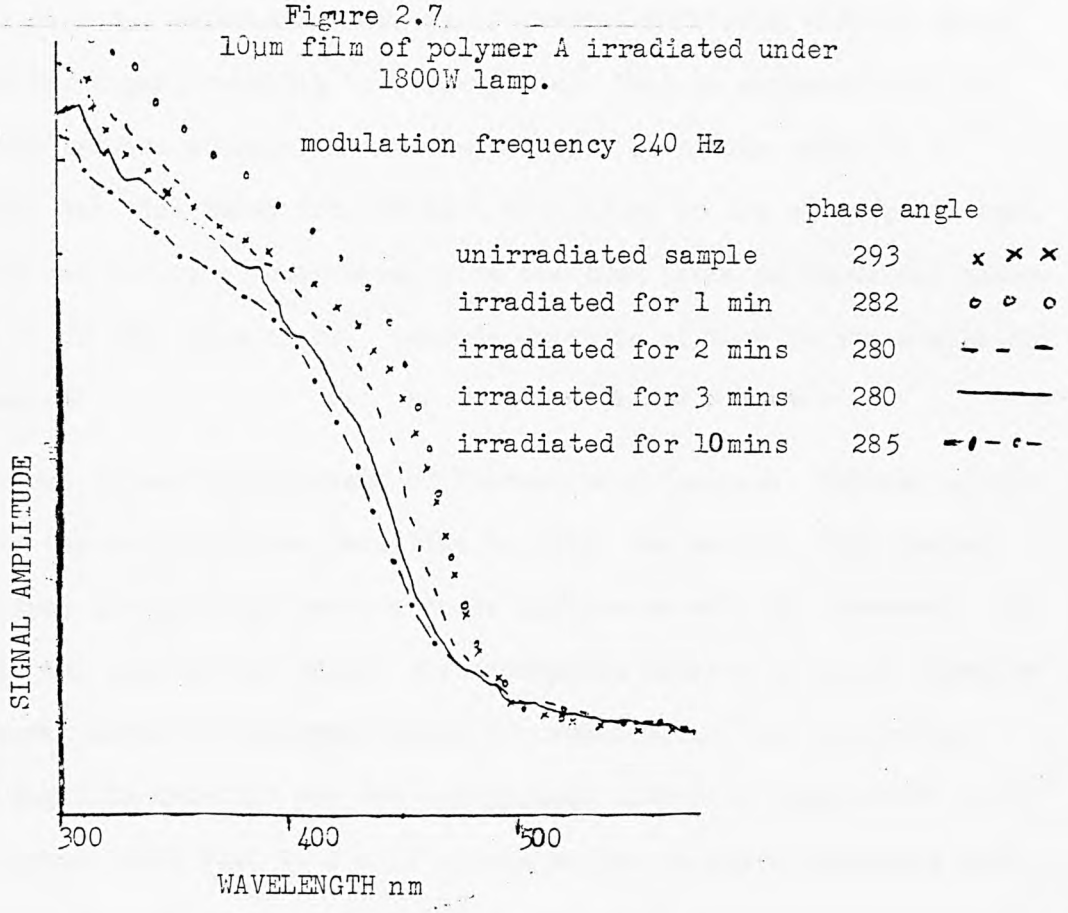

2.6.1 Depth Profiling - A Brief Introduction

Although photoacoustic saturation could not be removed it was hoped that the variation in the shape of the shoulder could be monitored at different depths.

Depth profiling is an important advantage of the photoacoustic technique and can be achieved in two ways. These are:-

i) variation of modulation frequency

ii) variation of phase angle

The first method relies upon the fact that at high modulation frequencies, the energy delivered to the sample when the light is 'on' is less than

the energy delivered at low modulation frequencies. Thus thermal waves will be more easily damped in the former case, and energy from deeper in the sample will not diffuse to the surface.

A phase angle is observed between the signal from the sample and the signal from the reference, because of thermal diffusion effects which delays the signal reaching the microphone. That is although the time interval between absorption and re-remission is of the order of 10^{-8} seconds, the time taken for the heat to diffuse to the surface, to heat the gas and set up a sound wave, plus the time taken to reach the microphone is of the order of 10^{-2} seconds which is similar to the modulation frequency.

The second method is the basis of thermal wave imaging. Thermal waves near to the top will take less time to reach the surface than thermal waves from the bulk and hence a phase difference will be observed. However in the case of the OAS400 the microphone detects a vector sumation of thermal waves of different phase and amplitude. Thus an average phase angle is detected and for homogeneous samples a phase shift to 90^{o} out of phase will lead to a null signal as the in phase component will be zero. However as Adams et al[105] demonstrated on spinach leaves, inhomogeneous samples do not produce a null response 90^{o} out of phase but actually give the spectrum of the other layer.

2.6.2 Experimental Method - Variation of Modulation Frequency

Depth profiling has been attempted using a variety of modulation frequency for a number of samples. Initially a two layer system was tried i.e. sellotape on a glossy blue substrate. The sensitivity was increased with modulation frequency and the phase angle was optimized in each case. A film of polymer A was deposited on the above sandwich using a No.2 K bar and spectra were again obtained at various modulation frequencies. Finally a very thick sample ($\simeq 35 \times 10^{-6}$m) of the same polymer was irradiated for 15 minutes under a 500W lamp. The teflon paper substrate was

removed and spectra were obtained of the irradiated face at modulation frequencies of 10 Hz and 240 Hz together with the unirradiated face.

2.6.3 Results and Discussion

The spectrum of the blue substrate on its own is shown in figure 2.8a.

The spectra of the blue substrate/sellotape sandwich with the sellotape layer uppermost (figure 2.8b), shows some interesting features. The spectrum taken at 240Hz shows a large peak around 500nm and an increase in signal amplitude after 650nm. The spectrum taken at 10Hz shows the spectrum of the blue substrate. The spectra obtained at the intermediate frequencies 40Hz and 80Hz show similarities to the spectrum taken at 240Hz, but a much flatter response is obtained. This maybe due to low sensitivity settings.

The thickness of the sellotape was measured with a micrometer and found to be 55×10^{-6}m.

Light modulated at 10Hz penetrates more than 55×10^{-6}m. However the other frequencies do not, and so depth profiling has been effected.

The spectra of polymer A on the above sandwich, taken at all five possible modulation frequencies. are shown in figure 2.9.

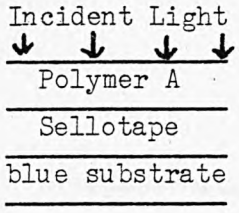

It is quite clear that both the 10Hz and 20Hz spectra have penetrated the first two layers.

Spectrum c does not increase in magnitude above 700nm and remains flat in the 500-700nm region. This indicates that a fairly large contribution to the signal is coming from the substrate. Spectrum d shows an increase above 700nm but also has a flat response between 500-700nm. This would suggest that at 80Hz a thermal diffusion depth of 60×10^{-6}m(sellotape

Figure 2.8a
PAS of shiny blue paper both in phase and 90 out of phase.

modulation frequency 240 Hz
phase angle 292

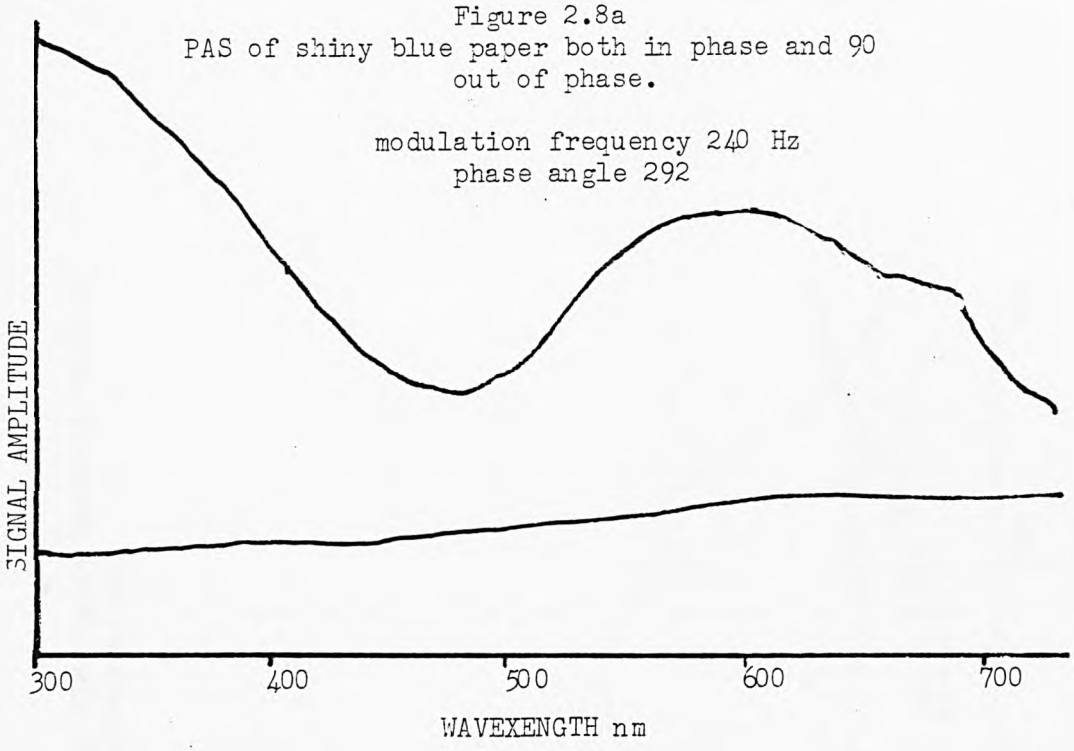

Figure 2.8b
PAS of Sellotape on blue paper at various modulation frequencies.

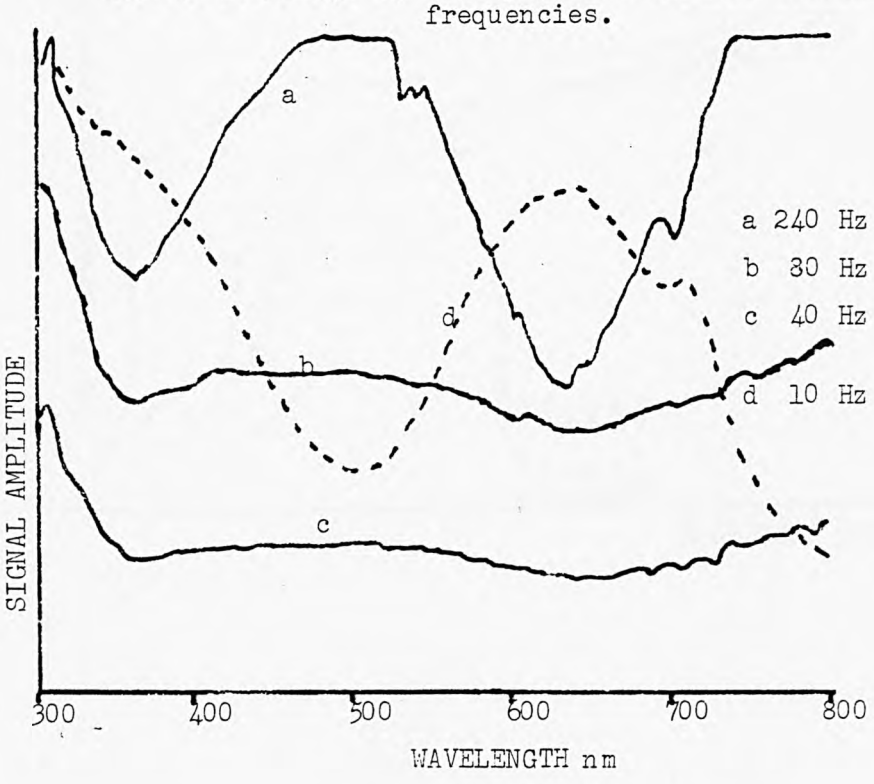

Figure 2.9
PAS of sample of polymer A/Sellotape/shiny blue paper sandwich taken at six modulation frequencies.

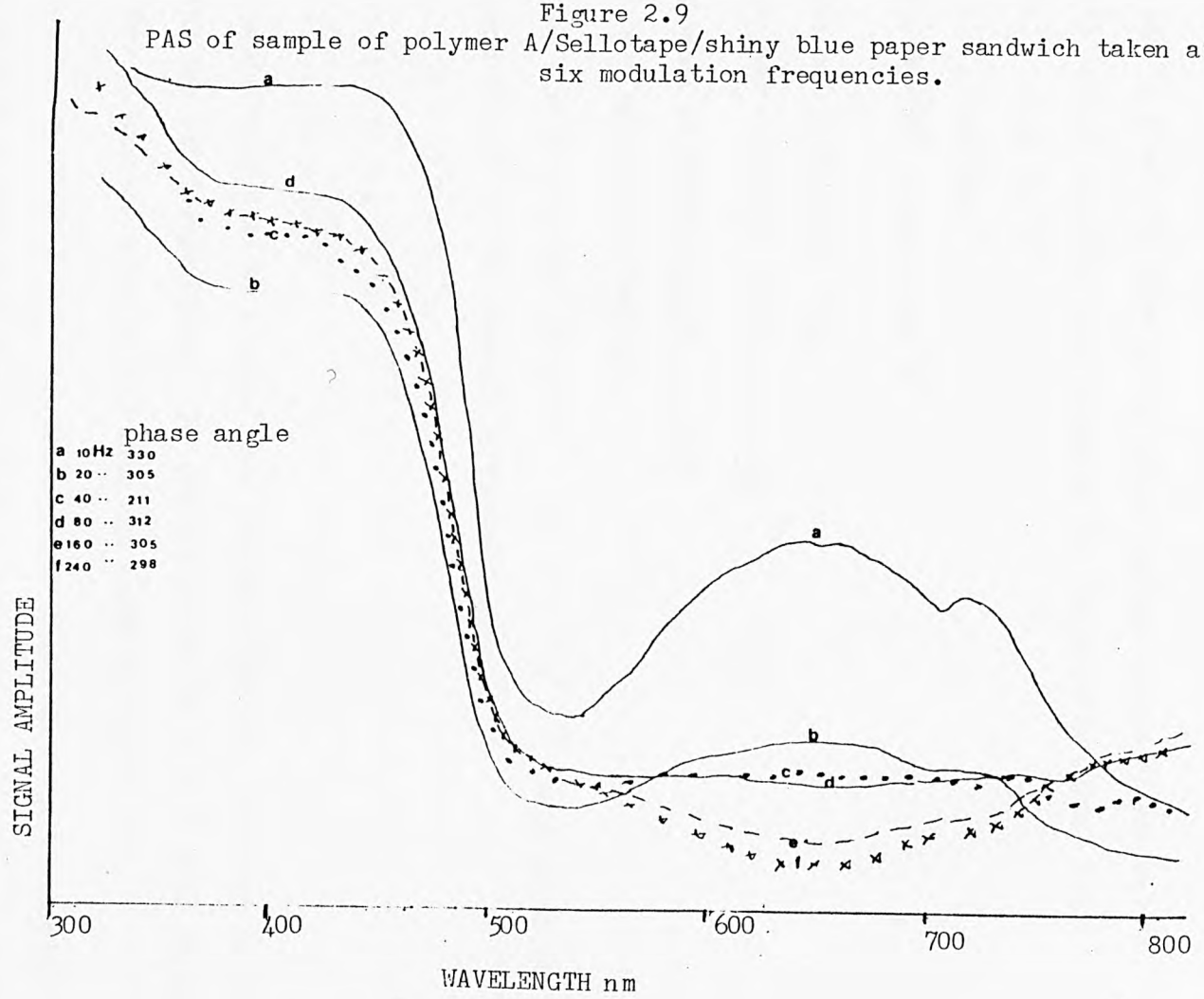

and polymer) is being attained, i.e. the sellotape/substrate boundary is being approached. The shape of spectra e and f above 650nm indicates that the sellotape is the main contributor to the signal as the polymer gives a flat response in this region. Thus all the possible modulation frequencies of the OAS 400 give a thermal diffusion depth (μ) of greater than 5×10^{-6}m for these polymers.

This can be predicted from theory using typical values of thermal (κ) density (ρ) and specific heat capacity (c) for epoxide resins i.e:-

$\kappa = 0.17 - 0.21\ Wm^{-1}K^{-1}$

$\rho = 1110 - 1400\ kgm^{-3}$

$c = 1.0\ Jg^{-1}K^{-1} = 1000\ J\ kg^{-1}K^{-1}$

α = thermal diffusivity = $\frac{\kappa}{\rho c}$

a = thermal diffusion coefficient = $\left(\frac{\omega}{2\alpha}\right)^{\frac{1}{2}}$

μ = thermal diffusion length = $\frac{1}{a} = \left(\frac{2\alpha}{\omega}\right)^{\frac{1}{2}}$

Where ω = modulation frequency.

Thus the limits of α are $1.2 \times 10^{-7} - 1.9 \times 10^{-7}\ m^2\ s^{-1}$ which gives the following values for the thermal diffusion length μ.

240Hz 31.6 - 39.7 x 10^{-6}m

80Hz 54.8 - 68.7 x 10^{-6}m

10Hz 155 - 190 x 10^{-6}m

These values were used as a basis when deciding upon the thickness of the film for the third experiment. The spectra of the 35×10^{-6}m film irradiated for 15 minutes under a 500W lamp are shown in figure 2.10.

By comparing spectrum 1 with spectrum 3 it is clear that the irradiated face has cured further than the unirradiated face. A comparison of spectra 1 and 2 shows that the 10Hz signal is emanating from this uncured layer whereas the 240Hz is more affected by the cured layer because less signal is coming from it. Thus depth profiling is clearly demonstrated in this thick sample.

Figure 2.10
PAS of 35μm film of polymer A irradiated for 15 minutes.

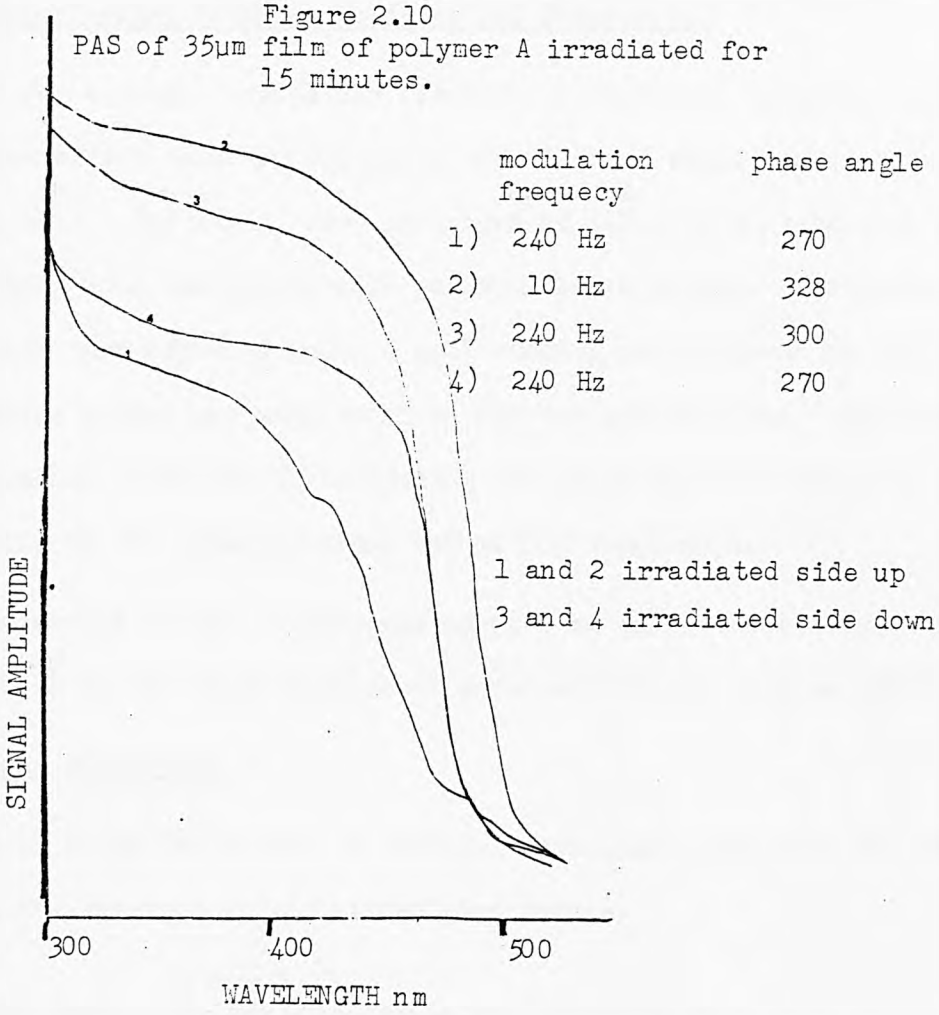

It is interesting to note that the calculated value for the thermal diffusion length (μ) at a modulation frequency of 240Hz is between $31\text{-}40 \times 10^{-6}$m for polymer A. However the spectra demonstrate an inhomogeneous sample 35×10^{-6}m thick. As a weaker signal reaches the surface from the uncured part, this strongly suggests that μ is smaller than the calculated value. Thus the thermal diffusivity (α) would be smaller which would mean that the thermal conductivity (κ) is smaller or the density (ρ) or the specific heat capacity (c) are larger.

2.6.4 Conclusion

It has been shown that depth profiling is possible using the limited modulation frequency range of the OAS 400. However only relatively thick samples can be profiled. Films of less than 10×10^{-6}m would require mod-frequencies greater than 10^{3}Hz.

2.6.5 Experimental Method - Variation of Phase Angle

Although for a single modulation frequency a variation in phase angle should not effect depth profiling an offset phase angle was used to demonstrate this. The signal were maximised at 440nm by switching to 90° out of phase with the approximate maximum sample signal. The phase control was then adjusted until a null reading was observed on the meter. The in phase signal was then regained and the spectrum run. The offset was determined by arbitarily selecting the phase angle of the 10Hz spectra and keeping it the same for other modulation frequencies.

The irradiations in the second experiment were carried out under a 500W lamp. Those in the third experiment were carried out under a 1800W lamp.

Results and Discussion

Figure 2.11 shows the effect of changing modulation frequency and phase angle on the spectrum of an unirradiated sample.

Figure 2.11
The effects of changing modulation frequency and phase angle on the PAS of polymer A.

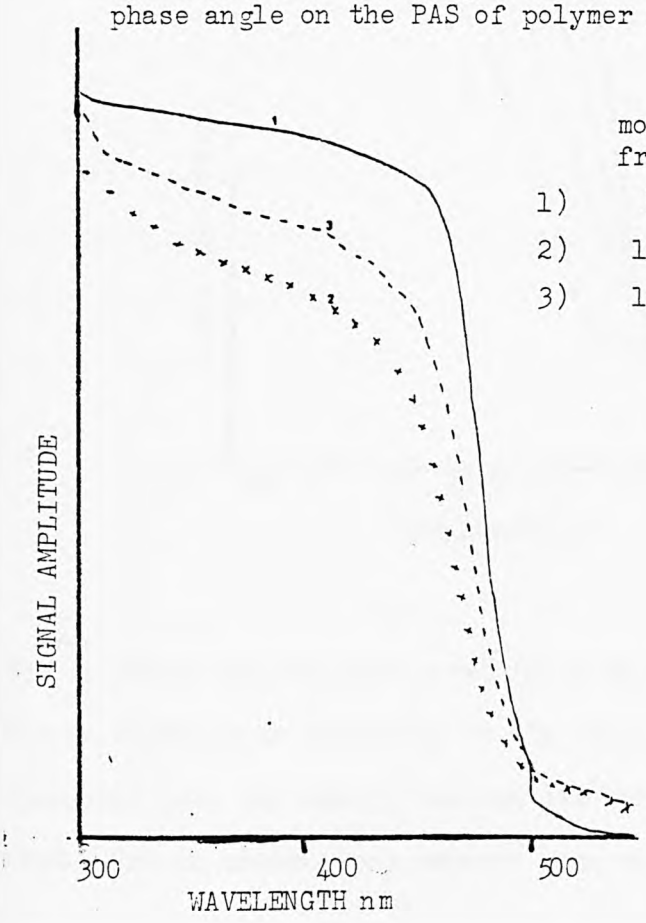

The 160Hz in phase spectrum is more rounded than the 10Hz in phase spectrum. The offset 160Hz spectrum is very similar to the in phase spectrum apart from the fact that it is smaller. The latter effect is due to a reduction in the in phase component. The former is probably due to the difference in signal intensity.

The results of irradiating a film deposited with a No.8 K Bar for 0, 20, 30 and 60 minutes are shown in figure 2.12. The spectra were taken at a modulation frequency of 240Hz. The signal was maximised at a phase angle of 293° the 30 and 60 minute spectra were also obtained with a 32° offset i.e. at 325°.

Figure 2.12
PAS of polymer A irradiated for various lengths of time and the effects of changing the phase angle.

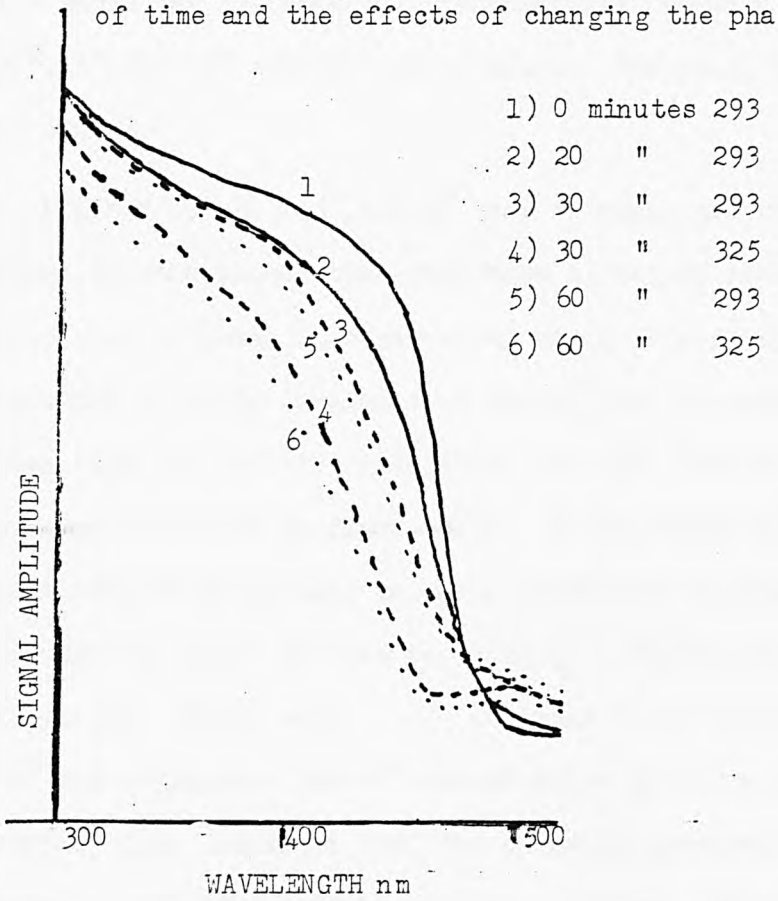

The in phase spectra show a reduction in the intensity of the shoulder and an increase in intensity at the foot. The 30 and 60 minute spectra show that cure has nearly reached its full extent after 30 minutes and that a lot of chromophore remains when cure can go no further after 60

minutes.

The out of phase spectra are similar to the in phase spectra except in the 500nm region where a small hump is resolved. This is attributed to the same chromophore that produces the increase in signal magnitude at the foot of the shoulder. The fact that this peak occurs at an offset frequency indicates that it is coming from a different depth than the main peak, which is consistent with this chromophore being initially formed at the surface.

Figure 2.13 shows spectra of an unirradiated 10 x 10^{-6}m film of polymer A on teflon paper. The modulation frequency was kept constant at 240Hz but the phase angle was systematically changed i.e. spectra were obtained at 0°,15°,30°,45°,60°,75° and 90° out of phase. The phase angle was maximised at 440nm.

The spectra obtained 15°,30°,45°,and 60° out of phase are very similar to the in phase spectra except that they have a flatter response below 450nm. The 75° out of phase spectrum shows signs of a peak appearing around 450nm which is fully developed in the 90° out of phase spectrum. A sample taken after 10 minutes irradiation was also treated in the same way. The spectra are shown in figure 2.14. As in figure 2.13 a decrease in signal amplitude with increase in phase difference is observed,and a peak appears when the phase difference is large. There are however 2 notable differences. These are:- i) The peak is no longer 90° out of phase but 75° out of phase. The 90° out of phase spectrum shows an inverted spectrum. This indicates that the in phase spectrum was not truely in phase. ii) The peak is shifted to 420nm. This second observation explains the change in phase angle on irradiation observed in section 2.5, because in the unirradiated sample the peak is at 440nm. Thus to obtain a null signal a smaller amount of phase difference will be required in the irradiated case than in the unirradiated case.

Figure 2.13
The effect of varying the phase angle on the PAS of an unirradiated sample of polymer A.

modulation frequency 240 Hz

1) in phase (290°)
2) 15° out of phase
3) 30° " "
4) 45° " "
5) 60° " "
6) 75° " "
7) 90° " "

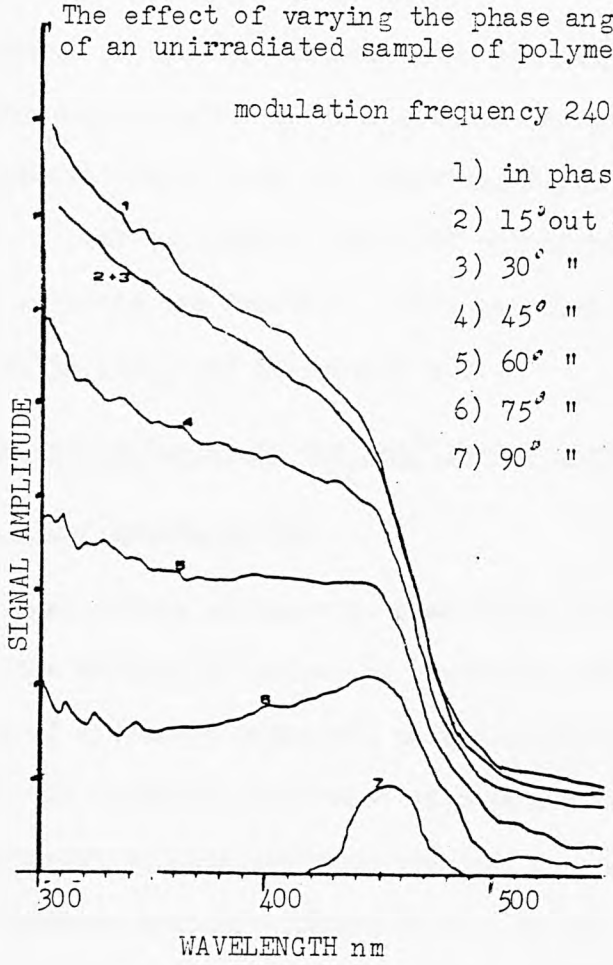

Figure 2.14
PAS of polymer A, irradiated for 10 minutes.
N.B. the base line in spectrum 7 has been raised.

modulation frequency 240 Hz

1) in phase (286°)
2) 15° out of phase
3) 30° " "
4) 45° " "
5) 60° " "
6) 75° " "
7) 90° " "

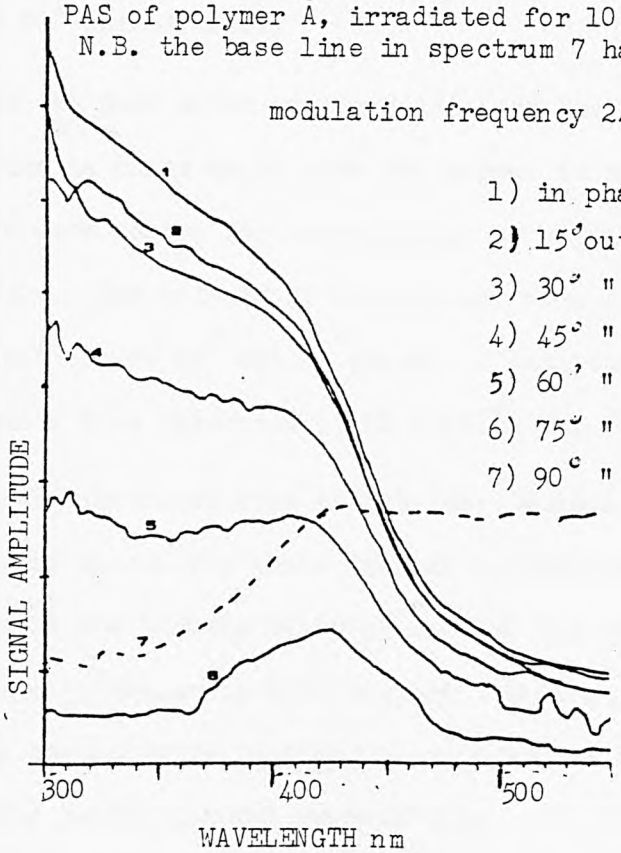

2.6.6 Conclusion

As expected it has been demonstrated that off setting the phase angle does not depth profile in this system. However as demonstrated in 2.4 a transparent layer over the absorbing layer does alter the phase angle. A peak in spectra taken 90° out of phase has been observed when a flat response was expected. This has been investigated further and the results presented in section 2.7.

2.7 Investigation in to the Peak that Occurs 90° Out of Phase

2.7.1 Experimental Method

So as to elucidate whether the peak which occurs 90° out of phase was due to the machine or caused by a genuine artefact of the polymer film, samples of different compounds that possessed a similar chromophore were tried. The compounds used were dibenzalacetone, 4,4-diglycidyl ether of 4,4-dihydroxy dibenzalacetone (compound S) and 4,4'-diglycidyl ether of 4,4'-dihydroxy chalcone (compound T). By way of a complete contrast a spectrum of the glossy blue substrate mentioned in 2.6.2 was also obtained 90° out of phase.

Because the peak moves on irradiation of the polymer films causing a variation in phase angle when the signal is maximised, different wavelengths were chosen for maximization of signal. These were 465nm, 420nm and 350nm. The effects of irradiation were studied in relation to the peak that occurs 90° out of phase. A modulation frequency of 240Hz was used and a film thickness of 10×10^{-6}m was obtained with a No.4 K Bar.

Two other substrates were also tried:- sodium chloride disc and tinfoil. These were chosen for their thermal conductivity properties as the properties of the backing material control the signal magnitude for optically transparent, thermally thin samples. Sodium chloride was chosen as its thermal conductivity is only a little better than teflon whereas tinfoil has a far better thermal conductivity.

Figure 2.15a
PAS of various compounds containing a similar chromophore to, that found in polymer A

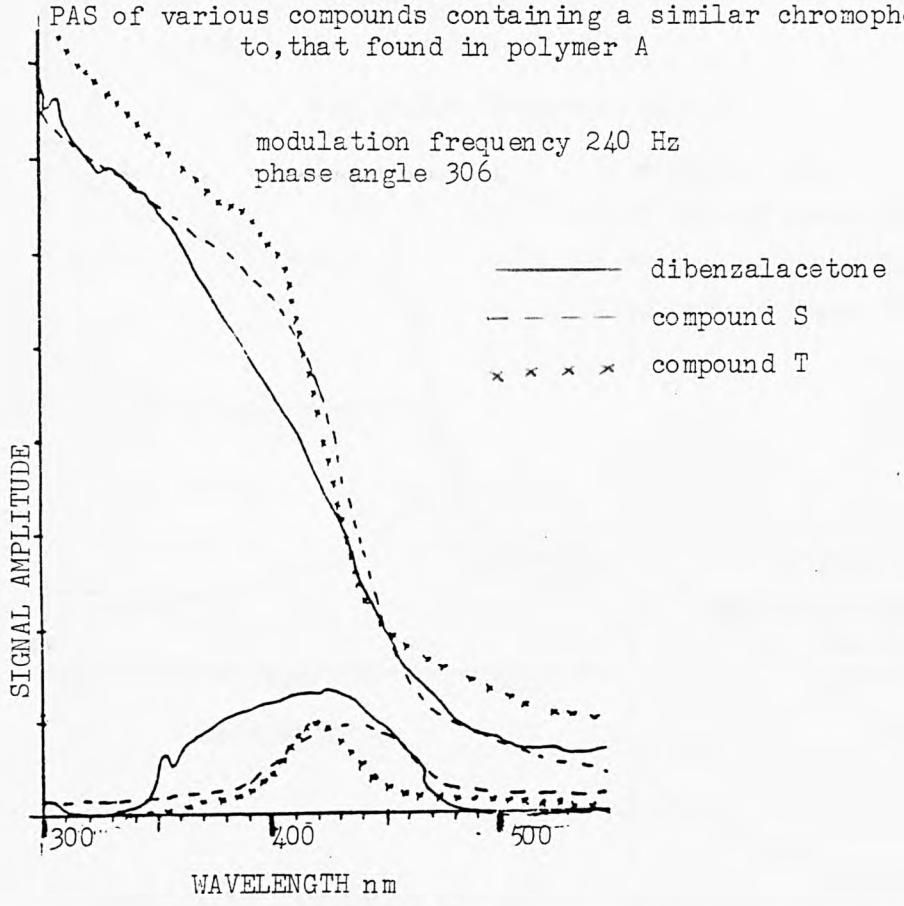

Figure 2.15b
PAS of shiny blue paper both in phase and 90 out of phase.

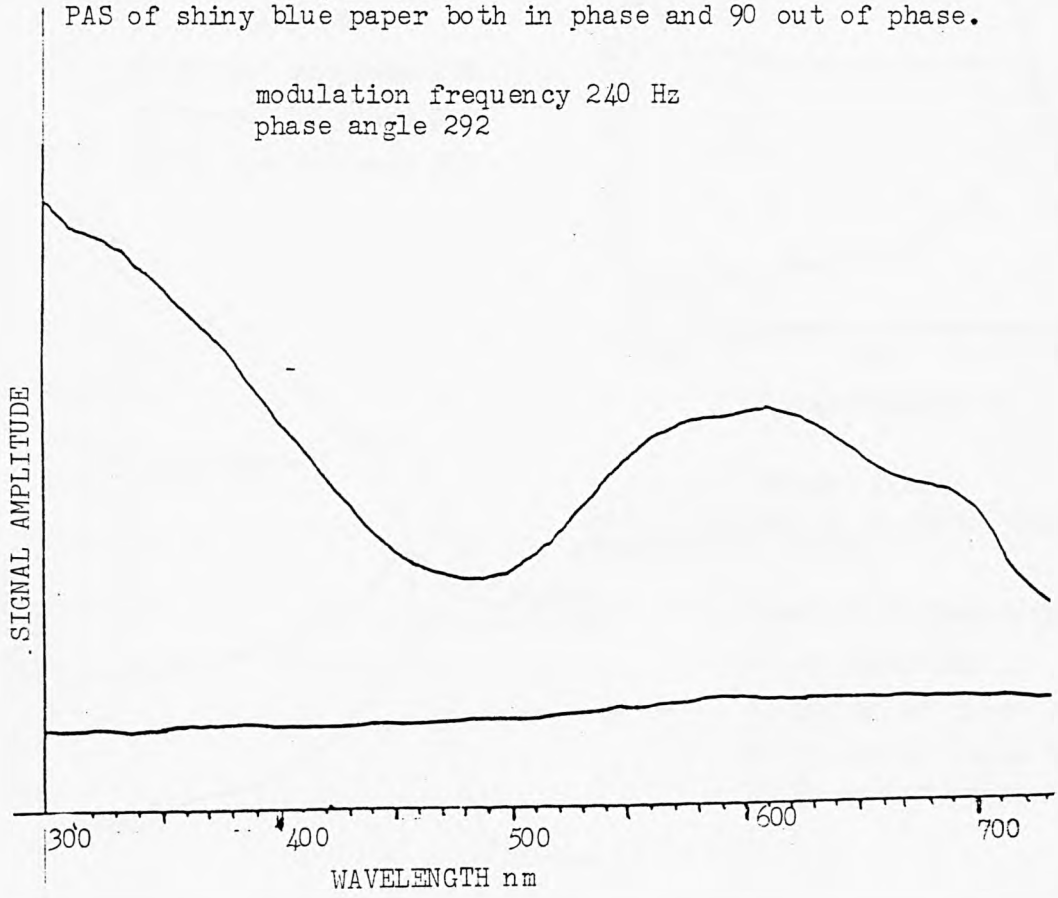

Figure 2.16a
PAS of polymer A in which the signal was optimised at 350nm

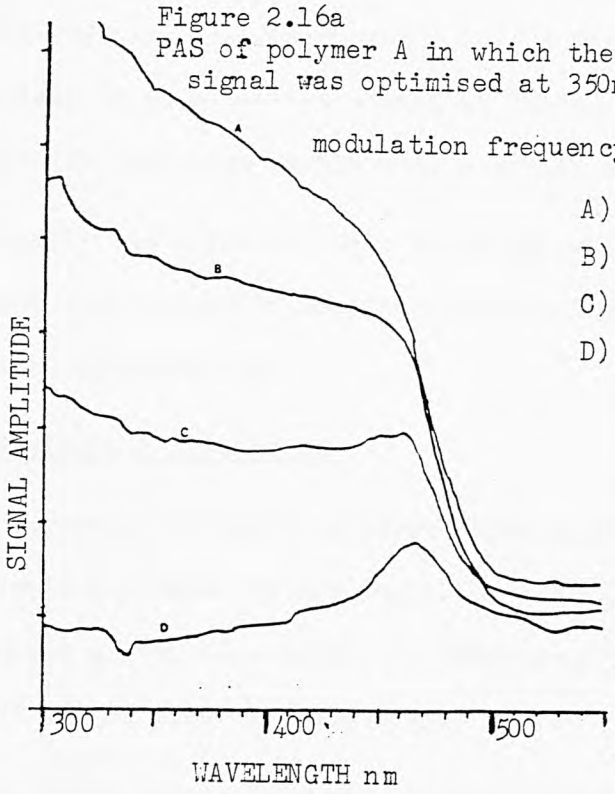

modulation frequency 240 Hz

A) in phase 299
B) 60 out of phase 239
C) 75 out of phase 224
D) 90 out of phase 209

Figure 2.16b
PAS of polymer A in which the signal was optimised at 440nm.

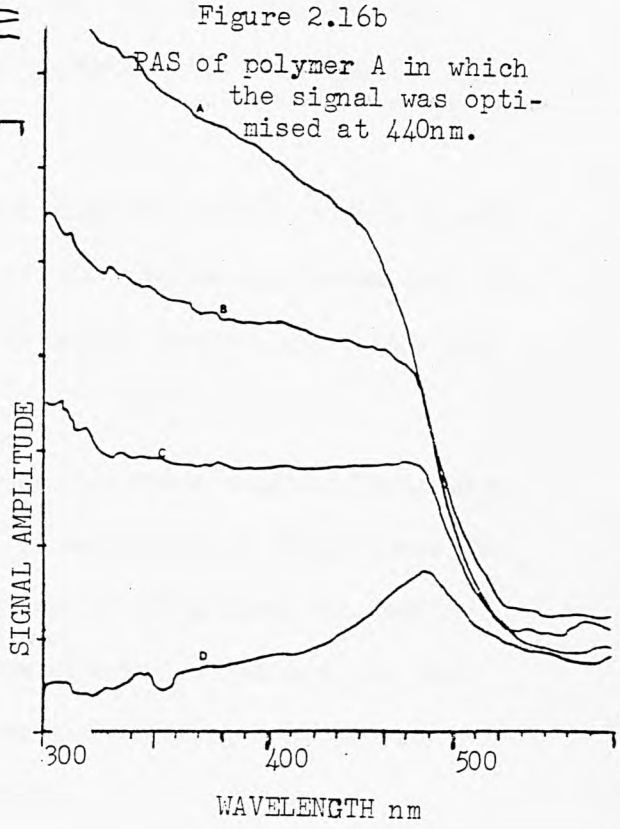

modulation frequency 240 Hz

A) in phase 298
B) 60 out of phase 238
C) 75 out of phase 223
D) 90 out of phase 208

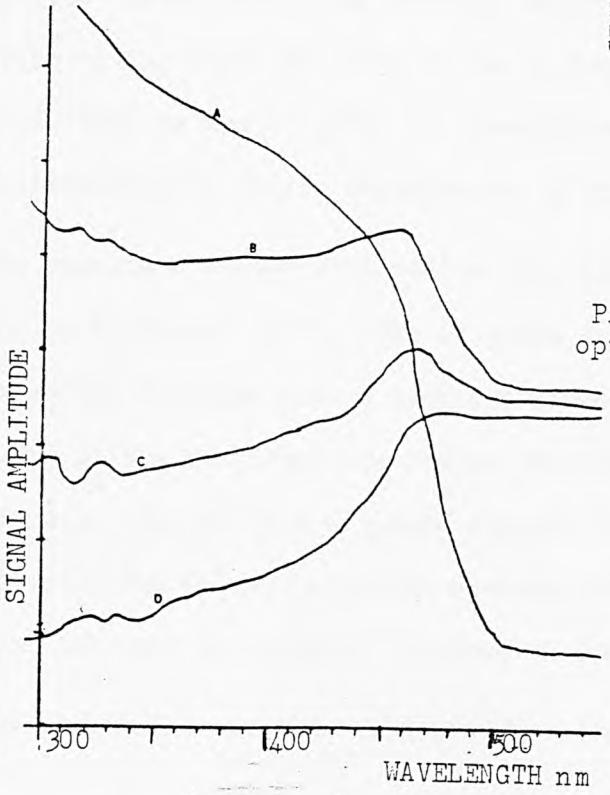

Figure 2.16c
PAS of polymer A in which signal was optimised at 465nm.

modulation frequency 240 Hz

A) in phase 281
B) 60 out of phase 221
C) 75 out of phase 206
D) 90 out of phase 191

The film was deposited with a No.4 K Bar and the phase angle was optimized to give maximum signal at 350nm. The effects of irradiation were studied using the sample with a sodium chloride substrate.

Finally the effect of film thickness was investigated. The thin films were produced as in section 2.4.1 i.e. dilution of the polymer solution with cyclohexanone.

Results and Discussion

The results of using different compounds including the glossy blue substrate are shown in figures 2.15a and 2.15b. It is clear that the opaque glossy blue substrate behaves as expected. i.e. the spectra taken 90° out of phase is essentially flat.

The three compounds with a similar chromophore to polymer A show a peak 90° out of phase. Careful examination of the spectra indicates that the peak starts around the point where the in phase spectra starts to come out of saturation.

The results of using different wavelengths for phase angle optimization are shown in figures 16a-16c. The spectra maximised at 350nm gives the flattest base line. The spectrum maximised at 465nm shows how maximising on the peak can distort the spectra obtained. Because the peak moves back to around 420nm on irradiation the wavelength chosen for optimization in future experiments is 350nm.

The results obtained with sodium chloride and tinfoil are shown in figure 2.17a and 2.17b. The in phase spectra of the irradiated sample on sodium chloride show a good consistency below 350nm. This is attributed to the fact that the sodium chloride prevents the polymer from curling. The 90° out of phase spectra show a very much diminished effect. The 90° out of phase spectrum obtained from the film on tinfoil does not show the effect. Instead it demonstrates an inverted signal.

The spectra of the thin film are shown in figure 2.17d. It is clear

Figure 2.17a
PAS of a film of polymer A on a sodium chloride substrate.

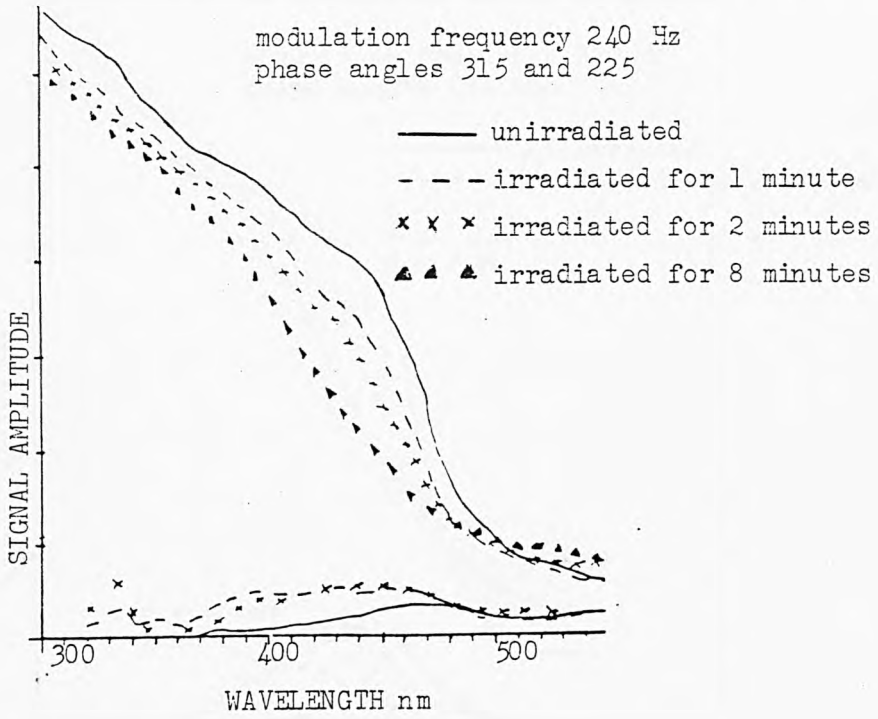

Figure 2.17b
PAS of a film of polymer A on a tin foil substrate.

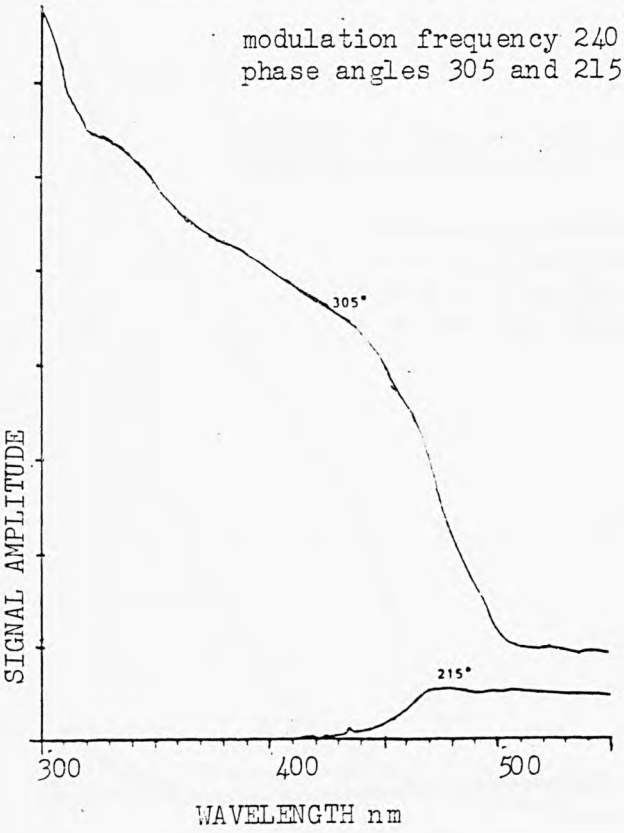

Figure 2.17c
Comparison of the in phase and the 90 out of phase spectra of an irradiated sample of polymer A.

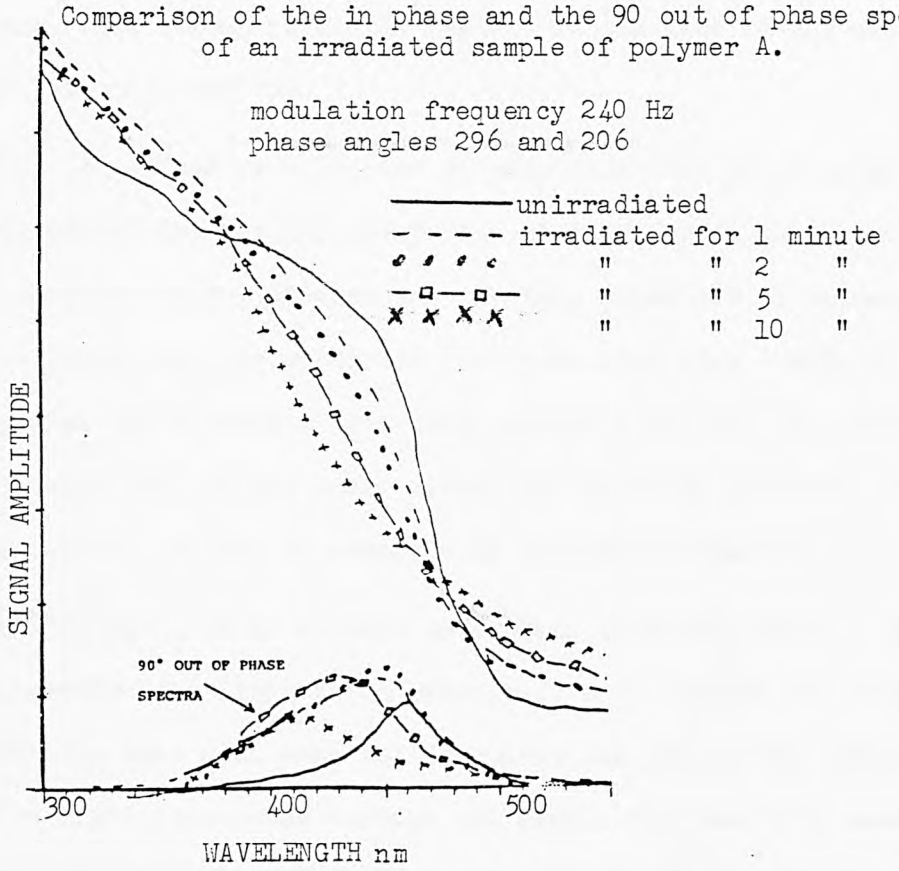

Figure 2.17d
PAS of a very thin film of polymer A

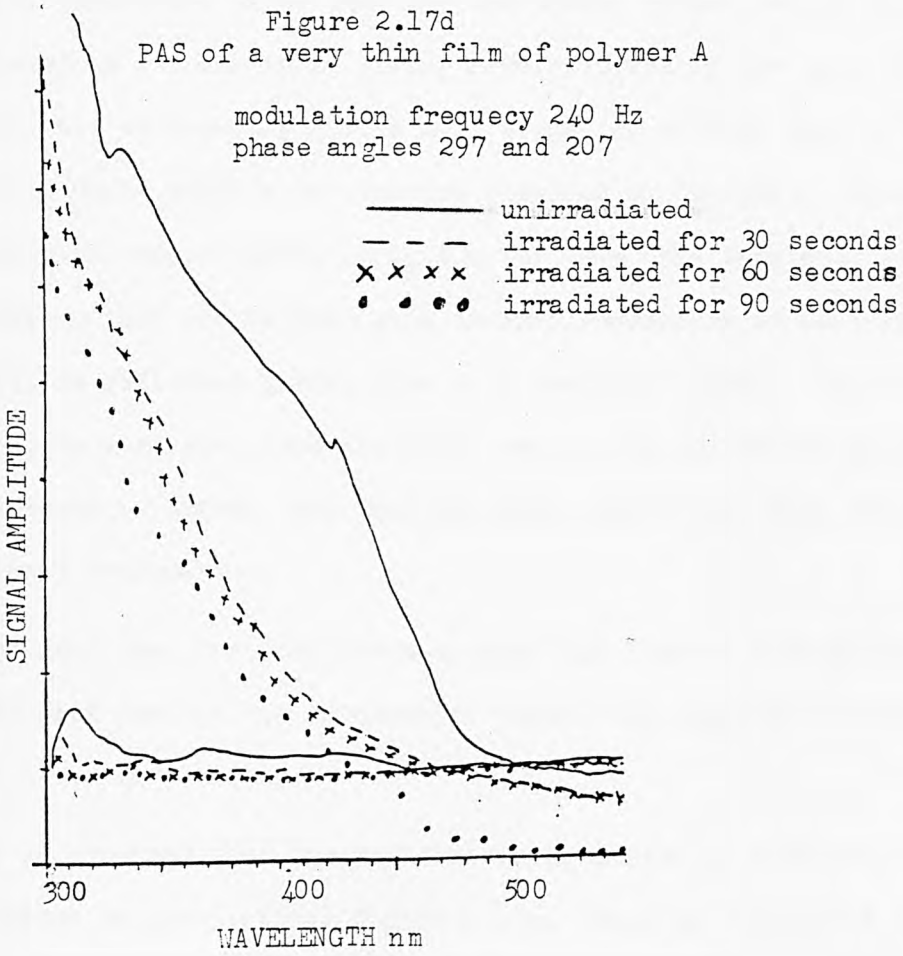

that cure is complete after only 30 seconds irradiation under the 1800W lamp. The second noticable feature is the lack of any peak in the 90° out of phase spectra.

Thus the effect is only seen in compounds that are transparent to some regions of the visible spectrum. It only occurs on the edge of the absorption band just when the spectrum comes out of saturation. It does not occur when the substrate is a good heat sink (chunk of sodium chloride) or when the substrate is a good conductor or when the film is very thin. The blue side of the peaks mirror the in phase spectrum. Another important point is that it occurs with homogenous samples.

The following is an attempt to explain this phenomenon. In the region of saturation the light is absorbed before it reaches the bottom of the sample. Thus the heat will come out from near the top of the sample. However, once light penetrates through the sample the heat will come from deeper down and takes longer to come out. The maximum amplitude of the heatwave will thus occur later than for the sample in saturation (c.f section 2.4). Therefore a phase angle giving a null signal in one part of the spectrum will not necessarily give a null signal on another part of the spectrum (this would explain the spectra obtained on tinfoil). This would not apply to samples where $\ell < \ell_\beta$ i.e.the very thin samples. However on substrates that are neither good thermal conductors or heat sinks, heat will be reflected giving rise to a positive signal. Thus reflected heat will be strongest from the lower regions of the sample as it has least distance to travel, and thus the peak occurs only when the sample becomes almost transparent.

The fact that the peak moves towards the blue on irradiation is due to the fact that as the chromophore reacts the compound becomes transparent at lower wavelengths.

It is observed that the peak intensity initially increases and then decreases on irradiation, figure 2.17c. This is attributed to the improve-

ment of the thermal properties on curing, which would increase signal magnitude and thus the inverted signal would increase and hence the increase in peak size. Reduction of the peak size on further cure ties up with a loss of chromophore nearer to the bottom of the sample.

2.8 A Study of the Amount of Cure Required to Effect Solvent Resistance

2.8.1 Experimental Method

It has been shown how UV/Visible PAS can be used to follow the photo-crosslinking of polymer A, in a qualitative fashion. This experiment was designed to find a correlation between time of irradiation, amount of cure and solvent resistance.

A film of polymer A was deposited on a Teflon paper substrate using K Bar No 4. The film was irradiated for 10 minutes under an 1800W lamp and samples were taken at 0,1,2,5 and 10 minutes. The spectra and instrumental conditions are shown in figure 2.17. From these films 6.45cm^2 samples were cut out and weighed at the same time as the 0,1,2 and 5 minute samples. These were stirred in a beaker with 25ml of cyclohexanone for 10 minutes at a constant stirring rate. They were then dried and reweighed.

Results and Discussion

wgt of 6.45cm^2 of Teflon paper =	0.0236g
" " " " " " + polymer A =	0.0317g
" " " " polymer A =	0.0081g
wgt of 0 min sample =	0.0317g
" " " " " after immersion =	0.0235g
wgt of 1 min sample =	0.0317g
" " " " " after immersion =	0.0319g
wgt of 1 min sample with substrate removed =	0.0080g
" " " " " " " " after immersion =	0.0069g

wgt. of 2 min. sample = 0.0315g

" " " " " after immersion = 0.0315g

wgt. of 2 min. sample with substrate removed = 0.0079g

" " " " " " " " after immersion = 0.0079g

wgt. of 5 min. sample = 0.0309g

" " " " " after immersion = 0.0309g

It has been shown previously that cure is 'complete' for a 10×10^{-6}m film of polymer A after 10 minutes under an 1800W lamp. The spectra show how little cure has been obtained after 1 minute irradiation and yet how close to complete cure the 5 minute sample is.

Comparison with the results for solvent resistance indicates that very little cure is required to establish a solvent resistant film but cure has only reached a little way into the sample. 'Complete' cure is not achieved until after 10 minutes irradiation. However it is not necessary to remove all the chromophores in reactive sites to achieve a crosslinked material. A quantitative assessment of how many chromophores have been removed is impossible as the spectra demonstrate only a shoulder and not a true peak.

Conclusion

On irradiation, a film of polymer A forms a crosslinked layer on the surface which effects solvent resistance. Full cure of thick samples does not occur until much later and it is not required. Thus if thin films are also etchant resistant, this would save on costs.

2.9 Effect of Interposing Different Filter Solutions Between The Lamp and The Sample.

2.9.1 Experimental Method

In order to get some idea of the wavelength sensitivity of polymer A two filter solutions were selected:-

i) a saturated solution of sodium nitrate

ii) a solution containing 0.27g/litre of potassium dichromate and 1g/litre of sodium carbonate.

The apparatus is as shown below:-

Figure 2.18

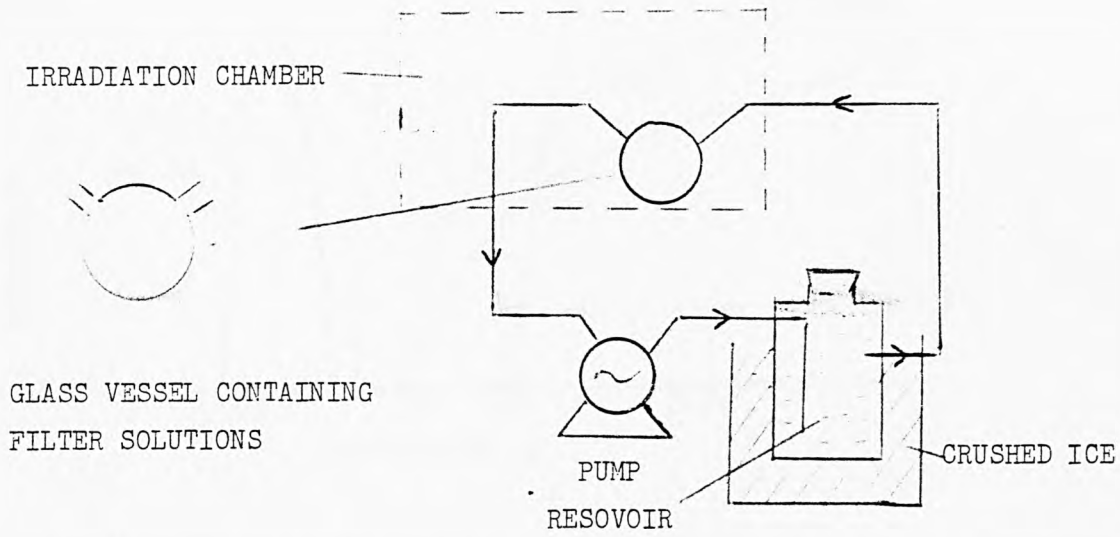

The UV absorption spectra are shown in figure 2.19, together with the spectrum of the glass container. It can be seen that any effect that the sodium nitrate solution may have will be masked by the glass container, except for a temperature effect.

In order to ascertain no light penetrated the K_2CrO_4/Na_2CO_3 solution, a recently prepared solution of anthracene was irradiated through this filter solution as this has no absorption above 380nm.

Spectra of polymer A were taken both in phase and 90° out of phase after 0, 1, 3 and 5 minutes of irradiation under the two filter solutions and also without any filter.

2.9.2 Results and Discussion

The lack of any apparent change in the anthracene spectrum (figure 2.20) even after 40 minutes irradiation through the potassium dichromate/ sodium carbonate solution demonstrates that the light below 410nm emitted from the 1800W UV source is completely absorbed by the solution.

Figure 2.19
UV absorbance spectra of filter solutions $K_2Cr_2O_4/Na_2CO_3$, $NaNO_3$ and water.

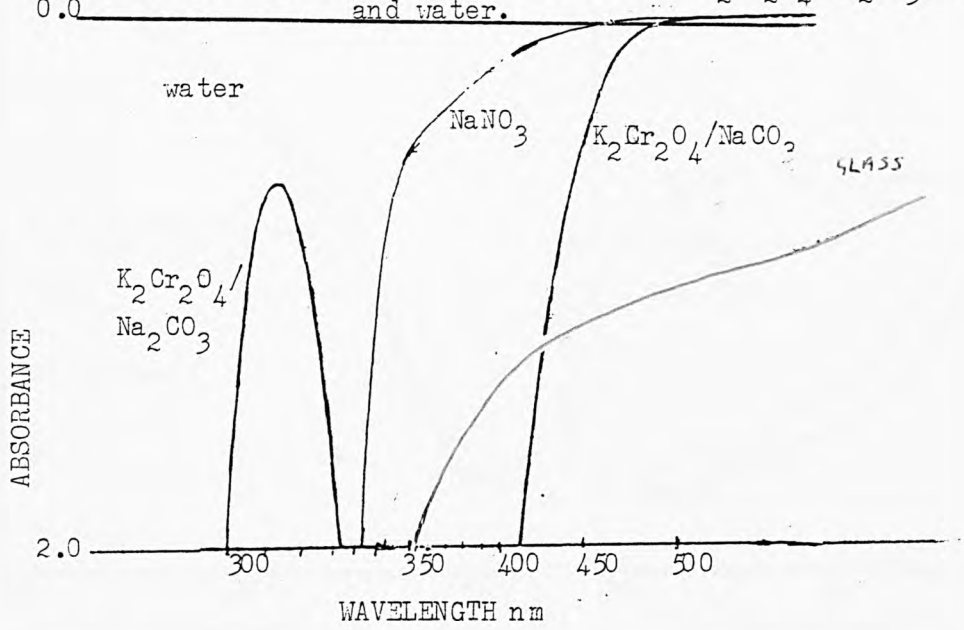

Figure 2.20
UV absorbance spectra of anthracene in acetonitrile before and after irradiation through the $K_2Cr_2O_4/Na_2CO_3$ solution.

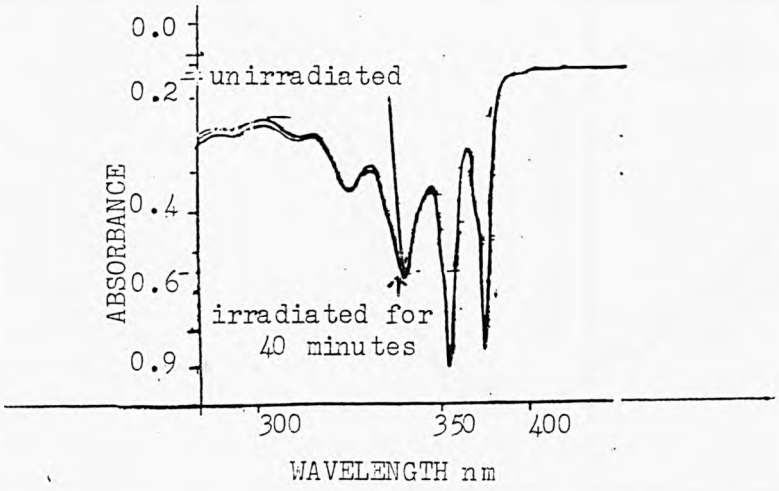

Figure 2.21a
PAS of samples irradiated for 1 minute through filter solutions.

modulation frequency 240 Hz
phase angle 296

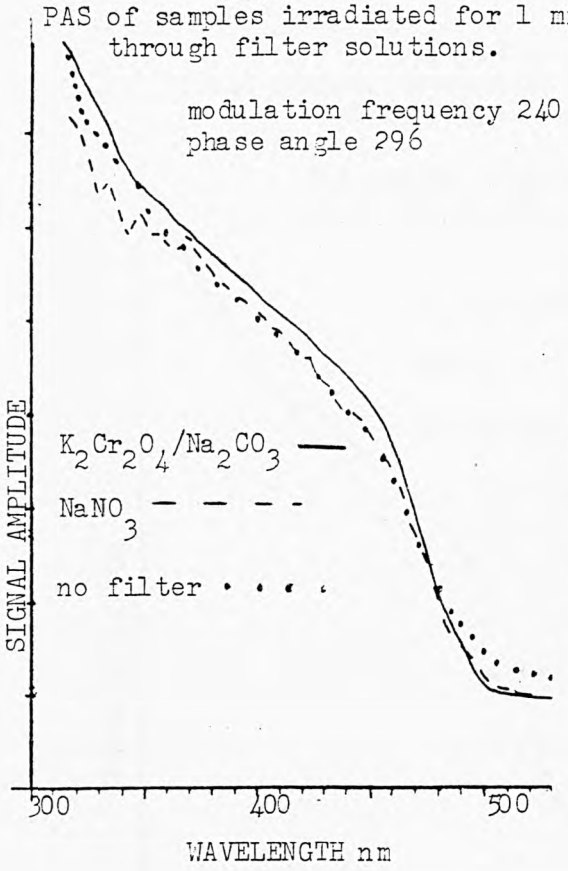

Figure 2.21b
PAS of samples irradiated for 1 minute through filter solutions.

modulation frequency 240 Hz
phase angle 206

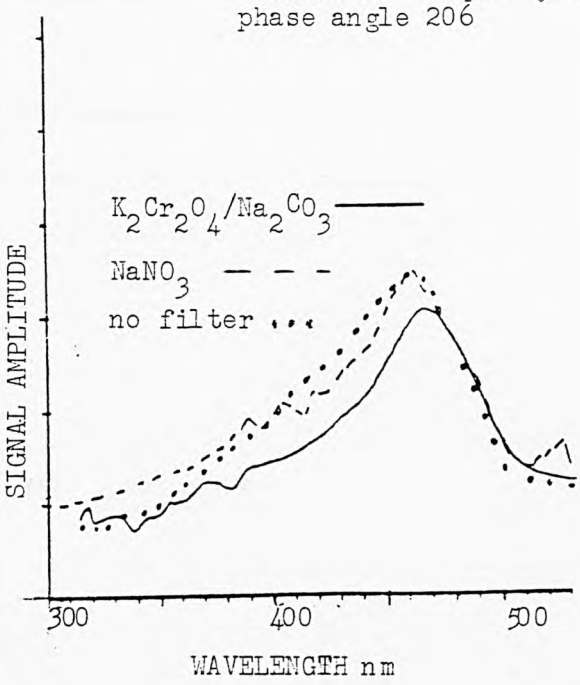

Figure 2.21c
PAS of samples irradiated for 3 minutes through filter solutions.

modulation frequency 240 Hz
phase angle 297

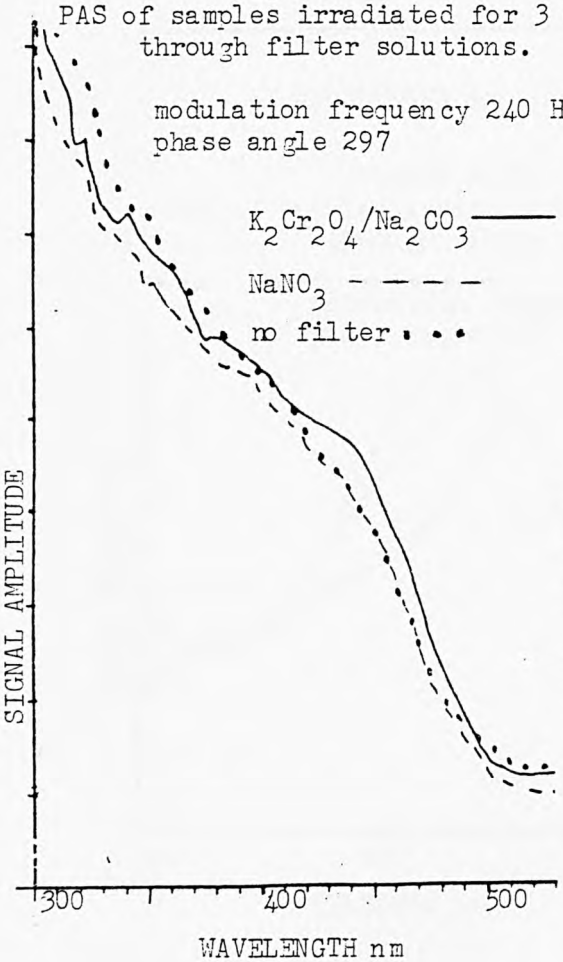

Figure 2.21d
PAS of samples irradiated for 2 minutes through filter solutions.

modulation frequency 240 Hz
phase angle 207

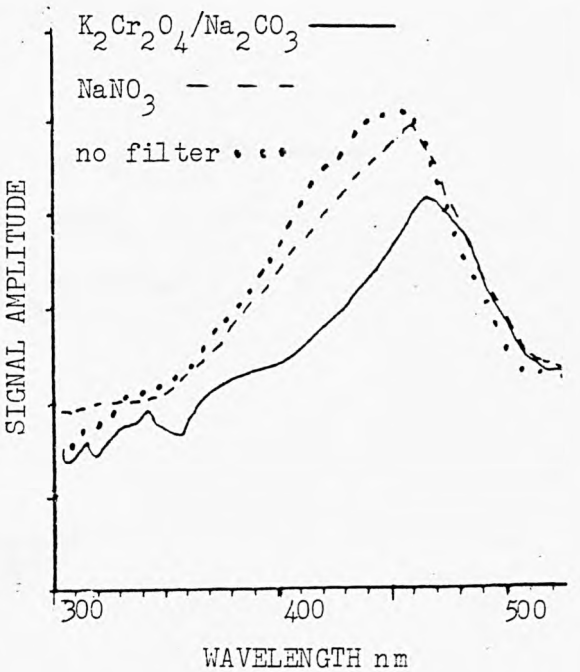

Figure 2.21e
PAS of samples irradiated for 5 minutes
through filter solutions.

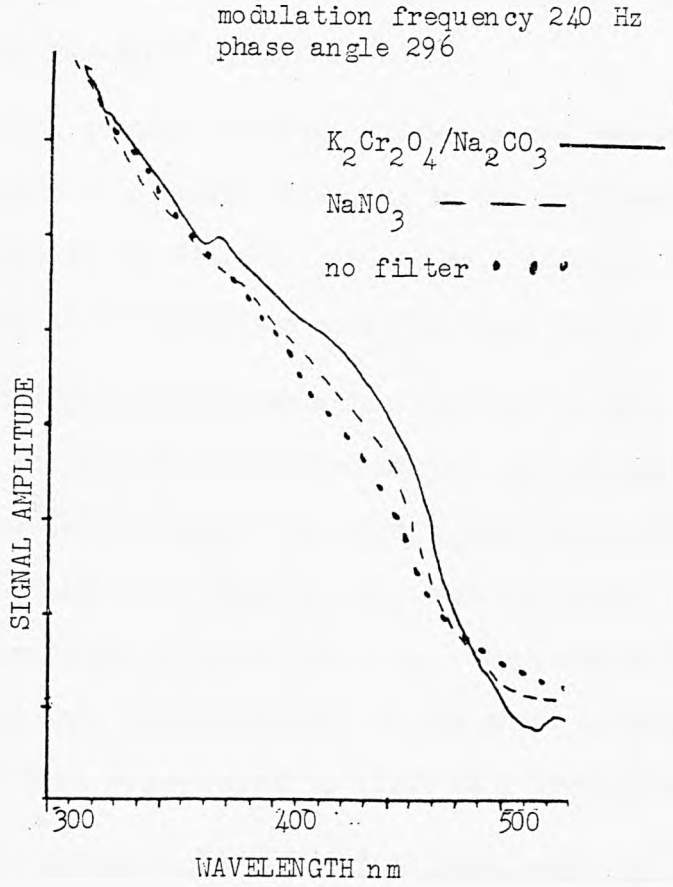

Figure 2.21f
PAS of samples irradiated for 5 minutes
through filter solutions.

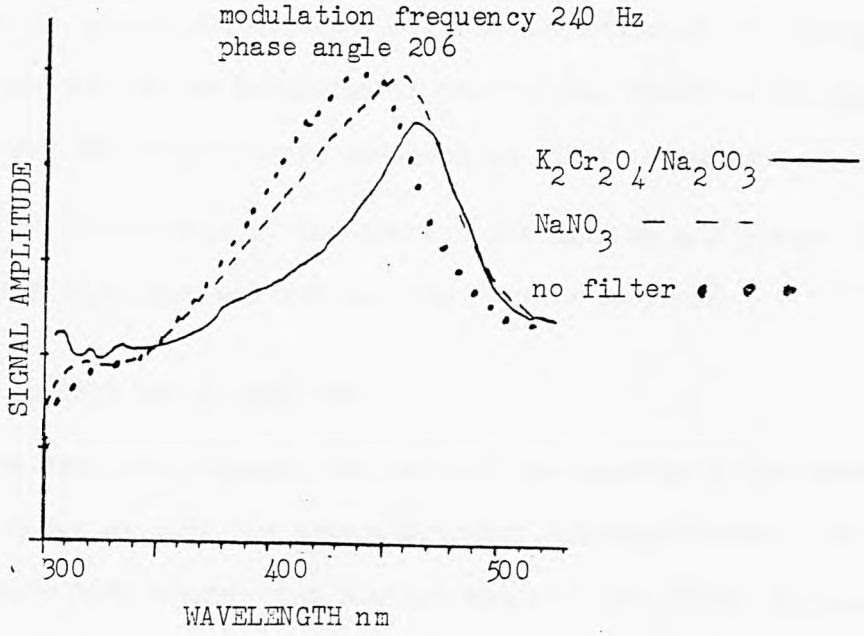

The photoacoustic spectra show that there is a distinct lack of reaction in polymer A when irradiated through the $K_2Cr_2O_4/Na_2CO_3$ solution. This is most apparent in the 90° out of phase spectra. Thus cure is effected by light of wavelength lower than 410nm.

Irradiation through the $NaNO_3$ filter causes reaction to occur however it takes place at a slower rate than in the unfiltered case. This has been attributed to the 30-45°C temperature difference that occurs because of introduction of the filter solution which also acts as a heat sink.

The most significant observation that can be made from the in phase spectra is that the samples irradiated without any filter solution have the typical increases in signal amplitude above 500nm which has been attributed to photo-oxidation. However this does not occur in samples that have been irradiated under a filter solution. The glass cuts out any light below 345nm and thus photo-oxidation or the photo induced cyclo-butane ring cleavage must be activated by light of a lower wavelength.

2.10 Estimation of the Extinction Coefficient of the 4,4'-Diglycidyl Ether of 4,4'-Dihydroxy Dibenzalacetone

2.10.1 Experimental Method

In order to ensure the absorption characteristics of the chromophore remain constant after inclusion in the polymer backbone UV spectra of the monomer and the polymer were obtained as dilute solutions in acetonitrite. A 2.5×10^{-5}m solution of the monomer was made up and placed in a 1cm cell. A UV spectrum was run and the results recorded.

2.10.2 Results and Discussion

As can be seen from figures 22a and 22b the spectra of the monomer and the polymer shows exactly the same absorption characteristics. On irradiation in solution both behave in a similar manner. The large increase in absorption after 320 minutes of irradiation together with the tail stretching

Figure 2.22a
UV spectra of monomer used in polymers A-F in acetonitrile.

a) unirradiated
b) irradiated for 10 minutes
c) " " 20 "
d) irradiated for 30 mins
e) " " 40 "

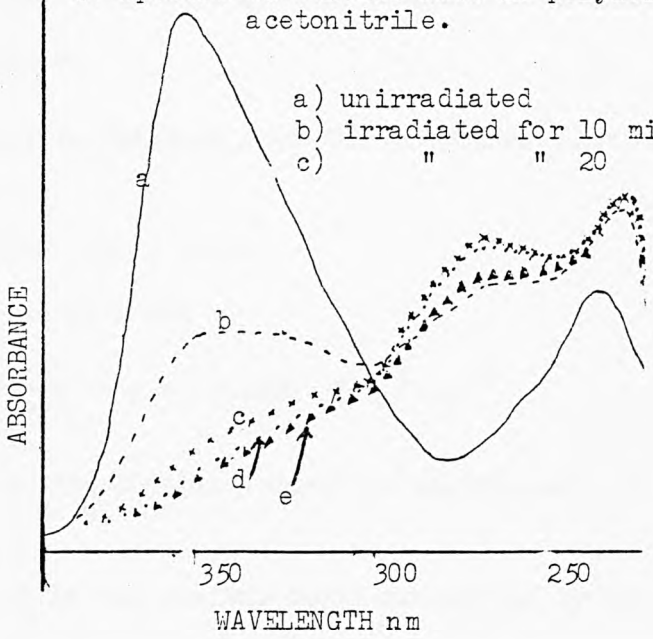

Figure 2.22b
UV spectra of polymer A in acetonitrile.

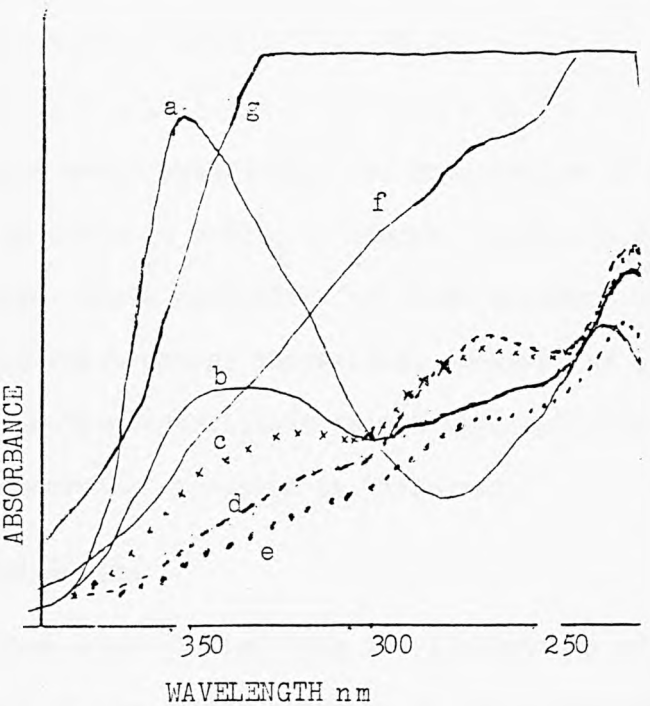

a) unirradiated
b) irradiated for 5 minutes
c) " " 10 "
d) " " 20 "
e) " " 40 "
f) " " 160 "
g) " " 320 "

into the visible region is consistent with an intense brown colour being produced after this length of time. Thus the chromophore produced by photo-oxidation has a greater extinction coefficient than the original chromophore.

The spectrum obtained from the 0.000025m solution is shown in figure 2.23.

The OD = 0.88

$\therefore$ as $OD = \varepsilon C \ell$

$$\frac{0.88}{2.5 \times 10^{-5} \times \ell} = \varepsilon = 35{,}200 \ \ell \ M^{-1} \ cm^{-1}$$

Now β = the optical absorption coefficient = $\frac{1}{\ell_\beta}$

Where ℓ_β is the maximum depth penetrated by the light.

However $\beta = \varepsilon C$

In the solid polymer film the concentration of chromophore in polymer A = $2.55 \ M\ell^{-1}$

$\therefore \beta = 35{,}200 \times 2.55 \ cm^{-1} = 89{,}760 \ cm^{-1}$

$\therefore \ell_\beta = 1.11 \times 10^{-5}.cm = 0.11 \times 10^{-6} m$

This value means that modulation frequencies of the order of MHz are required in order to reduce μ (thermal diffusion depth) lower than ℓ_β. Which makes depth profiling for these polymers using UV/visible photo-accoustic spectroscopy impossible. However as will be shown in Chapter 5 this extinction coefficient is not applicable to the solid polymer film as the absorption spectrum is different.

2.11 Conclusion

It has been demonstrated that the limitations of the instrument restrict the study of the curing reaction in these polymers to a qualitative nature.

Depth profiling has been shown to be a feasible technique if high enough modulation frequencies are attainable.

It has been shown that apart from the thinnest films complete through cure is not achievable but a layer at the top is cured sufficiently to effect solvent resistance.

There is evidence to suggest that the polymer is sensitive to light below 410nm.

CHAPTER THREE

STATISTICAL MODEL

3.1 Introduction

Egerton et al[155] have used a mathematical model to show the low proportion of adjacent chromophores that correspond exactly in the polyvinyl cinnamate matrix. They use as their basis the fact that the quantum yield reduces to zero after 50% of the chromophores have disappeared. Presented below is a less mathematical attempt to predict the percentage of unreactive sites in a photo-sensitive polymer, based on orientation of the chromophores. Only three cases are considered:- Total overlap, 50% overlap and zero overlap.

Molecular Model

The basis of this model is to find the number of combinations of 3 chromophores in a 3 dimensional matrix that would give rise to active sites. To do this the limits of the matrix must be clearly defined as must the relative size of the chromophore. The size of one repeat unit compared to the size of one chromophore is used to do this.

A molecule of polyvinyl cinnamate can be considered as a long aliphatic chain with large pendant groups that are photosensitive as shown below in figure 3.1.

Figure 3.1

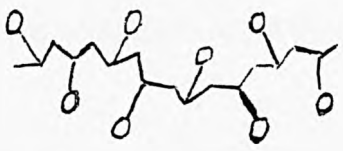

The repeat unit of four carbon atoms in the linear chain is shown in figure 3.2.

This planer configuration is assumed because it would allow closest

approach of chromophores from other chains. Otherwise the maximum distance for cyclodimerization as measured by Schmidt and Cohen[14] i.e: 4.1 Å would be exceeded.

Figure 3.2

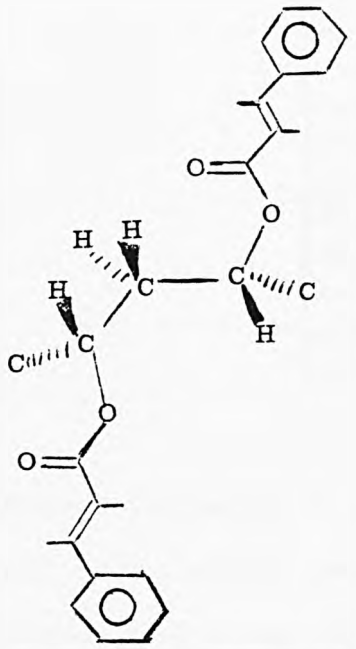

Using the following molecular dimensions the size of the repeat unit can be calculated.

C - C = 1.54Å C = O = 1.22Å C - O = 1.41Å

C - H = 1.10Å distance across a benzene ring = 2.41Å

C = C = 1.34Å Van der Waals radius for Hydrogen = 0.9Å

Because the C-H bond angle from the benzene ring is 120° the actual distance that the hydrogens protrude from the ring is 0.953Å.

Pendant group is 10.65Å. The length of the chromophore is about 3.5Å allowing for some conjugation with the carbonyl group and the benzene ring.

A factor of 1.45Å takes account of the nonlinear nature of the chain. The width of the repeat unit can be considered to be 3.5Å

Thus the dimensions of the repeat unit are 22.75Å by 3.5Å.

The distance between each chromophore is 5.1Å

Thus splitting the chromophore into two equal parts to allow for 50% overlap a matrix can be set up as shown below in figure 3.3.

Figure 3.3

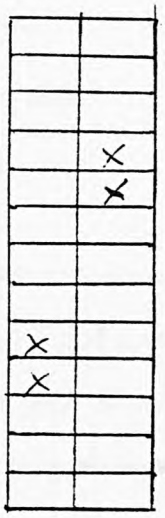

Where x designates an active centre. In the polymer this repeat unit will have a similar repeat unit above and below it.

Because each column will act in the same way the model will be reduced to consider only 1 pendant group which is free to move over the whole length of 2 pendant groups on opposite sides of the chain. That is the doubly active centre can take up any two adjacent boxes out of 13, which gives 12 different combinations.

Figure 3.3a

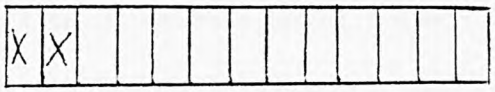

The situation with molecules above and below the plane can be scematically represented as follows.

Figure 3.4

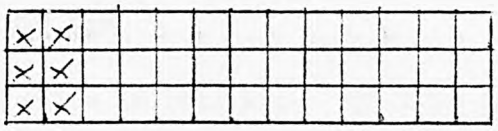

The above scheme would give rise to 12^3 combinations i.e. 1728.

An active combination is defined as when two boxes marked with x in different planes are adjacent, e.g.

Figure 3.5

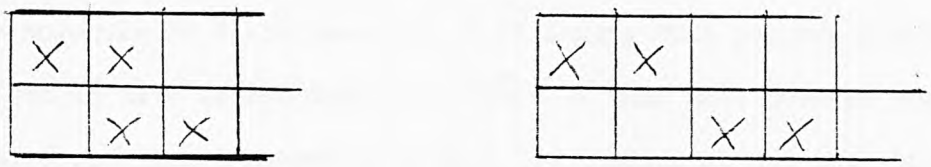

Active Unactive

In this way 718 combinations out of 1728 can be considered active which leads to approxiamtely 42% active. This short fall of 8% between this model and experiment may be due to the fact that an overlap of slightly less than 50% can be considered active or that the chromophore is longer than postulated above.

The repeat unit of Polymer 1 is shown below.

Figure 3.6

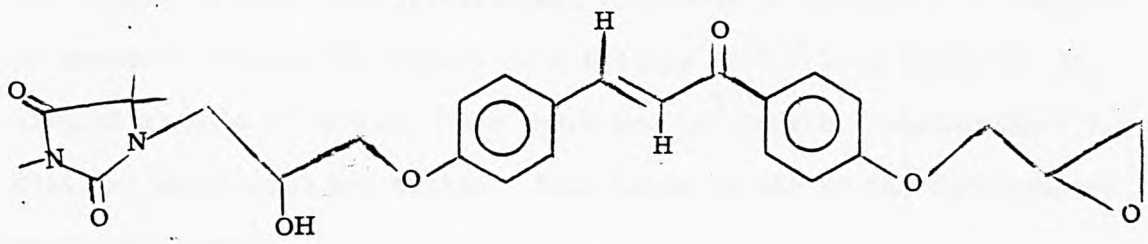

The dimensions of this are 22Å by 6Å by 4Å. i.e. the molecule can be no bigger than 4Å thick as this would prevent crosslinking due to the distance between chromophores being too big. Using a unit cell of this size the density can be calculated from $D = \frac{M}{V}$. i.e.

$$D = \frac{480 \times 10^{7}}{6.023 \times 10^{23} \times 6 \times 10^{-10} \times 4 \times 10^{-10} \times 22 \times 10^{-10}}$$

$$D = 1509 \text{ kgm}^{-3}$$

The measured value is 1443 kgm^{-3} which is in good agreement, indicating that the model is quite accurate.

This again can be considered as a linear chain of 13 boxes, which would

show 42% activity.

For polymer A the introduction of a second double bond requires that the model be adapted in the following way.

This molecule is 24.5Å long i.e. 2.5Å longer than polymer 1 which can be divided up into 14 sections of 1.75Å. In this case however because the chromophore cannot extend over both C = C bonds at the same time only 3 out of the middle 4 are considered active.

i.e. 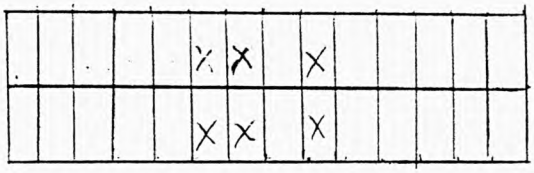

If reaction is considered to be possible between the top and bottom plains there will be a total of 11^3 combinations = 1331 of which 1031 are active i.e. 77%.

For polymer G where the 5,5-dimethyl hydantoin in polymer A is replaced by pentan-1,5-diol, the repeat unit becomes 29.7 Å long which can be divided up into 17 boxes. Thus there are 14^3 possible combinations i.e. 2744, of which 1862 are active. This leads to 68% of the chromophores in reactive sites.

Conclusion

This model predicts that the maximum number of chromophores available in reactive sites in polymer 1 is the same as polyvinyl cinnamate i.e. it should show the same sensitivity and no further reaction should take place after 50% have disappeared.

For polymer A there is a great increase in the number of chromophores in reactive sites and the sensitivity should be greater than polymer 1. Thetrue maximum percentage of chromophores available to react will be determined in the next chapter. However it is possible to predict that polymer A will be better than polymer G, and on the basis that the model predicts 42% as the maximum number of chromophores in reactive sites

for polymer 1, polymer should react further than 77%. For polymer 1, if one in ten of all chromophores are replaced only 40.5% of all sites will be reactive. However total number of chromophores will have dropped to 90% of the original number say .

$$\therefore \text{ percentage of active chromophores} = \frac{0.405}{0.9} \times 100$$

$$= 45\%$$

Therefore there should be no reduction in the percentage of active chromophores.

CHAPTER FOUR

INFRA-RED TRANSMISSION SPECTROSCOPY

4.1 General Comments

The results presented in chapter 2 clearly define the limitations of the OAS 400 photoacoustic spectrometer. In an effort to obtain quantitative data on rates of reaction and proportion of unreactive sites in a polymer film transmission infra-red spectroscopy was used.

On irradiation the double bonds are removed. Thus those bands in the infra-red associated with the double bond will diminish i.e. the sample will become more transparent at these wave numbers.

Spectra of model compounds have been obtained so that the bands in the more complex polymer spectra can be identified. The actual polymers used are described in tables 2.1a and 2.1b. In these polymers hydantoin carbonyl peaks act as internal standards so that thickness can be monitored throughout the irradiation process.

The method of determining the polymer density is described in chapter 7 together with details on the preparation of the 40mm KBr discs used in many of the following experiments.

4.2 Infra-red Spectra of Model Compounds

The reasons why certain bonds have been singled out are outlined in the following discussions.

Various bands in the infrared spectra of the photoresists change on irradiation. In order to establish some degree of consistency the changes in more than one of these bands were monitored. α,β-Unsaturated carbonyl compounds possess a C=O stretching mode which absorbs in the 1685-1665cm^{-1} region, aryl groups cause this band to occur at a lower

wave number, the actual position depending upon the degree of unsaturation in the vicinity of the carbonyl group e.g. in the polymer A series the band occurs around 1645cm^{-1} whereas in the polymer 1 series the band occurs near 1665 cm^{-1}. Carbonyl groups that are unconjugated absorb between 1725-1705cm^{-1}. It should be obvious from this that removal of unsaturation by either crosslinking or hydrogenation will shift the carbonyl bands to higher numbers, causing a reduction in the magnitude of the unsaturated carbonyl peak. It was thus hoped that curing could be followed using this band.

Carbon-carbon double bonds conjugated to carbonyl groups absorb at three places in the infra-red. Firstly there is a C=C stretching mode which appears in the 1640-1590cm^{-1} region. However C-C double bonds conjugated to aromatic groups give rise to a typically broad band with a side band. The second characteristic peak of the C=C double bond is caused by C-H out of plane deformation. If the molecule has trans-configuration the band lies around 970-960cm^{-1}. If the molecule has a cis-configuration the band occurs between 730-675cm^{-1}. The band due to the trans isomer is moved to higher wave numbers on conjugation with carbonyl and aromatic groups. Thus if the alkene character is reduced on crosslinking then these peaks should be affected. The other band is less useful than these, it is the C-H stretch between 3040-3010cm^{-1}.

If one obtains the transmission spectrum of a compound, then the absorption due to specific vibrational modes can be found using $A = \log\frac{1}{T}$. Now as $A = \varepsilon C\ell$ if ℓ and ε remain the same, then $A \propto C$, thus any variation in C can be monitored. ε = molar extinction coefficient ℓ = depth of sample.

By far the most consistent results have been obtained using the base line technique, where a tangent is drawn across the base of certain peaks and is then used as a baseline. The absorption can be calculated as follows:-

If T_b = transmission of background

T_p = transmission of band

then $A = \log \frac{1}{T_p} - \log \frac{1}{T_b}$

$$A = \log \frac{T_b}{T_p}$$

The model compounds used were: chalcone, 4,4'- diglycidyl ether of 4,4'- dihydroxy chalcone, 5,5- dimethyl hydantoin and dibenzalacetone. The spectra are shown in figures 4.1a-d. The interpretations are tabulated in tables 4.1a-d. All spectra were recorded on KBr discs.

The structure of chalcone is shown below. The spectrum can be seen in figure 4.1a, the interpretation can be seen below the structure.

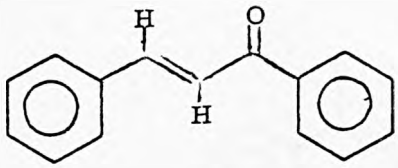

Table 4.1a

3090 cm^{-1}		aromatic C—H stretch
3060 cm^{-1}	weak	alkene C—H stretch
3030 cm^{-1}		
1665 cm^{-1}	strong	unsaturated carbonyl C=O stretch
1600 cm^{-1}		
1572 cm^{-1}	strong	aromatic and alkene C=C stretch
1495 cm^{-1}	medium	aromatic C—C stretch
1450 cm^{-1}	strong	aromatic C—C stretch
1337 cm^{-1}	strong	
1310 cm^{-1}	strong	
1285 cm^{-1}	strong	
1210 cm^{-1}	strong broad	

1180 cm^{-1}	medium	
1030 cm^{-1}	medium sharp	
1010 cm^{-1}	strong sharp	
987 cm^{-1}	strong broad	trans alkene C—H out of plane deformation
745 cm^{-1}	strong	aromatic C—H out of plane deformation (pattern expected for monosubst. aromatic)
685 cm^{-1}		
555 cm^{-1}	medium	
485 cm^{-1}	medium	

The structure of 4,4'-diglycidyl ether of 4,4'-dihydroxy chalcone is shown below. Its spectrum is shown in figure 4.1b and it has many features similar to the spectrum of chalcone. The interpretation is shown in table 4.1b.

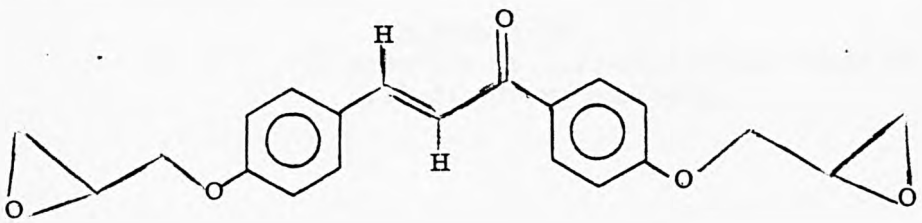

Table 4.1b

3410 cm^{-1}	weak	broad —O—H stretch
3065 cm^{-1}	weak	aromatic C—H stretch
3010 cm^{-1}	weak	alkene C—H stretch
2930 cm^{-1}	weak	CH_2 stretch
1655 cm^{-1}	strong	unsaturated carbonyl C=O stretch
1600 cm^{-1} 1572 cm^{-1}	strong	aromatic and alkenes C=C stretch
1505 cm^{-1}	strong	aromatic C—C vibration
1450 cm^{-1}	medium	aromatic C—C vibration
1420 cm^{-1}	medium	

Figure 4.1a
IR spectrum of chalcone.

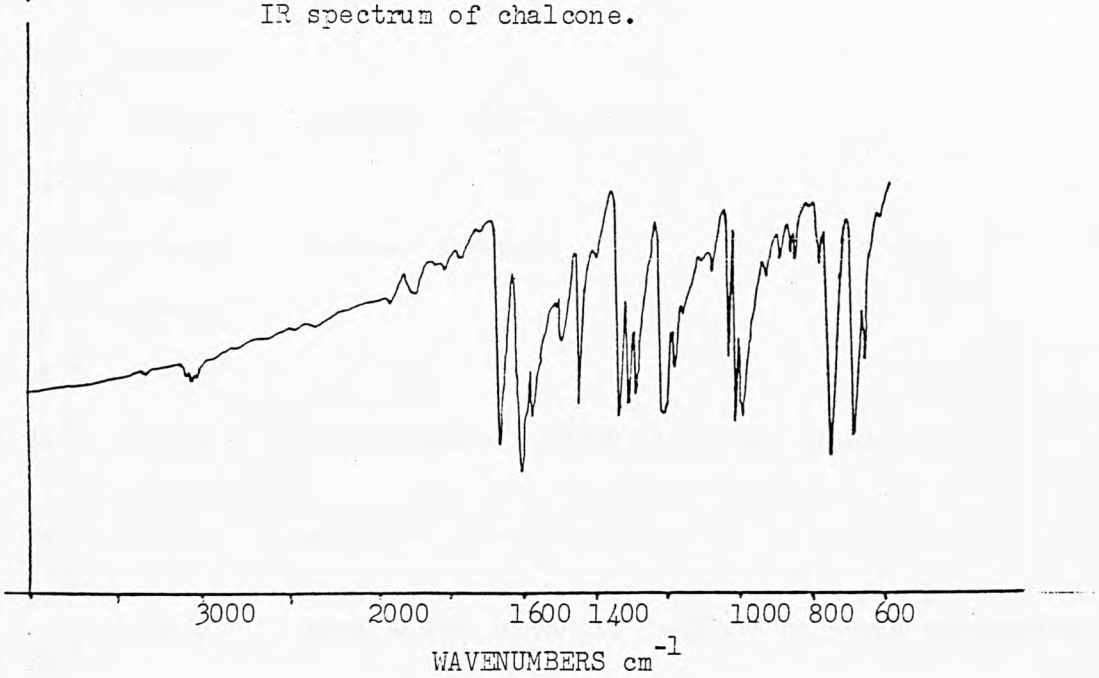

Figure 4.1b
IR spectrum of 4,4'-diglycidyl ether of
4,4'-dihydroxy chalcone.

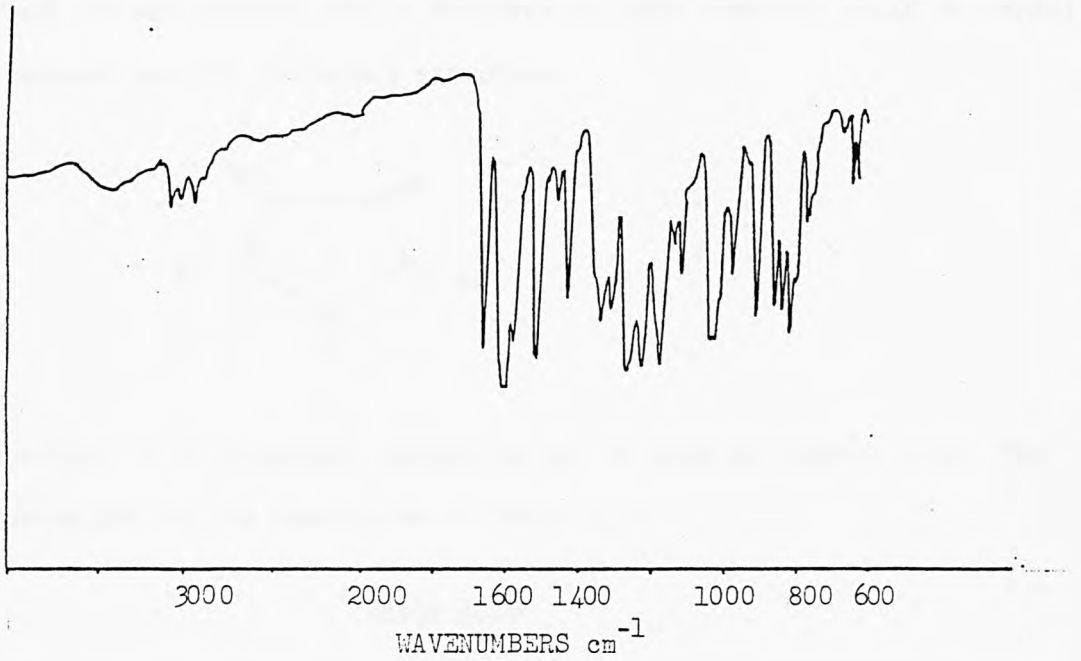

1330 cm^{-1}	medium		
1315 cm^{-1}	shoulder		
1303 cm^{-1}	medium		
1255 cm^{-1}	strong	epoxide	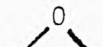 stretch
1215 cm^{-1}	strong		
1170 cm^{-1}	strong	C—O—C stretch	
1030 cm^{-1}	strong		
1015 cm^{-1}	strong		
970 cm^{-1}	strong	trans alkene C—H out of plane vibration	
907 cm^{-1}	strong	epoxide	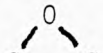
855 cm^{-1}	strong	para subst. aromatic C—H out of plane vaibration	
835 cm^{-1}			
815 cm^{-1}	strong	epoxide	
565 cm^{-1}	medium		

As polymers A-F and polymers 1-8 are all advanced with 5,5-dimethyl hydantoin it was thought that a spectrum of this compound would be useful. The compound has the following structure.

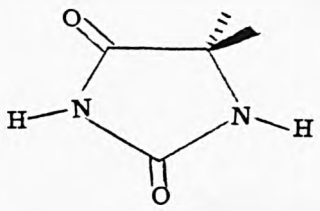

The spectrum of 5,5-dimethyl hydantoin can be seen in figure 4.1c. The interpretation can be seen below in Table 4.1c

Table 4.1c

3700 - 2700 cm^{-1}	V.broad	N-H, $-CH_3$ stretch
1780 cm^{-1}	strong	carbonyl stretch of imides in 5 membered ring
1720 cm^{-1}	strong	
1480 cm^{-1}	medium	N-H bending

1440 cm^{-1}	strong	
1390 cm^{-1}	medium	alkene C-H bending
1295 cm^{-1}	medium	
1220 cm^{-1}	medium	
1155 cm^{-1}	medium	Amide
1060 cm^{-1}	medium	C-C stretch
937 cm^{-1}	medium	
800 cm^{-1}	strong	
775 cm^{-1}	strong	NH and CH rocking
660 cm^{-1}	strong	
610-590 cm^{-1}	broad	

As dibenzal acetone (1,5-diphenyl penta-1,4-diene-3-one) is the photosensitive group in polymers A-F its spectra was obtained (figure 4.1d). The structure of dibenzal acetone is shown below and the interpretation of the spectrum is set out in Table 4.1d.

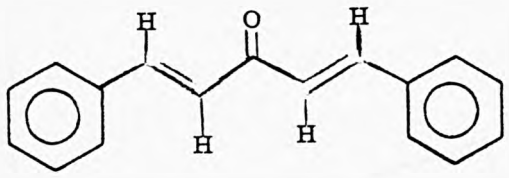

Table 4.1d

3080 cm^{-1}	weak	C-H stretch alkene
3055 cm^{-1}	weak	
3038 cm^{-1}	weak	C-H stretch aromatic
3020 cm^{-1}	weak	
1660 cm^{-1}	strong	αβ α'β' unsaturated C=O stretch
1610-1600 cm^{-1}	strong	C=C conjugated with carbonyl group.
1582 cm^{-1}	strong	aromatic C-C stretch
1518 cm^{-1}	strong	
1428 cm^{-1}	strong	

Figure 4.1c
IR spectrum of 5,5-dimethyl hydantoin.

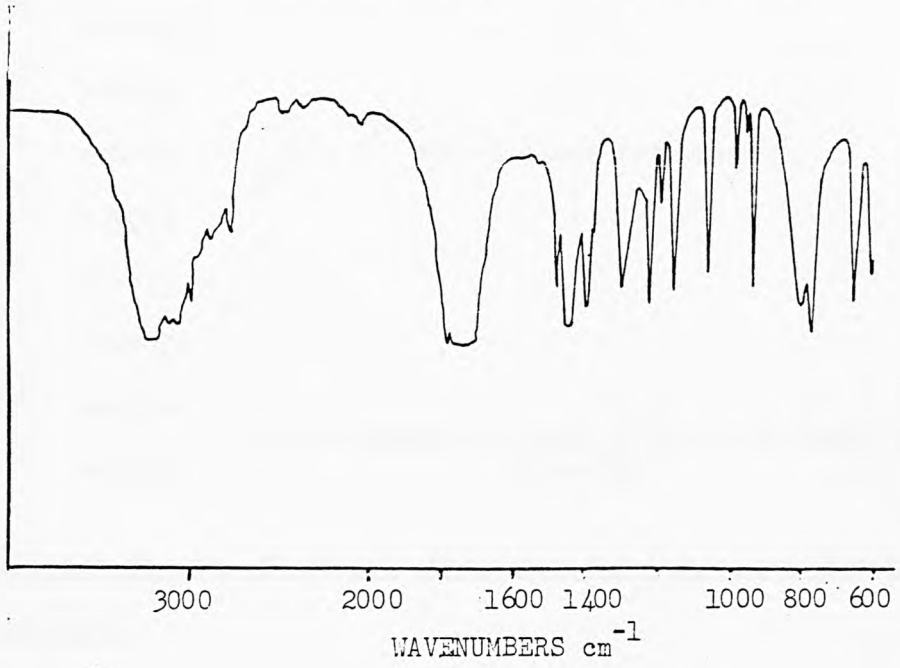

Figure 4.1d
IR spectrum of dibenzalacetone.

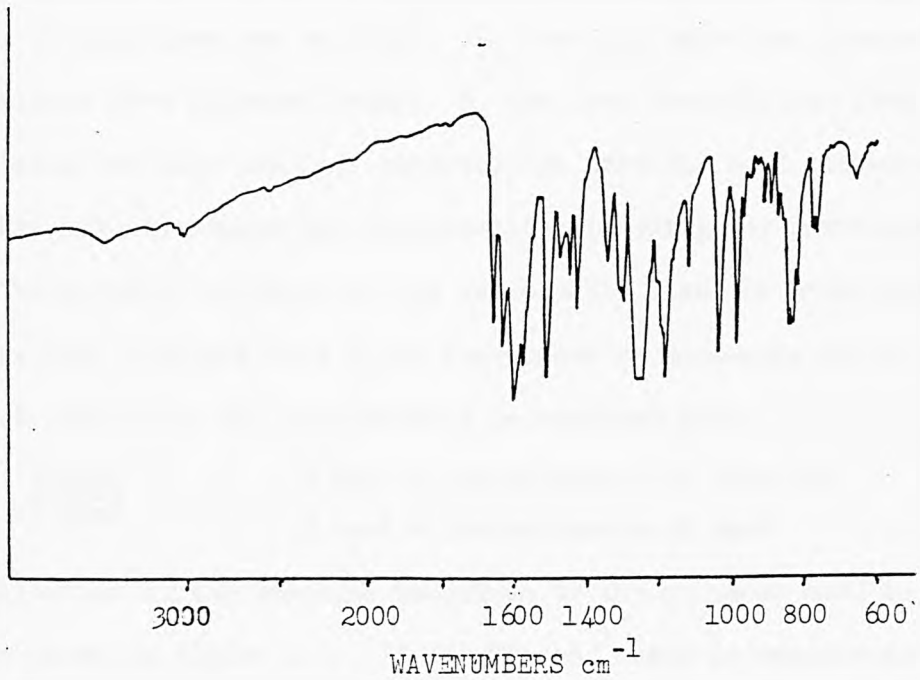

1311 cm^{-1}	strong	
1300 cm^{-1}	strong	
1268-1248cm^{-1}	strong	
1183 cm^{-1}	strong	
1035 cm^{-1}	strong	
987 cm^{-1}	strong	$H\diagup C = C \diagdown^{H}$ out of plane deformation.
840 cm^{-1}	strong	
879 cm^{-1}	strong	
815 cm^{-1}	strong	
772 cm^{-1}	medium	monosubstrated aromatic C-H out of plane bending vibration
761 cm^{-1}	medium	

4.3 Infra-red Spectra of Polymer Films and the use of the Baseline Technique.

The baseline technique is a method for obtaining quantitative data from infra-red spectroscopy. It entails drawing a base line between two points on a recorded infra-red spectrum. It can be seen from figure 4.2a that a number of baselines can be drawn. B_1 does not take into account the contributions from adjacent bands. B_2 has less contribution from adjacent bands but also has less contribution from the band understudy. Thus there are advantages and disadvantages in using any particular base line. The decision of which to use is normally based on which method gives the best straight line in an absorbance vs concentration plot. As explained previously the absorbance A is obtained from:-

$$A = \log \frac{T \text{ base}}{T \text{ band}}$$

T base = transmittance of baseline
T band = transmittance of band

The application of the baseline technique to the polymers used in this study is shown in figure 4.3. If the 984 cm^{-1} band is considered it is obvious that it almost completely disappears on irradiation and thus for most accurate results when following this band, the base line between 1800 cm^{-1} and 780 cm^{-1} was chosen. This base line has been used through-

out the study so as to obtain comparable results.

Table 4.2a

An interpretation of the major bands in the spectrum of a film of polymer A is presented below:-

3420 cm^{-1}	medium	broad -OH stretch
2980 cm^{-1}	weak	
2930 cm^{-1}	weak	alkene C-H stretch
2880 cm^{-1}	weak	
1765 cm^{-1}	medium	hydantoin saturated carbonyl stretch
1705 cm^{-1}	strong	
1645 cm^{-1}	medium	unsaturated C=O stretch
1620 cm^{-1}	medium	
1600 cm^{-1}	strong	pattern for C=C conjugated with aromatic ring
1572 cm^{-1}	medium	
1512 cm^{-1}	strong	aromatic C-C stretch
1460 cm^{-1}	medium	aromatic C-C stretch
1425 cm^{-1}	medium	CH_3- C-H bending mode
1386 cm^{-1}	weak	
1340 cm^{-1}	weak	broad
1305 cm^{-1}	weak	
1290 cm^{-1}	weak	
1257 cm^{-1}	strong	
1173 cm^{-1}	strong	C-O-C stretch
1100 cm^{-1}	medium	
1035 cm^{-1}	weak	
986 cm^{-1}	weak	trans alkene C-H bending
832 cm^{-1}	medium	
765 cm^{-1}	weak	
635 cm^{-1}	weak	
555 cm^{-1}	weak	broad
505 cm	weak	

Figure 4.2
Effects of irradiation on the IR spectrum of polymer 1.

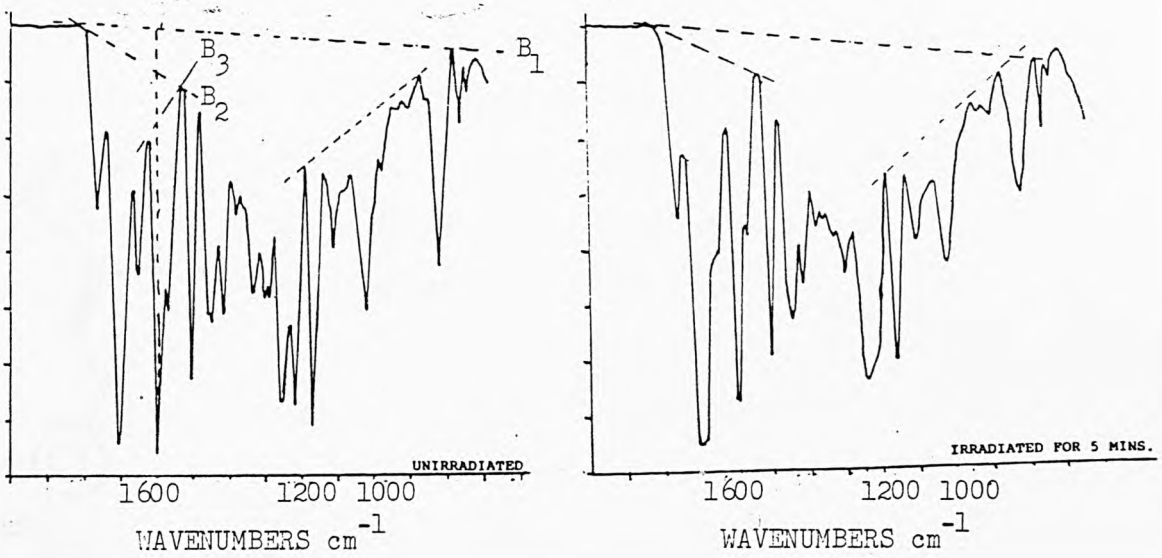

Figure 4.3
Effects of irradiation on the IR spectrum of polymer A.

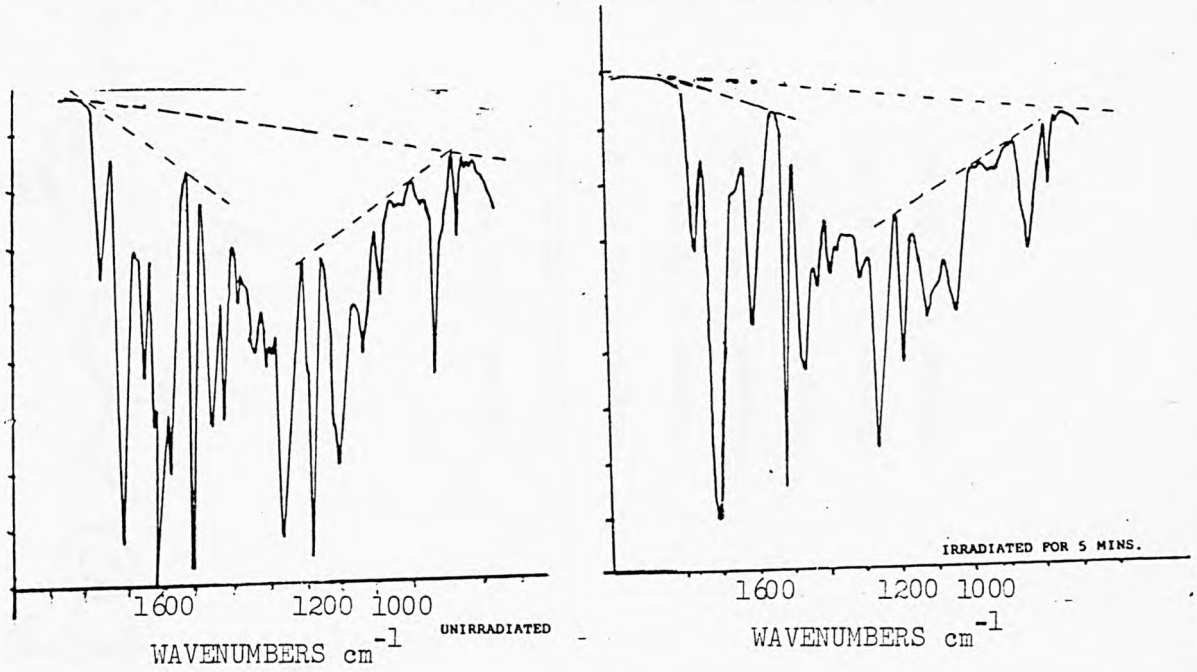

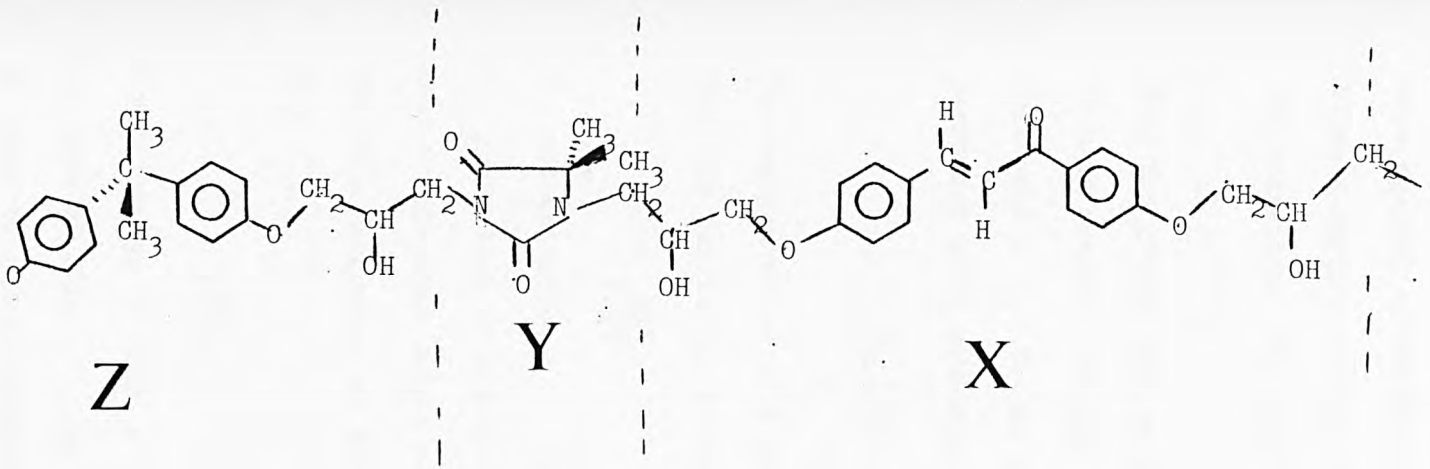

Polymer 1 10X 9Y

Polymer 2 9X 9Y 1Z

Polymer 3 8X 9Y 2Z

Polymer 4 7X 9Y 3Z

Polymer 5 5X 9Y 5Z

Polymer 6 3X 9Y 7Z

Polymer 7 1X 9Y 9Z

Polymer 8 9Y 10Z

4.4 Infra-red Study of the Photocrosslinking Reaction of Polymers 1-8.

4.4.1 Determination of Calibration Graphs.

4.4.1.1. Experimental Method.

In order to study a reduction in the concentration of a particular entity using a band in the IR region, it is necessary to have graphs of absorbance against concentration so that the absorbance of a particular band after a certain period of irradiation can be directly converted into a concentration. The Beer-Lambert law states that:-

$$A = \varepsilon C \ell \qquad 4.4.1$$

Thus the graphs must be plotted for a particular band at a particular film thickness. However conversion of an absorbance of a band at a film thickness ℓ (A_ℓ) to the absorbance at a specific thickness ℓs ($A_{\ell s}$) is performed using equation 4.4.2.

$$A_{\ell s} = \frac{A_\ell \times \ell s}{\ell} \qquad 4.4.2$$

The concentration of a particular entity in the film can be obtained from the density as follows.

$$C = \frac{x\rho}{M.wt} \qquad 4.4.3$$

C = concentration M/ℓ ρ = density of polymer g/ℓ

x = proportion of entity in original preparation of polymer.

M-wt = molecular weight of entity.

The film thickness can also be obtained from the density by using equation 4.4.4.

$$\ell = \frac{m}{A \times \rho} \qquad 4.4.4$$

ℓ = thickness of film m A = area of film m^2

m = mass of film kg ρ = density of polymer kgm^{-3}

In order to reduce weighing errors, which can be large when two large weights are subtracted to find a small difference, a substrate with a high surface area to weight ratio is required. If the curing of the film is to be monit-

ored using infra-red spectroscopy then a substrate, transparent to IR radiation would be an advantage. Large thin discs of KBr fit these conditions. Hence the use of the 40mm KBr discs (see chapter 7).

The band at 1765cm^{-1}, attributed to a carbonyl group in the hydantoin moiety, is well removed from the chromophore and it should remain constant on irradiation. Thus it has been used to determine thickness and as an internal standard to monitor change in thickness. To this end the extinction coefficient, as measured from the base line, was determined from samples of polymers 1-8 cast as films using k bars 1-3 so as to vary the film thickness. The thickness was determined by weighing the disc before and after coating it.

Data has also been extracted from the same spectra so that graphs of absorbance versus concentration would be plotted for the 1650cm^{-1}, 1600cm^{-1}, 1572cm^{-1}, 984cm^{-1} bands. Only the first five polymers have been considered, as absorbances in the other two are severely affected by background absorbance (see spectrum of polymer 8) The spectra of polymers 1-8 are shown in figure 4.4.

4.4.1.2 Results and Discussion.

The measurement of densities is detailed in chapter 6. The proportion of the entity in the original preparation is found by dividing the weight of the entity by the total weight of the reaction mixture, these figures are also given in chapter 6.

Table 4.3a

Polymer	Conc^{n} of Chalcone Moles/litre	Conc^{n} of DMH* Moles/litre	Conc^{n} of BADGE* Moles/litre	Density kg/m^3
1	3.21	2.44	-	1440
2	3.14	2.65	0.30	1550
3	2.41	2.29	0.51	1310
4	1.91	2.07	0.71	1180
5	1.36	2.06	1.15	1140
6	0.75	2.15	1.68	1110
7	0.26	2.26	2.29	1160
8	-	2.26	2.51	1140

* DMH = 5,5-dimethyl Hydantoin BADGE = BisphenolAdiglycidyl ether.

Figure 4.4a
IR spectrum of polymer 1

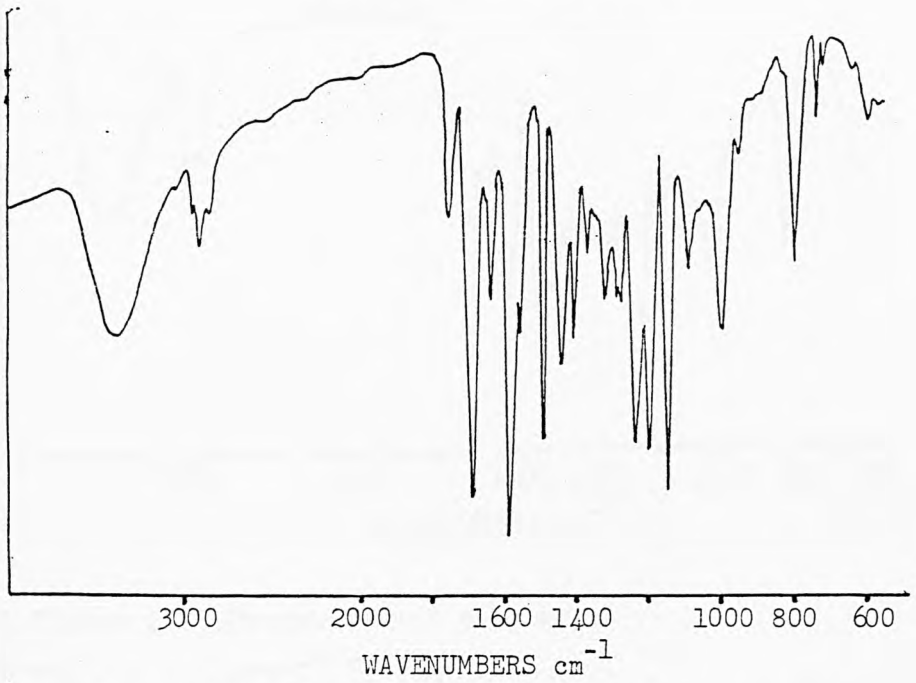

Figure 4.4b IR spectrum of polymer 2

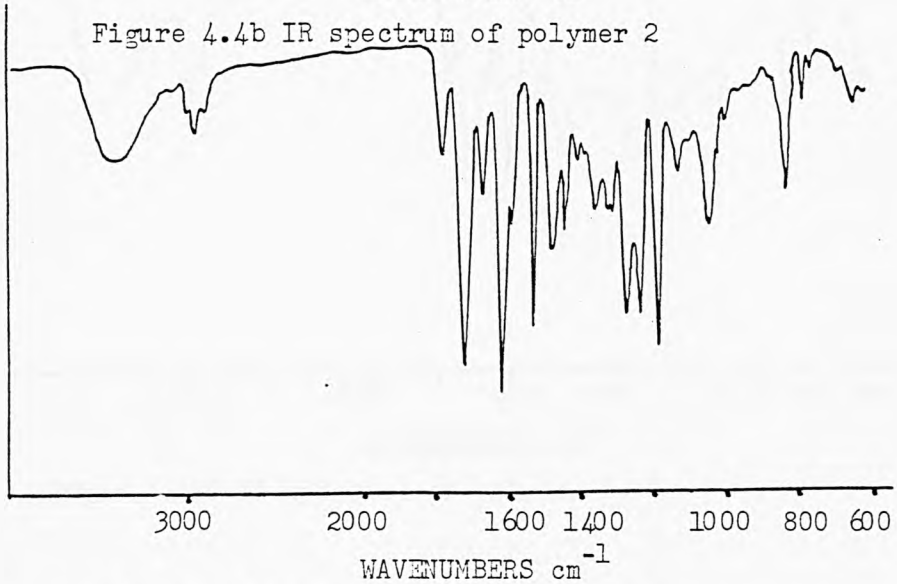

Figure 4.4c IR spectrum of polymer 3

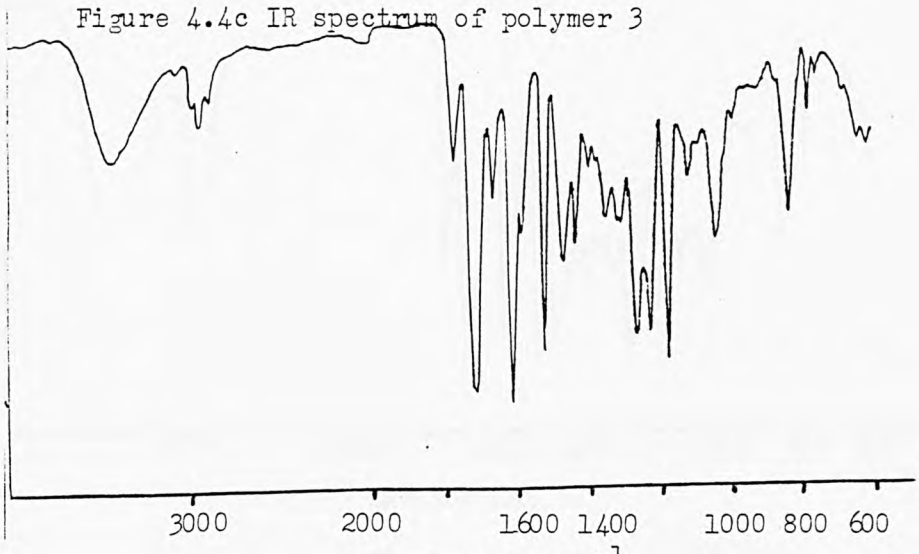

Figure 4.4d IR spectrum of polymer 4

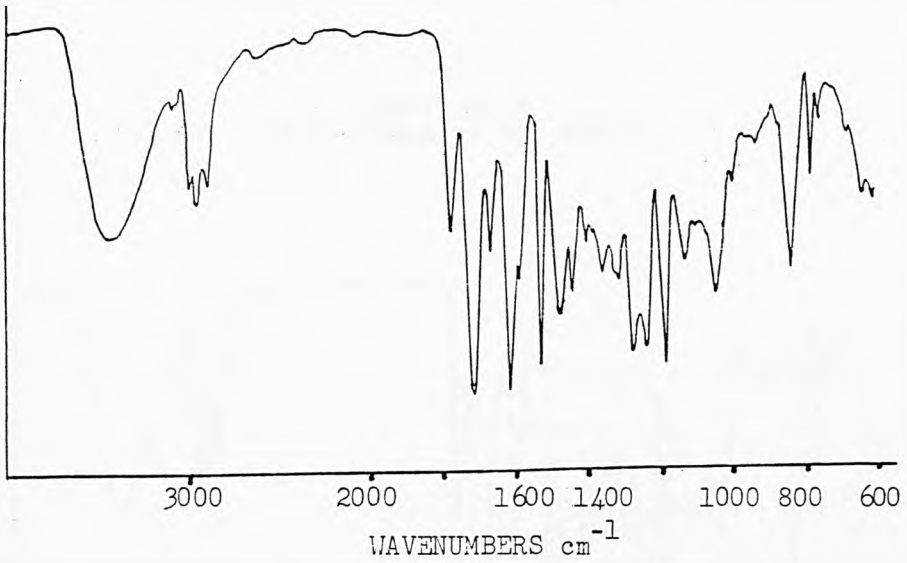

Figure 4.4e IR spectrum of polymer 5

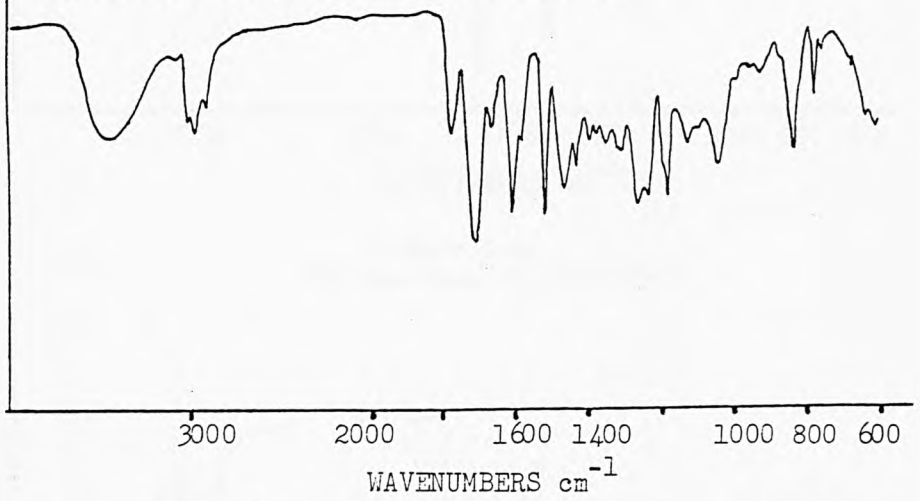

Figure 4.4f IR spectrum of polymer 6

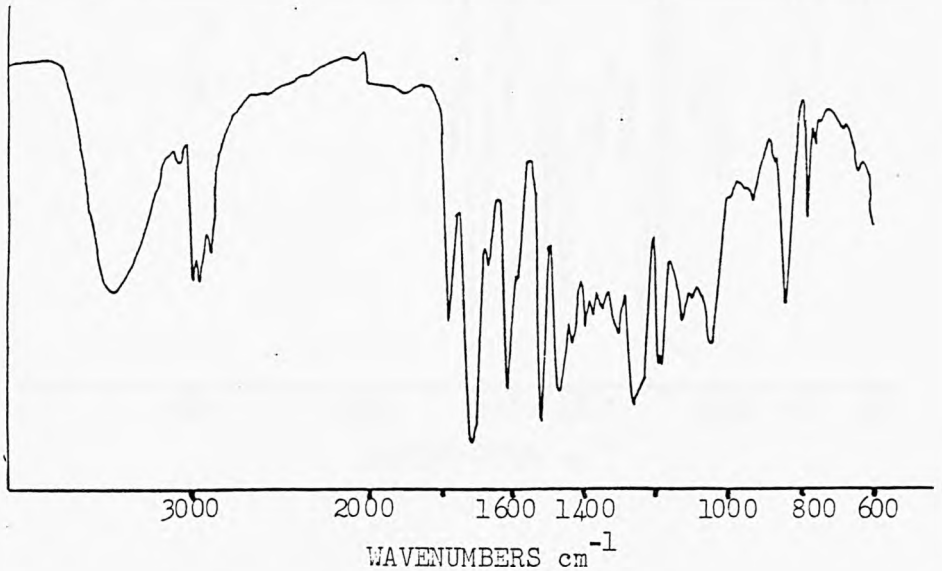

Figure 4.4g
IR spectrum of polymer 7

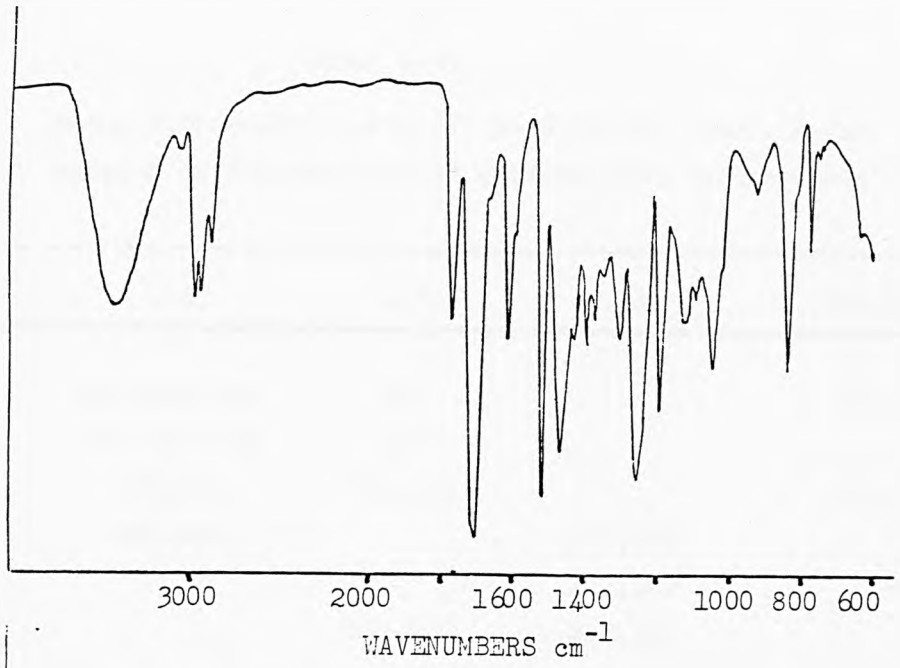

Figure 4.4h
IR spectrum of polymer 8

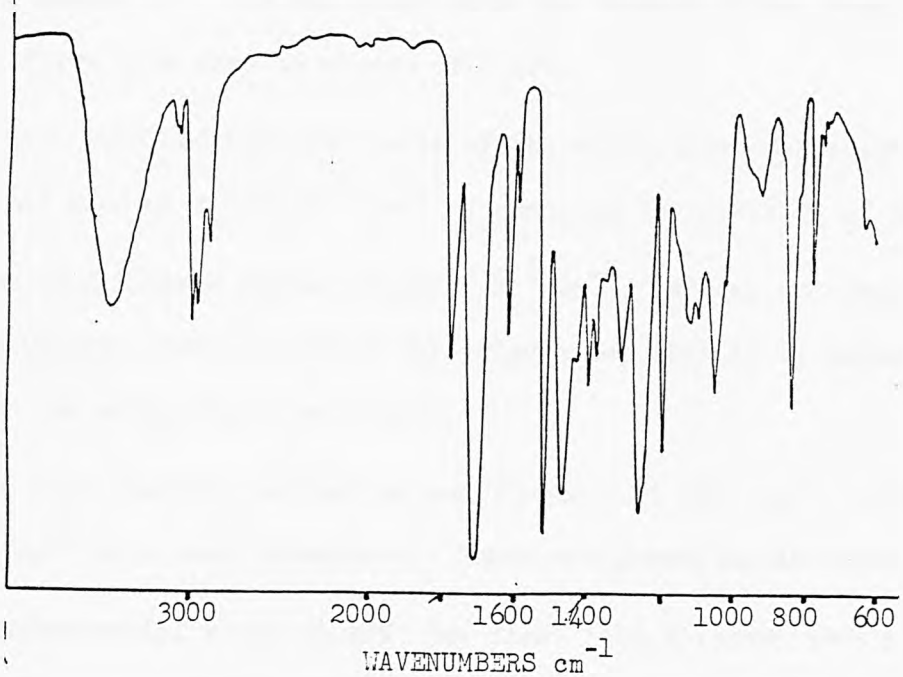

The sharp increase in the concentration of dimethyl hydantoin between polymers 1 and 2 and the small decrease in the concentration of chalcone between the same polymers is a reflection of the density increase which is explained by the bisphenol A improving molecular packing. This last statement has not been verified.

Table 4.3b

Extinction coefficients of the 1765 cm^{-1} band in the spectra of Polymers 1-8 at various film thicknesses.

Polymer	1-4μ	4-7μ	7-10μ	10-12μ
1	209,219,218	202		203
2	202,180,173	213		
3	237,214	224,236		224
4	220,222		173,206	
5			202,209	
6		234,207	206,214	
7			222.200	
8			208,210	

Possible errors of ± 30% can occur with the thinner films. Even the thicker films give rise to errors of ± 10%.

It has been observed that the value of the extinction coefficient can vary by as much as ± 10 ℓ M^{-1} cm^{-1} by changing the position of the disc. The mean of all these values is 207 ℓ M^{-1} cm^{-1}. As can be seen, most of the results are within ± 10% of this figure and thus it is taken as the value of the extinction coefficient.

From the same spectra, extinction coefficients at 1650 cm^{-1}, 1572 cm^{-1}, 1600 cm^{-1} and 984 cm^{-1} have been determined. These are presented in Table 4.4.1.

Within experimental error (± 10%) the first five polymers show a high degree of agreement. The other two polymers which contain a chromophore exhibit mildly different results because of residual absorbance. That

is if the spectra of polymer 8 are examined, a substantial absorbance can be found at the above wavenumbers or at slightly shifted wavenumber. This has little effect when the concentrations are high but it is significant at lower concentrations.

Table 4.3c

Extinction coefficients of the different bands.

Polymer 1	1650 cm^{-1} $\ell M^{-1} cm^{-1}$	1570 cm^{-1} $\ell M^{-1} cm^{-1}$	984 cm^{-1} $\ell M^{-1} cm^{-1}$
1	271,246,240	347,312,304	96.6,115,982
2	243,254	300,318	107,108
3	274,271	330,322	107,107
4	271,252,242	377,357,327	119,101,113
5	267,268	334,330	117,116
6	474,395,357	410,422,400	176,150,119
7	913	828	350
8	-	-	-

From the above results it follows that a graph of absorbance against concentration for a given thickness of film will give a straight line of gradient ε until low concentrations are reached.

In order to plot a calibration graph the absorbances, from which the above data is obtained, must be corrected for varying thickness. This is easily done because the concentration and the extinction coefficient remain constant.

Thus $A_1 = C\varepsilon\ell_1$

and $A_2 = C\varepsilon\ell_2$

$$A_2 = \frac{A_1\ell_2}{\ell_1}$$

A least square treatment was performed on the data of the first five polymers. The results can be seen under each table. The graphs obtained

are shown in figure 4.5. The graphs show deviation from linearity after the fifth polymer and hence polymers 6,7,8 were not considered in the least square treatment.

Table 4.4a

Correction of 1650 cm^{-1} band absorbances in the IR. spectra of polymers 1-5, for thickness.

Polymer	A_1	ℓ_1 ($\times 10^{-6}$ m)	ℓ_2 ($\times 10^{-6}$ m)	A_2	mean	Conc^{n} (M ℓ^{-1})
1	0.348	4	3	0.261		3.21
1	0.232	2.8	3	0.249	0.253	3.21
1	0.297	3.6	3	0.248		3.21
2	0.221	2.9	3	0.229		3.14
2	0.455	5.7	3	0.239	0.231	3.14
2	0.481	6.4	3	0.225		3.14
3	0.424	6.5	3	0.196		2.41
3	0.674	10.2	3	0.198	0.192	2.41
3	0.430	7.1	3	0.182		2.41
4	0.342	7.4	3	0.139		1.91
4	0.367	7.6	3	0.145	0.150	1.91
4	0.213	3.8	3	0.168		1.91
5	0.303	8.3	3	0.110	0.110	1.36
5	0.291	8.0	3	0.109		1.36
	Equation of line is :-					
	$y = 0.073x + 0.012$					
	error of slope = $\pm 0.005 = 6.8\ \%$					
8	0.023	1.95	3	0.035		0
8	0.032	2.83	3	0.034	0.034	0
8	0.094	8.51	3	0.033		0

Table 4.4b

Correction of 1600 cm^{-1} band absorbances in the IR spectra of polymers 1-5, for thickness.

Polymer	A_1	ℓ_1 ($\times 10^{-6}$ m)	ℓ_2 ($\times 10^{-6}$ m)	A_2	mean	Conc $\frac{n}{M\ell^{-1}}$
1	1.173	4.0	3	0.88		3.21
1	0.845	2.8	3	0.905	0.9	3.21
1	1.098	3.6	3	0.915		3.21
2	0.866	2.9	3	0.896		3.14
2	0.789	2.6	3	0.910	0.885	3.14
2	0.396	1.4	3	0.849		3.14
3	0.857	4.0	3	0.643		2.41
3	1.121	5.2	3	0.647	0.650	2.41
3	0.462	2.1	3	0.660		2.41
4	1.162	7.4	3	0.471		1.91
4	0.260	1.6	3	0.487	0.487	1.91
4	0.637	3.8	3	0.503		1.91
5	1.024	8.3	3	0.37		1.36
5	0.960	8.0	3	0.36	0.365	1.36

Equation of line is:-

$$y = 0.298x - 0.06$$

error of slope = $\pm 0.012 = 4.03\%$

Because of the large extinction coefficient only thin films (less than 6.0×10^{-6} m) of the first three polymers can be used for this band.

6	0.170	1.75	3	0.295		0.75
6	0.279	2.93	3	0.286	0.285	0.75
6	0.312	3.40	3	0.279		0.75
7	0.144	2.74	3	0.158	0.161	0.26
7	0.156	2.76	3	0.170		0.26
7	0.181	3.50	3	0.155		0.26

8	0.085	1.95	3	0.130		0
8	0.112	2.83	3	0.119	0.120	0
8	0.315	8.51	3	0.111		0

Table 4.4c

Correction of 1570 cm^{-1} band absorbances in the IR spectra of polymers 1-5, for thickness.

Polymer	A_1 ($x10^{-6}m$)	ℓ_1 ($x10^{-6}m$)	ℓ_2	A_2	mean	Conc^{n} $M\ell^{-1}$
1	0.446	4.	3	0.335		3.21
1	0.286	2.8	3	0.306	0.313	3.21
1	0.357	3.6	3	0.298		3.21
2	0.273	2.9	3	0.282		3.14
2	0.569	5.7	3	0.299	0.289	3.14
2	0.609	6.4	3	0.285		3.14
3	0.504	6.5	3	0.233		2.41
3	0.810	10.2	3	0.238	0.234	2.41
3	0.546	7.1	3	0.231		2.41
4	0.423	7.4	3	0.171		1.91
4	0.470	7.6	3	0.186	0.187	1.91
4	0.259	3.8	3	0.204		1.91
5	0.372	8.3	3	0.134	0.136	1.36
5	0.364	8.0	3	0.137		1.36

Equation of line is:-

$$y = 0.091x + 0.013$$

error of slope = $\pm 0.005 = 5.5\%$

6	0.062	1.75	3	0.106		0.75
6	0.091	2.93	3	0.093	0.099	0.75
6	0.112	3.40	3	0.099		0.75
8		1.95	3	0.053		0
8		2.83	3	0.050	0.049	0
8		8.51	3	0.044		0

Table 4.4d

Correction of $984cm^{-1}$ band absorbances in the IR spectra of polymers 1-5, for thickness.

Polymer	A_1	ℓ_1 ($x10^{-6}m$)	ℓ_2 ($x10^{-6}m$)	A_2	mean	$Conc^{\underline{n}}$ $M\ell^{-1}$
1	0.126	4.0	3	0.095		3.21
1	0.095	2.8	3	0.102	0.102	3.21
1	0.132	3.6	3	0.110		3.21
2	0.097	2.9	3	0.100		3.14
2	0.193	5.7	3	0.102	0.099	3.14
2	0.200	6.4	3	0.094		3.14
3	0.168	6.5	3	0.078		2.41
3	0.264	10.2	3	0.078	0.077	2.41
3	0.180	7.1	3	0.076		2.41
4	0.135	7.4	3	0.055		1.91
4	0.164	7.6	3	0.065	0.063	1.91
4	0.087	3.8	3	0.069		1.91
5	0.131	8.3	3	0.047	0.048	1.36
5	0.128	8.0	3	0.048		1.36

Equation of line is:-

$$y = 0.029x + 0.008$$

error of slope = $\pm 0.001 = 3.4\%$

Conclusion

The $984cm^{-1}$ band gives the best straight line. However because the $984cm^{-1}$ band merges into a shoulder and makes accurate assessment of absorbance difficult, whereas the next best band the $1600cm^{-1}$ band remains discreet and will therefore be used to follow the reaction.

Figure 4.5
Calibration graphs for the 1650 cm^{-1}, 1600 cm^{-1}, 1572 cm^{-1}, and 984 cm^{-1} bands in the IR spectra of polymers 1-8.

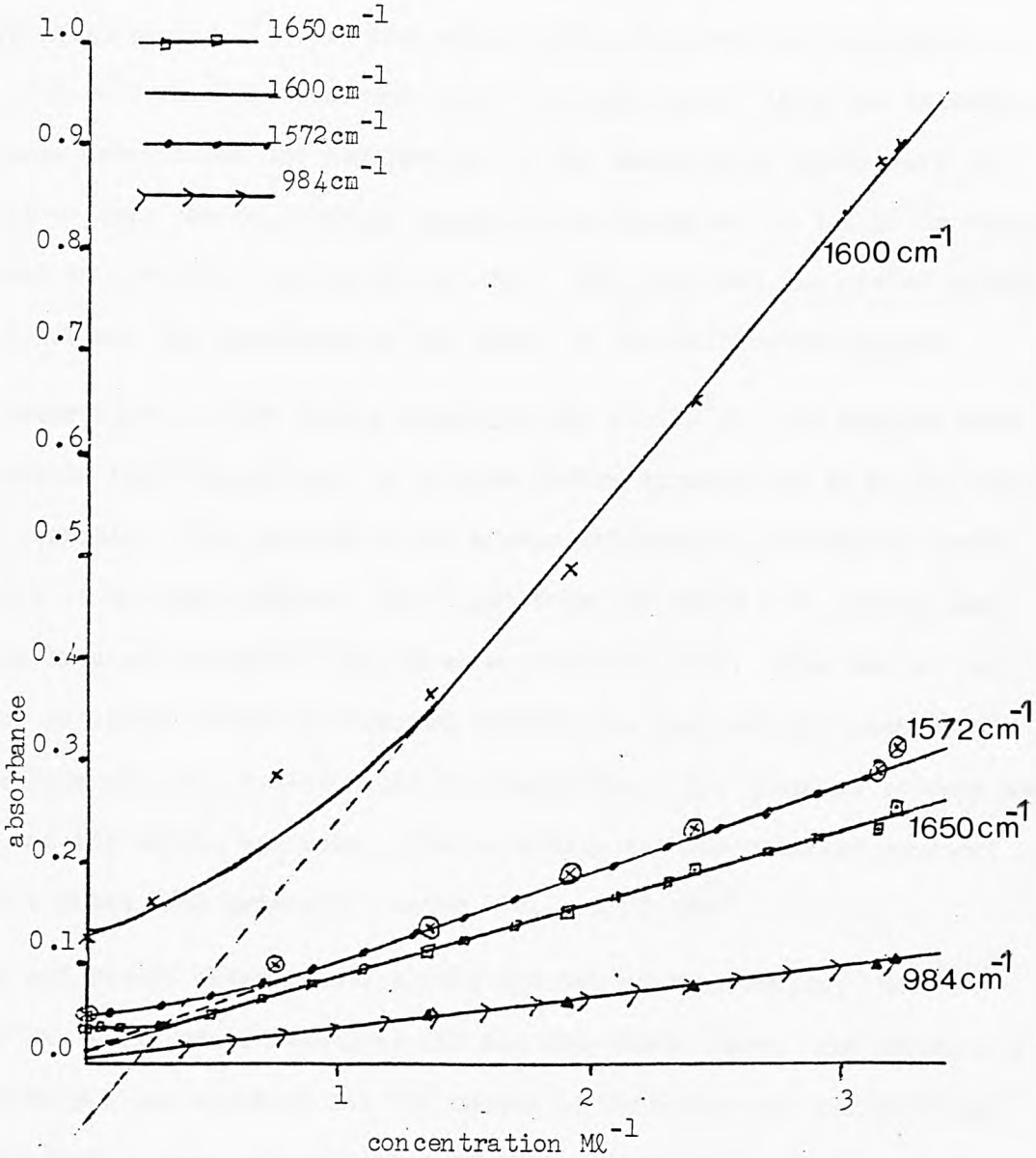

4.4.2 Photocrosslinking of Polymers 1-8

4.4.2.1 Experimental Method.

In order to follow the photocrosslinking reaction of these polymers, films were cast on potassium bromide discs. The thickness was determined by weighing the disc before and after application of the film and then using equation 4.4.4. A second method which utilised the absorbance of the 1765 cm^{-1} band and equation 4.4.1 was also used. Once the thickness had been established the absorbances of the bands under study were corrected so that the calibration graphs for a thickness of 3×10^{-6}m could be used to ascertain the concentration. This required the use of equation 4.4.2 and the equations of the lines on the calibration graphs.

The temperature in the curing apparatus was 80-100°C. The samples were brought to this temperature in an oven before irradiation so as to remove this variable. This procedure was always followed on successive irradiations of the same sample. The light from the 1800W U.V. curing lamp was restricted through a 7cm diameter circular hole. This was so that filter solutions could be inserted between the lamp and the sample at a later date and the results would be comparable. The distance between the lamp and the sample was 23cm. The intensity at this point as measured using a Macam Radiometer/Photometer R101 was 77 kWm^{-2}.

First and second order kinetics were applied to the results. Unfortunately the solid state reactions did not obey these laws. The absence of any mathematical equation for the curves of concentration against time of irradiation made determination of the gradient at a specific point on the curve impossible by mathematical means. This together with the inaccuracies of drawing tangents to the curve, has led to assessments of the rates of reaction being achieved by obtaining a mean gradient between the 0 and 60 second values. Although this does not give a true value for the rate of reaction, the gradient of the line will be equal to the gradient of the curve at one point between 0 and 60 seconds and

has been used to good effect in quantitative comparisons between polymers 1-8.

4.4.2.2 Results and Discussion

In order to compare the four bands which can be used to monitor the reaction, a film of polymer 1 was cast using K bar 2. Infra-red spectra were taken after 0,30,60,90,120,180,300,420,540 and 570 seconds.

Weight of disc and film = 3.0833g

Weight of disc = 3.0759g

Weight of film = 0.0074g

$$\therefore \quad \text{thickness} = \frac{0.0074}{1256.6 \times 10^{-3} \times 1440} = 4.1 \times 10^{-6}\,m \pm 0.4 \times 10^{-6}\,m$$

Absorbance of 1765 cm^{-1} band = 0.202

Extinction coefficient ε = 207 $\ell\, M^{-1}\, cm^{-1}$

Concentration of 5,5-dimethylhydantoin = 2.44 $M\, \ell^{-1}$

$$\therefore \quad \text{thickness} = \frac{0.202}{207 \times 2.44} = 3.99 \times 10^{-6}\ m \pm 0.5 \times 10^{-6}\ m\ *$$

The difference between the two values is well within experimental error. Although weighing is the most accurate technique and was used in most cases to confirm the actual thickness determined by the absorbance method, in the cases where the surface area to weight ratio was reduced i.e. when broken potassium bromide discs were used, the absorbance method only was applied. In the cases where the discrepancies were outside the range of experimental error the value from the absorbance was used as the surface of the disc was not always perfectly flat, and possible errors of $\pm 1 \times 10^{-6}$m were observed.

The absorbances of the four bands at the different irradiation times were corrected for thickness and then the concentration was determined from the equations of the calibration curves. The results are presented in tables 4.5 a,b,c and d and in figure 4.6.

* On the basis that the majority of experimentally determined values of

ε lie between $\pm 15\ \ell M^{-1} cm^{-1}$ which would give an error of $\pm 7.2\%$.

Table 4.5a

Correction of absorbances of 1650 cm^{-1} band for thickness and the calculated concentration of unreacted chromophore remaining.

Time (seconds)	A_1	ℓ_1 ($\times 10^{-6}$m)	ℓ_2 ($\times 10^{-6}$m)	A_2	Conc^{n} (M ℓ^{-1})
0	0.348	4	3	0.261	3.41
30	0.330	4	3	0.248	3.23
60	0.317	4	3	0.238	3.10
90	0.317	4	3	0.238	3.10
120	0.311	4	3	0.233	3.03
180	0.307	4	3	0.230	2.99
300	0.297	4	3	0.223	2.89
420	0.296	4	3	0.222	2.88
540	0.296	4	3	0.222	2.88
570	0.292	4	3	0.219	2.84

Table 4.5b

Correction of absorbances of 1600 cm^{-1} band for thickness and the calculated concentration of unreacted chromophore remaining.

Time (seconds)	A_1	ℓ_1 ($\times 10^{-6}$m)	ℓ_2 ($\times 10^{-6}$m)	A_2	Conc^{n} (M ℓ^{-1})
0	1.142	4	3	0.857	3.08
30	1.065	4	3	0.799	2.88
60	1.015	4	3	0.761	2.76
90	0.989	4	3	0.742	2.69
120	0.959	4	3	0.719	2.61
180	0.934	4	3	0.701	2.55
300	0.852	4	3	0.639	2.35
420	0.803	4	3	0.602	2.22
540	0.761	4	3	0.571	2.12
570	0.752	4	3	0.564	2.09

Table 4.5c

Correction of absorbances of 1572cm^{-1} band for thickness and the calculated concentration of unreacted chromophore remaining.

Time (seconds)	A_1	ℓ_1 (x10^{-6}m)	ℓ_2 (x10^{-6}m)	A_2	Conc^{n} (M ℓ^{-1})
0	0.446	4	3	0.334	3.52
30	0.406	4	3	0.305	3.21
60	0.390	4	3	0.293	3.08
90	0.378	4	3	0.284	2.98
120	0.362	4	3	0.272	2.85
180	0.349	4	3	0.262	2.74
300	0.318	4	3	0.239	2.48
420	0.300	4	3	0.225	2.33
540	0.288	4	3	0.216	2.23
570	0.286	4	3	0.214	2.21

Table 4.5d

Correction of absorbances of 984cm^{-1} band for thickness and the calculated concentration of unreacted chromophore remaining.

Time (seconds)	A_1	ℓ_1 (x10^{-6}m)	ℓ_2 (x10^{-6}m)	A_2	Conc^{n} (M ℓ^{-1})
0	0.126	4	3	0.095	3.00
30	0.111	4	3	0.083	2.59
60	0.109	4	3	0.082	2.55
90	0.103	4	3	0.077	2.38
120	0.098	4	3	0.074	2.28
180	0.092	4	3	0.069	2.10
300	0.083	4	3	0.062	1.86
420	0.081	4	3	0.061	1.83
540	0.078	4	3	0.058	1.72
570	0.074	4	3	0.056	1.66

Application of first and second order kinetics to the above data can be

Figure 4.6
Graphs of chromophore concentration versus irradiation time in polymer 1.

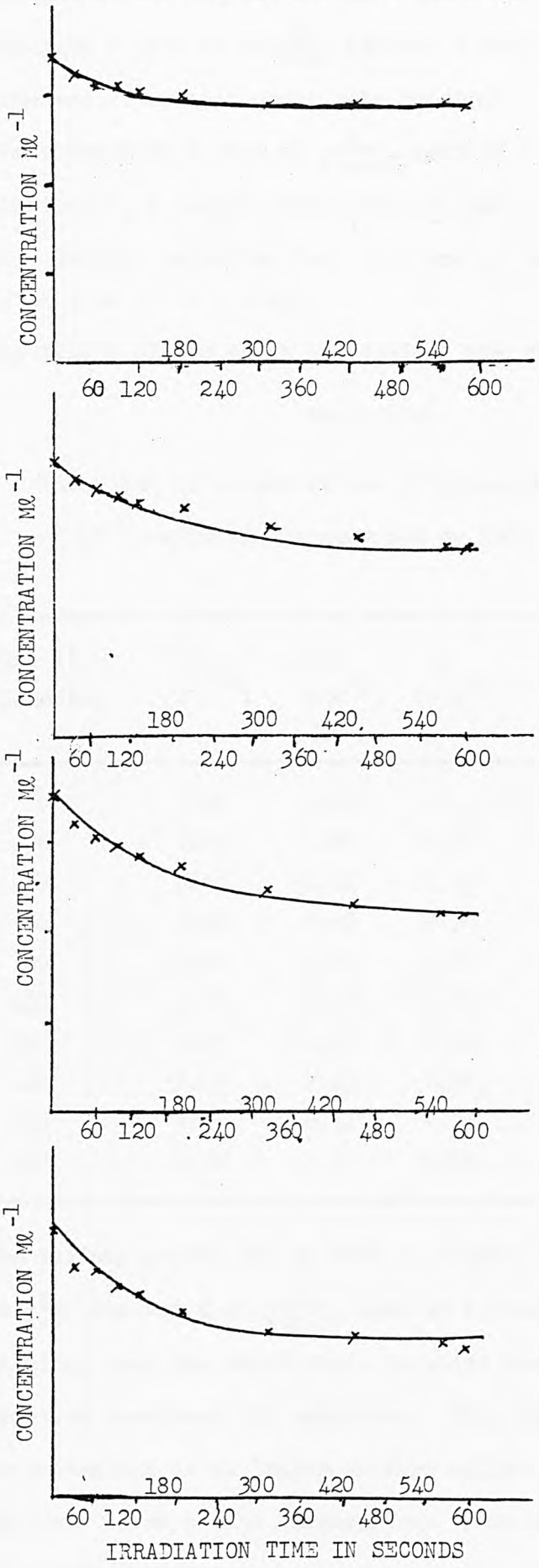

As measured by 1650cm^{-1} band.

As measured by 1600cm^{-1} band

As measured by 1572cm^{-1} band

As measured by 984cm^{-1} band

demonstrated using the 1600 cm^{-1} band. If a reaction is a first order reaction a plot of $\ln(\frac{a}{a-x})$ against t will yield a straight line of gradient k, a first order rate constant. If a reaction is a second order reaction a plot of $\frac{x}{a(a-x)}$ against t will yield a straight line of gradient k_2 a second order rate constant.

(a = initial concentration, x = amount reacted and a-x = amount left after time t, t = time).

The values of the above expressions are given in table 4.5e.

Table 4.5e

Variation of concentration of chromophore in polymer with time of irradiation as measured by 1600 cm^{-1} band.

Time (t) (Seconds)	a ($M\ \ell^{-1}$)	a-x ($M\ \ell^{-1}$)	x ($M\ \ell^{-1}$)	$\frac{a}{a-x}$	$\ln\frac{a}{a-x}$	$\frac{x}{a(a-x)}$ ($\ell\ M^{-1}$)
0	3.08	3.08	0	1	0	0
30	3.08	2.88	0.20	1.07	0.07	0.021
60	3.08	2.76	0.32	1.12	0.11	0.04
90	3.08	2.69	0.39	1.14	0.13	0.05
120	3.08	2.61	0.47	1.18	0.17	0.06
180	3.08	2.55	0.53	1.21	0.19	0.07
300	3.08	2.35	0.73	1.31	0.27	0.10
420	3.08	2.22	0.86	1.39	0.33	0.13
540	3.08	2.12	0.96	1.45	0.37	0.15
570	3.08	2.09	0.99	1.47	0.39	0.15

The various graphs can be seen in figure 4.7. As can be seen, neither $\ln\frac{a}{a-x}$ against t or $\frac{x}{a(a-x)}$ against t yield straight lines. Thus indicating that the solid state reaction does not follow simple rate kinetics developed for solutions. This is because on irradiation the concentration is no longer uniform unlike solution reactions. No account has been taken of the chromophores isolated in the solid matrix after surrounding chromophores have reacted, which absorb incident radiation but

Figure 4.7a
Graph of $\ln \frac{a}{a-x}$ against irradiation time for polymer 1.

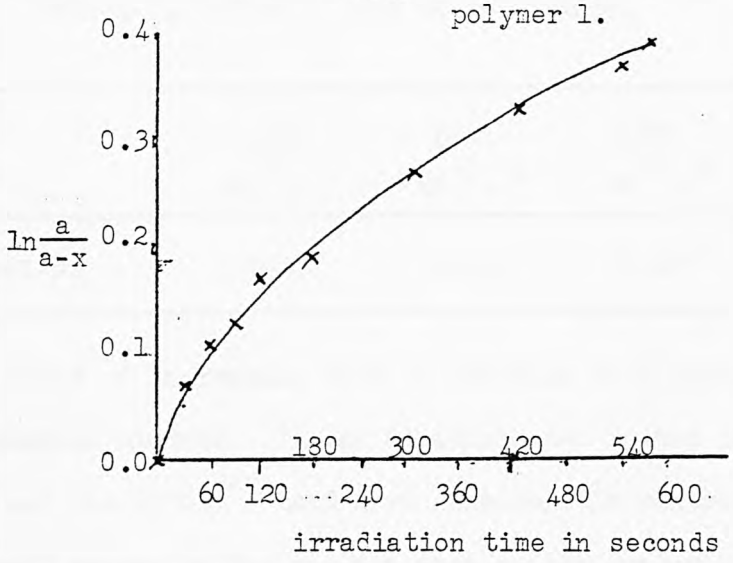

Figure 4.7b
Graph of $\frac{x}{a(a-x)}$ against irradiation time for polymer 1

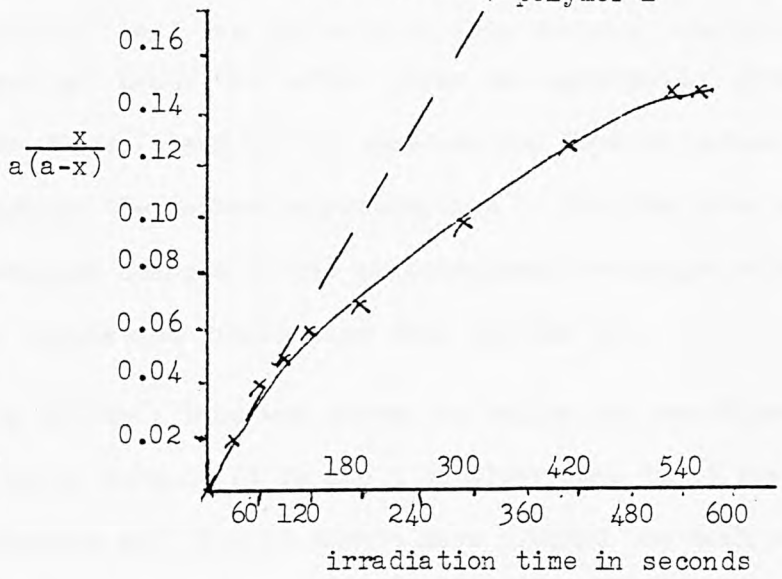

cannot react, thus reducing the effective incident light intensity.

The mean gradients between 0 and 60 seconds of the plots of concentration against time for the four different bands are presented in table 4.5f.

Table 4.5f

Mean gradients between 0-60 seconds for the 1650cm^{-1}, 1600cm^{-1}, 1572cm^{-1}, and 984cm^{-1} bands.

	1650 $M\ell^{-1}s^{-1}$	1600 $M\ell^{-1}s^{-1}$	1572 $M\ell^{-1}s^{-1}$	984 $M\ell^{-1}s^{-1}$
gradient	0.005	0.005	0.007	0.0075

This trend of increasing rate of reaction is a consistant feature of all the samples studied. It can be attributed to the fact that the 1600cm^{-1} band and the 1572cm^{-1} band have considerable contributions from other aromatic groups in the polymer such as the spacer bisphenol A group or the aromatics remaining after crosslinking has occured. However the 1600cm^{-1} band has far more of this residual absorption than the 1572cm^{-1} band and hence the latter gives the apparently greater rate of reaction. The 984cm^{-1} band has no contribution from any other source and gives perhaps the nearest approximation to the absolute rate. This could be verified using a UV/Vis photoacoustic technique with a much faster range of modulation frequencies than the OAS 400.

The 1600cm^{-1} band was chosen to follow the reactions for comparative studies because it is not a shoulder, and it is the largest band in the spectrum and thus it should have yielded the most accurate results. However it was discovered that this is only true in absorbance mode, as in the transmittance mode the low value of transmittance is seriously affected by reading errors, i.e. the error in measuring absorbance using the 1600cm^{-1}band is ±3.4% whereas the error in the smaller bands is ±2.5%.

4.4.2.3 Conclusion

It has been established that the photocrosslinking reaction can be monitored using IR spectroscopy.

4.4.3 The Effects of Varying Film Thickness and Concentration on the Measured Rate of Reaction.

4.4.3.1 Experimental Method.

The technique used was as explained in 4.4.2.1. Various thicknesses were obtained with different K bars.

4.4.3.2 Results and Discussion.

In cases where the film thickness is over 5×10^{-6}m only the $1572cm^{-1}$ band and the $984cm^{-1}$ band are used as the $1600cm^{-1}$ band absorbance is no longer proportional to concentration. The following data were extracted from spectra.

Table 4. 6a

Rates of reaction as measured by the $1600cm^{-1}$, $1572cm^{-1}$ and $984cm^{-1}$ bands for polymer 1.

Thickness $x10^{-6}$m	$1600cm^{-1}$ $M\ell^{-1}s^{-1}$	C_o $M\ell^{-1}$	$1572cm^{-1}$ $M\ell^{-1}s^{-1}$	C_o $M\ell^{-1}$	$984cm^{-1}$ $M\ell^{-1}s^{-1}$	C_o $M\ell^{-1}$
0.75	0.023	3.76	0.030	4.30	-	-
0.94	0.021	3.57	0.027	3.79	0.030	4.13
1.29	0.019	3.29	0.022	3.20	-	-
1.36	0.018	3.42	0.022	3.25	0.030	3.86
1.42	0.012	3.04	0.017	3.19	0.024	3.52
1.68	0.015	3.18	0.019	3.51	0.018	3.31
2.02	0.012	3.14	0.018	3.17	0.017	2.85
2.81	0.013	3.23	0.016	3.12	0.022	2.85
3.70	0.009	2.84	0.011	3.01	0.013	3.30
4.20	0.008	2.94	0.011	2.97	0.016	3.22

C_o = Initial concentration.

Figure 4.8a
Rate of reaction vs thickness for polymer 1.

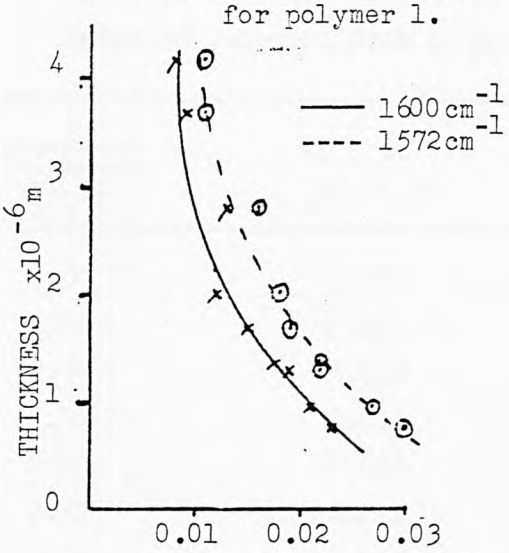

Figure 4.8b
Rate of reaction vs the inverse of thickness for polymer 1.

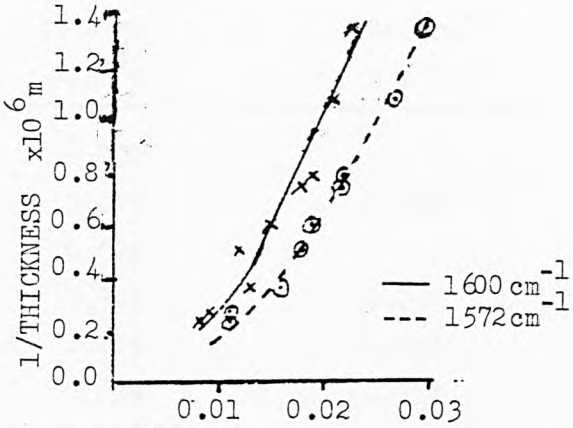

RATE OF REACTION M$\ell^{-1}s^{-1}$

Figure 4.8c
Rate of reaction vs thickness for polymer 2.

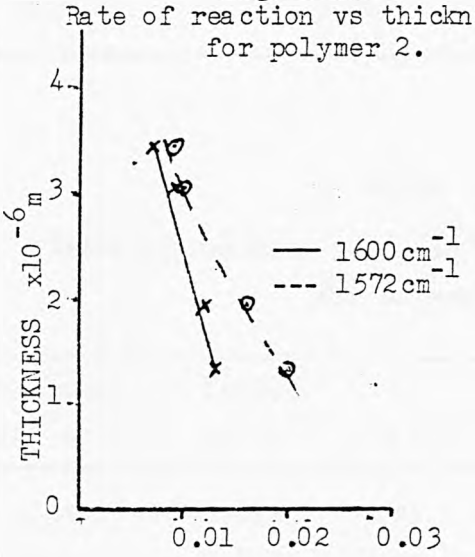

Figure 4.8d
Rate of reaction vs the inverse of thickness for polymer 2.

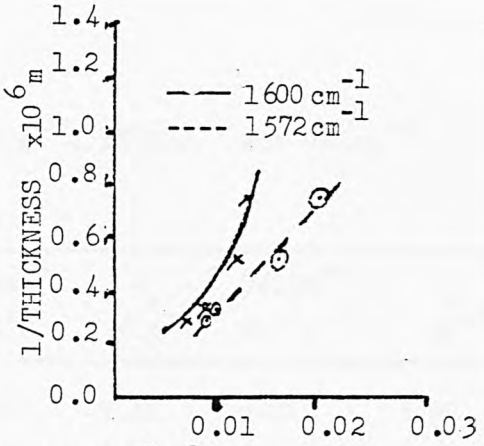

RATE OF REACTION M$\ell^{-1}s^{-1}$

Figure 4.8e
Rate of reaction vs thickness for polymer 3.

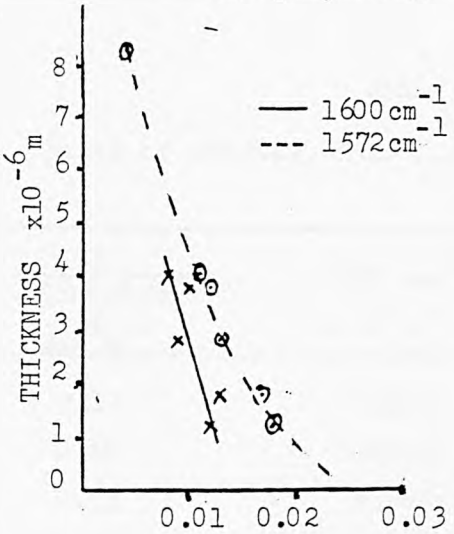

Figure 4.8f
Rate of reaction vs the inverse of thickness for polymer 3.

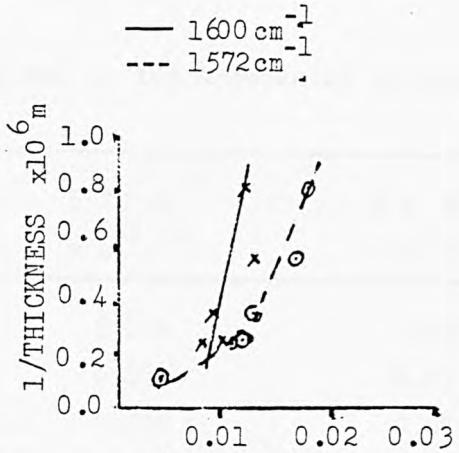

RATE OF REACTION M$\ell^{-1}s^{-1}$

Table 4. 6b

Rates of reaction from 4. 6a compared to inverse of thickness.

$\frac{1}{\text{Thickness}}$ $\times 10^{6}\,m^{-1}$	1600 cm^{-1} $M\,\ell^{-1}s^{-1}$	1572 cm^{-1} $M\,\ell^{-1}s^{-1}$	984 cm^{-1} $M\,\ell^{-1}s^{-1}$
1.33	0.023	0.030	-
1.06	0.021	0.027	0.030
0.78	0.019	0.022	-
0.74	0.018	0.022	0.030
0.60	0.015	0.019	0.018
0.50	0.012	0.018	0.017
0.36	0.013	0.016	0.022
0.27	0.009	0.011	0.013
0.24	0.008	0.011	0.016

Table 4.6c

Rates of reaction measured by 1600cm^{-1}, 1572cm^{-1} and 984cm^{-1} for polymer 2.

Thickness $\times 10^{-6}\,m$	1600cm^{-1} $M\ell^{-1}s^{-1}$	C_o $M\,\ell^{-1}$	1572cm^{-1} $M\ell^{-1}s^{-1}$	C_o $M\,\ell^{-1}$	984cm^{-1} $M\ell^{-1}s^{-1}$	C_o $M\ell^{-1}$
1.33	0.013	3.21	0.020	3.48	0.021	3.92
1.93	0.012	2.95	0.016	3.12	0.013	3.21
3.01	0.009	3.04	0.010	3.18	0.013	3.37
3.39	0.007	2.94	0.009	3.06	0.011	2.90

Table 4.6d

Rates of reaction from 4.6c compared to the inverse of thickness.

$\frac{1}{\text{Thickness}}$ $\times 10^{6}\,m^{-1}$	1600 cm^{-1} $M\,\ell^{-1}s^{-1}$	1572 cm^{-1} $M\,\ell^{-1}s^{-1}$	984 cm^{-1} $M\,\ell^{-1}s^{-1}$
0.75	0.013	0.020	0.021
0.52	0.012	0.016	0.013
0.33	0.009	0.010	0.013
0.29	0.007	0.009	0.011

Table 4.6e

Rates of reaction measured using 1600 cm^{-1}, 1572 cm^{-1} and 984 cm^{-1} bands for polymer 3.

Thickness x10^{-6} m	1600 cm^{-1} M $\ell^{-1}s^{-1}$	C_o Mℓ^{-1}	1572 cm^{-1} M $\ell^{-1}s^{-1}$	C_o Mℓ^{-1}	984 cm^{-1} M $\ell^{-1}s^{-1}$	C_o Mℓ^{-1}
1.20	0.012	2.48	0.018	2.74	0.020	2.83
1.79	0.013	2.73	0.017	2.62	0.022	3.14
2.80	0.009	2.56	0.013	2.59	0.016	2.57
3.79	0.010	2.73	0.012	2.53	0.015	2.51
4.05	0.008	2.52	0.011	2.49	0.011	2.38
8.33	-	-	0.004	2.30	0.009	2.48

Table 4.6f

Rates of reaction from table 4.6e compared to the inverse of thickness.

$\frac{1}{\text{Thickness}}$ x10^{6} m^{-1}	1600 cm^{-1} M $\ell^{-1}s^{-1}$	1572 cm^{-1} M $\ell^{-1}s^{-1}$	984 cm^{-1} M $\ell^{-1}s^{-1}$
0.83	0.012	0.018	0.020
0.56	0.013	0.017	0.022
0.36	0.009	0.013	0.016
0.26	0.010	0.012	0.015
0.25	0.008	0.011	0.011
0.12	-	0.004	0.009

Table 4.6g

Rates of reaction measured by 1600 cm^{-1}, 1572 cm^{-1} and 984 cm^{-1} bands for polymer 4.

Thickness x10^{-6} m	1600 cm^{-1} M$\ell^{-1}s^{-1}$	C_o Mℓ^{-1}	1572 cm^{-1} M$\ell^{-1}s^{-1}$	C_o Mℓ^{-1}	984 cm^{-1} M$\ell^{-1}s^{-1}$	C_o Mℓ^{-1}
0.89	0.016	2.46	0.02	2.60	-	-
2.17	0.009	2.12	0.012	2.09	0.015	1.77
2.24	0.008	2.11	0.011	2.11	0.013	2.32
3.83	0.006	2.02	0.009	2.03	0.011	2.07

Table 4.6h

Rates of reaction from table 4.6g compared to the inverse of thickness.

$\frac{1}{\text{Thickness}}$ $\times 10^{6}\,m^{-1}$	$1600\,cm^{-1}$ $M\,\ell^{-1}s^{-1}$	$1572\,cm^{-1}$ $M\,\ell^{-1}s^{-1}$	$984\,cm^{-1}$ $M\ell^{-1}s^{-1}$
1.12	0.016	0.020	-
0.46	0.009	0.012	0.015
0.45	0.008	0.011	0.013
0.26	0.006	0.009	0.011

Table 4.6i

Rates of reaction measured by $1600\,cm^{-1}$, $1572\,cm^{-1}$ and $984\,cm^{-1}$ bands for polymer 5.

Thickness $\times 10^{-6}\,m$	$1600\,cm^{-1}$ $M\ell^{-1}s^{-1}$	C_o $M\ell^{-1}$	$1572\,cm^{-1}$ $M\ell^{-1}s^{-1}$	C_o $M\ell^{-1}$	$984\,cm^{-1}$ $M\ell^{-1}s^{-1}$	C_o $M\ell^{-1}$
1.45	0.007	1.73	0.008	1.63	-	-
2.25	0.007	1.53	0.009	1.41	-	-
3.42	0.005	1.58	0.006	1.34	-	-
5.11	0.003	1.29	0.005	1.34	-	-
5.39	0.004	1.46	0.004	1.20	-	-
5.68	0.003	1.32	0.005	1.34	-	-

Table 4.6j

Rates of reaction from table 4.6i compared to inverse of thickness.

$\frac{1}{\text{Thickness}}$ $\times 10^{6}\,m^{-1}$	$1600\,cm^{-1}$ $M\ell^{-1}s^{-1}$	$1572\,cm^{-1}$ $M\ell^{-1}s^{-1}$
0.69	0.007	0.008
0.44	0.007	0.009
0.29	0.005	0.006
0.20	0.003	0.005
0.19	0.004	0.004
0.18	0.003	0.005

The results for polymers 6 and 7 came within the nonlinear section of the curve which requires further calibration and thus they are not presented here.

The errors involved are as follows:-

±1% error in reading absorbance and ±10% in estimating thickness by weighing or ±12% by using the 1765cm^{-1} band. This gives rise to a minimum error of ±11% in concentration which converts to a 53% error in the calculated rates of reaction. This is because the initial concentration and the concentration after 60 seconds may both be wildly out. This could be significantly reduced by increasing the statistical confidence in the figure of 207 $\ell\ M^{-1}cm^{-1}$ which is used for ε, the extinction coefficient of the 1765cm^{-1} band. This would be done by increasing the number of experiments performed to discover the extinction coefficient. As an example, the application of the above errors to the 1.29×10^{-6}m film of polymer 1 would give a rate of reaction between 0.009 and 0.028 $M\ell^{-1}s^{-1}$ virtually wiping out the trends shown in table 4.6a. However although the large errors stated account for the more inconsistent results, the majority of the results show a linear relationship between the inverse of the film thickness and the rate of reaction, i.e. the thinner the film the faster the measured rate of reaction, (except at high thicknesses when the line starts to tail off. This is possibly due to all the light being absorbed so that at the lower depths cure will be slow if it goes at all). This relationship is caused by measuring the chromophore concentration through the whole film whereas the reaction gradually works down from the top giving rise to the thicker films having more chromophore remaining. Another factor is that 50% of the chromophore remains after cure is complete reducing the intensity more in the lower regions of the thicker films. Errors also seem to occur in the estimation of initial concentration, the thicker films giving lower values. This has been attributed to the deviation from the Beer-Lambert law observed when the transmittance is under 40%.

Figure 4.8g
Rate of reaction vs thickness for polymer 4.

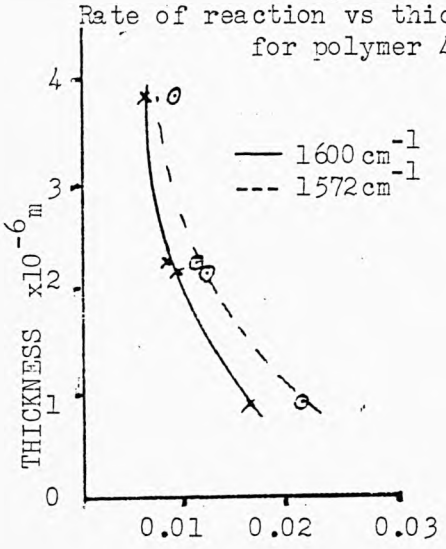

Figure 4.8h
Rate of reaction vs the inverse of thickness for polymer 4.

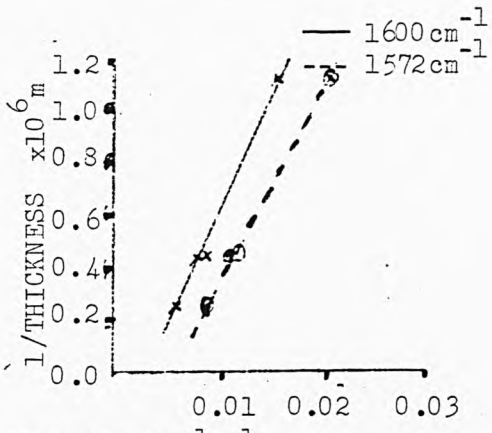

RATE OF REACTION M$\ell^{-1}s^{-1}$

Figure 4.8i
Rate of reaction vs thickness for polymer 5.

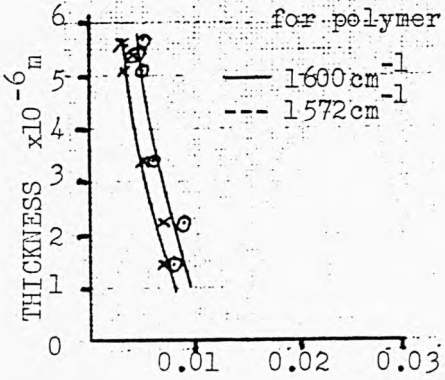

Figure 4.8j
Rate of reaction vs the inverse of thickness for polymer 5.

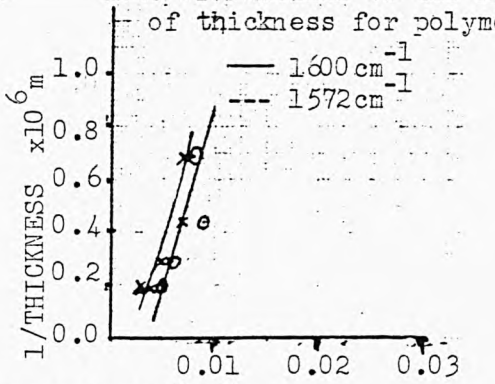

RATE OF REACTION M$\ell^{-1}s^{-1}$

Figure 4.8ℓ
Rate of reaction vs initial concentration over 0.85 - 1.35µm.

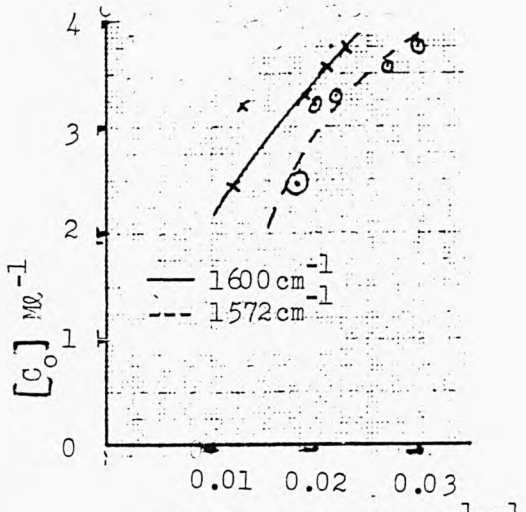

RATE OF REACTION M$\ell^{-1}s^{-1}$

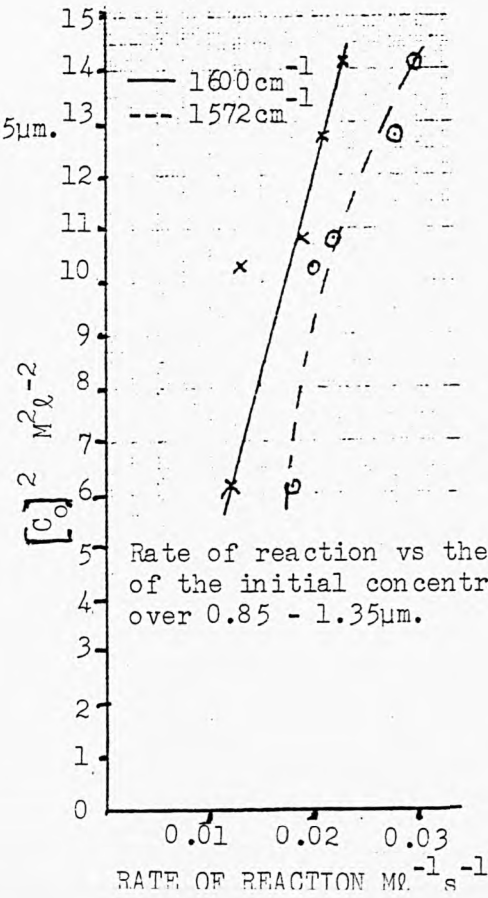

Rate of reaction vs the square of the initial concentration over 0.85 - 1.35µm.

RATE OF REACTION M$\ell^{-1}s^{-1}$

A variation in the ratios of the bands due to the chromophore and to the 1765cm^{-1} band of the hydantoin was observed. This could be caused by high or low concentrations of the chromophore compared to the overall bulk concentration because of a variation in the number of branched chains caused by reaction of epoxide groups with hydroxyl groups formed from previous epoxide ring opening.

A result that confirms the dependance of rate of reaction on thickness is the time taken to reach 45% cure as measured by the 1600cm^{-1} band. The fact that polymers 2,3,4,5 all go to 45% cure and more was predicted by the model presented in chapter 3. However the times to achieve the extra cure are considerable, e.g. polymer 3 45% after 840 seconds, 49% after 1560 seconds. Taking the forcing conditions into account i.e. 20 minutes spent at 80-100^{o}C under very strong UV light it is not inconcievable that some of the 'extra cure' is due to photo-oxidation.

Table 4.6k

Length of irradiation time required to reach 45% cure as measured by the 1600cm^{-1} band. For polymers 1,2,3,4,5,6 and 7 of various film thicknesses.

Polymer 1		Polymer 2	
Film Thickness x 10^{-6}m	Irradiation Time seconds.	Film Thickness x 10^{-6}m	Irradiation Time seconds.
4.00	700	3.39	660
2.81	480	3.01	660
2.02	420	1.93	540
0.94	180	1.33	450

Polymer 3		Polymer 4	
Film Thickness x 10^{-6}m	Irradiation Time seconds	Film Thickness x 10^{-6}m	Irradiation Time seconds
4.05	840	3.83	960
3.79	840	2.24	690
2.80	660	0.89	210
1.79	540		
1.20	500		

Polymer 5

Film Thickness x 10^{-6}m	Irradiation Time seconds
5.39	1140
3.42	1020
2.25	780
1.45	620

The results obtained for polymer 5 fall into the region of nonlinearity and thus not much weight can be put on these times to reach 45% cure.

It should be noted here that when the 1600 cm^{-1} band indicates 45% cure has taken place, the 1572 cm^{-1} band shows 55% cure. This difference is again attributed to the greater amount of residual absorption remaining because of the aromatic groups present at 1600 cm^{-1}. In a lot of cases the estimation of the transmittance and hence absorbance at 984 cm^{-1} is made difficult by the lack of any definite peak. Thus the errors involved in this case are very large.

By presenting the data shown in tables 4.6a -4.6j in a different way the effect of varying the chromophore concentration can be demonstrated. By taking film thicknesses over a range 0.5μm (or 0.8μm for the thicker films) the following tables can be generated.

Table 4.6ℓ

Variation of rate of reaction with concentration over thickness range 0.85 - 1.35 x 10^{-6}m.

Initial Conc^{n} $M\,\ell^{-1}$	1600 cm^{-1} $M\,\ell^{-1}s^{-1}$	1572 cm^{-1} $M\,\ell^{-1}s^{-1}$	984 cm^{-1} $M\,\ell^{-1}s^{-1}$	(Conc^{n})^{2} $M^{2}\ell^{-2}$
3.76	0.023	0.030	-	14.14
3.57	0.021	0.027	0.03	12.74
3.29	0.019	0.022	-	10.82
3.21	0.013	0.020	0.021	10.30
2.48	0.012	0.018	0.020	6.15

Table 4.6m

Variation of rate of reaction with concentration over thickness range 1.35 - 1.85 x 10^{-6}m.

Initial Conc^{n} $M\,\ell^{-1}$	1600 cm^{-1} $M\,\ell^{-1}s^{-1}$	1572 cm^{-1} $M\,\ell^{-1}s^{-1}$	984 cm^{-1} $M\,\ell^{-1}s^{-1}$	(Conc^{n})^{2} $M^{2}\,\ell^{-2}$
3.42	0.018	0.022	0.030	11.70
3.18	0.015	0.019	0.018	10.11
3.04	0.012	0.017	0.024	9.24
2.93	0.012	0.016	0.013	8.58
2.73	0.013	0.017	0.022	7.45
1.73	0.007	0.008	-	2.99

Table 4.6n

Variation of rate of reaction with concentration over thickness range 1.85 - 2.35 x 10^{-6}m.

Initial Conc^{n} $M\,\ell^{-1}$	1600 cm^{-1} $M\,\ell^{-1}s^{-1}$	1572 cm^{-1} $M\,\ell^{-1}s^{-1}$	984 cm^{-1} $M\,\ell^{-1}s^{-1}$	(Conc^{n})^{2} $M^{2}\,\ell^{-2}$
3.14	0.012	0.018	0.017	9.86
2.95	0.012	0.016	0.013	8.70
2.12	0.009	0.012	0.015	4.49

Table 4.6n continued.

Initial Conc^{n} $M\,\ell^{-1}$ ..	1600 cm^{-1} $M\,\ell^{-1}s^{-1}$	1572 cm^{-1} $M\,\ell^{-1}s^{-1}$	984 cm^{-1} $M\,\ell^{-1}s^{-1}$	$(Conc^{n})^{2}$ $M^{2}\,\ell^{-2}$
2.11	0.008	0.011	0.013	4.45
1.53	0.006	0.009	-	2.34

Table 4.6o

Variation of rate of reaction with concentration over thickness range 2.6 - 3.4 x 10^{-6}m.

Initial Conc^{n} $M\,\ell^{-1}$	1600 cm^{-1} $M\,\ell^{-1}s^{-1}$	1572 cm^{-1} $M\,\ell^{-1}s^{-1}$	984 cm^{-1} $M\,\ell^{-1}s^{-1}$	$(Conc^{n})^{2}$ $M^{2}\,\ell^{-2}$
3.23	0.013	0.016	0.022	10.43
3.04	0.009	0.010	0.016	9.24
2.94	0.007	0.009	0.011	8.64
2.56	0.008	0.012	0.016	6.55
1.58	0.005	0.006	-	2.50

Table 4.6p

Variation of rate of reaction with concentration over thickness range 3.6 - 4.4 x 10^{-6}m.

Initial Conc^{n} $M\,\ell^{-1}$	1600 cm^{-1} $M\,\ell^{-1}s^{-1}$	1572 cm^{-1} $M\,\ell^{-1}s^{-1}$	984 cm^{-1} $M\,\ell^{-1}s^{-1}$	$(Conc^{n})^{2}$ $M^{2}\,\ell^{-2}$
2.84	0.009	0.011	0.013	8.076
2.92	0.007	0.011	0.016	8.53
2.73	0.010	0.012	0.015	7.45
2.52	0.008	0.011	0.011	6.35
2.02	0.006	0.009	0.011	4.08

The above results give a reasonable straight line plot when the rate is plotted against the square of the <u>initial</u> concentration. Thus indicating that over the first minute the reaction posesses a large degree of second order character. However in the previous section 4.4.2 it was shown that

Figure 4.8m

Rate of reaction vs initial concentration over 1.35 - 1.85μm.

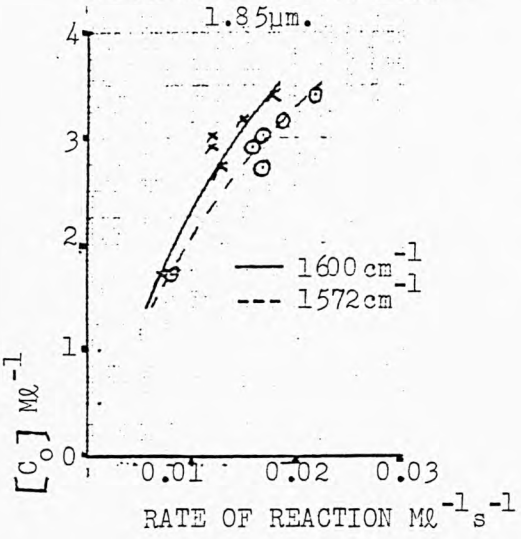

Rate of reaction vs the square of the initial concentration over 1.35-1.85μm.

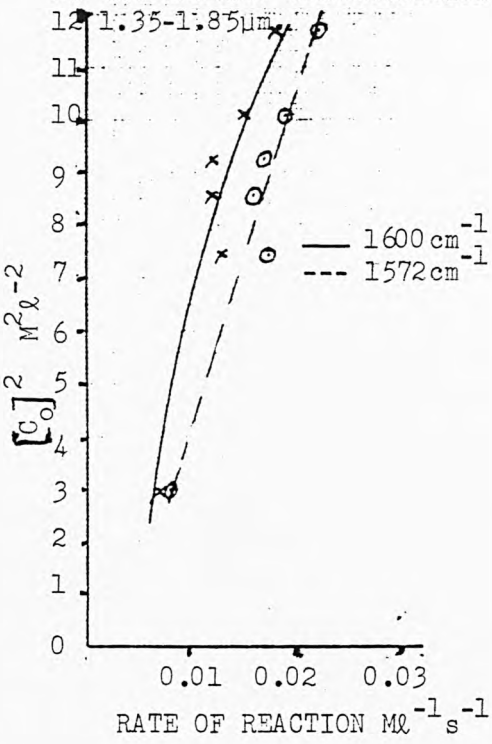

Figure 4.8n

Rate of reaction vs initial concentration over 1.85 - 2.35μm.

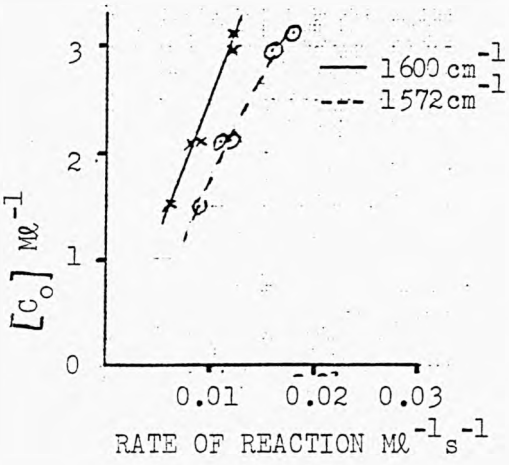

Rate of reaction vs the square of the initial concentration over 1.85 - 2.35μm.

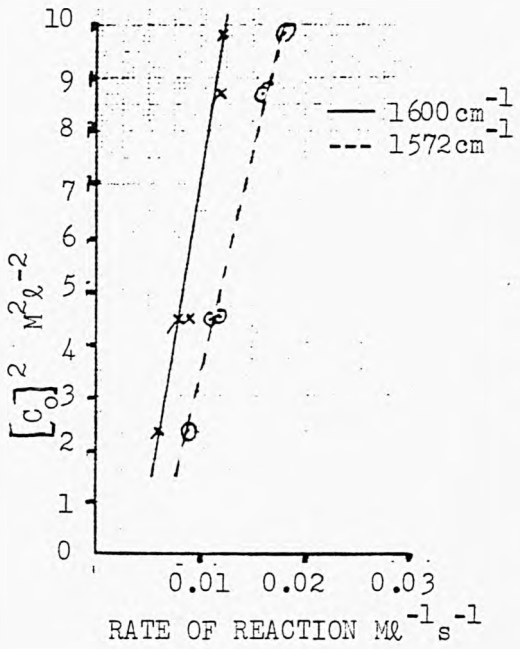

Figure 4.8o
Rate of reaction vs initial concentration over 2.6 - 3.4μm.

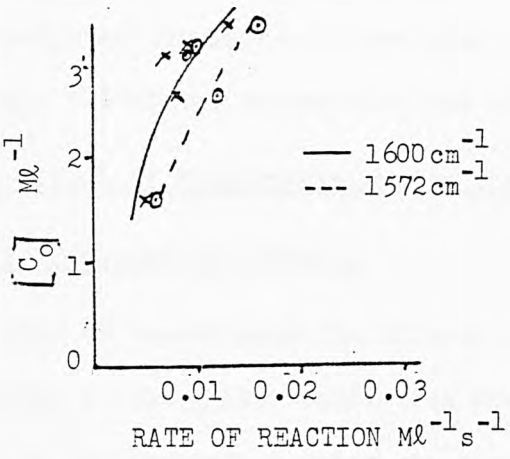

Rate of reaction vs the square of the initial concentration over 2.6 - 3.4μm.

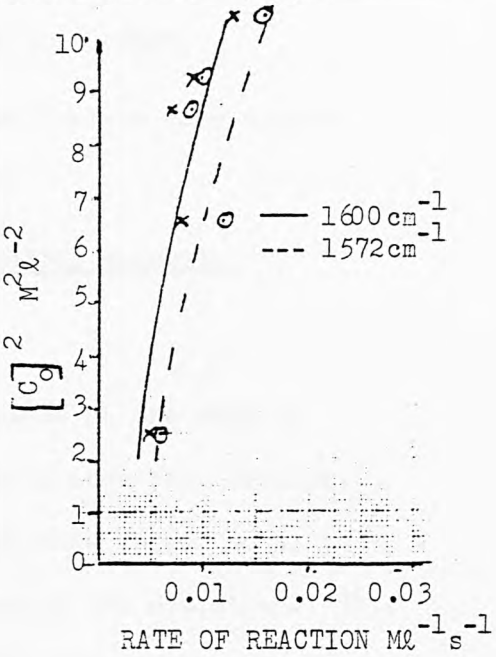

Figure 4.8p
Rate of reaction vs initial concentration over 3.6 - 4.4μm.

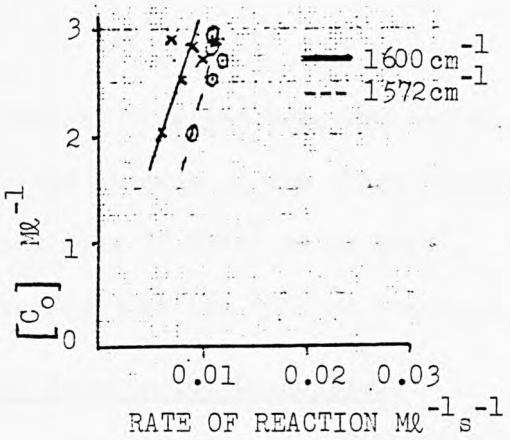

Rate of reaction vs the square of the initial concentration over 3.6 - 4.4μm.

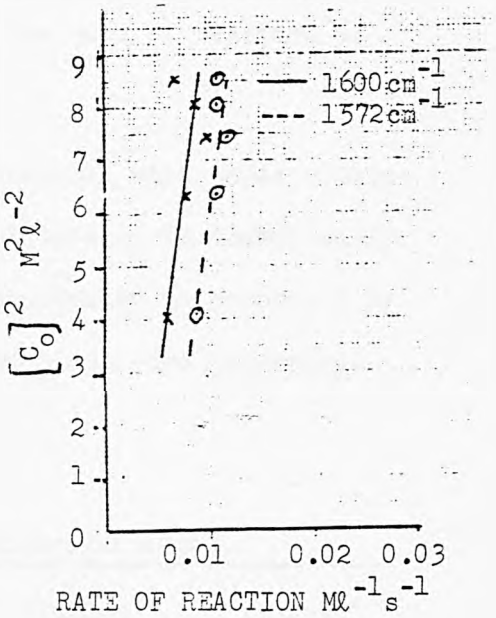

simple second order kinetics are not followed once a significant reduction in chromphore concentration is reached. In conclusion it can be said that the rate is dependant upon the inverse of the thickness and the square of the initial concentration up to a point.

As predicted in chapter 3 cure will not proceed further once approximately 50% of the chromophore has crosslinked.

4.5 Effect of Temperature on the Photodimerization Reaction.

4.5.1 Experimental Method.

In order to investigate the effects of temperature on the rate of reaction a flat glass vessel (8cm diameter) was placed over the 7cm hole in the apparatus, water was pumped through this vessel so as to remove heat generated by the absorption of some of the radiation. This had the added effect of cooling the irradiation compartment. However the equilibrium temperature of the compartment was still 55-60^{o}C. In order to reduce the temperature further, ice-baths were placed inside the compartment, which allowed measurement of the rate of reaction at both 40^{o}C and 25^{o}C.

The results obtained here are not directly comparable with those obtained in the absence of the glass vessel, as the intensity is dramatically reduced from 77 kW/m^{2} to 64 kW/m^{2}. It was demonstrated in chapter 2 by UV/Vis PAS that the rate of reaction is dependant upon the intensity.

4.5.2 Results and Discussion.

Table 4.7

Effect of temperature on rate of crosslinking.

Temperature ^{o}C	Thickness x10^{-6}m	Initial Conc^{n} M ℓ^{-1}	1600cm^{-1} M $\ell^{-1}s^{-1}$	1572cm^{-1} M $\ell^{-1}s^{-1}$
25	3.52	3.06	0.002	0.003
40	3.15	3.24	0.003	0.004
60	2.79	3.42	0.005	0.006

The results are for films of comparable thickness and show that there is a temperature dependance of the rate of reaction. This is attributed to the higher mobility of the polymer chains at higher temperatures which allows chromophores to move into reactive positions.

4.6 Infra-red Study of the Photocrosslinking reaction of Polymers A-F.

4.6.1 Introduction.

The method outlined in section 4.4 was extended to the system in which the chromphore was changed by adding an extra C-C double bond i.e. where chalcone was replaced by dibenzal-acetone

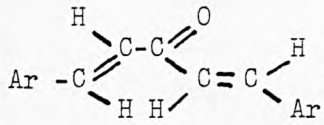

in place of

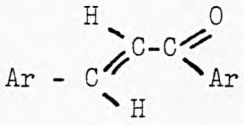

It was again necessary to calibrate the IR spectra using polymers with varying concentrations of chromophore. Thus polymers A-F were made (see chapter 6). Films were produced on KBr discs, the thickness of which was obtained by weighing the disc before and after the film was deposited, and then dividing this weight by the density and the area. The thickness was also assessed using the 1765cm^{-1} absorption band in the spectrum attributed to a carbonyl group of the hydantoin moiety. A sample of polymer A in which the concentration of the starting materials was unknown (polymer X made by Ciba-Geigy, Duxford) was used in many of the experiments hence the high initial concentration. It is postulated that the original diglycidyl ether of 4,4-dihydroxy-benzalacetone had a low epoxy value and thus a considerable amount over the stated ratio for polymer A was added.

4.6.2 Determination of Calibration Graphs.

The densities of the polymers A-F and the concentrations of the various components are presented in table 4.8a.

A decrease in the density with increase in the concentration of bisphenol A is again observed (The density of a polymer containing only bisphenol A and dimethylhydantoin is 1140kg m^{-3}). The anomally of polymer A is explained by the fact that the initial dibenzalacetone

Table 4.8a

Concentrations of the different components in polymers A-F together with the densities.

Polymer	Density kg/m^3	Conc^n DBA M/ℓ	Conc^n BPA M/ℓ	Conc^n DMH M/ℓ
A	1175	2.39	0	2.12
B	1260	2.34	0.25	2.24
C	1270	2.12	0.51	2.32
D	1196	1.77	0.72	2.19
E	1126	1.22	1.16	2.11
F	1146	0.76	1.71	2.18

DBA = dibenzalacetone derivative BPA = bisphenol A derivative DMH = dimethylhydantoin

diglycidyl ether was of a higher epoxy value than that used for the other polymers(i.e.5.19 compared to 5.06). Thus less of the higher density component was added as the amount used is calculated from an effective molecular weight which is based on the 'purity' of the reactant as given by the epoxy value. The error in the density is again ±4%.

In order to assess the validity of the assumption that the extinction coefficient of the carbonyl band at 1765 cm^{-1} does not vary between the 2 polymer series, films of the polymers were formed on the large KBr discs. The thicknesses calculated from the weighing and from the spectra are presented in table 4.8b. The spectra are shown in figure 4.9.

Although some variation is observed, the results are consistent in most cases. The anomalies can be explained by the slight uneveness of the KBr discs.

A large number of spectra of all six polymers were obtained, and the thickness of the films was estimated using the 1765 cm^{-1} band. A representative sample of the data is presented in the following tables. The data is corrected to a thickness of 3×10^{-6}m as in the previous series studied. The points were treated using a least square computor pro-

Figure 4.9a IR spectrum of polymer A.

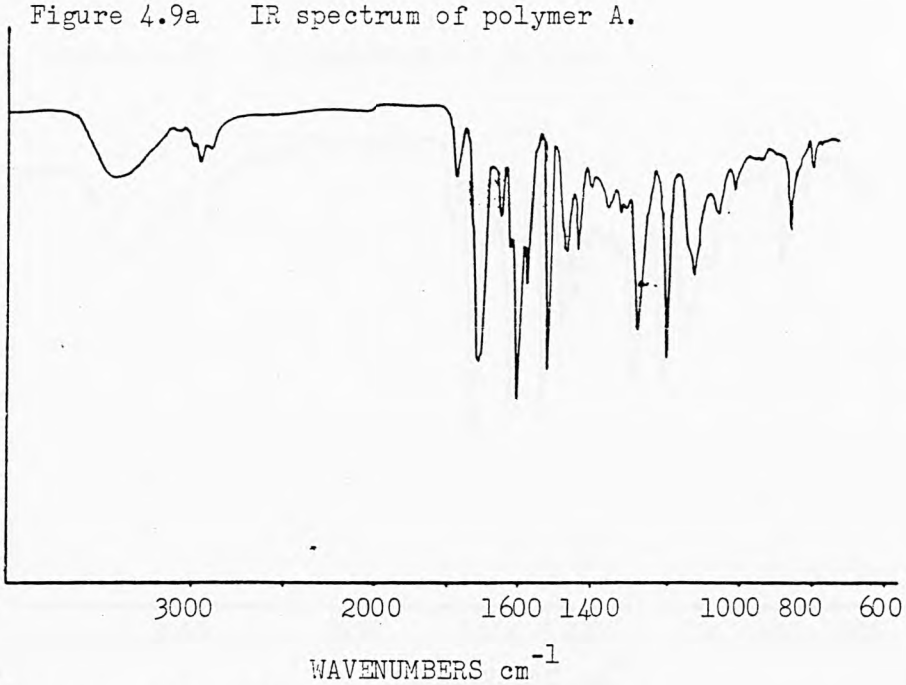

Figure 4.9b IR spectrum of polymer B.

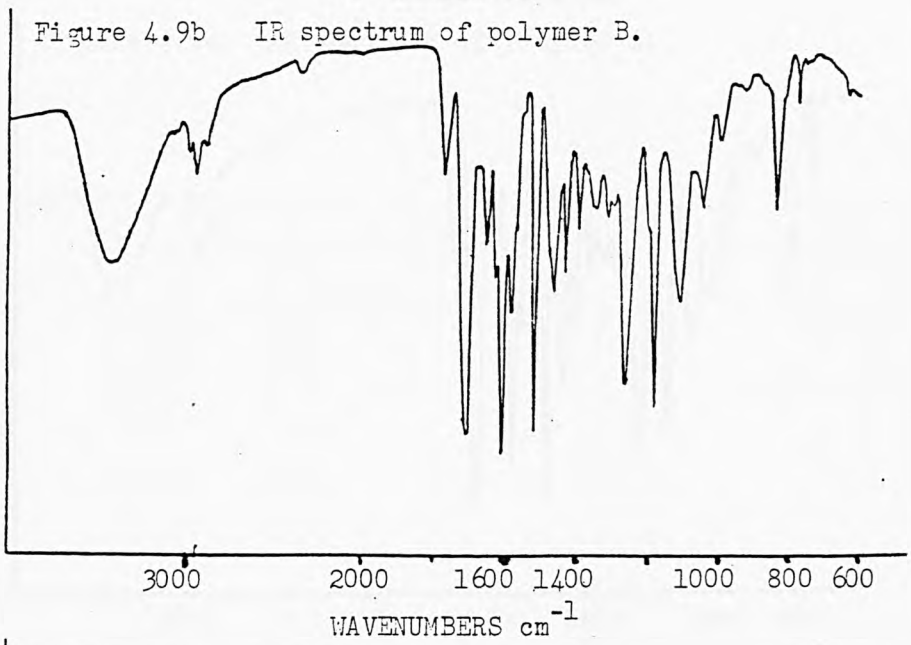

Figure 4.9c IR spectrum of polymer C.

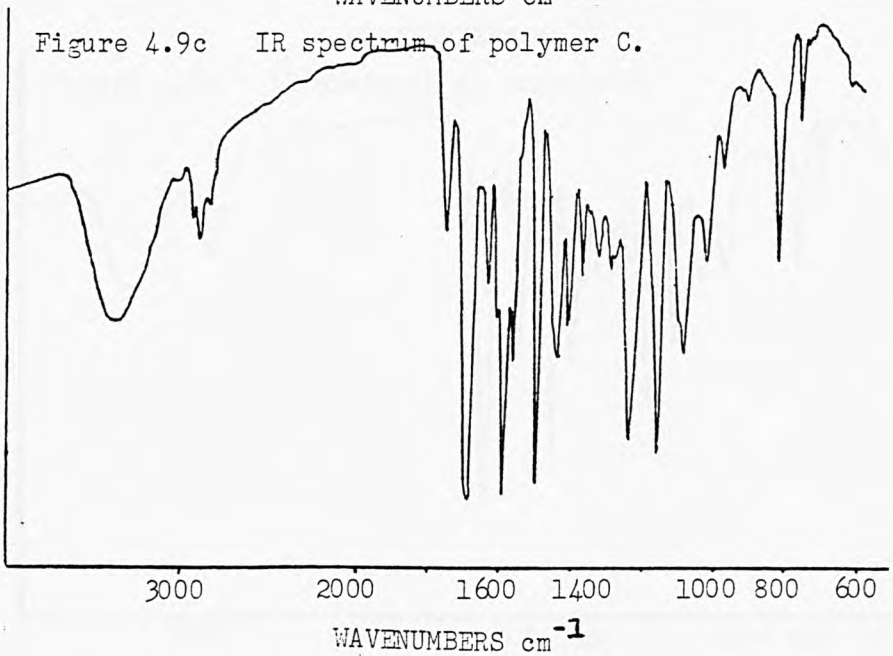

Figure 4.9d IR spectrum of polymer D.

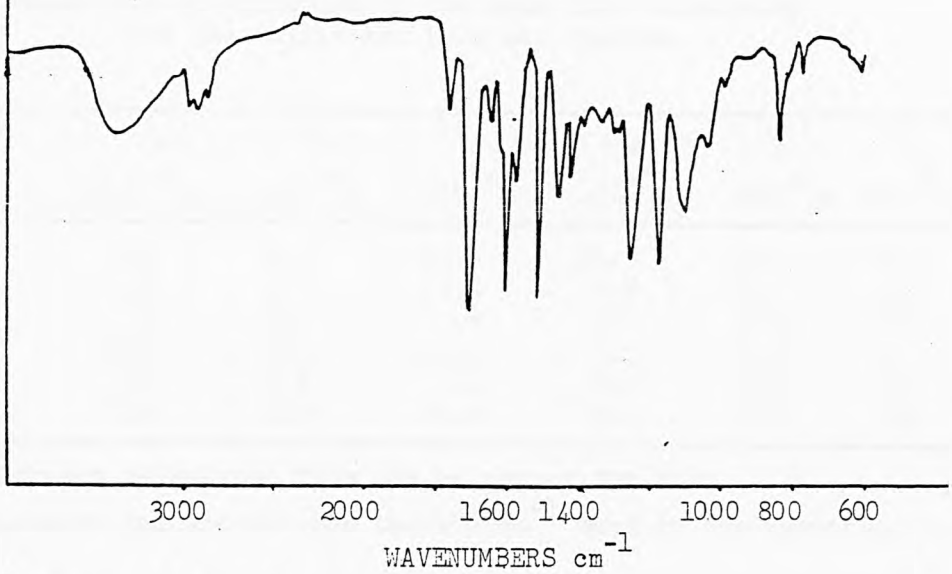

Figure 4.9e IR spectrum of polymer E.

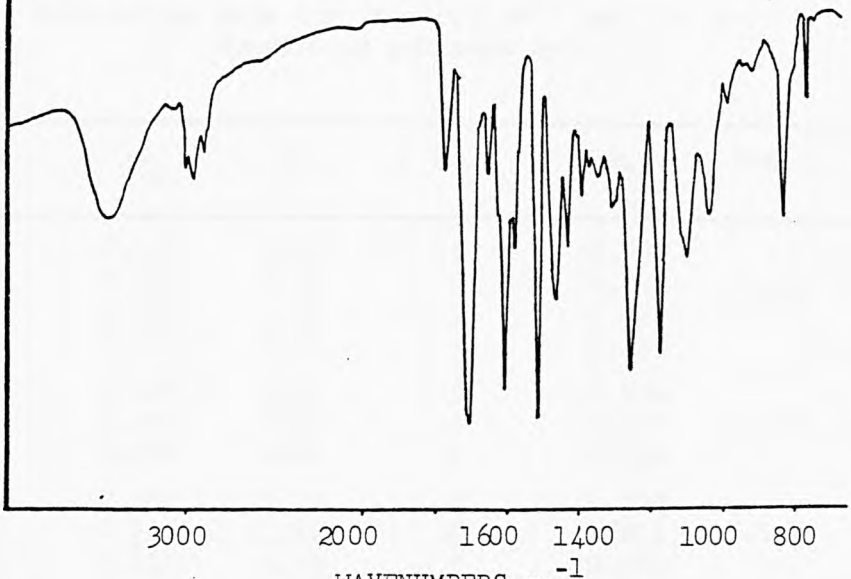

Figure 4.9f IR spectrum of polymer F.

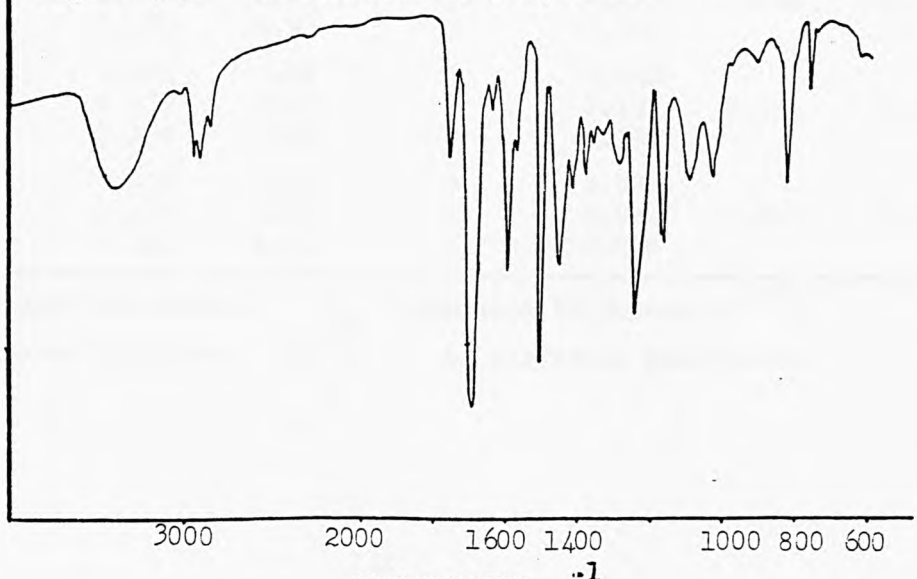

gramme in order to find the best straight line.

Table 4.8b

Comparison of thickness of the same film calculated from the weight and from the spectra.

Polymer	ℓ_w x10^{-6}m	ℓ_s x10^{-6}m	ℓ_w x10^{-6}m	ℓ_s x10^{-6}m	ℓ_w x10^{-6}m	ℓ_s x10^{-6}m
A	2.7	2.4	10.0	10.3	3.2	3.2
B	2.2	1.6	5.8	5.9	2.2	2.3
C	3.3	3.2	1.8	1.7	1.6	2.0
D	8.5	8.9	3.3	3.3	1.3	1.7
E	7.4	7.4	3.4	3.0	1.6	1.8
F	3.8	3.5	8.6	8.3	3.5	3.8

ℓ_w = thickness calculated from the weight of the film.

ℓ_s = thickness calculated from the 1765cm^{-1} band in the spectrum.

Table 4.8c

Calibration data for the 1645 cm^{-1} band in the spectra of polymers A-F.

Polymer	A_1	ℓ_1	ℓ_2	A_2	Mean	Conc^n M/ℓ
A	0.129	1.63	3	0.237		
A	0.233	3.12	3	0.224	0.230	2.39
A	0.143	1.91	3	0.225		
A	0.175	2.23	3	0.235		
B	0.220	2.80	3	0.236		
B	0.227	2.87	3	0.237	0.237	2.34
B	0.079	1.01	3	0.238		
C	0.510	8.01	3	0.198		
C	0.112	1.65	3	0.204	0.198	2.12
C	0.213	3.19	3	0.200		
D	0.183	3.23	3	0.170		
D	0.095	1.65	3	0.173	0.168	1.77
D	0.475	8.90	3	0.160		
E	0.094	1.98	3	0.142		
E	0.137	3.00	3	0.137	0.136	1.22
E	0.238	5.35	3	0.133		
F	0.059	1.93	3	0.092		
F	0.106	3.77	3	0.084	0.085	0.76
F	0.223	8.34	3	0.080		

A_1 = measured absorbance ℓ_2 = standard thickness x10^{-6}m

ℓ_1 = measured thickness x 10^{-6}m A_2 corrected absorbance.

Equation of the line $y = 0.088x + 0.02$

Gradient of line $= \varepsilon\ell = 0.088 \pm 0.01 = 12.5\%$ error

$\therefore \varepsilon = \frac{0.088}{3 \times 10^{-4}} = 293.3\ \ell\ M^{-1}cm^{-1}$

$\therefore$ optical absorption coefficient of polymer A(β) $= \varepsilon c = 700.1 cm^{-1}$

$\therefore$ optical absorption depth (ℓ_β) $= \frac{1}{\beta} = 1.43 \times 10^{-5} m$

Table 4.8d

Calibration data for the 1600 cm^{-1} band in the spectra of polymers A-F.

Polymer	A_1	ℓ_1 $\times 10^{-6}$ m	ℓ_2 $\times 10^{-6}$ m	A_2	Mean	Conc^{n} M/ℓ
A	0.423	1.63	3	0.774		
A	0.791	3.12	3	0.761	0.767	2.39
A	0.504	1.91	3	0.790		
A	0.549	2.23	3	0.739		
B	0.705	2.80	3	0.760		
B	0.378	1.53	3	0.741	0.745	2.34
B	0.708	2.87	3	0.740		
C	0.374	1.65	3	0.682		
C	0.717	3.19	3	0.674	0.686	2.12
C	0.421	1.80	3	0.702		
D	0.620	3.20	3	0.576		
D	0.323	1.65	3	0.587	0.593	1.77
D	0.334	1.63	3	0.615		
E	0.327	1.98	3	0.495		
E	0.479	3.00	3	0.479	0.489	1.22
E	0.877	5.35	3	0.492		
F	0.191	1.93	3	0.297		
F	0.364	3.77	3	0.290	0.291	0.76
F	0.791	8.34	3	0.285		

Equation of line $y = 0.274x + 0.112$

Gradient of line $= \varepsilon\ell = 0.274 \pm 0.018 = 6.6\%$ error.

$\therefore \varepsilon = \frac{0.274}{3 \times 10^{-4}} = 913.3\ \ell\ M^{-1}cm^{-1}$

$\therefore$ optical absorption coefficient (β) of polymer A $= \varepsilon c = 2182.9\ cm^{-1}$

$\therefore$ optical absorption depth $\ell_\beta = \frac{1}{\beta} = 4.58 \times 10^{-6} m$

Table 4.8e

Calibration data for the 1572 cm^{-1} band in the spectra of polymers A-F.

Polymer	A_1	ℓ_1 $\times 10^{-6}$ m	ℓ_2 $\times 10^{-6}$ m	A_2	Mean	Conc^n M/ℓ
A	0.200	1.63	3	0.368		
A	0.367	3.12	3	0.353	0.353	2.39
A	0.226	1.91	3	0.355		
A	0.248	2.23	3	0.334		
B	0.278	2.80	3	0.298		
B	0.179	1.53	3	0.351	0.331	2.34
B	0.329	2.87	3	0.344		
C	0.741	8.01	3	0.278		
C	0.174	1.65	3	0.316	0.304	2.12
C	0.330	3.19	3	0.310		
D	0.290	3.23	3	0.269		
D	0.740	8.90	3	0.249	0.265	1.77
D	0.153	1.65	3	0.278		
E	0.148	1.93	3	0.230		
E	0.221	3.00	3	0.221	0.223	1.22
E	0.389	5.35	3	0.218		
F	0.084	1.93	3	0.131		
F	0.162	3.77	3	0.124	0.124	0.76
F	0.354	8.34	3	0.127		

Equation of line $y = 0.124x + 0.049$

Gradient = $\varepsilon\ell = 0.124 \pm 0.01$ (8.1% error)

$\therefore\ \varepsilon = \frac{0.124}{3\times10^{-4}} = 413.3\ \ell\ M^{-1}cm^{-1}$

$\therefore$ optical absorption coefficient of polymer A = $c = 987.9 cm^{-1}$

$\therefore$ optical absorption depth $\ell_\beta = \frac{1}{\beta} = 10.1 \times 10^{-6}$m.

As in the previous series the best straight line is given by the 1600 cm^{-1} band, as demonstrated by the standard deviation and also by eye from the graph. The deviations from a straight line are attributable to inaccurate determinations of the concentration because of the crudity of the method used to measure density. The fact that there is some residual absorption at 1600 cm^{-1} will give rise to a difference between rates measured using the 1600 cm^{-1} band and these measured using the 1572 cm^{-1}.

Figure 4.10
Calibration curves for the 1600 cm^{-1}, 1645 cm^{-1}, 1572 cm^{-1} and 984 cm^{-1} bands in the IR spectra of polymers A-F.

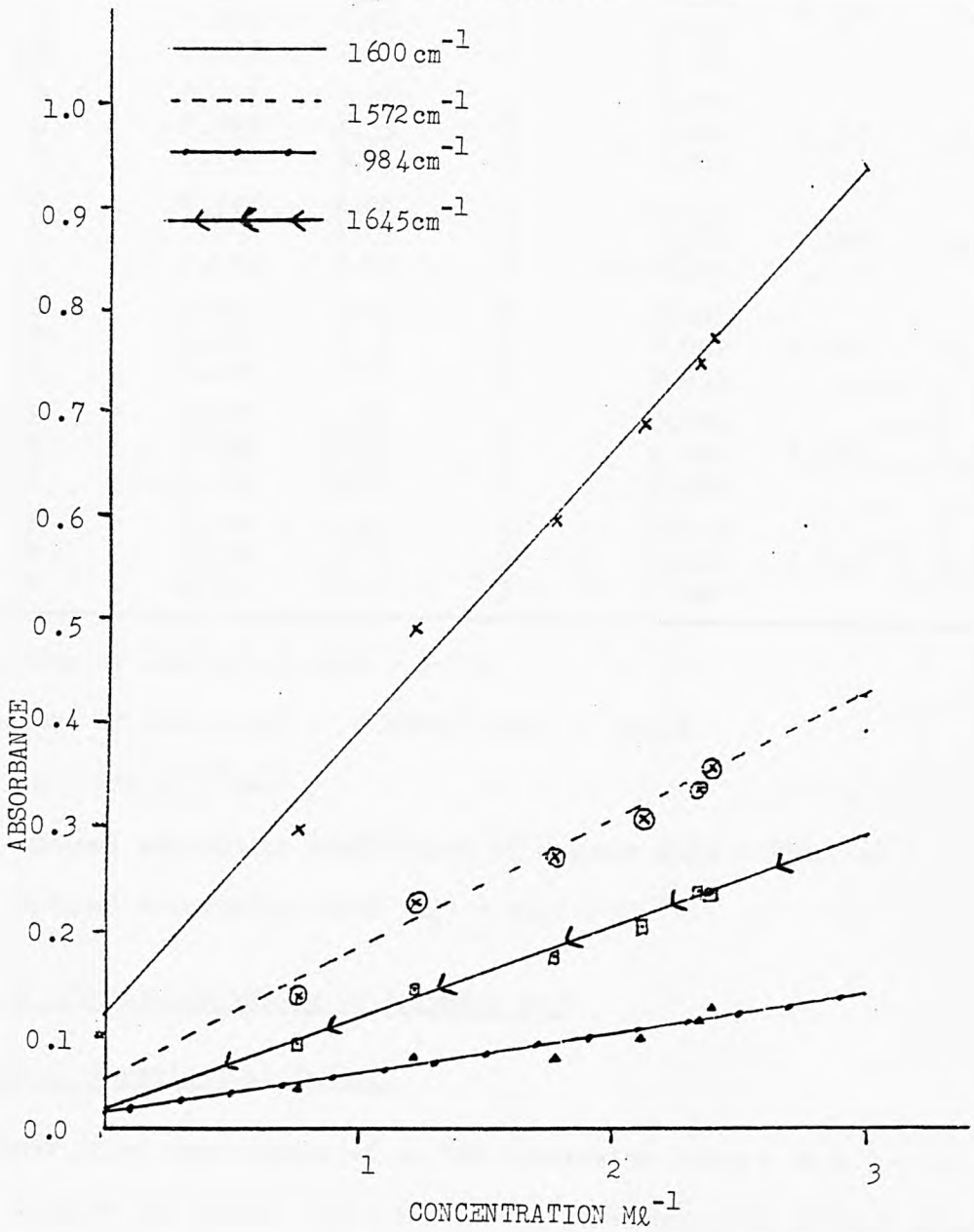

Table 4.8f.

Calibration data for the 984cm^{-1} band in the spectra of polymers A-F.

Polymer	A_1	ℓ_1 x10^{-6}m	ℓ_2 x10^{-6}m	A_2	Mean	Conc^{n} M/ℓ
A	0.071	1.63	3	0.131		
A	0.108	3.12	3	0.104	0.116	2.39
A	0.073	1.91	3	0.115		
A	0.083	2.23	3	0.112		
B	0.087	2.80	3	0.093		
B	0.063	1.53	3	0.124	0.105	2.34
B	0.190	5.64	3	0.101		
C	0.242	8.01	3	0.091		
C	0.050	1.65	3	0.091	0.089	2.12
C	0.051	1.80	3	0.085		
D	0.087	3.23	3	0.081		
D	0.045	1.65	3	0.082	0.072	1.77
D	0.158	8.90	3	0.053		
E	0.050	1.98	3	0.076		
E	0.068	3.00	3	0.068	0.071	1.22
E	0.123	5.35	3	0.069		
F	0.029	1.93	3	0.045		
F	0.052	3.77	3	0.041	0.042	0.76
F	0.111	8.34	3	0.040		

Equation of line $y = 0.039x + 0.014$

Gradient of line = $\varepsilon\ell$ = 0.039 ± 0.006 = 15.4%

$\therefore$ $\varepsilon = 130\ \ell\ M^{-1}cm^{-1}$

$\therefore$ optical absorption coefficient of polymer A(β) = 310.7 cm^{-1}

$\therefore$ optical absorption depth (ℓ_β) = 32.2 x 10^{-6}m.

4.6.3 Photocrosslinking of Polymers A-C

4.6.3.1 Experimental Method.

Polymer films were deposited on KBr substrates using K bars 1-3 in order not to have too great a film thickness which cannot be studied using infra-red spectroscopy. The solvent was evaporated by placing the sample in an oven at 80°C for 10 mins. The sample was then cooled and the IR spectrum obtained. Before placing under the curing lamp samples were heated to 80°C in an oven. Some samples were taken to full cure

but because of an inadequate kinetic model the only rate over the first minute was monitored. Thus other samples were only studied over the first minute.

The results of using an intensity meter under a glass plate with a polymer film laid on top of it are also presented. In this case difficulty was encountered because the response of the detector is temperature dependant.

4.6.3.2 Results and Discussion.

The following results were obtained from the spectra.

Table 4.9a

Rates of reaction of polymer A measured using $1600 cm^{-1}$ and $1572 cm^{-1}$ bands.

Thickness x 10^{-6}m	$1600 cm^{-1}$ $M\ell^{-1}s^{-1}$	Initial C $M\ell^{-1}$	$1572 cm^{-1}$ $M\ell^{-1}s^{-1}$	Initial C $M\ell^{-1}$
0.83	0.037	2.62	0.041	3.00
1.75	0.032	2.43	0.035	2.58
2.20	0.023	2.20	0.030	2.86
3.58	0.022	2.25	0.026	2.81

Table 4.9b

Rates of reaction of polymer B measured using $1600 cm^{-1}$ and $1572 cm^{-1}$ bands.

Thickness x 10^{-6}m	$1600 cm^{-1}$ $M\ell^{-1}s^{-1}$	Initial C $M\ell^{-1}$	$1572 cm^{-1}$ $M\ell^{-1}s^{-1}$	Initial C $M\ell^{-1}$
1.01	0.035	2.67	0.038	2.84
2.29	0.024	2.14	0.029	2.32
3.04	0.025	2.29	0.029	2.43

Taking into account the error in measuring thickness i.e.12% (see 4.4.2.2.) and the error determining concentration i.e.4% and the error in time (1%) the maximum error in the estimates of reaction rates is $\pm$ 0.01 $M\ell^{-1}s^{-1}$.

Table 4.9c

Rates of reaction of polymer C measured using $1600 cm^{-1}$ and $1572 cm^{-1}$ bands.

Thickness $\times 10^{-6} m$	$1600 cm^{-1}$ $M \ell^{-1} s^{-1}$	Initial C_o $M \ell^{-1}$	$1572 cm^{-1}$ $M \ell^{-1} s^{-1}$	Initial C_o $M \ell^{-1}$
1.21	0.029	2.17	0.033	2.30
3.23	0.019	1.64	0.024	2.05
5.14	0.015	1.89	0.017	2.01

The dependance of reaction rate on film thickness is again demonstrated with these polymers. However it is difficult to isolate the effect of measuring the concentration through the whole film which possesses a concentration gradient from the actual effect of thickness on the rate of curing. The dependance of reaction rate on initial concentration is seen here. However it is more clearly demonstrated by comparing the following results obtained for polymer X with those presented previously.

Table 4.9d

Rates of reaction of polymer X measured using $1600 cm^{-1}$ and $1572 cm^{-1}$ bands.

Thickness $\times 10^{-6} m$	$1600 cm^{-1}$ $M \ell^{-1} s^{-1}$	Initial C_o $M \ell^{-1}$	$1572 cm^{-1}$ $M \ell^{-1} s^{-1}$	Initial C_o $M \ell^{-1}$
0.82	0.045	3.32	0.048	3.59
1.99	0.036	3.32	0.039	3.59
3.42	0.028	3.28	0.029	3.30
3.54	0.022	2.67	0.031	3.29

The concentrations estimated using the $1572 cm^{-1}$ band are consistently higher than those estimated using the $1600 cm^{-1}$ band.
The $1600 cm^{-1}$ band results are closer to those presented in table 4.8a. Thus the calibration curve for the $1572 cm^{-1}$ band requires further investigation.

Following is a table in which the two series are compared using results from the $1600 cm^{-1}$ band.

Table 4.9e

Comparison of the rate of reaction of the two series of polymers.

Series A-F			Series 1-7		
$Conc^{n}$ $M\,\ell^{-1}$	Thickness $x10^{-6}m$	Rate $M\ell^{-1}s^{-1}$	$Conc^{n}$ $M\,\ell^{-1}$	Thickness $x10^{-6}m$	Rate $M\ell^{-1}s^{-1}$
3.32	0.82	0.045	3.76	0.75	0.023
3.32	1.99	0.039	3.14	2.02	0.012
3.28	3.42	0.028	2.84	3.70	0.009
2.43	1.75	0.035	2.73	1.79	0.013
2.25	3.58	0.022	2.73	3.79	0.010
2.17	1.21	0.029	2.46	0.89	0.016

Within the limits of experimental error the inclusion of a second double bond doubles the rate of reaction.

Another interesting point is the smaller spread of initial concentrations as thickness is increased (estimated using the 1600 cm^{-1} band) for the series A-F compared to the series 1-7, indicating that the calibration curve for the former is better than that of the latter.

The maximum amount of cure seems to be between 80-90% which is again higher than that predicted by the statistical model presented in chapter 3. This again is indicative of chromophores being able to react when the overlap is less than 50%. The following results demonstrate this .

Table 4.9f

Comparison of times to reach 'Full cure' for polymers X, A and B.

Polymer X

$0.82 \times 10^{-6}m$		$1.99 \times 10^{-6}m$		$3.42 \times 10^{-6}m$	
Time (s)	$Conc^{n}$ $M\ell^{-1}$	Time (s)	$Conc^{n}$ $M\ell^{-1}$	Time (s)	$Conc^{n}$ $M\ell^{-1}$
0	3.32	0	3.32	0	3.28
120	0.52	240	0.61	420	0.67
180	0.45	360	0.53	540	0.55
%cure = 86%		%cure = 84%		%cure = 83%	

Polymer A

0.83×10^{-6}m.

Time (s)	Conc^{n} $M\ell^{-1}$
0	2.62
60	0.41
120	0.41

%cure = 84%

Polymer B

1.01×10^{-6}m

Time (s)	Conc^{n} $M\ell^{-1}$
0	2.67
120	0.46
180	0.41

%cure = 85%

2.29×10^{-6}m

Time (s)	Conc^{n} $M\ell^{-1}$
0	2.14
180	0.37
240	0.33

%cure = 85%

Glass plates were placed on top of a light intensity meter and exposed to the curing lamp. Films of various thicknesses were spread on these glass plates and the intensity monitored with time, the results are presented in table 4.9g Before each irradiation through the uncoated glass plate was checked because the detector response varied with temperature.

Table 4.9g

The intensity of light measured through films of polymer X.

Thickness x10^{-6}m	I_o Wm^{-2}	I_g Wm^{-2}	I_{gf} at t=0s Wm^{-2}	I_{gf} at t=60s Wm^{-2}	I_{gf} at t=600s Wm^{-2}
0.9	77,000	68,000	61,000	66,000	66,000
3.9	77,000	72,000	58,000	60,000	60,000
5.1	77,000	67,000	57,000	57,000	57,000
11.2	77,000	72,000	58,000	58,000	58,000

I_o = incident intensity I_g = intensity measured through glass plate

I_{gf} = intensity measured through glass and film.

These results show that light which initiates photocrosslinking can

eventually penetrate 4 x 10^{-6}m into the sample. However before the ray reaches a depth 5 x 10^{-6}m it is attenuated to such an extent that it is not possible to detect the cure which is initiated. The film will still absorb a little more irradiation as demonstrated by the 11.2μm film, but this is of insufficient energy to initiate a reaction. This high attenuation of light by films in which the concentration has been reduced to about 15% of the original concentration is attributed to the high extinction coefficients below 400nm.

The intensity of light absorbed is given by:-

$$I_{abs} = I_o(1-10^{-\varepsilon C\ell}) \qquad 4.6.3.2$$

When $\ell = \frac{5}{\varepsilon C}$ $\quad -\varepsilon C\ell = -5 \quad$ $I_{abs} \simeq I_o$

∴ the wavelength of the light above which initiation is impossible can be found by determining the extinction coefficient (ε).

i.e. $\varepsilon = \frac{5}{4\text{x}10^{-4}\text{x}3.3} = 3790\ \ell M^{-1}cm^{-1}$

4.6.4 Photocrosslinking Using a 5000W Lamp.

4.6.4.1 Experimental Method.

The irradiation procedure was the same as above, however the sample was placed 73cm from the lamp. The temperature was about 55°C and the measured intensity 49,000Wm^{-2}. The sample in this case was only irradiated for 30 seconds. The spectral output of this lamp is compared to that of the 1800W lamp in figure 4.11.

4.6.4.2 Results and Discussion.

Table 4.10

Variation of concentration of chromophore in the uncharacteristic polymer with time of irradiation.

Time (secs)	A_1	ℓ_1 x10^{-6}m	ℓ_1 x10^{-6}m	A_2	Conc^n $M\ell^{-1}$	Rate $M\ell^{-1}s^{-1}$
0	0.861	2.46	3	0.893	2.85	0.026
30	0.571	2.59	3	0.677	2.06	

Figure 4.11a
Spectral power distribution of 1800W lamp.

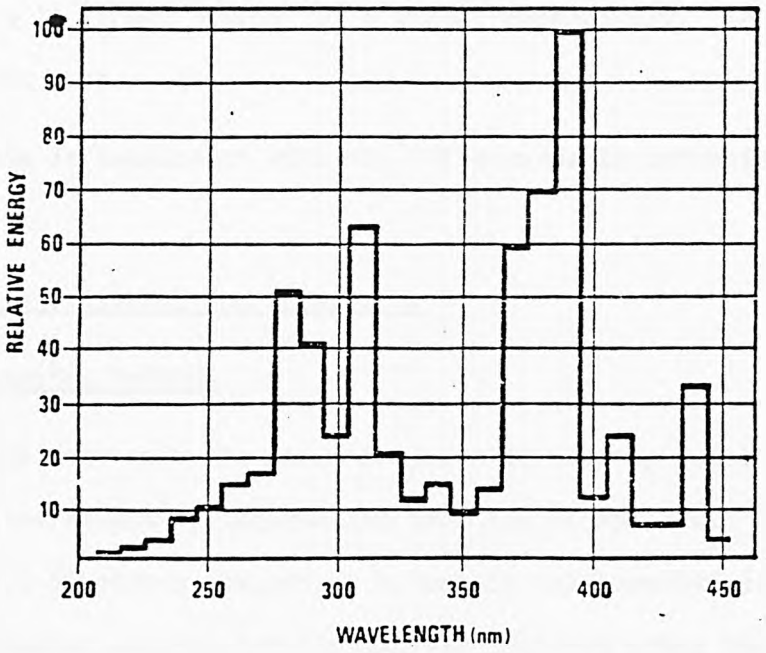

Figure 4.11b
Spectral power distribution of 5000W lamp.

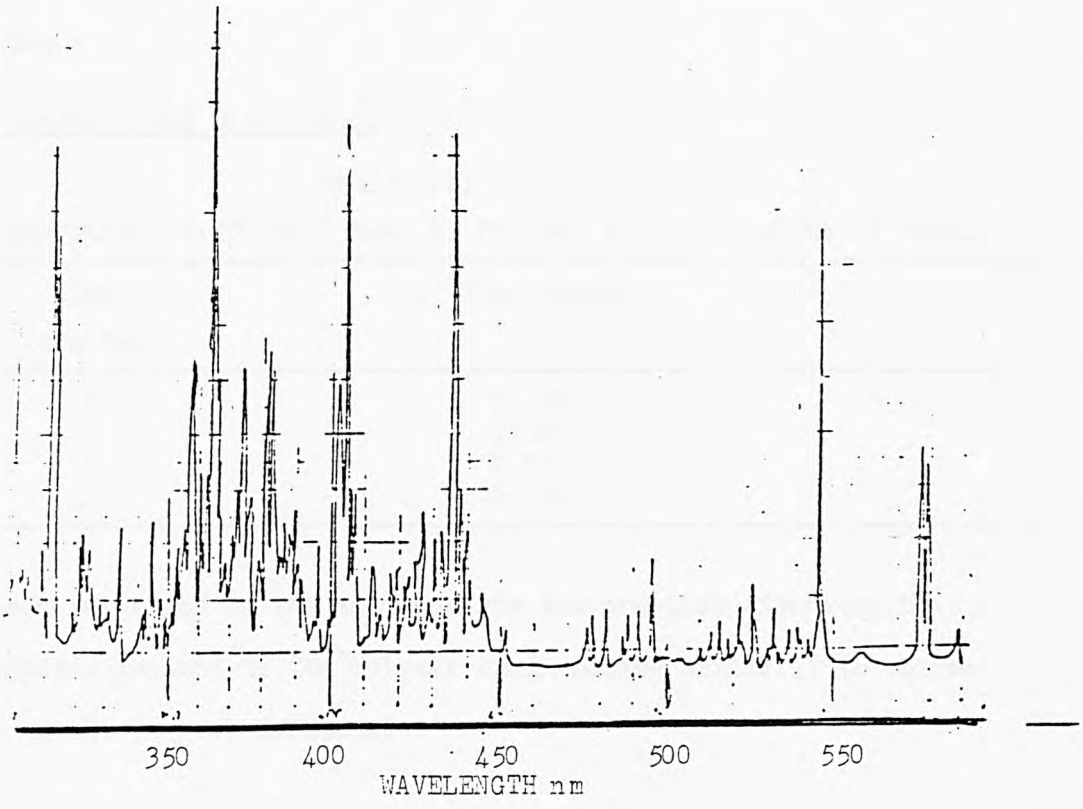

This value for rate of reaction compares with values over the first 30 seconds of 0.059 $M\ell^{-1}s^{-1}$ and 0.039 $M\ell^{-1}s^{-1}$ for films of the same polymer 1.99 x 10^{-6}m and 3.42 x 10^{-6}m thick respectively. Irradiated under the 1800W lamp.

This lower rate is consistent with the differences in intensity and temperature.

4.7 A Study of Polymer 9 and Polymer G.

4.7.1 Experimental Method.

As no standards were made for these polymers it is only possible to obtain a limited amount of information from the IR spectra. Polymer 9 made from 3,4-dihydroxy chalcone + hydantoin was irradiated for a total of 12 minutes and the irradiation was followed using the 1600 cm^{-1} band after 0,4,9 and 12 minutes. Polymer G prepared from bis(4-glycidyl ether) of 4,4-dihydroxy dibenzal acetone and 1,5-pentandiol, gave a tacky film when the solvent had been removed, which meant that density measurement was difficult. Consequently the estimation of concentration was rendered difficult. The changes in the IR spectrum on irradiation were observed and the total percentage of groups in reactive sites estimated.

4.7.2 Results and Discussion.

Table 4.11
Absorbance of 1600 cm^{-1} band in Polymer 9 as a function of time.

Time (minutes)	Absorbance.
0	0.458
4	0.329
9	0.272
12	0.246

This is a reduction of 46% and supports the previous discovery that chromophores pendant to the polymer chain behave similarly to chromophores in the polymer backbone.

Figure 4.12a IR spectrum of polymer 9.

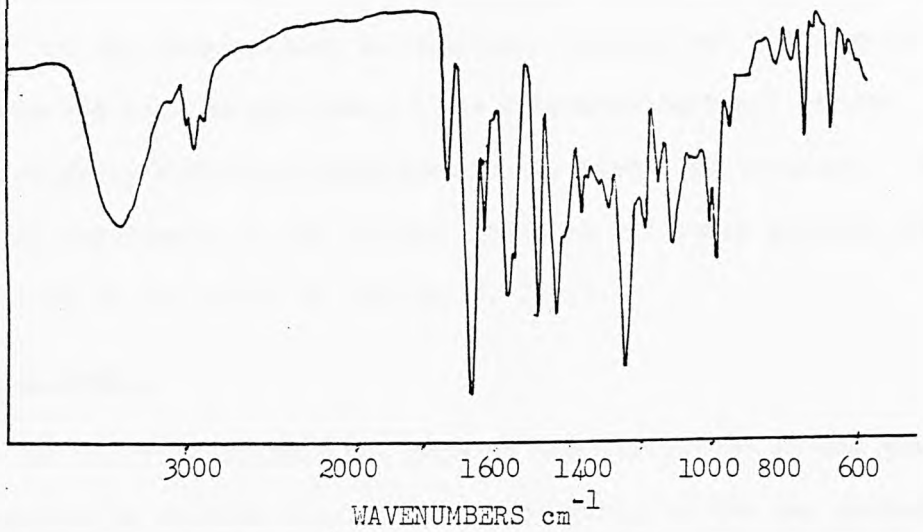

Figure 4.12b
IR spectrum polymer G.

unirradiated

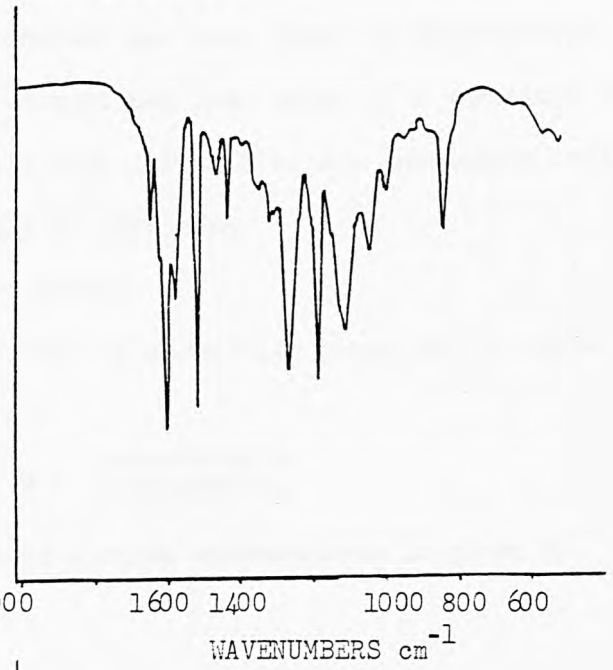

Figure 4.12c
IR spectrum of polymer G.

irradiated for 12 minutes.

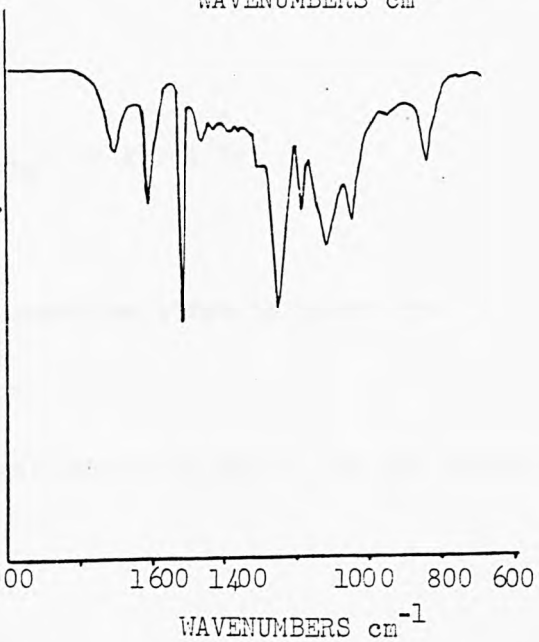

The 1600cm^{-1} absorption band of polymer G decreases in intensity as can be seen in figure 4.12. The 1645cm^{-1} band attributed to an α,β-unsaturated carbonyl group also decreases in intensity and shifts to 1703cm^{-1} as the unsaturation is removed. Because not all unsaturation is removed and because some of the saturated carbonyl groups will have slightly different environments the band also broadens. The reduction in absorbance of the 1600cm^{-1} band is 73% again greater than that predicted by the model in chapter 3. (66%).

4.8 Kinetic Model.

There are two major approximations made in the derivation of the kinetic model presented in section 1.4.4 that do not apply to the two systems understudy. There are: i) no account has been taken of chromophores in unreactive sites and ii) no account has been taken of a variation in concentration throughout the film when thick films are considered. That is solution kinetics do not apply in this case.

Considering first the unreactive sites.

The rate of excitation is unaffected by unreactive sites and is therefore given by equation 1.4.3 i.e.

$$k_1(C) = \frac{\alpha I_{abs}}{\ell} \qquad \text{where} \quad \alpha = \frac{1}{6.023 \times 10^{23} h\nu}$$

and therefore the concentration of excited chromophores is given by equation 1.4.2 i.e.

$$[C^*] = \frac{k_1[C]}{k_4} = \frac{\alpha I_{abs}}{\ell k_4}$$

The light intensity absorbed (I_{abs}) is given by:

$$I_{abs} = 2.303\varepsilon[C]\,\ell I_o$$

However I_{abs} by chromophores in reactive sites is given by:

$$I_{abs} = 2.303\varepsilon[C]-[xC_o]\,\ell I_o$$

where x = the proportion of unreactive sites and C_o is the concentration at time zero.

Figure 4.13
Irradiation time vs kt for a film of polymer 1, 4μm thick.

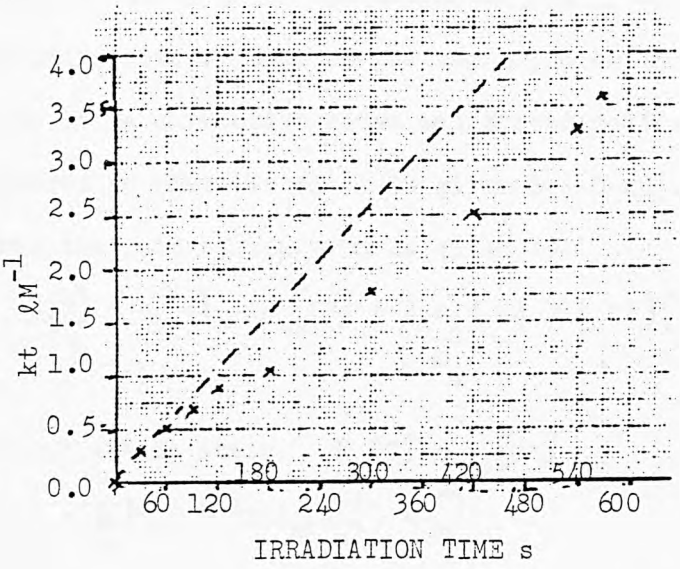

Figure 4.14
Irradiation time vs kt for films of
polymer 1(0.94μm) and polymer B(0.82μm).

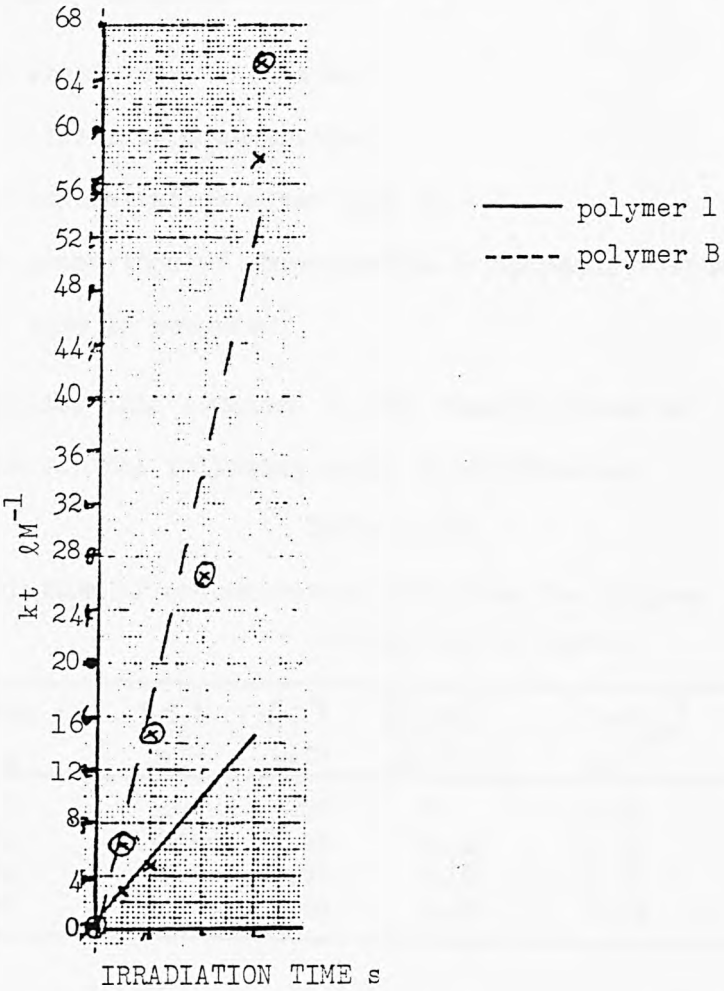

$$\therefore \quad [C^*] = \frac{(\alpha\ 2.303\varepsilon I_o)}{k_4}[C\text{-}x\ C_o] \qquad 4.8.1$$

Equation 4.7.1 gives the concentration of excited chromophores in reactive sites. Some of the chromophores in the ground state must also be in unreactive sites and therefore the concentration of chromophores in reactive sites is given by $C\text{-}xC_o$.

Thus the rate of reaction is given by:

$$-\frac{d[C]}{dt} = k_1[C] - k_4[C^*] + 2\frac{k_2}{k_4}(\alpha 2.303\ \varepsilon I_o)[C\text{-}xC_o][C\text{-}xC_o] \qquad 4.8.2$$

but at steady state $k_1[C] = k_4[C^*]$

$$\therefore \quad -\frac{d[C]}{dt} = (4.606\alpha\varepsilon I_o)\frac{k_2}{k_4}[C\text{-}xC_o]$$

$$-\frac{d[C]}{dt} = k[C\text{-}xC_o]^2$$

$$\text{Thus} \quad \frac{[C_o\text{-}C]}{[C\text{-}xC_o]C_o(1\text{-}x)} = kt \qquad 4.8.3$$

k = observed rate constant

C_o = initial concentration

C = concentration after line t

x = proportion of chromophores in unreactive sites

t = time in seconds

Applying this equation to the results presented in table 4.5e where x is 0.5 the following table is constructed.

Table 4.12a

Variation of concentration with time for polymer 1 taking unreactive sites into account.

Time t s	$[C_o]$ $M\ell^{-1}$	$[C]$ $M\ell^{-1}$	$[C_o\text{-}C]$ $M\ell^{-1}$	$[C\text{-}xC_o]$ $M\ell^{-1}$	kt ℓM^{-1}
0	3.08	3.08	0	1.54	0
30	3.08	2.88	0.20	1.34	0.30
60	3.08	2.76	0.32	1.22	0.52
90	3.08	2.69	0.39	1.15	0.68

table 4.12a continued.

Time t s	C_o $M\ell^{-1}$	C $M\ell^{-1}$	$C_o - C$ $M\ell^{-1}$	$C - xC_o$ $M\ell^{-1}$	kt ℓM^{-1}
120	3.08	2.61	0.47	1.07	0.88
180	3.08	2.55	0.53	1.01	1.05
300	3.08	2.35	0.73	0.81	1.80
420	3.08	2.22	0.86	0.68	2.53
540	3.08	2.12	0.96	0.58	3.31
570	3.08	2.09	0.99	0.55	3.60

A graph of kt against time is shown in figure 4.13

The same treatment was applied to a thinner film of polymer 1 (0.94×10^{-6}m) and a thin film of polymer B. The results are presented below.

Table 4.12b

Variation of concentration with time for a film of polymer 1, 0.9×10^{-6}m thick taking unreactive sites into account.

Time s	C_o $M\ell^{-1}$	C $M\ell^{-1}$	$C_o - C$ $M\ell^{-1}$	$C - xC_o$ $M\ell^{-1}$	kt ℓM^{-1}
0	3.57	3.57	0	1.78	0
30	3.57	2.53	1.04	0.74	2.81
60	3.57	2.31	1.26	0.52	4.85
180	3.57	1.87	1.74	0.06	58.0

Table 4.12c

Variation of concentration with time for a film of polymer B, 0.82×10^{-6}m thick taking unreactive sites into account.

x = 0.12

Time s	C_o $M\ell^{-1}$	C $M\ell^{-1}$	$C_o - C$ $M\ell^{-1}$	$C - xC_o$ $M\ell^{-1}$	kt ℓM^{-1}
0	3.32	3.32	0	2.92	0
30	3.32	0.84	2.48	0.44	6.40
60	3.32	0.61	2.71	0.21	14.66
120	3.32	0.52	2.80	0.12	26.52
180	3.32	0.45	2.87	0.05	65.23

The graphs of kt against time are shown in figure 4.14

In all three cases there are obvious deviations from linearity. The leastdeviation would seem to be in the graph of polymer B. In each case there is a point of inflection which would indicate an initial

slowing down of the rate and then an acceleration. However the effect of attenuated intensity has not been accounted for in this model which may explain some of the deviation.

For cases of thick films where the absorbed intensity (I_{abs}) is equal to the incident intensity the following treatment is suggested. Firstly divide the film into layers of thickness ℓ (where ℓ is comparable to a thickness in which the concentration gradient is negligable).

For top layer of thickness ℓ

$$I_{abs} = L_1 = I_o (1-10^{-\varepsilon C_1 \ell})$$

ε = extinction coefficient C_1 = concentration in layer 1

For the next layer

$$I_{abs} = L_2 = I_1 (1-10^{-\varepsilon C_2 \ell})$$

but $I_1 = I_o 10^{-\varepsilon C_1 \ell}$

$$\therefore \quad L_2 = I_o (10^{-\varepsilon C_1 \ell} - 10^{-\varepsilon \ell (C_1+C_2)})$$

In general $L_n = I_o (10^{-\varepsilon \ell\ C_1+C_2 \cdots C_{n-1}} - 10^{-\varepsilon \ell\ C_1+C_2 \cdots C_n})$ 4.8.4

$\therefore$ For any layer $k_1 C_n = \frac{\alpha L_n}{\ell}$

Substitution in the rate equation gives:

$$\frac{-dC_n}{dt} = \frac{2k_2\alpha}{\ell k_4} L_n C_n \qquad 4.8.5$$

For the simplest case of the first layer

$$\int_{C_o}^{C_t} \frac{-dC_n}{(1-10^{-k_3 C_n})C_n} = \int_0^t I_o K \, dt \qquad 4.8.6$$

where $k_3 = \varepsilon \ell$ and $K = \frac{2k_2\alpha}{\ell k_4}$

Equation 4.8.6 can be solved by numerical techniques however more information about the concentrations in very thin films is required.

Summary

Inclusion of unreactive sites in the model has not improved it because account has not been taken of attenuation of the incident intensity. In order for this to be included more information concerning reaction in very thin films is required.

4.9 Conclusion

The extension of the infra-red spectroscopy to the study of these systems has proved highly successful. A dependance of rate of curing on concentration, temperature, incident intensity and film thickness has been established. Infra-red spectroscopy could also be used as a form of actinometry.

It has been demonstrated by means other than IR spectroscopy, that the high absorbancy of the polymer films only allows the top 4×10^{-6}m to be cured. This could be checked by using either the $1572cm^{-1}$ band or the $984cm^{-1}$ band. However calibration curves at higher concentrations are required.

The films are essentially solid hence little or no mixing will occur on reaction which causes a concentration gradient to be set up, because the intensity of the activating radiation is attenuated which means lower concentrations of excited species at greater depths. It is for this reason that the application of solution kinetics to this system failed.

CHAPTER FIVE

UV/VISIBLE DIFFUSE REFLECTANCE SPECTROSCOPY

5.1 General Comments

Diffuse reflectance was first suggested as a possible analytical tool by A.H.Taylor in 1919[156]. (A sophisticated spectrophotometer type of reflectometer was built by Hardy in 1929[157].) Reflectance spectroscopy uses the amount of radiant energy reflected from a sample surface as the measured variable. The data is generally reported as percent reflectance R.

Where $R = I/I_o \times 100$ 5.1

I = Intensity of reflected radiation

I_o = Intensity of reflected radiation from a standard reflecting surface.

5.2 Some Theoretical Considerations

In general there are two types of reflectance:-
specular or regular reflectance and diffuse reflectance. These are two ideal limiting cases and most samples yield remitted radiation that is composed of a contribution from each.

Specular reflectance is mirrorlike reflectance and has a well defined reflectance angle.

Diffuse reflectance has no defined reflectance angle and in ideal diffuse reflectance the angular distribution of the reflected radiation is independant of the angle of incidence.

Ideal regular reflectance has been well defined by the Fresnel equations. In the derivation of which light is resolved into two components, one parallel and the other perpendicular to the plane of incidence. The amount reflected and the amount refracted is given by a function of the angle of incidence and the angle of refraction.

The regular reflectance of a non-absorbing medium can be expressed as:-[158]

$$R_{reg} = \frac{1}{2}\left[\frac{\sin^2(\alpha-\beta)}{\sin^2(\alpha+\beta)} + \frac{\tan^2(\alpha-\beta)}{\tan^2(\alpha+\beta)}\right] \qquad 5.2$$

α = angle of incidence β = angle of refraction

for $\alpha = \beta = 0$ i.e. perpendicular incidence.

$$R_{reg} = \left[\frac{N_1 - N_o}{N_1 + N_o}\right]^2 \qquad \text{where } N_1 > N_o \qquad 5.3$$

For strongly absorbing materials the regular reflectance is given by;-

$$R_{reg} = \frac{(N_1 - N_o)^2 + (N_1K_1)^2}{(N_1 + N_o)^2 + (N_1K_1)^2} \qquad \text{for } \alpha = \beta = 0 \qquad 5.4$$

$N_1 > N_o$ K = absorption coefficient.

Thus when the absorbance of material 1 is large ($N_1K_1 > N_1$) the reflectance of the material is large, a fact which is well known from the reflectance of metals.

The Lambert Cosine law for diffuse reflectance is derived by considering a fraction of the remitted radiation flux per unit surface area of an irradiated disc. This is then integrated over the total hemisphere of remitted radiation and then related to the incident radiation by a constant. The Lambert Cosine law is expressed as:-

$$\frac{dIr/df}{d\omega} = \frac{\text{Const.}S_o}{\pi} \cos\alpha \cos\theta \qquad 5.5$$

$$= \beta \cos\theta$$

dIr/df = remitted radiation flux per unit surface area.

$d\omega$ = the solid angle .

S_o = irradiation intensity (Watts/m^2).

α = angle of incidence.

θ = angle of observation.

β = radiation density (Watts/ω cm^2).

i.e. the remitted radiation flux per square centimeter and unit solid

angle is proportioned to the cosine of the incident angle(α) and to the cosine of the angle of observation (θ).

Bouguer[159] tried to explain diffuse reflectance by assuming regular reflectance was occuring from the elementary mirrors of the crystal faces whose surface planes have a symmetrical statistical distribution of orientations. Grabowski[160] showed that this was incompatible with the Lambert Cosine law.

However Berry[161] and Rense[162] showed that a Gaussian distribution of orientations gives predictions very close to experimental results of angles of incidence and observation of less than 45° are used. Thus as long as the dimensions of the crystal exceed the wave length of incident light the Fresnel formulas will be valid for the elementary mirror.

Deviations from the Lambert law occur particularly at high angles of incidence and observation. This is partly due to some radiation being regularly reflected. The proportion increases with increasing angle of incidence. Regular reflectance is appreciable when $\alpha + \theta$ are large and equal and the azimuth (ϕ, the angle between the incident and reflected ray in the plane of the mirror) is 180°.

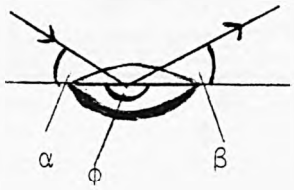

Plots of $\frac{B_{rel}}{\cos\alpha}$ against θ or goniophotometric curves where:-

α = angle of incidence $B_{rel} = \frac{B(\alpha,\theta)}{B\ 0^{\circ},45^{\circ}}$ i.e. the relative radiation.

density is normalised to $\alpha=0^{\circ}$ $\theta = 45^{\circ}$, should yield a straight line parallel to the x axis if the reflector obeys the Lambert Cosine law. Various researchers showed[103,164] that except at low values of α deviations are observed. Powder samples of barium sulphate yielded

curves in which $B_{rel}/\cos\alpha$ increased with θ. At $\alpha = \theta$ peaks were observed which were accredited to regular reflectance. These peaks were very large when surfaces were prepared by high pressure, however if paper was placed inbetween the die and the powder these peaks were removed. At high values of α the gradient of the slope was larger than at low values of α.

Other white standards such as rutile, magnesium oxide and Aerosil (SiO_2) were investigated in the same manner, the resulting curves were similar. However the increase in gradient increased in the order of rutile, magnesium oxide, barium sulphate and silicon dioxide. If the regular reflectance of these materials is plotted against the angle of incidence, the dependance upon the refractive index is observed.

Figure 5.1

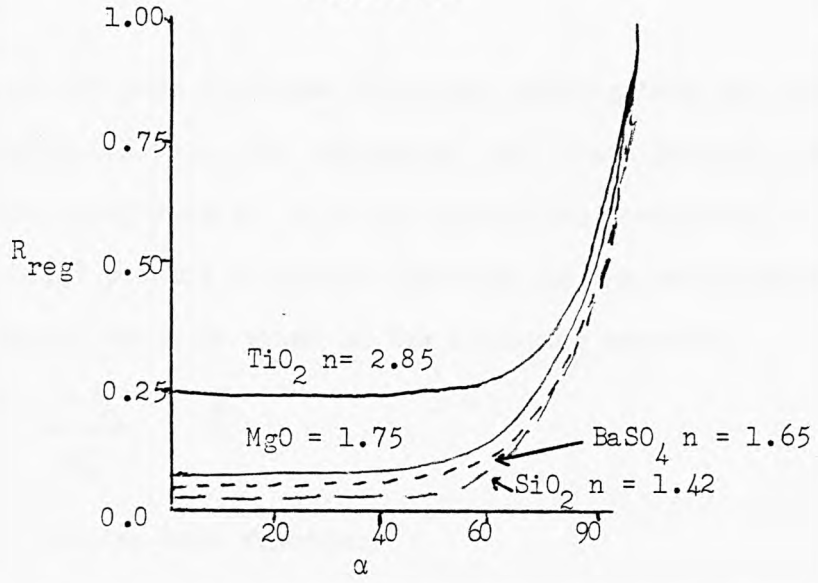

Because B_{rel} is a ratio of the reflected radiation density at angle θ to the reflected radiation density at $\theta = 45^{\circ}$ the substance with the lowest refractive index and shortest range of constant behaviour, will give the steepest curves. Hence the dependance of reflected radiation on the refractive index of the sample.

For absorbing materials two effects change the spectral composition of the reflected radiation. Radiation in a certain wavelength region is

selectively absorbed thus the diffuse light being remitted from the interior of the sample lacks that which is absorbed. However because of the Fresnel laws (equation 5.4) this same radiation will be preferentially reflected, from the sample surface at the Bouguer elementary mirrors. Hence the two processes are working against each other. For highly absorbing compounds at high values of α and θ very large scale deviations are observed.

Diffuse reflectance is described by the Kubelka-Munk theory[165,166]. The assumptions made during the development of the theory are:- the Lambert Cosine law is obeyed i.e. regular reflectance is ignored, the particles in the layer are regarded as randomly distributed and very much smaller than the thickness of the layer i.e. the layer has essentially infinite thickness, the layer is subject to diffuse irradiation.

Equations are then developed for light passing into the layer and for light reflected out. Two constants K and S are invoked. K is the absorption coefficient. S is the scattering coefficient. The ratio of the light passing in either direction is the reflectance (R_∞) of the material which is given in the following equation.

$$F(R_\infty) \equiv \frac{(1-R_\infty')}{2R_\infty'} = \frac{K}{S} \qquad 5.6$$

$F(R_\infty)$ = Kubelka-Munk function.

where R_∞' = the absolute reflectance of the layer.

However it is more convenient to use the relative diffuse reflectance R_∞ which is measured against standards such as MgO or $BaSO_4$. It is assumed that K=0 and $R_\infty' = 1$ for these standards. However R_∞' is less than 1 thus the reflectance of the sample given by $\frac{R_\infty' \text{ sample}}{R_\infty' \text{ standard}} = R_\infty$ is dependant on the standard used.

S is constant with wavelength only when the particle size is much

greater than the wavelength used. Thus for sample with small absorption coefficients or for samples diluted with a low absorbing powder K maybe replaced by $2.30\varepsilon C$ where ε = extinction coefficient and C= concentration. Hence a plot of $F(R_\infty)$ against C should yield a straight line of gradient K' where $K' = \frac{2.30\varepsilon}{S}$.

Deviations from linearity occur when the layer is not infinitely thick because background interference occurs.

A decrease in the slope also occurs with large particle sizes and high concentrations. This is attributed to the regular reflectance portion of the remitted radiation. That is at high values of K equation 5.4 becomes significant. Regular reflectance can be eliminated by dilution and by reducing particle sixe.

For low concentrations

$$\log F(R_\infty) = \log\varepsilon + \log 2.303\ C/S \qquad 5.7$$

and thus a plot of $\log F(R_\infty)$ against wavelength should yield a similar spectrum to the absorption spectrum obtained from transmission spectroscopy. This was found to be the case with anthraquinone[167]. However at high concentrations the spectrum showed little resemblance to that obtained in solution.

5.3 Applications of Diffuse Reflectance Spectroscopy.

The most important industrial application of UV-Vis diffuse reflectance spectroscopy, is the measurement and adjustment of the colour of 'bulk dyes'.[168] The technique was first used in the 1930's for this application.[169]

When the concentrations are low and the dyes are mixed with an excess of white pigment the Kubelka-Munk theory is applicable. However for high concentrations and for surfaces which remit a lot of regular reflectance an amended form of the K-M theory is required.

$$\text{i.e. } R^*_\infty = \frac{0.472\ R_\infty}{1.059\ R_\infty} \qquad 5.8$$

For a mixture of coloured pigments with an excess of white pigment, the

K-M function can be written for a particular wavelength.

$$F(R'_\infty) = \frac{C_1K_1 + C_2K_2}{S} = \frac{\sum_1^n C_iK_i}{S} \qquad 5.9$$

For large particles S does not vary with wavelength. Thus for wavelength λ_1 $F(R')_{\lambda_1} = K_1(\lambda_1)C_1 + K_2(\lambda_1)C_2$

wavelength λ_2 $F(R'_\infty)_{\lambda_2} = K_1(\lambda_1)C_1 + K_2\lambda_1 C_2$

These equations are fitted with the aid of a computer to reflectance data until the concentrations don't change. In this way the dyeing recipe can be calculated.

Diffuse reflectance was applied to samples from TLC plates in the 1960's.[168] This application was also suggested for PAS in the 1970's.[170].

The use of diffuse reflectance for studying surface absorbed substances was reviewed by Frei and MacNeil in 1971.[168] The subject of colour change in organic systems upon absorption onto an active surface was covered in detail. More recently Hurtubise and co-authors have studied room temperature phosphorescence in aromatic compounds absorbed on solid supports. Diffuse reflectance was used to confirm the prescence of hydrogen bonding.[171,172]

Diffuse reflectance has been used in the infra-red region to study ultra thin films of organic phase on chromatographic packings,[173] and to follow the reaction between silane coupling agents and glass fibres.[174]

The spectra of inorganic salts have been obtained by U.V.diffuse reflectance, a subject which has again been reviewed by Frei and MacNeil.[168] The first spectrum of Holmium Oxide (Ho_2O_3) which is now used to calibrate photoacoustic instruments, was obtained in 1967.[175] A comparison of diffuse reflection to PA Spectroscopy was made using Holmium Oxide[176] by Röhl et al. These workers found that they were complementary techniques but in this case the PA technique was more

noisy and had smaller peak intensities.

UV/Vis diffuse reflectance has also been compared to PAS by Davidson and King.[177] They studied the effect of particle size, and thus surface area, in potassium chromate and potassium ferricyanide diluted with magnesium oxide. It was shown that surface area is as critical to photoacoustic signals as absorption, i.e. although samples of small particle size absorb less radiation the PA signals are greater for weak absorbers.

It has been mentioned above that the Kubelka-Munk theory is only applicable over a limited range of concentrations and that at high concentrations large deviations occur. Other theories of diffuse reflectance have been put forward and in a series of papers Hecht[178,179,180] has compared two of them to experimental results.

The first theory, attributed to Rozenburg, is developed by considering successive scattering of the incident radiation, and the following equation is eventually generated:-

$$\frac{R_o}{R} = \frac{(1+\beta)^2}{1+\frac{\beta}{Q}}$$

R_o = the reflectance of the background.

R = the reflectance of the sample.

β = α/σ the ratio of the absorption and scattering coefficients.

Q = $1 + \frac{t}{r+t}$ where t = proportion of incident light forwardly scattered
r = proportion of incident light reflected.

Hecht has verified that at high values of absorption $Q \simeq 1$ and

thus $\frac{R_o}{R} \simeq 1+\beta$

The second theory was developed by Pitts and Giovanelli and is a development of the radiative transfer equation and includes a coefficient for anisotropic scattering caused by regular reflectance. However this equation is very cumbersome and Hecht found that it did not always work

although a good fit was found when the equation did work. At high values of absorption the Rozenburg equation is a better fit than the Kubelka-Munk theory. However at low values of absorption the K-M theory is better than the Rozenburg theory essentially because an accurate value for Q cannot be found.

Different types of samples give different performances i.e. the K-M theory is good for solid solutions and adsorbed absorbers, and fair for mixtures and paper chromatographs. However it is poor for suspensions for which the Rozenburg theory gives a good fit.

The general conclusion was that no theory was significantly better than any other.

5.4 The Study of the Photocrosslinking Reaction of Polymer A using UV Reflectance Spectroscopy.

5.4.1 Experimental Method.

The polymer was deposited using K bars on teflon paper and the solvent was removed in an oven at 80°C. Samples were cut from the film after various irradiation times and placed in the reflectance attachment of the Perkin Elmer Lamda 5 UV spectrometer.

5.4.2 Results.

A comparison of the reflectance spectrum of the solid with the polymer in dilute acetonitrile solution yields some significant differences. (figure 5.2)

i) In the solid there are maxima at 445nm and 320nm in the solution maxima occur at 352nm and 235nm.

ii) On irradiation the 445nm maxima at first decreases in intensity and then as it receeds towards the blue it increases in intensity only to fall again after longer periods of irradiation. However the band never decreases to zero and does not move below 410nm. The solution band maxima at 352nm does start to approach zero absorbance after long

Figure 5.2a
UV absorption spectrum of polymer A
in acetonitrile.

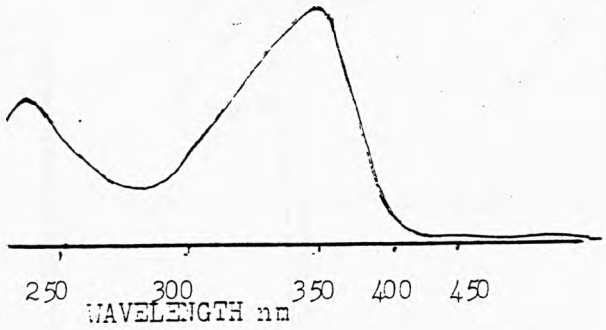

Figure 5.2b
UV reflectance spectrum of a solid film of
polymer A.

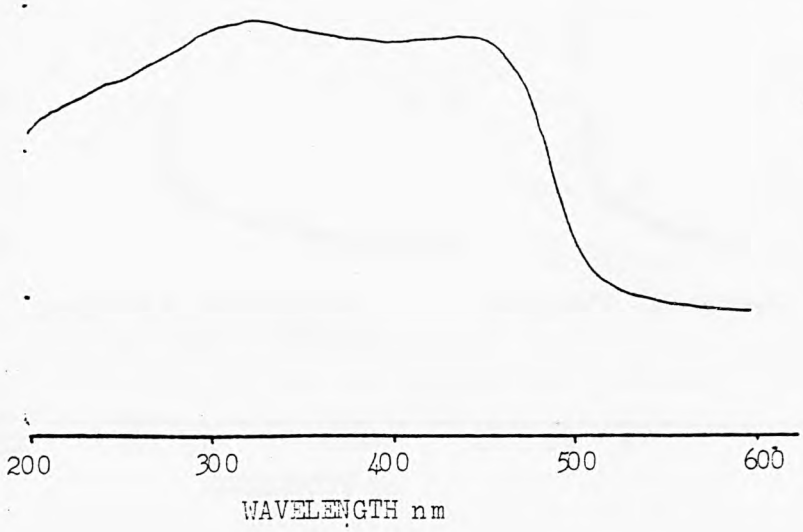

Figure 5.2c
UV reflectance spectra of polymer A, irradiated for: 0,1,2,3,5,7 and 9 minutes.

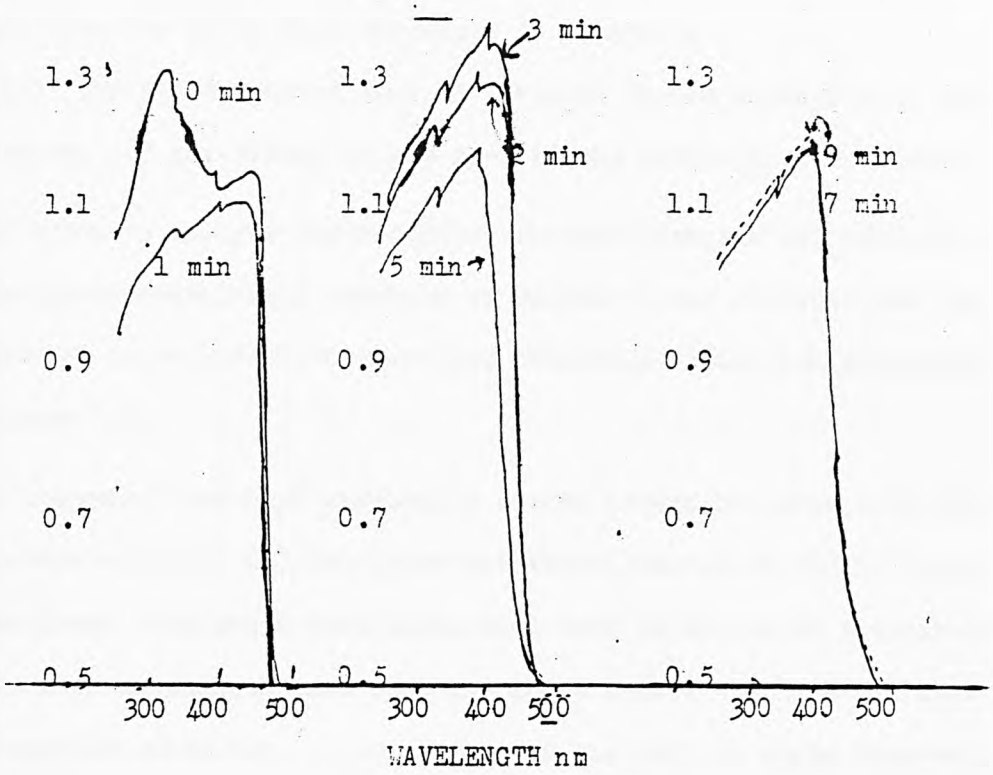

Figure 5.3
UV reflectance spectra of polymers 1-8 and bisphenol A diglycidyl ether, the spectra of polymer 1 irradiated for 1 and 3 minutes are also included.

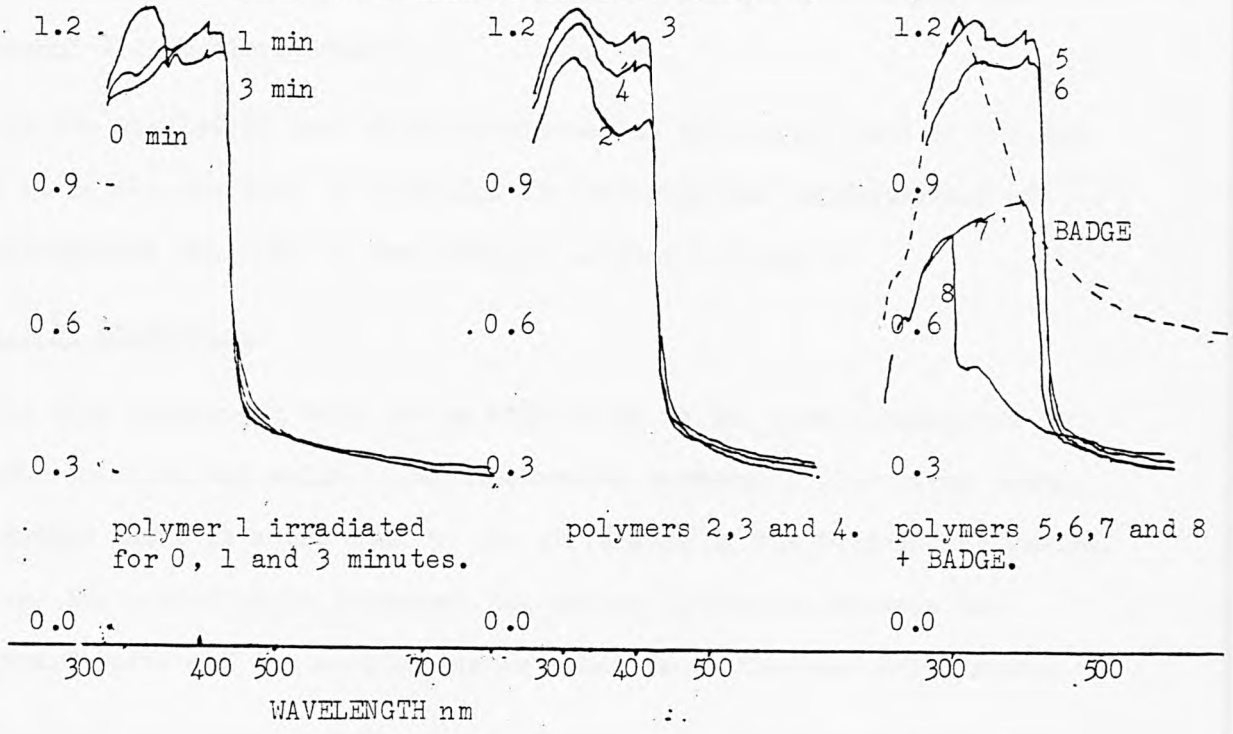

periods of irradiation. The 320nm band in the solid spectrum disappears extremely quickly when compared to the 445nm band and in the solution the 235nm band increases in intensity.

iii) The solid spectra show an increase in the intensity of the tail between 450 and 500nm, as was seen in the photoacoustic spectra.

In order to analyse these results further research was required, thus the photocrosslinking reaction of polymer 1 was followed and the spectra of polymers 2-8 were also obtained. These are presented in figure 5.3.

In polymer 1 the high wavelength maxima occurs at 410nm (c.f 332nm in acetonitrile ref 25) the lower wavelength maxima at 310nm. Here again the lower wavelength band disappears very quickly upon irradiation. The high wavelength band does not shift toward the blue but does increase in intensity. A broadening of the tail is again observed.

Inspection of the spectra of the other polymers indicates that the high wavelength band appears at 410nm in all but the spectrum of polymer 8, which contains no chromophore. The band below 300nm in polymer 8 is attributed to the bisphenol A moiety (c.f. the spectrum of the bisphenol A diglycidyl ether).

The low wavelength band slowly decreases in intensity until in polymer 7 it is not visible. A variation at odds with the concentration of chromophore can also be seen between polymer 1,2 and 3.

5.4.3 Discussion.

The high wavelength band can be attributed to the same chromophore in both solution and solid (i.e. unsaturated carbonyl). The large bathochromic shift is attributed to the difference in the surrounding medium, i.e. the acetonitrile increases the energy difference between the ground state and the excited states relative to the pure solid state.

The fact that there remains a considerable absorbance even after long

irradiation times is due to the fact that chromophore remains in unreactive sites after irradiation, (12-15% in polymer A 45-50% in polymer 1). Because of the high absorbtivity of these chromophores the remaining absorbance will be large. The fact that in polymer A the band receeds to 410nm whereas the band in polymer 1 does not move, is attributable to the fact that the chromophores left in polymer 1 are the same as the original. However the chromophores left in polymer A will generally have had one of the two double bands removed and thus will be essentially the same as those left in polymer 1.

The unexpected increase in absorbance or decrease in reflectance can be explained by considering the regular reflectance part of the reflected radiation. The regular reflectance is dependant upon the refractive index and absorption coeficient of the sample which will change on irradiation. The subsequent decrease may be due to differences in sample size, preparation or surface area presented to the incident radiation.

The low wave-length peaks can be attributed to an intermolecular interaction. This conclusion is reached by observing the changes that occur with change in the concentration of chromophore. It is weak in polymer 6 because only a few chromophores are within the distance required for this interaction to take place and in polymer 7 the concentration is so low that the effect cannot be observed at all. The very quick disappearance of the peak is attributable to a change in crystal structure or irradiation which puts the chromophores out of reach of each other. This must be the case because the effect is still visible in polymer 5 where 50% of the original chromophores have been removed. The effect is not seen in solution because the molecules cannot approach close enough due to the solvent.

5.5 A Comparison of UV/Visible Diffuse Reflectance Spectroscopy with Photoacoustic Spectroscopy.

5.5.1 Experimental Method.

A number of films of polymer A were produced using a No.4 Kbar. These films were irradiated for 0,2,5 and 9 minutes. Samples were obtained and placed in the reflectance attachment of the Lamda 5, and spectra obtained. The samples were then cut so that they would fit into the cell of the photoacoustic spectrometer.

5.5.2 Results and Discussion.

The spectra obtained are shown in figures 5.4a and 5.4b. The similarities are that both spectra of the unirradiated sample absorb strongly until about 450nm, and then there is a sharp drop in absorbance. The spectra of the irradiated samples seem to move back towards the blue end of the spectrum at about the same rate, they both stop at about 410nm and both have an increase in absorbance above 450nm.

The differences are that the photoacoustic spectra yield plateaus whereas the reflectance spectra have a little more structure. The photoacoustic spectra go off scale below 350nm. This is explained by photoacoustic saturation, and poor optics and low source output. Thus the band at 320 nm is not visible in the PA spectra. Because the PA spectra are in saturation and the band is not visible, the apparent disappearance of this band seen in figure 5.4 cannot be confirmed. It is possible that the band may have been swamped in the irradiated spectra. However, on the evidence of figure 5.2a in which polymer A has been irradiated for 1 minute and the band at 320nm is still visible, this is unlikely.

The PA spectra do not increase in absorption at larger wavelengths indicating that the apparent rise in absorbance in the reflectance spectra is due to reflectance phenomenon as the PA technique is unaffected by reflected light.

Figure 5.4a
UV reflectance spectra of polymer A irradiated for
0,2,5 and 9 minutes.

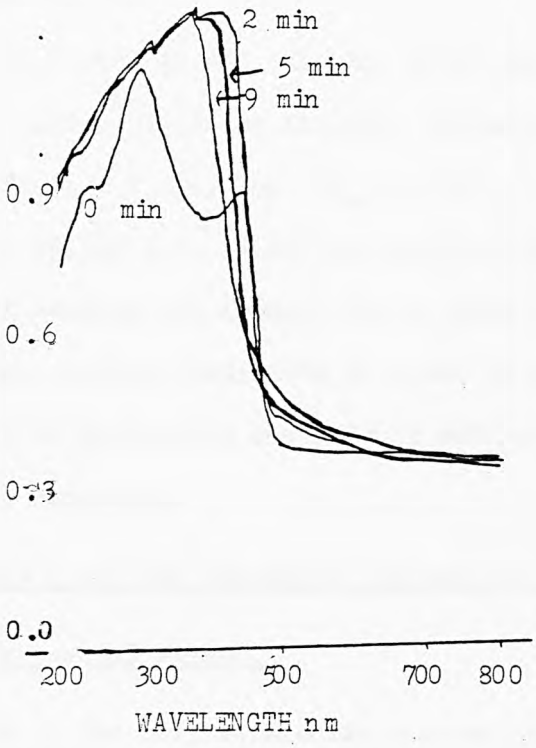

Figure 5.4b
UV PAS of polymer A irradiated for 0,2,5 and 9 minutes.

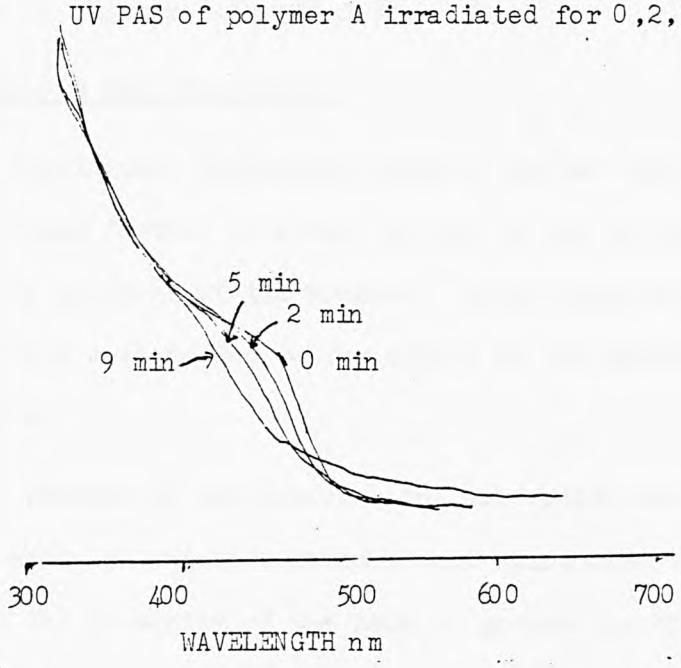

Consider equation 7, in this case for t = 0 min.

$$\log F(R_\infty) \simeq 0.9 = \log \frac{(1-R)^2}{2R}$$

or $7.943 = (1-R)^2/2R$

or $15.886R = R^2 - 2R + 1$

$R^2 - 17.886R + 1 = 0$

$R = 0.056$ or 17.83. As $R \leq 1$ only the first answer has any physical significance, i.e. 5.6% of the incident radiation is remitted.

Similarly for t = 9 min. $\log F(R_\infty) = 1.2$

$R = 0.03$ or 33.668 i.e. 3% of the incident radiation is remitted. As regular reflectance can account for a great deal of the remitted radiation when diffuse incident radiation is used, slight changes in the absorption coefficient or refractive index could well account for the small change in remitted radiation.

5.6 Polymer A and the Monomeric Chromophore.

5.6.1 Experimental Method.

The spectra of the polymer and the monomer were obtained as before and are shown in figures 5.5a and 5.5b.

5.6.2 Results and Discussion.

The most significant difference between the two spectra is that the shoulder comes further into the visible in the spectrum of the polymer than in the spectrum of the monomer. As no difference is observed in solution this must be due to the effect of the materials being in the solid state.

The other feature of the spectra, the absorption band at shorter wavelengths, again undergoes a bathochromic shift when the monomer is polymerised. The intensity of the peak is greater in the polymer than in the monomer, relative to the longer wavelength band. This would strengthen the suggestion that it is caused by intermolecular interaction as dibenzalacetone will not udergo photocrosslinking in the

Figure 5.5a
UV reflectance spectrum of the monomer used
in polymers A-F.

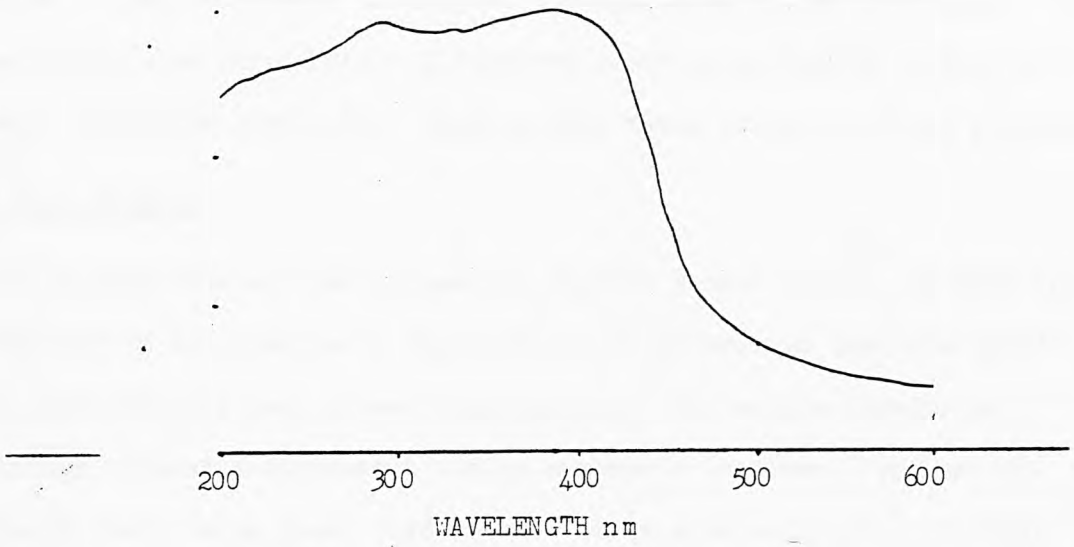

Figure 5.5b
UV reflectance spectrum of polymer A.

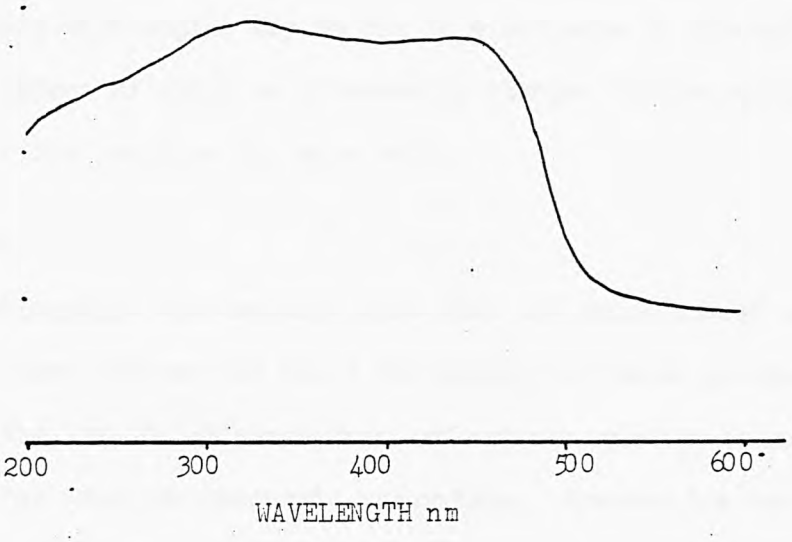

pure solid state due to spatial arrangement. To take this work a stage further the spectrum of dibenzalacetone is required.

5.7 Irradiation Through Filter Solutions.

5.7.1 Experimental Method.

Films of polymer A were irradiated through three filter solutions. The solutions used were potassium dichromate/sodium carbonate, sodium nitrate, and water (see 2.9). Samples were taken after 0,1,5 and 9 minutes.

5.7.2 Results.

The spectra obtained can be seen in figures 5.6a,b and c. If they are compared to the spectra in figure 5.4a, it is obvious that the speed of photocure has been slowed considerably. The sample irradiated through potassium dichromate/sodium carbonate is slowed furthest although there is no great difference. It is interesting to note that the band around 320nm is still just visible after 9 minutes irradiation indicating that there are some chromophores close enough to interact.

The reduction in cure rate is attributable to a reduction in temperature and photon flux. The fact that cure still occurs through potassium dichromate/sodium carbonate indicates a sensitivity to light above 410nm.

The increase after 5 minutes and then decrease (after 9 minutes) in the absorption at long wavelengths may be due to a decrease in absorption coefficient the effect of which is reversed by changes in the refractive index. However this requires far more work.

5.8 Conclusion.

Both PAS and reflectance spectroscopy show that the films absorb out to 445nm. However more information about the absorption bands particularly at low wavelengths, can be obtained from reflectance spectra because they do not suffer from photoacoustic saturation. However the variation in absorbance in the reflectance spectra, attributed to variations in

Figure 5.6
UV reflectance spectra of films of polymer A irradiated through different filter solutions.

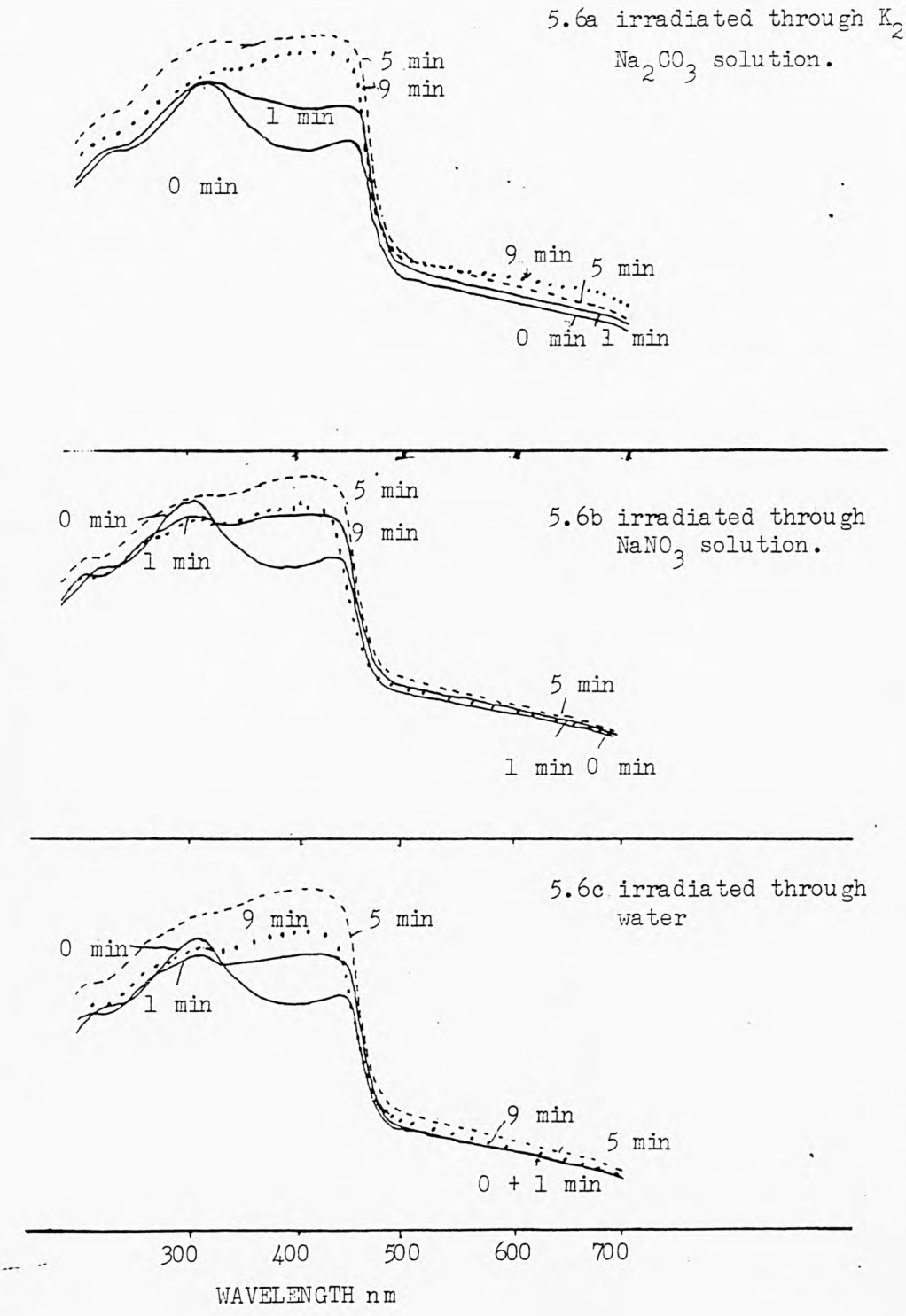

regular reflectance, which cannot be removed because of the nature of the sample, means that reflectance spectroscopy cannot be used quantitatively.

A lot more work is required to investigate the short wavelength band and to discover precisely why the absorbance of the high wavelength band goes up on irradiation.

The experiments done on the effects of filter solutions give results that contradict those found in chapter 2 i.e. some sensitivity light of wavelength greater than 410nm has been found. This requires further investigation.

CHAPTER SIX.

FOURIER TRANSFORM INFRA-RED PHOTOACOUSTIC SPECTROSCOPY

6.1 General Comments and Applications.

Fourier Transform Infra-red Spectroscopy (FT-IR) is based upon a Michelson interferometer. The interferometer consists of 2 mirrors set at right angles. One of the mirrors is fixed the other is moveable. A beam splitter divides the light from the source and an interference pattern is set-up by the recombination of the reflected light at the beam splitter. The interference pattern or interferogram is generated because the moving mirror introduces phase differences between the reflected rays from the two mirrors as one ray travels further than the other.

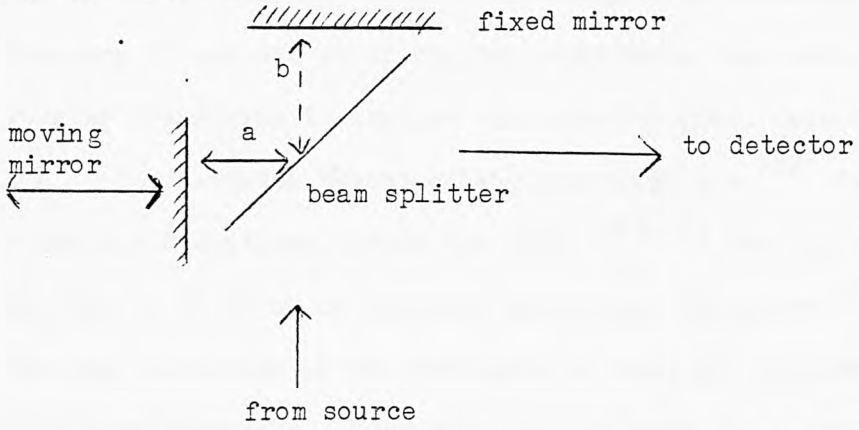

Let the distance moved by the mirror be xcm.

Thus the extra distance travelled by the light is 2xcm.

When $x = 0$ let $a = b$ i.e. no path difference. Thus when $x = 0$ all light frequencies will be inphase on reflection to the beam splitter and constructive interference will occur.

When $2x = n\lambda$ for monochromatic light of wavelength λnm no phase difference will be observed at the beam splitter and maximum intensity attained providing n is a positive integer.

When $2x = \frac{m\lambda}{2}$ where m is both a positive and odd integer the reflected

rays will be exactly out of phase at the beam splitter and destructive interference will occur. Thus the intensity will be zero and modulation is effected.

The number of times the rays are exactly in phase during one sweep of the mirror from x = 0 to x = x_{max} cm is given by:

$$\frac{2\,x_{max}}{\lambda}$$

The number of sweeps/second = V/x_{max} where V = mirror velocity in cm s^{-1}.

$\therefore$ Modulation frequency = $\frac{2x_{max}V}{\lambda x_{max}} = \frac{2V}{\lambda}$

Modulation frequency = $\omega = 2V\bar{\nu}$ Hz

$\bar{\nu}$ = wavenumber of light in cm^{-1}.

The interferometer was originally designed by Michelson in 1881.[181] However, it was not until digital computers, that were able to use Fourier Transforms to analyse the interferogram, were developed, that the interferometer became of any practical use.[182] Improvements in computing techniques during the 1960's[183,184] has led to the increaseing use of FT-IR as on everyday analytical technique.[185]
The main advantage of the technique is that all wavelengths are measured simultaneously. This cuts out the need for a monochromater and its associated light losses and therefore, helpsto overcome the inherent detector noise limitations of the photoacoustic technique.

FT-IR was first applied to photoacoustic spectroscopy by Buose and Bullemer in 1978.[186] They obtained the spectrum of methanol vapour. The first FT-IR-PA spectra of solids were obtained independantly in 1979 by Vidrine[187] and Rockley.[188] Since then there has been considerable activity in the field.[190-202]

The FT-IR-PA technique is a single beam technique and thus corrections

are required for variation in source output. The conventional approach to this correction was to use carbon black as a black absorber.[189,190] However Riseman and Eyring have shown how the spectra of carbon black samples vary with mirror velocity and also the origin of the samples.[191] These workers suggested that the response of a standard detector made from triglycine sulphate (TGS) would prove to be a better reference, as the spectral features of the carbon black would not be present. A second point would be the absence of any absorption bands due to absorbed carbon dioxide and water.

Recently Rockley et al[192] have shown that the TGS detector has regions of increased sensitivity which would result in anomalous bands, shoulders and band widths. They concluded that the best type of reference material was actually carbon black obtained from hexane soot.

The photoacoustic signal at constant light intensity is inversley proportional to the frequency of modulation. However as demonstrated above, in FT-IR-PAS the frequency of modulation is dependant upon the mirror velocity and the frequency or wavenumber of the radiation. However the energy of a photon is directly proportional to the frequency, and these effects work in opposite directions effectively counteracting each other.

Another important factor is the variation in the thermal diffusion depth with frequency. This causes the signal at large wavenumbers to be low. Teng and Royce[193] devised a method for overcoming this, which involves varying the mirror velocity of the interferometer. However this method can only be applied to samples having a thickness of more than six times the thermal diffusion length.

Krishnan[194] demonstrated the applicability of the Rosencwaig-Gersho theory to the spectrum of Plexiglas. He calculated the thermal diffusion length of the material for a mirror velocity of 0.16cm s^{-1} at wavenumbers 1700 cm^{-1} and 1000 cm^{-1} . These were 6.46 and 8.43nm res-

pectively. He assumed that all the light was absorbed within a depth $\ell_\beta = \frac{1}{\beta}$ where β is the product of the extinction coeficient (ε) and the concentration (C). For the 1730cm^{-1} carbonyl band ℓ_β = 5μm spectra were obtained of films 0.3,0.7,3.7 and 13.8 μm thick. For the first three the carbonyl band intensity showed a linear dependance on thickness and the relative intensities of the other bands remained constant. However the spectrum of the fourth sample was quite different. The relative intensity of the carbonyl band at 1730cm^{-1} had become weaker and it had developed a lower frequency shoulder. A considerable loss in spectral definition was also observed.

The explanation offered for this effect was that the strong bands had gone into photoacoustic saturation, whereas the weaker bands were still increasing in intensity as thickness increased. McClelland and Kniseley[195] have suggested that saturation would not occur until the thermal diffusion depth was ten times the inverse of the absorption coefficient ($\ell_\beta = \frac{1}{\beta}$), i.e. the light is considered to be totally absorbed within this depth. The fact that saturation occurs well before this criterea is reached can be explained by considering the Beer-Lambert law.

$$I_{abs} = I_o(1 - 10^{-\varepsilon C \ell})$$

I_o = Incident intensity ε = extinction coefficient $\varepsilon C = \beta$

I_{abs} = Absorbed intensity C = Concentration

ℓ = Sample thickness.

When $\ell = \frac{1}{\beta}$ (i.e.$\ell\beta$) then 90% of the incident light is absorbed. When $\ell = 2\ell_\beta$ 99% of the incident light is absorbed. In FT-IR-PAS the intensity of the light at each wavenumber is small, and the sensitivity of the microphone is low. Thus light that is absorbed inbetween ℓ_β and $2\ell_\beta$ will not significantly contribute to the acoustic signal, and the band would show the characteristics of saturation.

The first samples to be studied using FT-IR-PAS included:[189,190,196]

electrical insulation tape, polyurethane feedstock chips, analgesic tablets, polystyrene beads, tobacco leaves, nitrile plastic with different surface morphologies and various coal samples. Other notable applications since 1980 have been:

i) The study of bonding effects in a formulated pesticide[197]. By subtraction of the spectrum of the carrier from the spectrum of the carrier and the pesticide combined and comparing to a transmission spectrum of the pesticide it was possible to show that the hydrogen of the amine group of the pesticide was forming a hydrogen bond with the carrier.

ii) The use of FT-IR-PAS to obtain spectra of compounds on TLC plates.[198] In this case both microphonic and piezoelectric detector systems were employed. Subtraction techniques were again used to eliminate the spectrum of the support so as the spectrum of the applied compound could be obtained. The position of the bands was found to be in good agreement with the transmission spectrum but the relative intensities varied. Some quantitative results were obtained by loading with different amounts of the compound and then plotting a calibration graph.

iii) The determination of catalytic surface adsorption sites[199], which involved studying the effects of introducing carbon monoxide into a PA cell first containing silica and then containing a nickel/silica catalyst.

iv) The analysis of wool/man made fibre blends[200]. The spectrum of wool was subtracted from that of a wool/polyester blend until the spectrum became similar to that of the polyester. In this case 60% of the wool spectrum had to be subtracted indicating that the blend had a 60/40 composition. Following this success spectra of wool and nylon were added together in different proportions to make 'synthetic' spectra. The 'synthetic' spectrum made from 80% wool spectrum/20% nylon spectrum compared well with the actual spectrum of an 80/20 blend, apart from bands at 1700 cm^{-1} and 3000 cm^{-1} which were possibly affected by differences in hydrogen bonding.

v) The quantitative determination of phencyclidine and phenobarbital in complex mixtures.[201] This involved subtracting different proportions of spectra of the compounds that made up the mixture until a flat base line was obtained. Some problems were encountered in trying to achieve a flat base line. These were attributed to differences in the amount of light reflected due to different particle sizes or to saturation effects.

vi) A comparison between ATR and PAS [202] was made during the surface analysis of polymer mixtures. Two mixtures were studied which were:

i) Toluene 2,4-di-isocyanate with 1,2-diamino ethane as chain extender and polyether (tetra-methylene oxide).

ii) Toluene 2,4-di-isocyanate with 1,4-butan-diol as chain extender, poly(dimethyl siloxane) and polyether (polypropylene glycol).

In the second polymer mixture the dimethyl siloxane character increased as the angle of incidence in the ATR experiments increased. That is more DMS was found at the surface. This was done by measuring the relative intensities of the C-H bands due to DMS and the polyurethane N-H bands. In the first mixture the softer component separated towards the surface.

The photoacoustic technique detected impurities which segregated to the surface that ATR did not pick up. This indicated that the photoacoustic technique profiled to a shallower depth.

6.2 The Measurement of the Thermal Conductivity (κ) of the Polymer X.

6.2.1 Experimental Method.

In PAS the maximum thickness of sample that can contribute to the signal, the thermal diffusion depth (μ) is given by:-

$$\mu = \left(\frac{2\kappa}{\omega\rho C}\right)^{\frac{1}{2}}$$

κ = thermal conductivity.
ρ = density
C = specific heat capacity
ω = modulation frequency

In the literature the first three values are available for general

types of polymers but not specific types. The density of polymer X has been measured previously (7.6) and the specific heat capacities do not seem to vary a great deal. However not a lot was known about the thermal conductivity and so this was measured using the following technique. A disc of the polymer, of known area and thickness is placed between two metal rods of the same cross sectional area. The temperature of the two rods is measured using 2 thermocouples. One of the rods is heated by an electrical coil.

The power flowing across the disc at steady state (Q) is given by:-

$$Q = \frac{\kappa A \Delta T}{\Delta x}$$

κ = thermal conductivity $Wm^{-1}K^{-1}$
A = area of disc m^2
ΔT = temperature gradient K^{-1}
Δx = thickness of disc. m

A diagram of the apparatus is shown below.

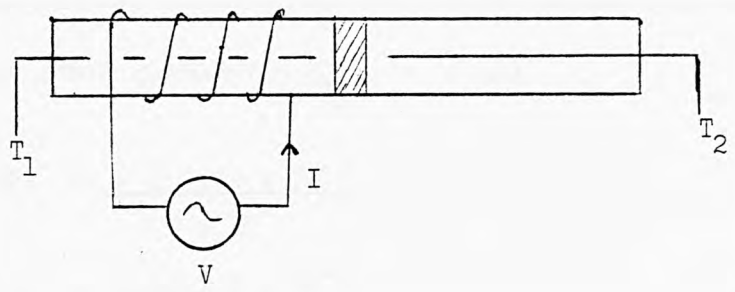

The rods were lagged so that the flow of heat was unidirectional i.e. through the sample. Thus under steady state conditions the power supplied by the electrical circuit (VI) is equal to the power flowing across the sample.

A disc of area $7.85 \times 10^{-5} m^2$ and thickness $4.5 \times 10^{-5} m$ was prepared by placing powdered polymer in a press. The disc was then placed between the two rods and a voltage of 2V was applied across the coil. When steady state had been reached i.e. when T_1 and T_2 were constant, the voltage (V) the current(I) and temperatures T_1 and T_2 were noted. The voltage was then increased in increments up to a value of 7.7V. The system was allowed to equilabrate each time before readings were taken.

A graph of Q against ΔT should yield a straight line of gradient $\frac{\kappa A}{\Delta x}$ hence κ can be found.

The results are given in Table 6.1 and plotted in figure 6.1.

Table 6.1

V (Volts)	I (Amps)	Q (Watts)	T_1 °C	T_2 °C	ΔT K
2	0.05	0.10	22.1	21.5	0.6
2.5	0.09	0.225	22.6	21.5	1.1
3.1	0.10	0.31	23.6	21.6	2.0
3.5	0.12	0.42	24.7	21.8	2.9
4.1	0.14	0.574	26.7	22.1	4.6
4.7	0.16	0.752	29.5	22.9	6.6
5.1	0.18	0.918	31.3	23.3	8.0
5.7	0.20	1.14	33.4	23.6	9.8
6.1	0.22	1.34	35.3	23.8	11.5
6.7	0 24	1.61	37.9	24.5	13.4
7.2	0.26	1.87	40.8	25.2	15.6
7.7	0.28	2.16	43.8	25.9	17.9

From the graph gradient = $\frac{2.18}{18} = 0.121$

$$\therefore \quad 0.721 = \frac{\kappa \times 7.85 \times 10^{-5}}{4.5 \times 10^{-5}}$$

$$\kappa = 0.0694 \text{ W m}^{-1}\text{K}^{-1}$$

This value is much lower than the literature value for epoxy resins (0.17-0.21 W $m^{-1}K^{-1}$) one reason for this is that thermal contact in the powdered form maybe less than in film form.

Thus one suggestion for further work is to measure the thermal conductivity of a film. The easiest way to do this would be to take a sample on a Teflon paper substrate as the uncrosslinked polymer is not mechanically very strong. Hence the thermal conductivity of the Teflon paper would be required.

6.3 Calculation of Thermal Diffusion Depths (μ) and Optical Absorption Lengths (ℓ_β) for Three Bands in the FT-IR-PA Spectrum of Polymer X At Six Mirror Velocities.

From the literature values of κ,ρ and C the thermal diffusivity (α)

Figure 6.1
A graph of power supplied vs temperature gradient for a disc of polymer A.

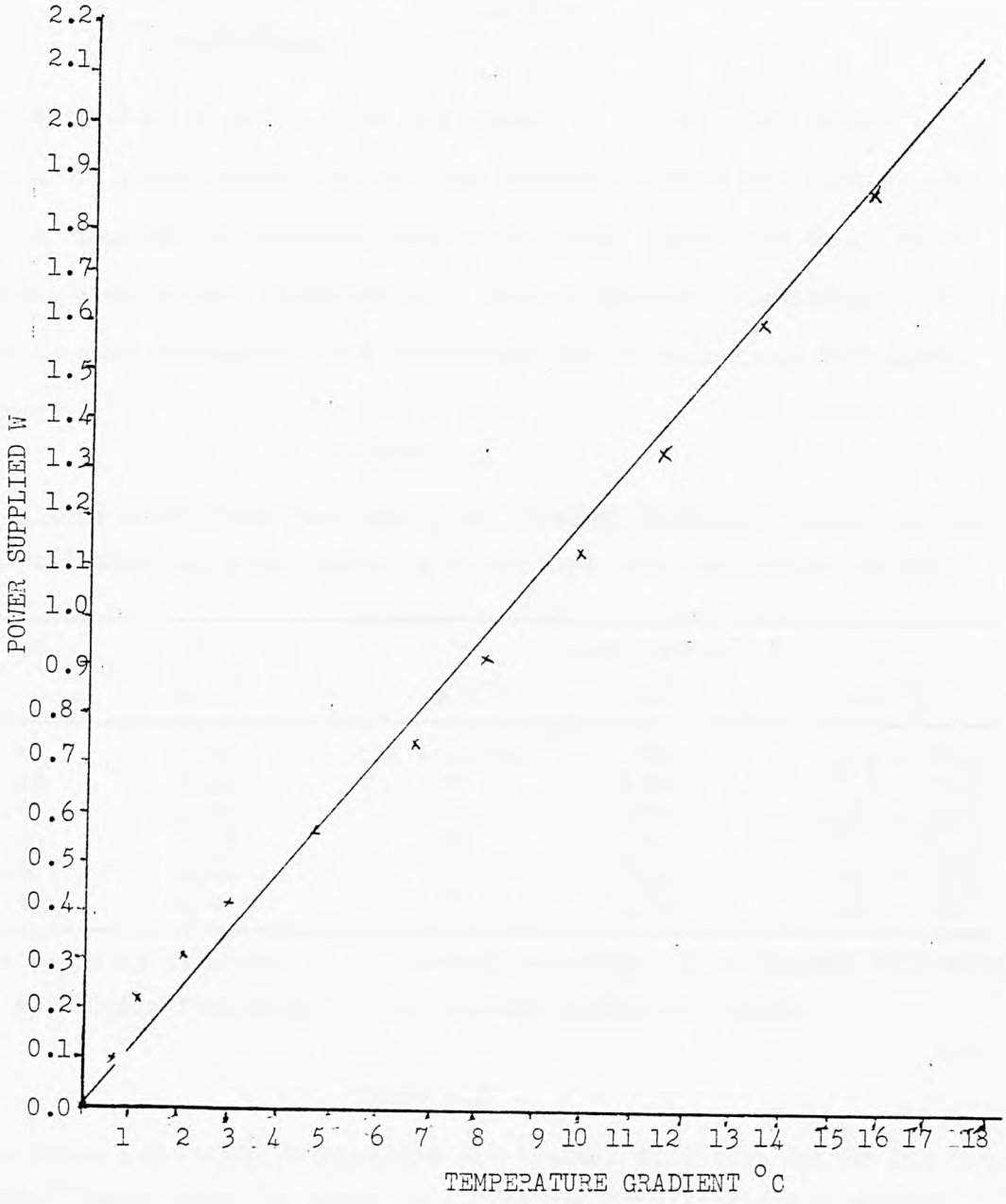

for epoxy resins is 1.2 - 1.9 x $10^{-7} m^2 s^{-1}$ (see section 2.6.3), if the value for thermal conductivity from 6.2 and the density from 7.6 are used. Assuming that the specific heat capacity is the same as the literature value the thermal diffusivity is given by

$$\alpha = \frac{\kappa}{\rho C} = \frac{0.007}{1290 \times 1000} = 5 \times 10^{-8} m^2 s^{-1}$$

The bands used to follow cure are 1600 cm^{-1}, 1572 cm^{-1} and 984 cm^{-1}. In the following tables the extreme lefthand numbers are labels used by the computer for specific mirror velocity. There are 61 of these ranging from 00-60. Although they have no physical significance they will be used throughout as a convenient way of specifying the mirror velocity.

Table 6.2

Calculated modulation frequencies and thermal diffusion depths for the 1600 cm^{-1} band using the value of α obtained from literature values.

CV	V $cm\ s^{-1}$	α $m^2 s^{-1}$	ω at 1600 cm^{-1} s^{-1}	μ $x10^{-6} m$
20	0.28	1.2 - 1.9x10^{-7}	896	16.4 - 20.6
25	0.41	"	1312	13.5 - 17.0
30	0.56	"	1792	11.6 - 14.6
40	1.12	"	3584	8.2 - 10.3
50	2.24	"	7168	5.8 - 7.3
60	4.49	"	14368	4.1 - 5.1

CV = computor velocity V = actual velocity α = thermal diffusivity
ω = modulation frequency μ = thermal diffusion length.

Table 6.3

Calculated modulation frequencies and thermal diffusion depths for the 1572 cm^{-1} band using the value of α obtained from literature values.

CV	V $cm\ s^{-1}$	α $m^2 s^{-1}$	ω at 1572 cm^{-1} s^{-1}	μ $x10^{-6} m$
20	0.28	1.2-1.9x10^{-7}	880	16.5 - 20.8
25	0.41	"	1289	13.6 - 17.2
30	0.56	"	1761	11.7 - 14.7
40	1.12	"	3521	8.3 - 10.4
50	2.24	"	7043	5.8 - 7.3
60	4.49	"	14117	4.1 - 5.2

Table 6.4

Calculated modulation frequencies and thermal diffusion depths for the $984cm^{-1}$ band using the value of α obtained from literature values.

CV	V $cm\ s^{-1}$	α m^2s^{-1}	ω at $1572cm^{-1}$ s^{-1}	μ $x10^{-6}m$
20	0.28	$1.2\text{-}1.9x10^{-7}$	551	20.9 - 26.3
25	0.41	"	807	17.2 - 21.7
30	0.56	"	1102	14.8 - 18.6
40	1.12	"	2204	10.4 - 13.1
50	2.24	"	4408	7.4 - 9.3
60	4.49	"	8836	5.2 - 6.6

Table 6.5

Calculated modulation frequencies and thermal diffusion depths for the $1600cm^{-1}$ band using experimental values to obtain α.

CV	V $cm\ s^{-1}$	α m^2s^{-1}	ω at $1600cm^{-1}$ s^{-1}	μ $x10^{-6}m$
20	0.28	0.5×10^{-7}	896	10.6
25	0.41	"	1312	8.7
30	0.56	"	1792	7.6
40	1.12	"	3584	5.3
50	2.24	"	7168	3.7
60	4.49	"	14368	2.6

From chapter 4 the values of β ($=\varepsilon C$) for the three bands in polymer X are:-

$$\beta_{1600} = 913 \times 3.3 = 3013$$

$$\beta_{1572} = 413 \times 3.3 = 1363$$

$$\beta_{984} = 130 \times 3.3 = 429$$

$$\ell_\beta = \frac{1}{\beta} \quad \therefore \quad \ell_\beta \text{ at } 1600cm^{-1} = 3.32 \times 10^{-6}m$$

$$\ell_\beta \text{ at } 1572cm^{-1} = 7.34 \times 10^{-6}m$$

$$\ell_\beta \text{ at } 984cm^{-1} = 23.31 \times 10^{-6}m$$

From the values of μ and ℓ_β it is obvious that any film greater than $3.3 \times 10^{-6}m$ thick will give a saturated band at $1600cm^{-1}$ for any mirror velocity below 50. For the $1572cm^{-1}$ band saturation will occur below velocity 30. The $984cm^{-1}$ band will show saturation below velocity 20.

6.4 The Instrument.

The instrument used to obtain the spectra was a Nicolet 60 SX FT-IR spectrometer fitted with an EG and G Princeton photoacoustic cell. The resolution of the instrument is determined by the number of transform points taken, the greater the number of transform points the better the resolution. In this case a resolution of 8 cm^{-1} was used.

As mentioned above there are 60 possible mirror velocities ranging from 0.07cm/sec to 4.48cm/sec. Unfortunately the spectrometer would not operate below mirror velocity 21 i.e. 0.3cm s^{-1}. The same carbon black sample was used to correct each spectrum thus the results will be internally consistent. However as demonstrated by Riseman and Eyring[191] the spectral features of the carbon black may produce anomalous bands in the spectra. The spectra of carbon black was obtained at five mirror velocities 25,30,40,50 and 60. However the polymer films gave weak and uncorrectable interferograms above velocity 40. Thus a restriction was placed on the range of velocities available.

Unfortunately a standard sample size was not used due to the lack of an appropriate cutting tool.

6.5 Experimental Method.

K bars 1 and 2 used to lay down the films on Teflon paper. Thus film thicknesses were approximately 3 x 10^{-6}m and 5 x 10^{-6}m. These films were irradiated for various lengths of time under the 1800W UV curing lamp. The film on the KBr disc was deposited by K bar 4. This gave a thickness of 9 x 10^{-6}m as measured by transmission IR spectroscopy. This same technique was used to establish when 25% of the original double bond content had disappeared. The powdered sample was obtained by scraping the unirradiated polymer off the Teflon paper substrate.

6.6 Results and Discussion.

The spectrum of the powdered unirradiated polymer X was obtained at

Figure 6.2
FT-IR-PA spectrum of a powdered sample
of polymer X.

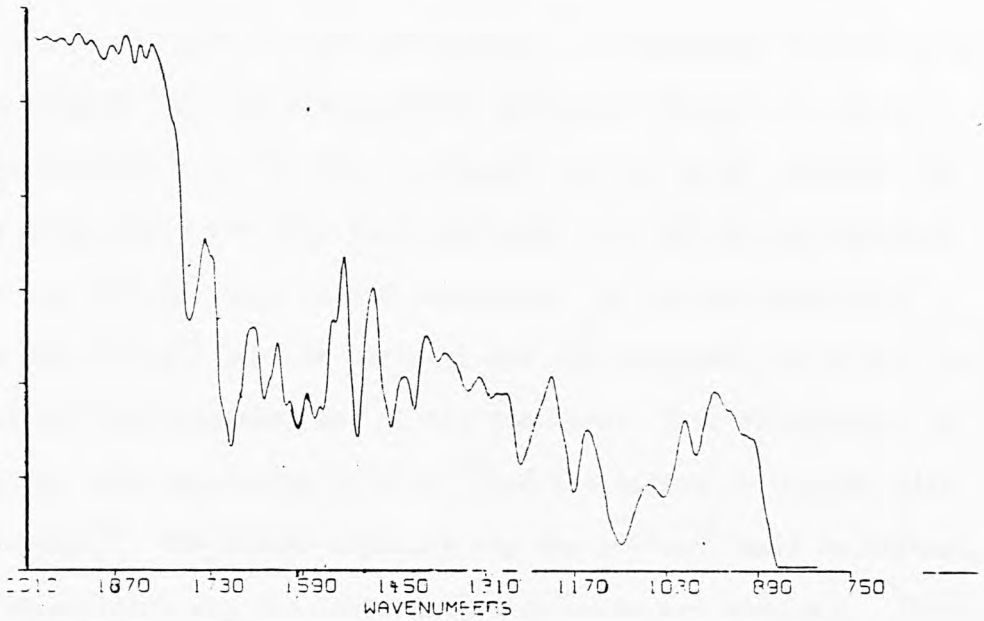

Figure 6.3
IR transmission spectrum of polymer X.

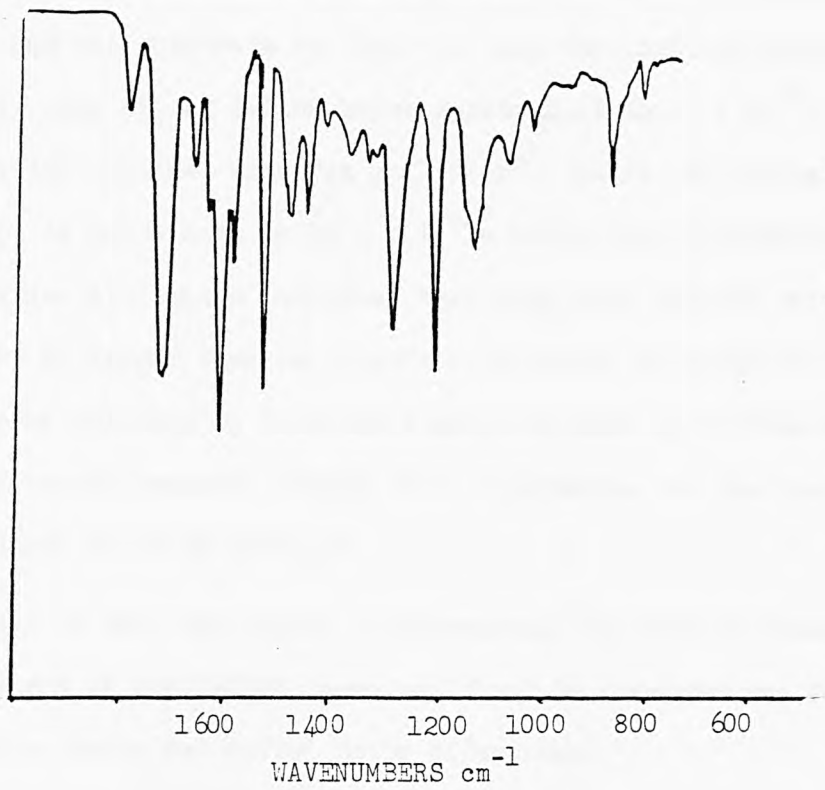

mirror velocity 40. The absorption spectrum was inverted after ratio ing to carbon black, in order to make comparison with transmission spectra easier and also to aid subtraction. A comparison between this spectrum (figure 6.2) and transmission spectrum (figure 6.3) shows many similarities, i.e. the band positions are the same. However the relative intensities are very much different i.e. in the transmission spectrum the 1600 cm^{-1} band is the strongest. In the photoacoustic spectrum the 1700 cm^{-1} band is stronger and the strongest bands are observed at the low frequency end of the spectrum. This observation is explained by both saturation effects[194] and the effect of thermal diffusion depths.[193] The former explains why the 1600 cm^{-1} band is weaker, the latter explains why the lower frequency bands are stronger. These bands are stronger because a greater depth of sample is giving rise to a greater signal.

The spectra of the films on the Teflon paper substrate are far more complicated (figure 6.4b). This is due to the Teflon paper spectrum being superimposed on the polymer spectrum. Figure 6.4 shows the polymer and the substrate on their own and the combined spectrum. The fact that some of the Teflon paper spectrum of the 5×10^{-6} m film appears in the combined spectrum at 1790 cm^{-1}, where the thermal diffusion depth (μ) is calculated to be 5×10^{-6} m using the experimentally determined values of κ and ρ indicates that they need further investigation, as μ must be larger than calculated at a mirror velocity of 1.12cm/sec. If a mirror velocity 60 (4.49cm/s) could be used by introducing Helium as the acoustic transfer medium, more information on the thermal diffusion depth could be obtained.

An attempt to test the theory by increasing the film thickness until the spectrum of the Teflon paper could not be observed was thwarted by the spectra being too noisy to be of any use.

Figure 6.4
FT-IR-PAS of polymer, substrate and the polymer/ substrate combined.

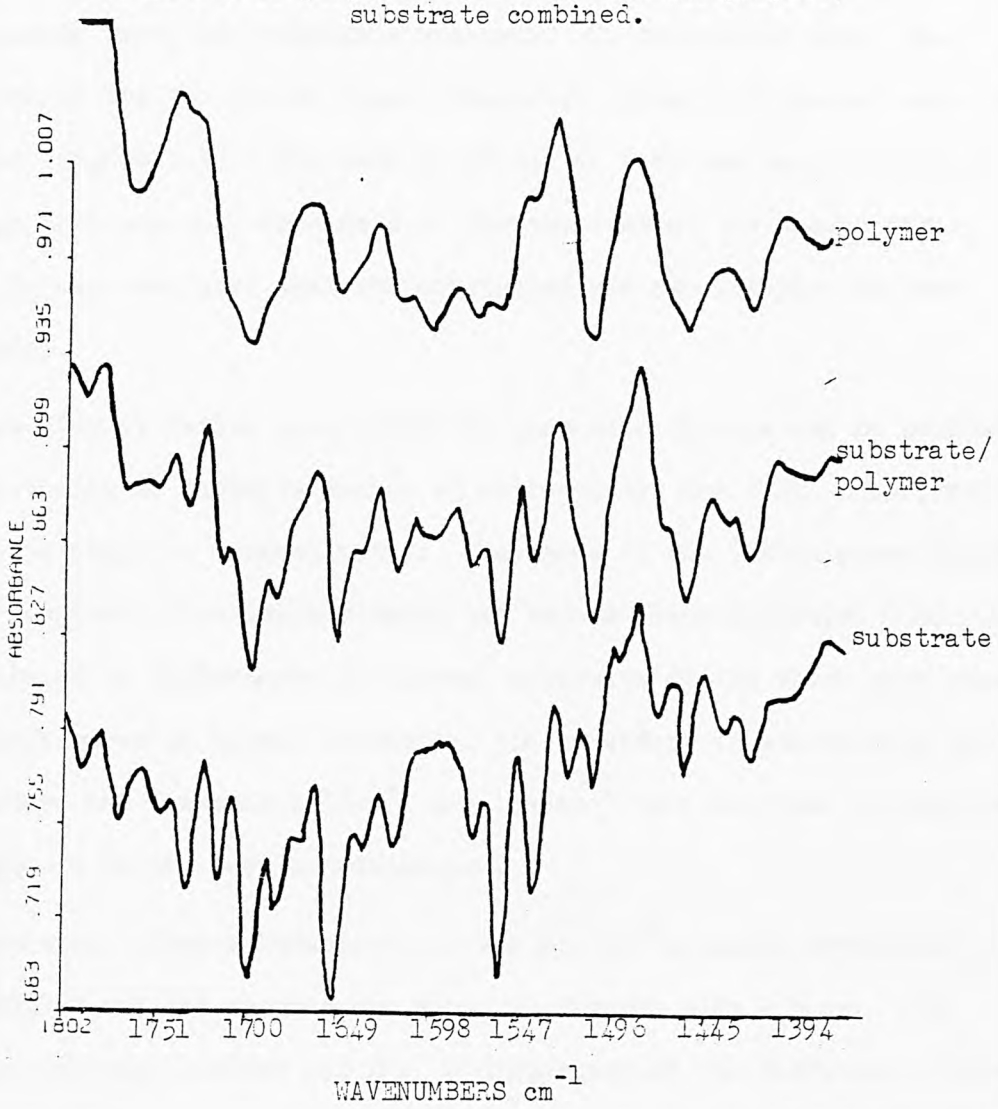

Figure 6.5
FT-IR-PAS of the two different Teflon papers, clear and opaque.

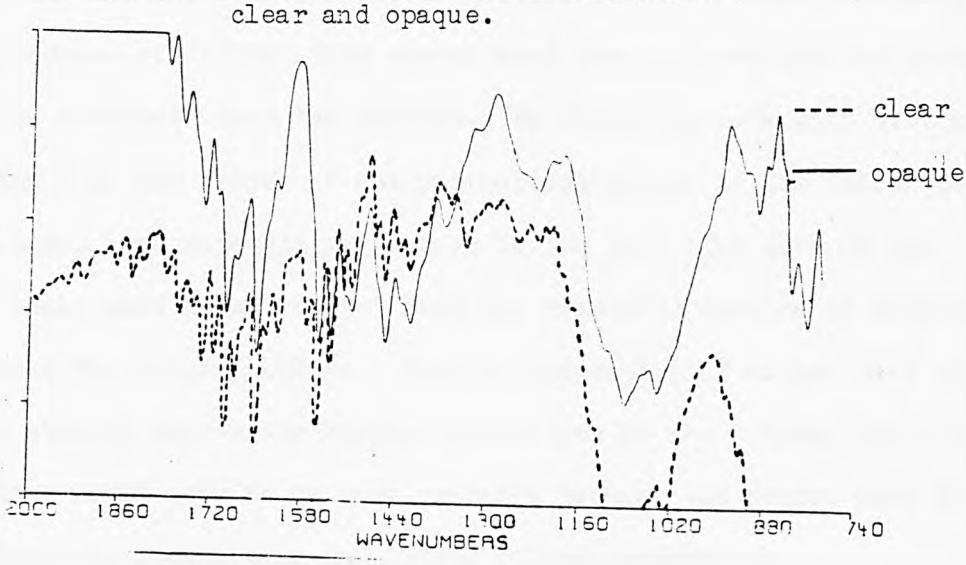

In order to make comparisons easier the spectrum of Teflon paper was subtracted from each composite spectrum. To facilitate this, the spectra of the two Teflon paper substrates (clear and opaque) were obtained (figure 6.5). The band positions in both are very similar although some are only shoulders in the spectrum of the opaque paper. Thus it was concluded that the substrates are essentially the same material.

Subtraction of Teflon paper from the composite spectra can be performed at virtually an infinite number of ratios using the 60SX. The problem was obtaining the correct ratio. When some of the Teflon paper bands were smoothed, some polymer bands had become unrecognisable. This was attributed to differences in thermal diffusion depths which give rise to differences in signal intensity. In an effort to standardise the procedure the bands at $1553cm^{-1}$ and $1537cm^{-1}$ were smoothed to what was thought to be the best approximation.

The spectra, after subtraction, of the $5 \times 10^{-6}m$ sample irradiated for 60,180,360 and 540 seconds are shown in figures 6.6a - 6.6g. The mirror velocity setting was 40. A comparison of the different irradiation times shows a decrease in the intensity of both the $1600cm^{-1}$ and the $1645cm^{-1}$ bands. Thus qualitatively one can say reaction has occured however any quantitative conclusion would be subject to large errors because of difficulties encountered when subtracting the correct amount of substrate from the spectra. By comparing 6.6a with 6.6b and 6.6e with 6.6f the effect of not subtracting enough of the Teflon paper can be seen. One interesting feature is the fact that more of the Teflon paper must be subtracted from the composite spectra of samples irradiated for longer periods. This is indicative of either more light getting through and/or the thermal properties of the polymer improving. The latter would seem to be more probable because the region used for optimizing the subtraction has little polymer absorption.

Figure 6.6a
0.5 Times the Teflon paper spectrum subtracted from the spectrum of polymer X, irradiated for 60 seconds.

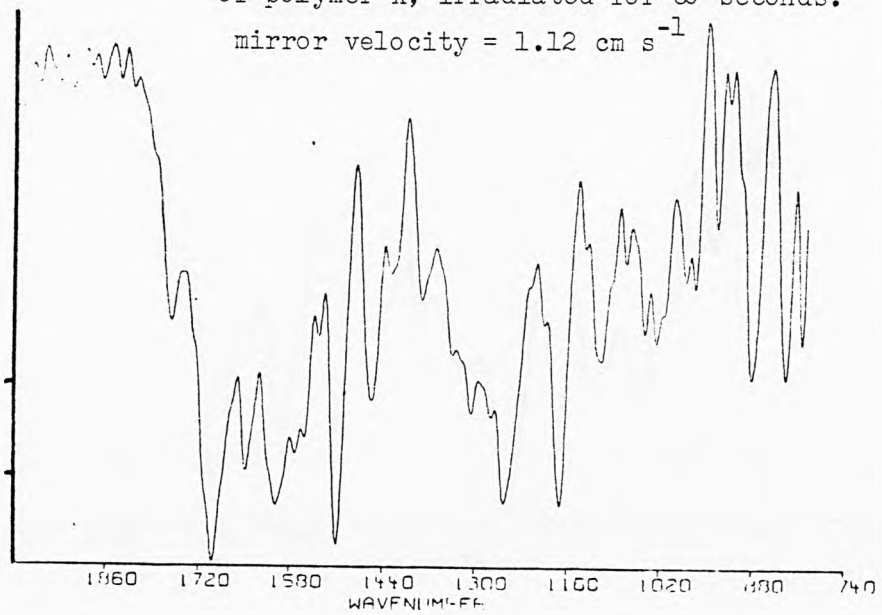

Figure 6.6b
0.6 Times the Teflon paper spectrum subtracted from the spectrum of polymer X, irradiated for 60 seconds.

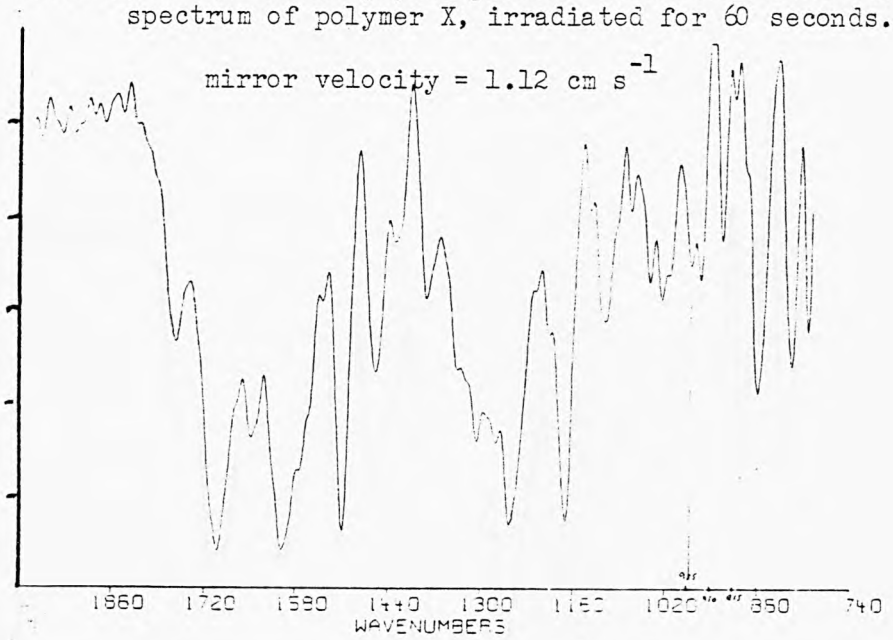

Figure 6.6c
0.5 Times the Teflon paper spectrum subtracted from the spectrum of polymer X, irradiated for 180 seconds.

mirror velocity = 1.12 cm s^{-1}

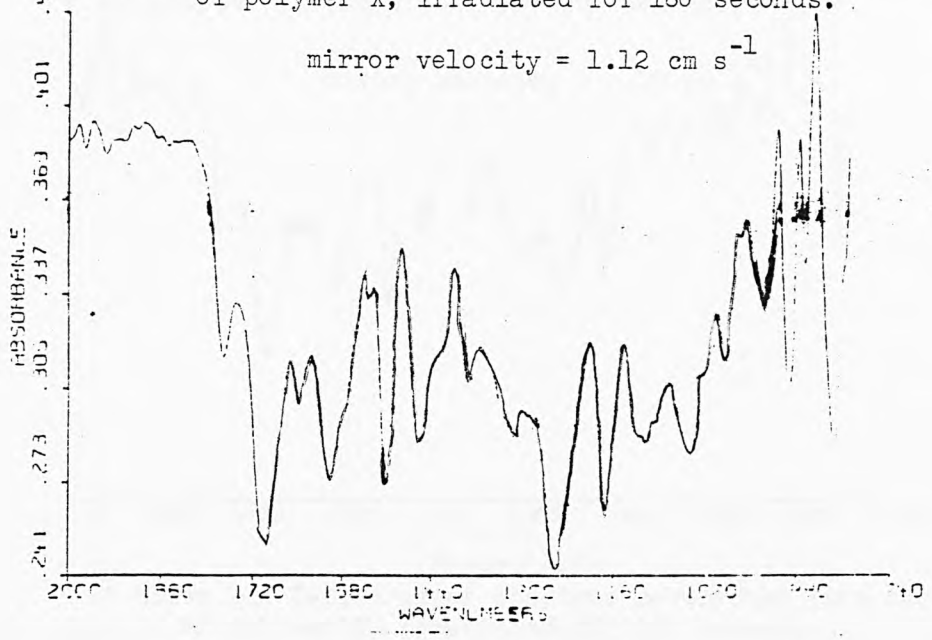

Figure 6.6d
0.6 Times the Teflon paper spectrum subtracted from the spectrum of polymer X, irradiated for 180 seconds.

mirror velocity = 1.12 cm s^{-1}

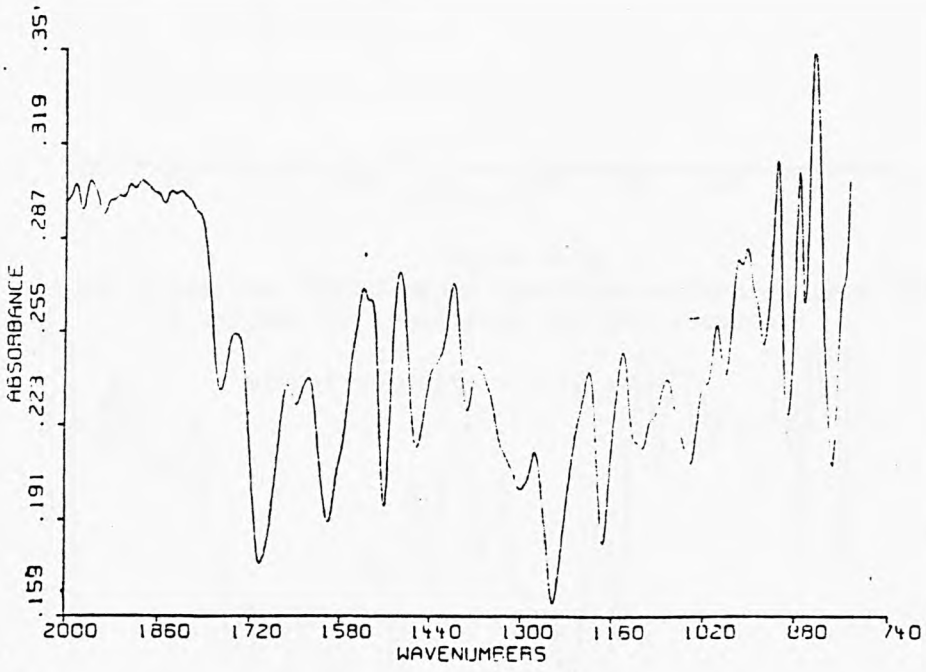

Figure 6.6e

0.8 Times the Teflon paper spectrum subtracted from the spectrum of polymer X, irradiated for 360 seconds.

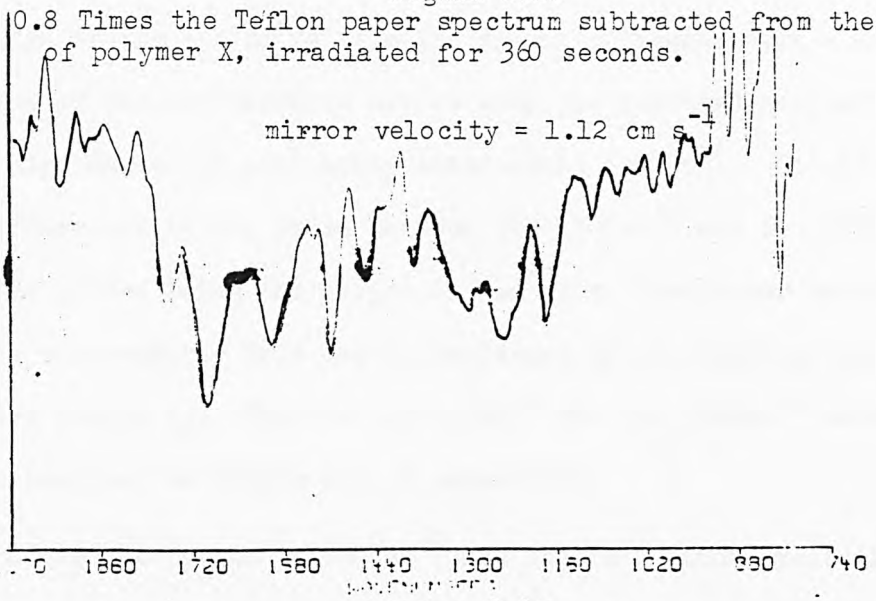

Figure 6.6f

0.5 Times the Teflon paper spectrum subtracted from the spectrum of polymer X, irradiated for 360 seconds.

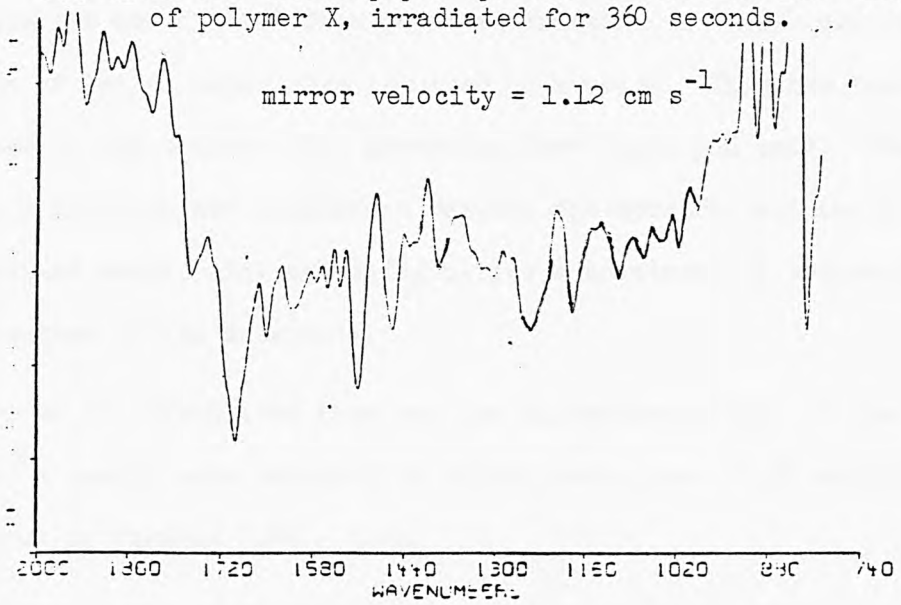

Figure 6.6g

1.0 Times the Teflon paper spectrum subtracted from the spectrum of polymer X, irradiated for 540 seconds.

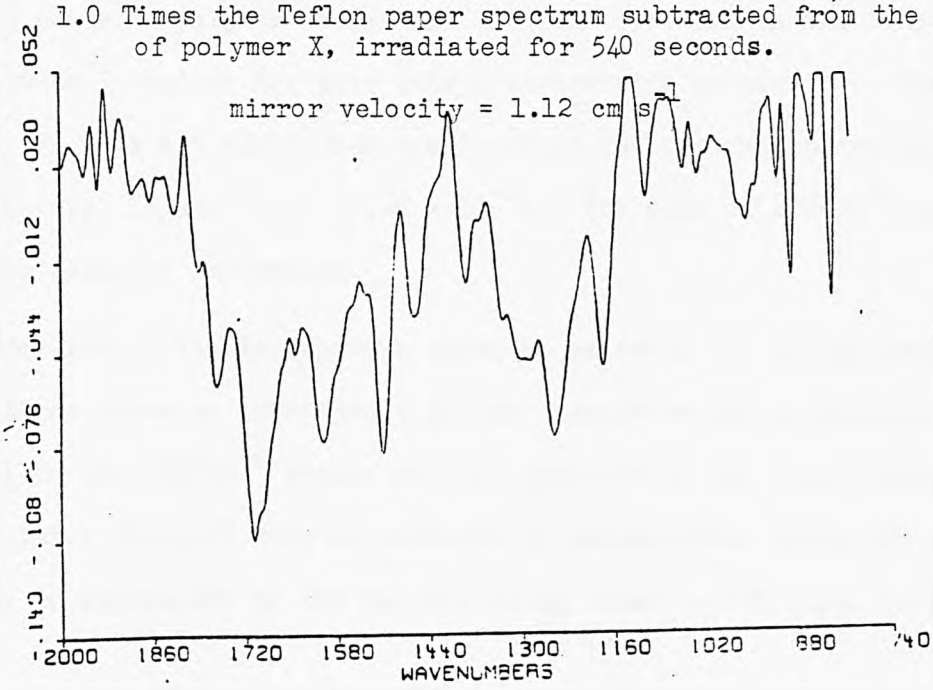

The spectra of the 3×10^{-6}m film are shown in figures 6.7a - 6.7f. A comparison of the unirradiated sample with the powdered polymer sample shows a high degree of similarity above about $1000 cm^{-1}$. One of the major differences is the ratio between the $1700 cm^{-1}$ and the $1600 cm^{-1}$ bands, the latter being the larger in the film, the former being the larger in the powder. This may be explained by considering the optical absorption length ℓ_β. This is 3.32×10^{-6} for the $1600 cm^{-1}$ band and thus the band may be coming out of saturation.

By monitoring the $1645 cm^{-1}$, $1600 cm^{-1}$ and $1572 cm^{-1}$ bands cyclodimerization is again seen to have occurred. Here again there was a need to increase the amount of Teflon paper subtracted. In this case larger amounts of Teflon paper were required on average. This has been attributed to the thinner film absorbing less light and heat. The units of the y axis are not consistant between the spectra because of lack of constant sample size and difficulties encountered in subtracting the spectrum of the substrate.

Spectra of the irradiated face and the unirradiated face of the 9×10^{-6}m sample were obtained at mirror velocities 25,30 and 40. These are shown in figures 6.8a - 6.8d.

A spectrum of the unirradiated side taken at velocity 25 is compared to the powdered polymer shows that the film spectrum in the $1705 cm^{-1}$ and $1600 cm^{-1}$ regions has gone into photoacoustic saturation. The reasons for this are clear when one looks at the optical absorption lengths e.g. $1600 cm^{-1}$ $\ell_\beta = 3.32 \times 10^{-6}$m. The peak at $1572 cm^{-1}$ is also showing signs of saturation.

A comparison of the two spectra taken at velocity 25, of the front and back faces shows an improvement in fine structure and a slightly weaker signal in the $1600 cm^{-1}$ region for the spectrum of the front face. For a 9μm thick film 25% cure as measured by transmission infra-red spectroscopy is equivalent to the top 3μm being cured to 85%, i.e. no further

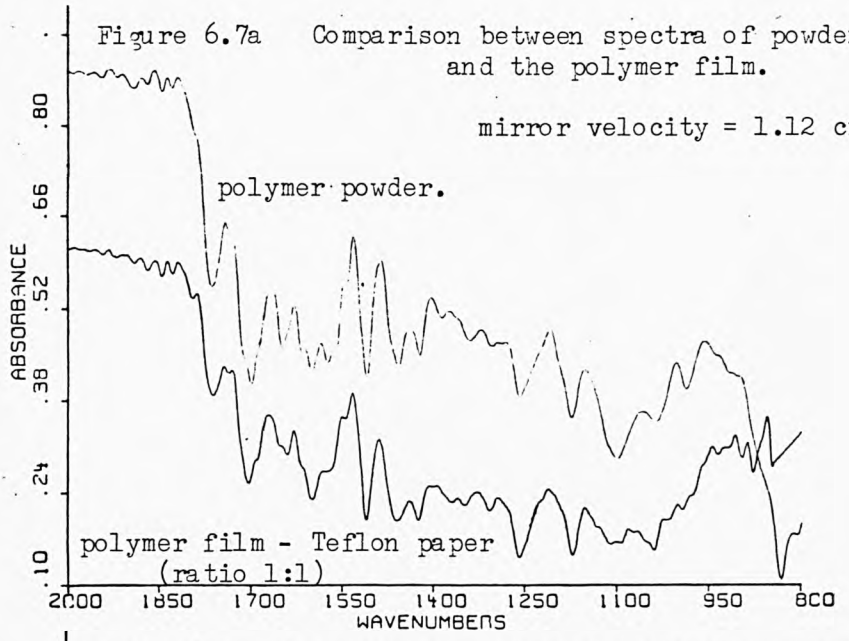

Figure 6.7a Comparison between spectra of powdered polymer X and the polymer film.

mirror velocity = 1.12 cm s^{-1}

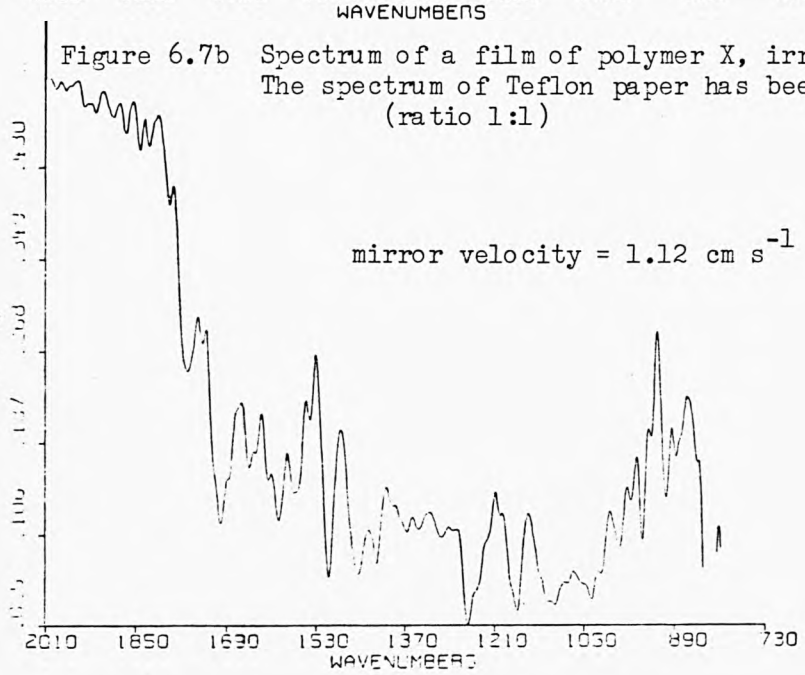

Figure 6.7b Spectrum of a film of polymer X, irradiated for 30s. The spectrum of Teflon paper has been subtracted out. (ratio 1:1)

mirror velocity = 1.12 cm s^{-1}

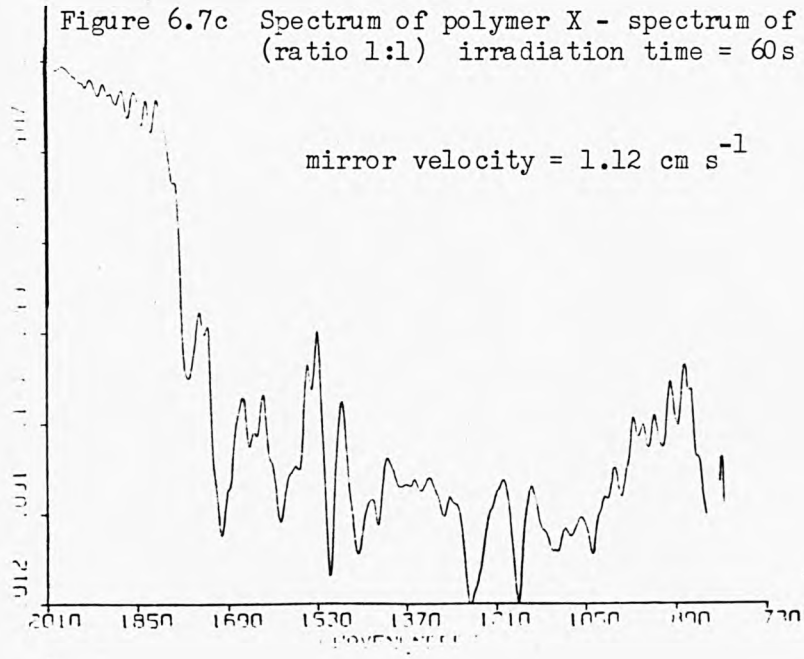

Figure 6.7c Spectrum of polymer X - spectrum of Teflon paper. (ratio 1:1) irradiation time = 60s

mirror velocity = 1.12 cm s^{-1}

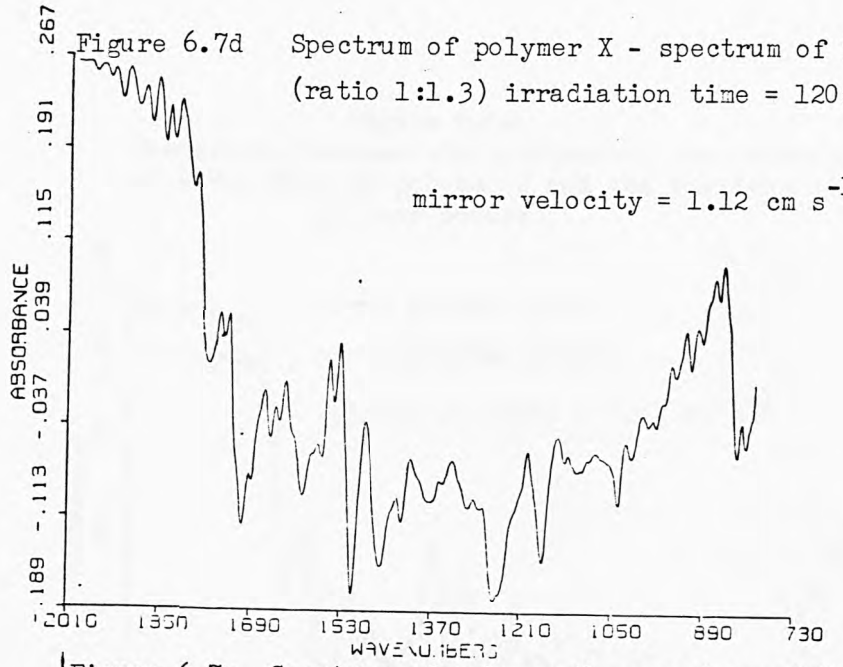

Figure 6.7d Spectrum of polymer X - spectrum of Teflon paper. (ratio 1:1.3) irradiation time = 120s

mirror velocity = 1.12 cm s^{-1}

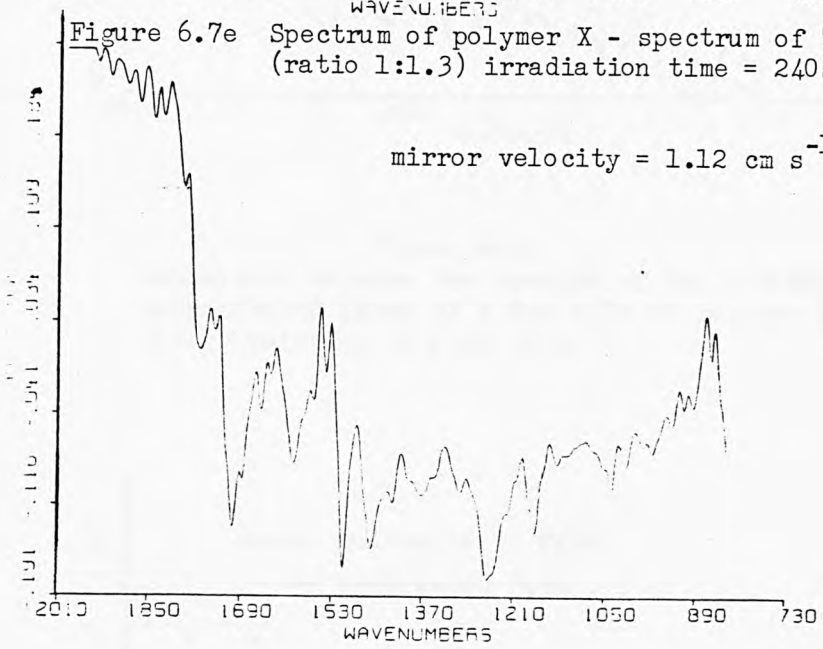

Figure 6.7e Spectrum of polymer X - spectrum of Teflon paper. (ratio 1:1.3) irradiation time = 240s

mirror velocity = 1.12 cm s^{-1}

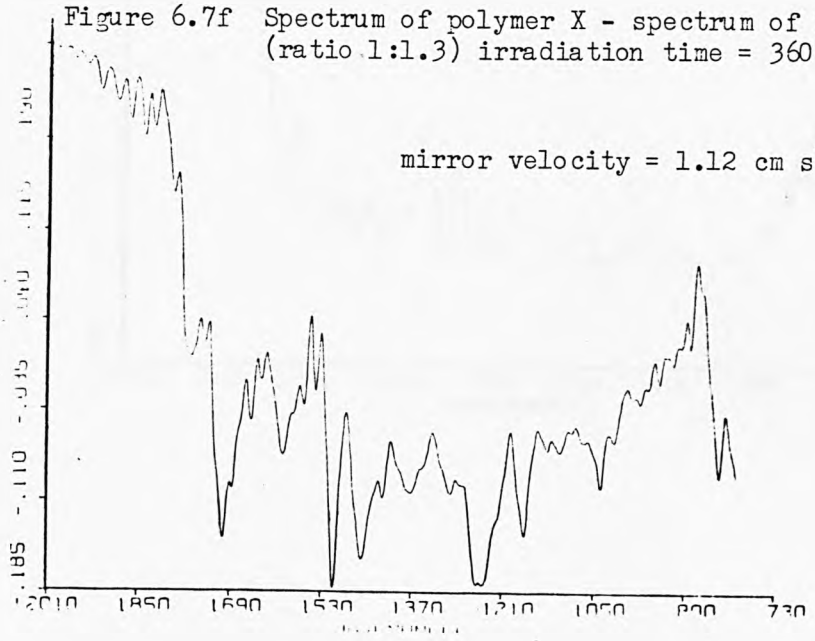

Figure 6.7f Spectrum of polymer X - spectrum of Teflon paper. (ratio 1:1.3) irradiation time = 360 s

mirror velocity = 1.12 cm s^{-1}

Figure 6.8a
Comparison between the spectrum of the unirradiated face of a 9μm film of polymer X and the spectrum of unirradiated polymer powder.

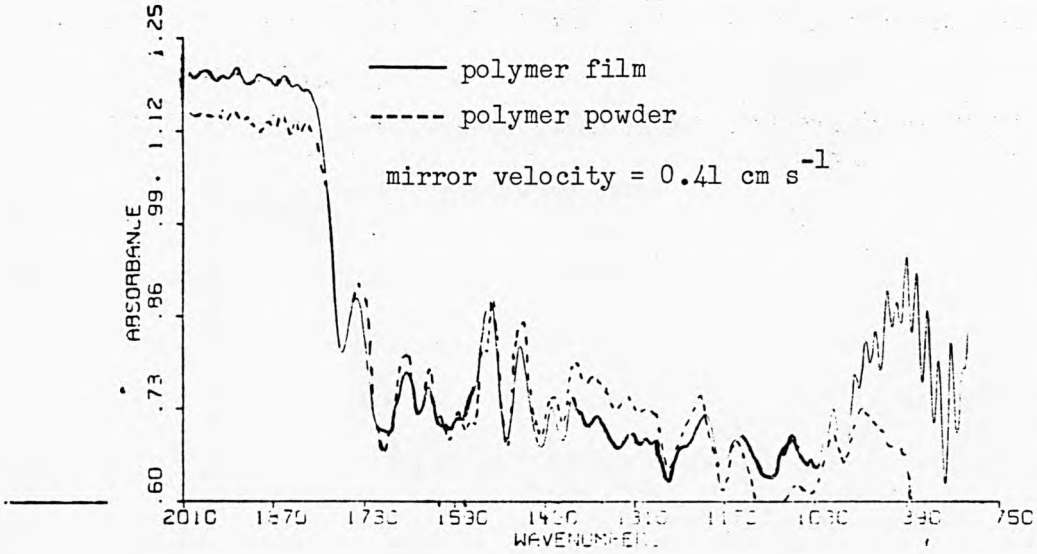

Figure 6.8b
Comparison between the spectra of the irradiated and unirradiated faces of a 9μm film of polymer X at a mirror velocity of 0.41 cm/s.

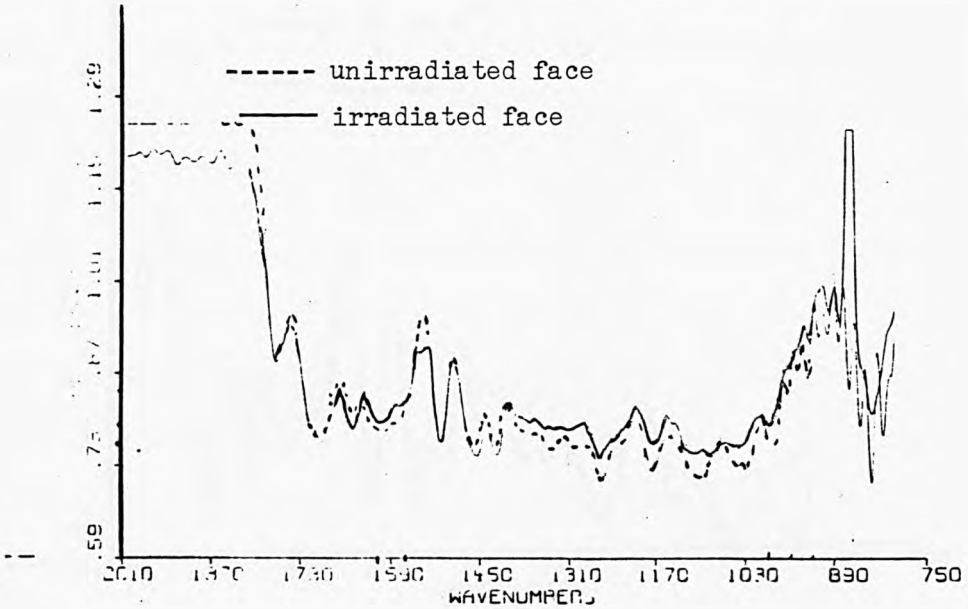

Figure 6.8c
Comparison between the spectra of the irradiated and unirradiated faces of a 9μm film of polymer X at a mirror velocity of 0.56 cm/s.

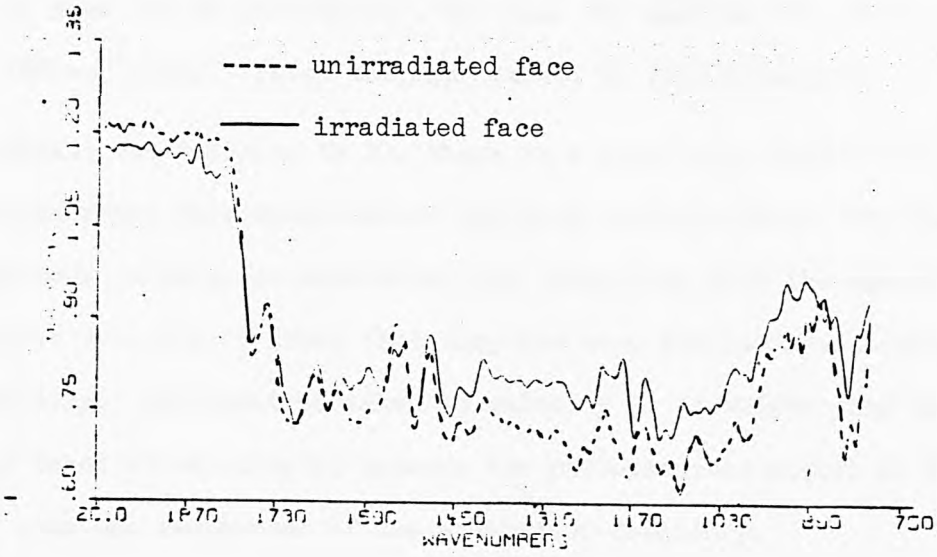

Figure 6.8d
Comparison between the spectra of the irradiated face of a 9μm film of polymer X, taken at mirror velocities of 0.56 and 1.12 cm/s.

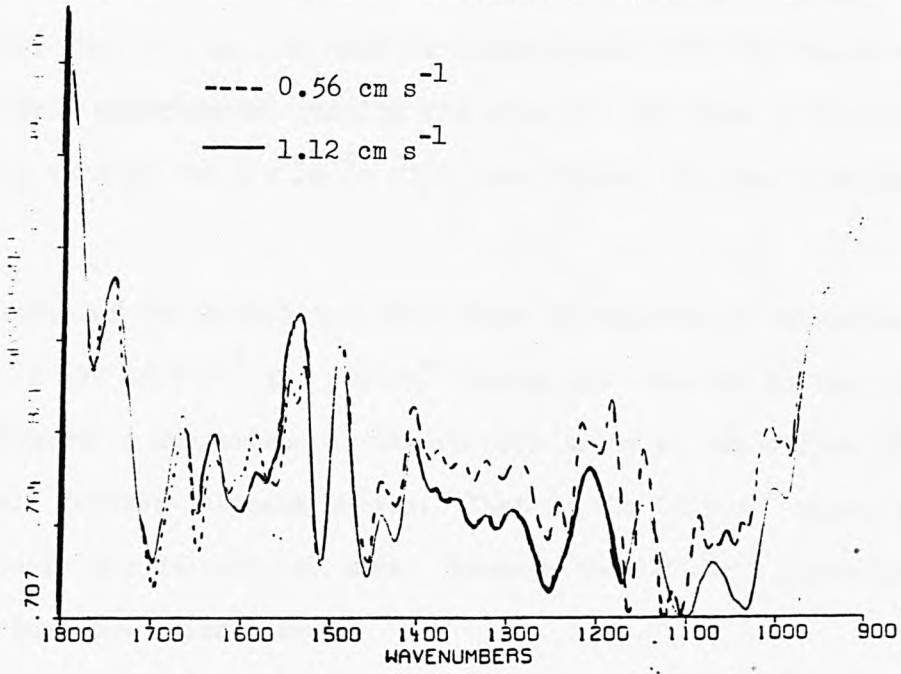

cure can occur in the top 3μm because the rest of the chromophores are in unreactive sites. Thus the back face would give saturated signals for the 1572cm^{-1}, 1600cm^{-1} and 1705cm^{-1} bands. However because chromophore has been removed from the front face of the sample the 1572cm^{-1} band will come out of saturation , and also the band on the otherside of the 1600cm^{-1} band. Hence the improvement in fine structure.

On increasing the velocity to 30, there is a very large difference between the front face spectrum and the back face spectrum. The back face spectrum is still in saturation and comparison with the spectra obtained at velocity 25 shows that they are very similar apart from the intensity. The spectrum taken at velocity 30 is weaker than the spectrum taken at velocity 25 because the photoacoustic signal is dependant upon the reciprocal of the modulation frequency.

The front face spectrum shows that a lot of the 1600cm^{-1} band has disappeared although the 1645cm^{-1} remain virtually unchanged. The loss of the 1600cm^{-1} would indicate that the thermal diffusion length (μ) is shorter than 3-4 μm. As this is inconsistent with the value calculated from experimental results and with the spectrum of Teflon paper appearing through the 5 x 10^{-6}m film (see above), further work must be done.

The spectrum of the irradiated face taken at velocity 40 shows cure has occured if the 1645cm^{-1} and 1600cm^{-1} bands are compared to the 1705cm^{-1} band. However a comparison of the spectra taken at velocities 30 and 40 reveals further inconsistancies. That is the 1645cm^{-1} shows a lot more cure in the velocity 40 case. However the 1600cm^{-1} shows less cure as does the 984cm^{-1} band.

6.7 Conclusion.

The Princeton photoacoustic cell combined with the Nicolet 60SX can give well resolved infra-red spectra of very small samples in a short

time. However the quality of the spectra depends upon the type of sample and how highly absorbing it is. That is powders give better spectra than films, highly absorbing compounds may go in to photoacoustic saturation. A correction ought to be applied in any further work so that the relative intensities of the bands, affected by variations in thermal diffusion depth, can mirror those in transmission spectra more closely.

If the samples are thermally thin, problems occur with the substrate spectrum being superimposed on the sample spectrum. This can be overcome by subtraction of the substrate spectrum from the composite spectrum. Complications arise because of variations in thermal diffusion depth which causes the intensity of the substrate spectrum to vary from one end of the spectrum to the other.

Low mirror velocities limit the range of thermal diffusion lengths in theory, to those outside some important optical absorption lengths at particular wavenumbers. Although Helium may allow faster mirror velocities to be used, the frequency response of the microphone <10 k Hz may become a second limiting factor.

Although some of the results obtained from the 9μm sample without a substrate, give encouraging signs that depth profiling is possible using this system inconsistent results mean that further work must be done.

CHAPTER SEVEN

EXPERIMENTAL

7.1 Photoacoustic Instrumentation

The photoacoustic spectrometer used during this project was the OAS 400 spectrometer built by EDT Research. The source of light is a short arc xenon continuum source. The light is modulated using a rotating disc, which can rotate at 6 different speeds so as to give modulation frequencies of 10,20,40,80,160 and 240 Hz. After modulation the light is passed through and f/4 monochromator, the scan rate of which can be altered between 10 and 200 nm/minute using 5 selectors.

On emerging from the monochromator the light is split into two beams of unequal intensity. The smaller fraction is reflected onto a pyroelectric detector to provide a reference signal. This signal is used to correct the photoacoustic signal for variation in source intensity with wavelength and time. The larger fraction is reflected onto the cell, which is an aluminium non resonant cell with transparent fused silica windows. The cell contains a microphone whose diaphragm forms part of the wall.

The signals from the cell and the pyroelectric detector are passed into two separate lock-in amplifiers which consist of 6 tuned amplifiers tuned to a narrow band of frequencies (within ±5Hz of the modulation frequency), and are brought into operation separately. That is when a certain modulation frequency is chosen the corresponding amplifier is also selected. The reference signals for the phase sensitive detectors in these amplifiers are provided from the rotating sector source modulator.

The outputs from the lock-in amplifiers are fed into a ratiometer, where they are mixed and the resultant signal is taken to a displaymeter and

to an X-Y recorder.

There is a capability to adjust the sensitivity of the microphone. This consists of a selector switch with settings between 10μV and 300mV, in a 1-3-10 sequence, the latter being the least sensitive. A variable potentiometer acts in sympathy with the selector and it is used to adjust the sensitivity between the set values.

The phase difference between the signal from the sample and that from the rotating sector can be monitored using the phase angle facility. The optimum phase angle giving maximum signal is determined as follows:-

1) Find the approximate phase angle that gives maximum signal.
2) Shift to 90° out of phase (when the 2 signals are exactly 90° out of phase no signal is obtained).
3) Adjust phase control to null reading.
4) Shift back by 90°.

Figure 7.1

A schematic diagram of the PAS spectrometer.

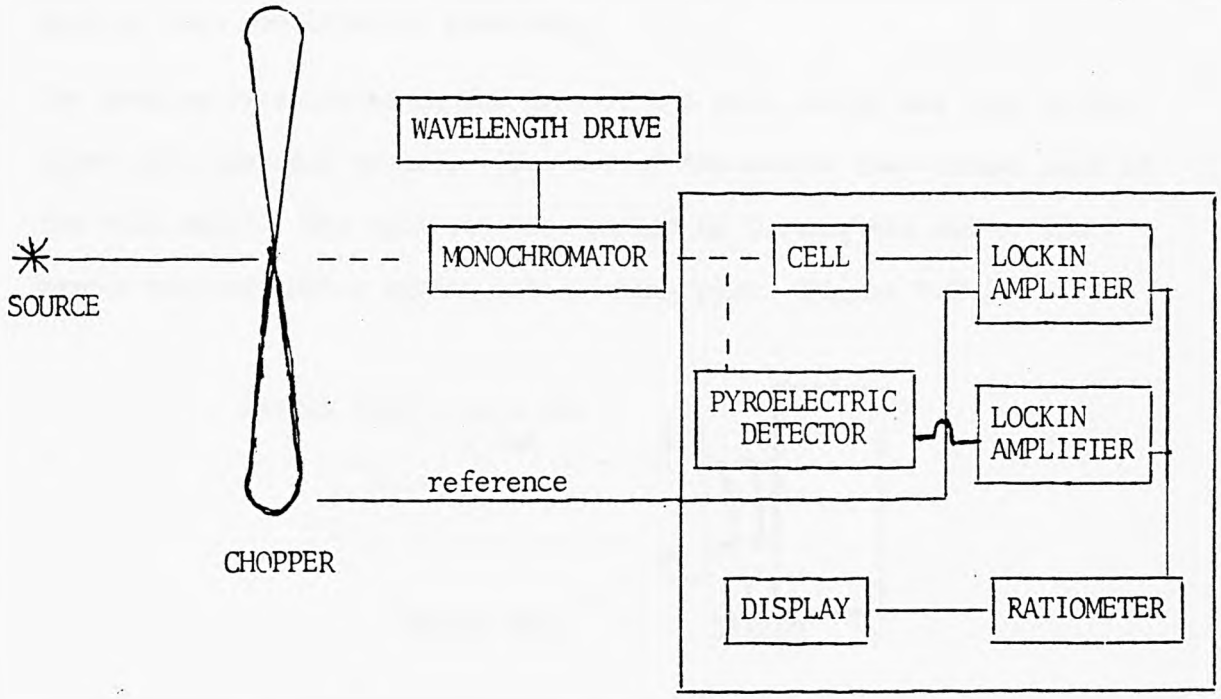

Samples of films were cut using the punch and die method mentioned in section 2.3.1. The two punches are shown in figure 7.2a.

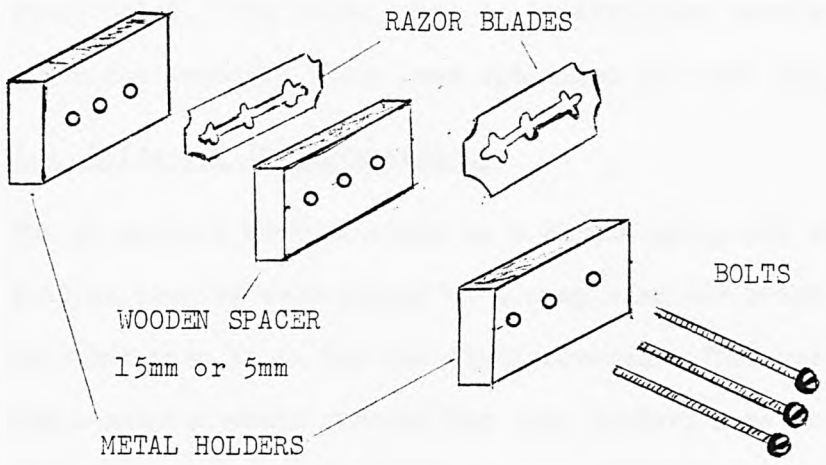

Figure 7.2a Exploded diagram of punches used to cut out samples for the PA Spectrometer.

Hard wood was found to be the best die. Using these tools 15mm x 5mm samples were consistantly produced.

The samples were placed in the tray of the cell, which was then introduced into the cell casing. (One end of the sample tray formed part of the cell wall). The cell was then sealed by turning the end of the sample tray against a spring onto locking pins. (Figure 7.2b.)

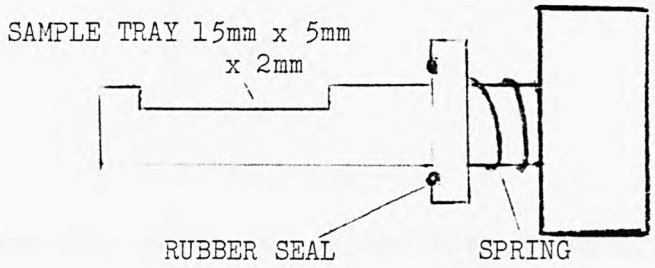

Figure 7.2b Sample tray of the photoacoustic cell in the OAS 400.

The required modulation frequency was selected as was the scan rate, the slit width and hence the time constant. The sensitivity was adjusted to bring the signal onto scale, as measured by a meter on the front panel. The phase angle at a particular wavelength (initially 440nm but latterly 350nm) was optimized and then the spectrum was run.

7.2 Infra-red Instrumentation.

The IR spectra were obtained on a Perkin Elmer 599 spectrometer. In general samples were placed on a sample holder which had a 15mm x 5mm hole cut into it to let the light through. This was used so that small samples would present the same surface area as larger samples without radiation going around the sides.

The majority of the samples were run as 40mm discs but with only the 15mm x 5mm portion which covered the hole in the sample holder presented to the beam. As mentioned previously the discs were used to increase the surface area/weight ratio. They were prepared using a 40mm Specac press.

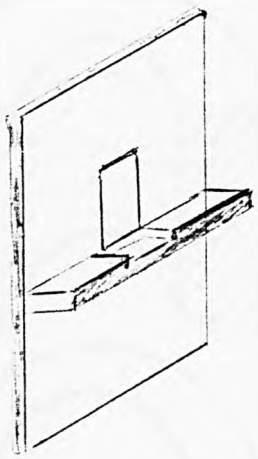

Figure 7.3 Sample holder for IR spectrometer.

It was found that the optimum weight of KBr required is about 3g, any lower than this and the discs are mechanically weak. Above this and the surface area to weight ratio starts to become smaller and the ad-

vantages are reduced.

These discs could not be made without opacities in them. However opacities were reduced if the plunger of the press was placed on top of the KBr powder and turned for about 5 minutes. The plunger was then removed and the second anvil was placed into the press followed by the plunger.

Best results were obtained when high pressures and long pressing times were used and the press was evacuated. The highest pressure available was 25 tons, the optimum pressing time was found to be about 3 hours although shorter times gave reasonable results.

The clear parts of the discs tended to go cloudy even if left in a desicator, however, this did not adversely affect the region of interest i.e., 2000 cm^{-1} to 600 cm^{-1}.

The area of the surface of the disc = $\pi \times 20 \times 20$

$= 1256.6mm^2$

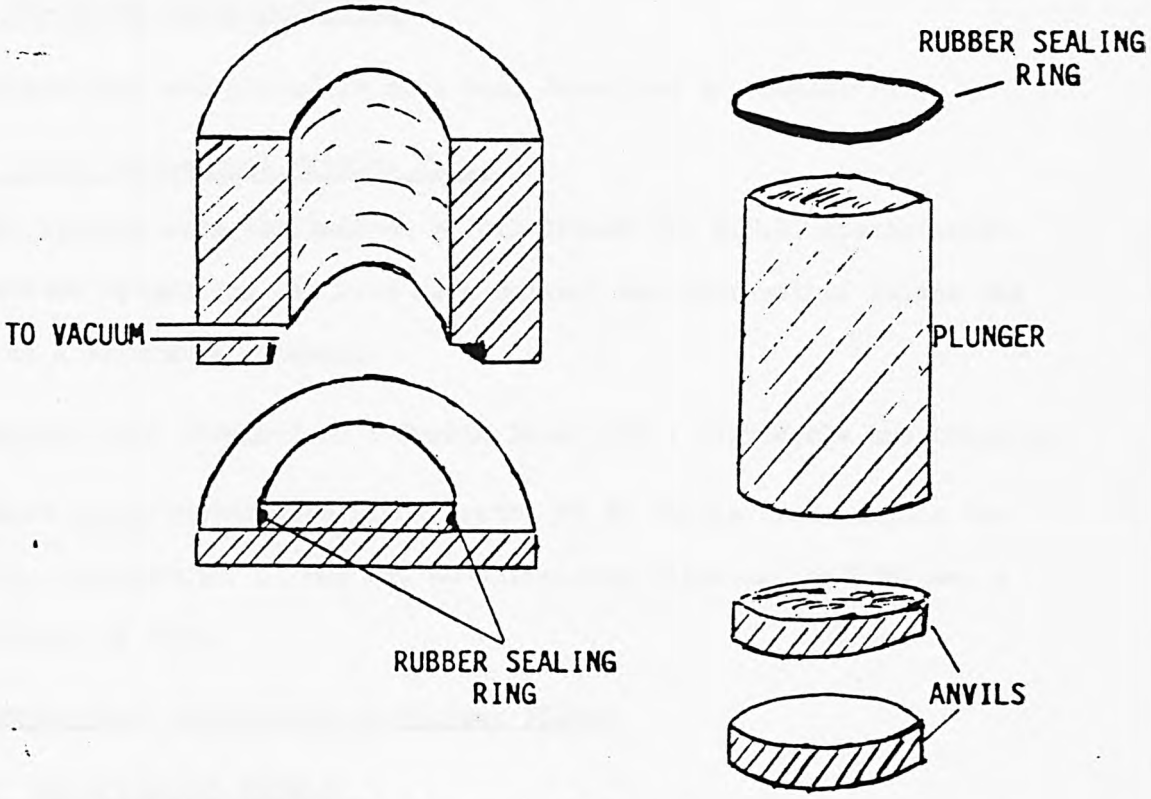

Figure 7.4 Exploded diagram of 40mm Specac press.

7.3 UV Diffuse Reflectance.

The instrument used for the application of this technique was a Perkin Elmer Lamda 5, with a UV reflectance attachement. This instrument was a double beam instrument with a filter grating monochromator. The light sources were a tungsten/halogen lamp and a deuterium lamp.

The diameter of the intensity sphere was 76mm and it gave an energy throughput of 40%. The detector was an end window photomultiplier tube mounted at a right angle to the plane of the sample.

The procedure was as follows. Initially a background spectrum was obtained of the barium sulphate standard so as to ensure no anomalous bands occured. The sample was then placed in the sample holder under a quartz plate and secured with the back plate of the sample holder. The whole assembly was then slotted into place in the spectrometer and the spectrum run. Barium sulphate was used in the reference section of the sample holder.

7.4 FT-IR-PAS Instrumentation.

The instrument and procedure have been described in chapter 6.

7.5 Other Instumental Methods Used.

N.M.R. spectra were obtained on a Joel JNM-MH 100 N.M.R. spectrometer. Deuterated chloroform was used as a solvent and tetramethyl silane was used as a reference material.

UV spectra were obtained on a Perkin Elmer 402 - UV/visible spectrometer.

The mass spectrometer used was a Kratos MS 30 double beam, double focussing instrument. It was run at an ionising potential of 70eV and a resolution of 1000.

7.6 Measurement of Density of Polymer Films.

7.6.1 Experimental Method.

The density of the polymers is required in order that the concentration

of the chromophore can be found. This can be done by weighing a substrate with and without a film and by measuring the area and the thickness of the film.

The use of a micrometer to measure film thickness gave errors larger than the thickness of many films, i.e. the error was ±0.5 thou = 12μm. Thus another method was required. An elcometer 250W was chosen, as this was found to give errors of ±0.5μm. The drawback of this instrument is that it can only be used with a non-ferrous metal substrate. Many readings were taken and then a mean value found.

The measurement of the area was performed with a millimeter rule giving errors of ±0.5mm. The weights were obtained using a four figure balance which gives errors of ±0.0010g.

7.6.2 Results.

Polymer (1) Area = 74 x 62.5 = 4625mm^2 ±68mm^2

weight of substrate + film = 14.0889g

weight of substrate = 13.9279g

weight of film = 0.1629g ±0.001g

film thickness = 24.4 ± 0.5μm

$$D = \frac{0.1629 \times 10^{-3}}{24.4 \times 10^{-6} \times 4625 \times 10^{-6}} = 1443.5 \pm 60 \text{ Kg/m}^3$$

By a similar calculation the density of polymer 6 is:-

$$1109 \pm 42 \text{ Kg/m}^3$$

Both errors are 4%.

7.6.3 Discussion.

The error would be reduced by using a five figure balance and by using a travelling microscope to measure area. The error could then be as low as ± 2.5%.

It can be seen from table 7.1 that polymer 1 has no BADGE (see 2.2) in it and polymer 8 has no chalcone in it. Table 7.1 shows that the den-

sity of polymer 1 is 1443 kg/m^3 and the density of polymer 8 is 1140 kg/m^3. Thus it would be expected that the densities of the polymers in between would decrease as the amount of chalcone decreased. This is in fact observed except for polymer 2 which has a higher density. This anomaly probably occurs because a little BADGE helps the molecules to pack more closely.

Table 7.1

Measured weights and volumes and calculated densities for polymers 1-8

Polymer	Weight (g)	Volume (ℓ)	Density kg/m^3
1	0.1629	1.129×10^{-4}	1443
2	0.2019	1.304×10^{-4}	1549
3	0.1349	1.026×10^{-4}	1314
4	0.1571	1.334×10^{-4}	1177
5	0.2494	2.195×10^{-4}	1136
6	0.1613	1.455×10^{-4}	1109
7	0.1379	1.186×10^{-4}	1162
8	0.1433	1.256×10^{-4}	1140

Table 7.2

Measured weights and volumes and calculated densities for polymers A-F

Polymer	Weight (g)	Volume (ℓ)	Density kg/m^3
A	0.1623	1.381×10^{-4}	1175
B	0.1295	1.029×10^{-4}	1260
C	0.1915	1.508×10^{-4}	1270
D	0.1419	1.186×10^{-4}	1196
E	0.1249	1.109×10^{-4}	1126
F	0.1447	1.263×10^{-4}	1126

From the above data, together with the knowledge of the composition of each polymer, i.e. % chalcone, % dimethylhydantoin and % bisphenol A, the concentration of the various compounds may be obtained, e.g. polymer 1.

% of dimethylhydantoin = 21.6%

$$C = \frac{0.216 \times 1440}{128}$$

$$= 2.44 \text{ moles/litre}$$

Similarly, $\frac{0.784 \times 1440}{352}$

= 3.21 moles/litre

Table 7.3

Variation of concentration of the three components that make-up polymers 1-8

Polymer	Conc^{n} chalcone m/ℓ	Conc^{n} DMH* m/ℓ	Conc^{n} BADGE* m/ℓ
1	3.21	2.44	-
2	3.14	2.65	0.30
3	2.41	2.29	0.51
4	1.91	2.07	0.71
5	1.36	2.06	1.15
6	0.75	2.15	1.68
7	0.26	2.26	2.29
8	-	2.26	2.51

* DMH = Dimethylhydantoin

BADGE = Bisphenol A. Diglycidyl ether

Table 7.4

Variation of the three components that make-up polymers A-F

Polymer	Conc^{n} of Dibenzal acetone m/ℓ	Conc^{n} of DMH m/ℓ	Conc^{n} BADGE m/ℓ
A	2.39	2.12	-
B	2.35	2.24	0.25
C	2.12	2.32	0.51
D	1.77	2.19	0.72
E	1.22	2.11	1.16
F	0.76	2.18	1.71

7.7 Estimation of Epoxy Values.

7.7.1 Experimental Method.

Approximately 0.2g of the 4,4'-diglycidyl ether of 4,4'-dihydroxy chalcone was weighed accurately and dissolved in cyclohexanone (25 ml). Glacial accetic acid (25 ml) was also added together with tetraethyl ammonium bromide (2.5g) ensuring an excess. One drop of crystal violet

in glacial acetic acid was used as an indicator. This mixture was titrated against N/10 perchloric acid in glacial acetic acid. The colour change was from purple through blue and turquoise to apple green.

7.7.2 Results.

Weight of chalcone = 0.2038g

Titre of N/10 perchloric acid = 9.78 mls.

Epoxide value per kilogramme = $\frac{9.78}{10 \times 0.2038}$

= 4.80 equivalents/kilogramme

Theoretical EV = $\frac{2000}{352}$ = 5.68 " "

84.5% of the prepared chalcone was the diepoxide. This gives an effective molecular weight of 416.7g.

The same method as above was used to determine the epoxide value of bisphenol A diglycidyl ether (BADGE)

Weight of BADGE = 0.2530g

Titre of N/10 perchloric acid = 14.51 mls.

Epoxide value per kilogramme = $\frac{14.51}{10 \times 0.2530}$ = 5.735

Theoretical value = $\frac{2000}{340}$ = 5.88 epoxide groups/kilogramme

97.5% of the compound is the diepoxide. This gives an effective molecular weight of 348.7g.

7.8 Preparation of Polymers 1-8.

7.8.1 Preparation of 1,3-bis(4-hydroxy phenyl) prop-2-en-1-one (4,4'-dihydroxy chalcone).

1-(4-Hydroxyphenyl) ethan-1-one was dissolved in ethanol, heated and then decolourising charcoal was added. This mixture was filtered hot and the ethanol was removed on the rotary evaporator. 1-(4-Hydroxyphenyl) methanal was recrystallised from water during which a hot filtration was carried out.

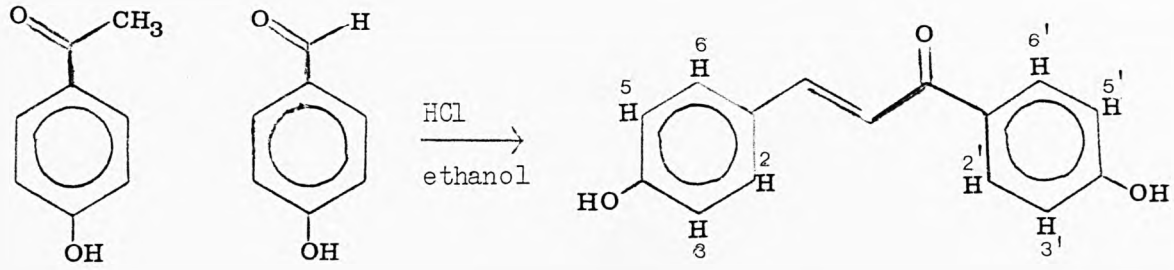

The purified 1-(4-hydroxyphenyl) ethan-1-one (2,72g) was added to absolute ethanol (40ml) in a 250ml round bottomed flask with side arm. 1-(4-Hydroxyphenyl) methanal (2.44g) was added to the mixture whilst it was cooled to $5^{o}C$ using an ice/water bath.

HCl gas was then bubbled through the mixture for 1 hour, which was left stirring for another four hours. HCl was bubbled through at intervals during this time.

The red liquor was filtered and washed with water, which turned the red crystals to green, which gave a yellow product upon recrystallisation from ethanol and water.

Yield = 3.41g = 74%

M.p. = 202-203° lit[25] 208°C.

Mass spectral data gave a molecular ion at m/e = 240 and fragmentation peaks at 223 (loss of hydroxide group) and 147 loss of 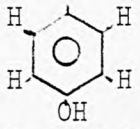

The UV spectrum in methanol gave a λ_{max} at 250nm and another at 236nm and at 206nm. (cf ref.25).

The N.M.R. spectrum was run in deuterated DMSO and gave the following:-

6.86δ (2H, d J=8Hz H-3,5) 6.92δ (2H, d, J=8Hz H-3',5')

7.69δ (2H, s CH=CH), 7.73δ (2H, d, J=8Hz H-2.6)

8.09δ (2H, d J=8Hz H-2',6') 10.30δ (2H, s, OH)

Because of the presence of the carbonyl group para to the hydroxyl group

on the primed ring (see figure 7.8.1a), the hydrogens are less perturbed and hence the doublets at 8.09 and 6.92 are almost equal heights. That is because as the chemical shifts are pulled further apart perturbation is reduced.

It must be purely accidental that the vinyl protons are magnetically equivalent.

The 3 and 5 protons are shifted upfield by the electron donating hydroxyl group. The 2 and 6 protons are shifted downfield by the electron withdrawing carbonyl and alkene groups. The different powers of these two latter groups accounts for the difference in position i.e. carbonyl is the stronger.

The reaction time of five hours was taken from reference 25 where a large scale reaction was undertaken. Therefore reaction time could possibly be cut to two hours in this case.

7.8.2 Preparation of 4,4'diglycidyl ether of 4,4'dihydroxy chalcone.

4,4'Dihydroxy chalcone (0.01M(2.4g)) was mixed with epichlorohydrin (0.088M(8.14g)) in isopropanol (20ml). This was brought up to about 75°C then a 50% aqeous solution of sodium hydroxide (0.022M (0.88g)) was added over a period of 10 minutes. No reflux was observed as the alkali was added unlike Zahir[25]. The resulting mixture was heated to 83°C for a further 4 hours.

A yellow precipitate was formed on cooling but the bulk of the product was precipitated out using water. The yellow powder was recrystallised from an alcohol/chloroform mixture, in the ratio 2:1v/v.

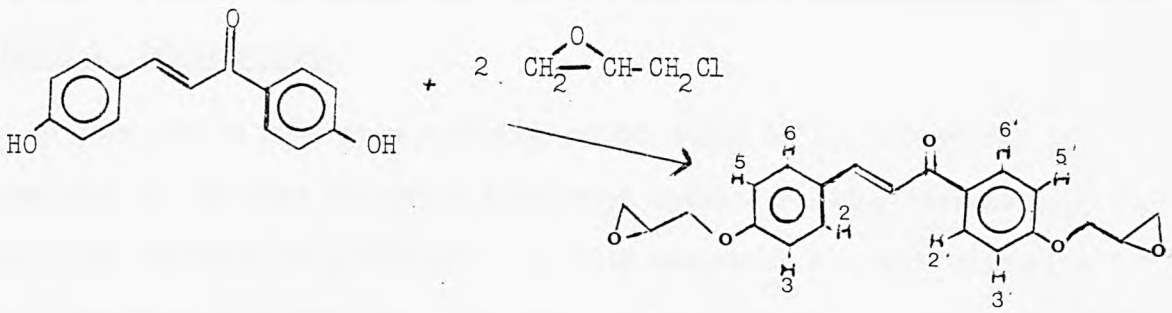

For other compounds formed see reference 25.

Yield = 2.65g = 75% m.p. 109-110C lit[25] 116°C

The mass spectrum showed a parent ion peak at 352 and a fragment peak at 295 showing the loss of a glycidyl group.

The N.M.R. spectrum in $CDCl_3$ gave the following:-

2.68 - 3.0δ (4H, M, CH_2—C(O)—C), 3.20 - 3.44δ (2H, M, C(O)—CH—C)

3.80 - 4.40δ (4H, M, C(O)—C-CH_2), 6,86δ (2H, d, J=8.5Hz, H-3, 5)

6.90δ (2H, d, J=8.5Hz, H-3' ,5'), 7,49δ (2H, Q, J=15Hz — CH=CH—)

7.50δ (2H, d, J=8.5Hz, H-2,6), 7.90δ (2H, d, J=8.5Hz, H-2' ,6')

The rationalisation of the N.M.R. spectrum is as follows:-
The aromatics are as before. The vinylic protons are exhibiting typical behaviour of an AB system with a coupling constant of 15Hz indicating trans substitution.

The methylene protons of the epoxide group are nonequivalent hence a quartet split into doublets which gives rise to a multiplet. The single proton is split by both of these methylene protons and by the other methylene group.

The UV spectrum was found to yield λ_{max} at 337nm and 229nm. However these were found to interchange during the determination indicating trans-cis isomerisation.

7.8.3 Advancement of 4,4'-Diglycidyl ether of 4,4'-dihydroxy chalcone

7.8.3.1 Introduction.

A polymer can be made from 4,4'-diglycidyl ether of 4,4'-dihydroxy chalcone by reacting it with 5,5-dimethyl hydantoin using tetramethylammonium chloride as a catalyst. As both compounds are bifunctional a polymer chain will develop. The concentration of the chromophore in

the polymer chain can vary by using a spacer molecule of similar molecular weight, in this case BADGE. The chemicals should be mixed in the following proportions.

Table 7.5

Constituents of polymers 1-8

Polymer	Chalcone Derivative	BADGE	5,5-Dimethyl hydantoin
1	10	0	9
2	9	1	9
3	8	2	9
4	7	3	9
5	5	5	9
6	3	7	9
7	1	9	9
8	0	10	9

In this way it is hoped that polymers of similar molecular weights will be obtained. Thus hoping to calibrate infra-red spectra, and the only factor affecting sensitivity towards UV radiation will be the concentration of chromophore.

Another control over the molecular weight is to monitor the epoxide value (i.e. the number of equivalents/kg) of the solutions at intervals and stop each reaction when a certain value has been reached.

The minimum E.V.'s of the reaction are:-

1. 0.376 epoxide equivalents/kg
2. 0.381 " " "
3. 0.386 " " "
4. 0.391 " " "
5. 0.402 epoxide equivalents/kg
6. 0.413 " " "
7. 0.425 " " "
8. 0.436 " " "

This would lead to chains containing 10 units of chalcone and 9 units of hydantoin and thus each chain would terminate at both ends in epoxide groups.

7.8.3.2 Method

The same method was used for all eight polymers only the amounts differed, thus only the method used to synthesis polymer 1 will be des-

cribed.

4,4'-Diglycidyl ether of 4,4'-dihydroxy chalcone (4.9998g) was placed in a 100ml three necked round bottomed flask with 5,5'-dimethylhydantoin (1.380g). Tetramethyl ammonium chloride was added as a catalyst (0.0102g) i.e. 0.2% by weight. 2-Ethoxy ethanol was added (9.57g) so as to produce a 40% solution. The solution was heated to 115°C and stirred with a mechanical stirrer. The flask was wrapped in a cloth throughout the preparation in order to keep out any radiation that would cause cross-linking.

Approximately 0.2g aliquots were taken after various times and the epoxide values determined. The factor of 2.5 is introduced to take account of the solvent.

After one hour weight of sample from reaction = 0.2184g

Titre of N/10 perchloric acid = 1.67 ml

$$EV = \frac{1.67 \times 2.5}{10 \times 0.2184} = 1.911$$

7.8.3.3 Results.

Table 7.6

Weights of compounds used in polymers 1-8

Reaction	weight of chalcone derivative	weight of BADGE	weight of 5,5-dimethyl hydantoin	Total
1	4.9998g	0	1.3807g	6.3805g
2	4.9987g	0.4639g	1.5361g	6.9987g
3	5.0000g	1.0436g	1.7283g	7.7719g
4	5.0003g	1.8031g	1.9744g	8.7778g
5	10.0005g	9.2924g	6.2230g	25.5159g
6	5.0009g	10.8200g	5.2150g	21.0359g
7	2.0000g	16.7361g	6.2120g	24.9481g
8	-	25.0000g	8.2592g	33.2592g

Table 7.7

Ratios of compounds used in polymers 1-8

Polymer	Chalcone derivative	Bisphenol A derivative	5,5-Dimethyl hydantoin
1	10	0	9
2	9	1	9
3	8	2	9
4	7	3	9
5	5	5	9
6	3	7	9
7	1	9	9
8	0	10	9

Table 7.8

Epoxide values taken during the preparation of polymers 1-8

Time	1	2	3	4	5	6	7	8
1hr	1.91	-	-	-	1.88	-	-	-
2	-	1.57	-	-	1.59	1.32	1.52	-
3	-	-	1.52	-	-	-	-	-
3	1.40	-	-	-	-	-	-	-
4	_	-	-	1.40	-	1.20	-	-
5	1.14	-	-	-	-	-	-	1.22
6	1.17	1.00	1.26	1.10	-	-	-	-
7	-	-	-	-	-	-	0.96	-
8	-	-	-	-	1.07	-	-	-
9	-	0.93	-	-	-	-	-	-
10	-	-	-	-	0.91	0.81	0.81	-
11	1.10	1.04	1.04	0.93	-	-	-	-
13	1.00	0.85	1.01	0.98	-	-	-	0.92
14	0.95	0.87	0.93	0.92	-	-	-	-

The accuracy of the EV is ±0.1 hence these values were taken as the same.

7.8.4 Gel Permeation Chromotography.

In order to check that there were no major differencies in molecular weight distribution between the polymers G.P.C. analysis was performed. The G.P.C. system used consisted of a Pye LC3 pump, three columns used in series and a Walters Associates 440 UV detector.

The eluting solvent was dried and distilled dimethyl formamide, the flow rate of which was 0.4mls/min.

The three columns were:- i) PL Gel 500A (polystyrene column)
ii) PL Gel 100A (polystyrene column)
iii) Dupont PSM1000S (silicil column)

The detector was set at 280nm, with a sensitivity variable between 1 and 0.1 the latter being the most sensitive.

Before injection into the column the polymer solutions were diluted by a factor of 100.

The first four polymers give similar profiles although polymers 1 and 2 may have a little more of the higher molecular weight component than polymers 3 and 4. The general reduction in size of the profile is attributed to the reduction in concentration of the chalcone chromophore which affects the response of the detector. The reversal of this trend for polymer 4 may be due to a high polymer content in the 2-ethoxy ethanol solution or by an inaccurate dilution.

Although a comparison of polymers 4,5,6 and 7 is made difficult by a variation in sensitivity, made necessary by a variation in concentration of chalcone, similarities can be observed. There are minor variations on the low molecular weight side possibly caused by the bisphenol A having a molecular weight 12 units smaller than the chalcone.

It can be postulated that the first two peaks nearest the 20cm mark are due to the two monomers, molecular weights:- 352 and 128. If that is so then the third peak will be for a compound of the two in a ratio of 1:1. Subsequent peaks are due to oligmers/polymers whose molecular weights have been built up step by step. On the basis of this assumption it is possible to estimate the molecular weight of the component present in the highest proportion. In this case it has a molecular weight of 3048-3400 and contains either six or seven chalcone units

Figure 7.5a

A GPC of polymers 1 - 4.

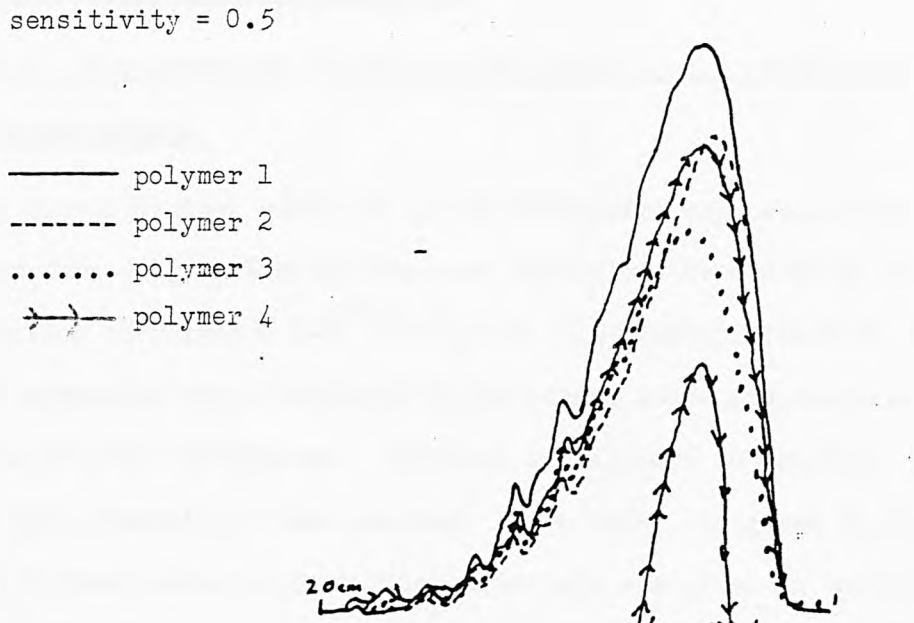

Figure 7.5b
A GPC of polymers 4 - 7.

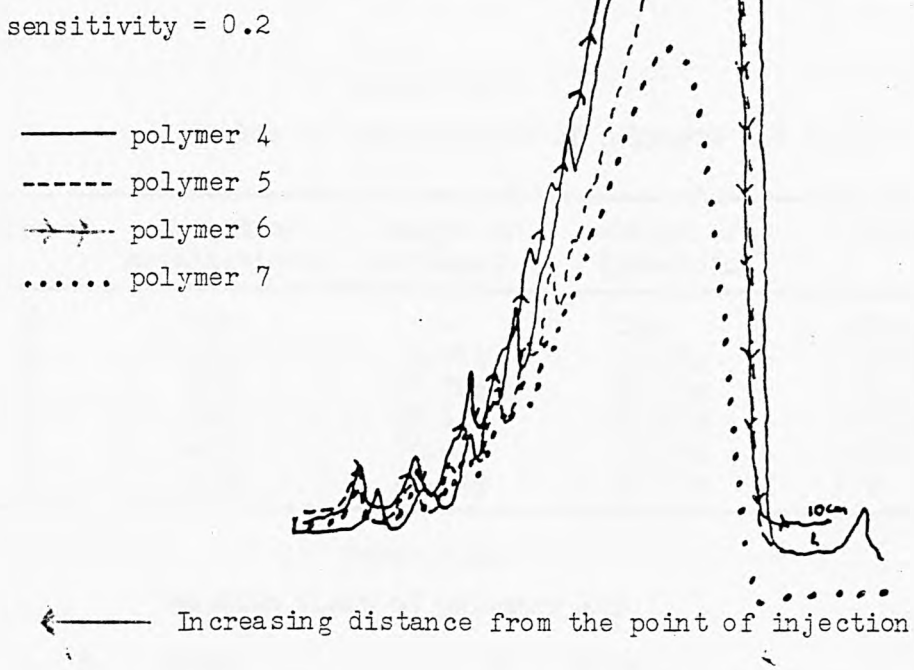

with seven associated hydantoin units!

In conclusion, the molecular weight distributions of the polymers 1-7 are similar and thus spectra and sensitivity should not be affected.

7.9 Preparation of Polymers A-F.

7.9.1 Advancement of 4,4-Diglycidyl Ether of 4,4 -Dihydroxy dibenzalacetone.

The 4,4-diglycidyl ether of 4,4-dihydroxydibenzalacetone was obtained from Ciba Geigy. Exactly the same conditions were used as in the preparation of polymers 1-8[7.8.3], i.e. 5,5-dimethylhydantoin was used as the advancing agent bisphenol A diglycidyl ether was used as a substitute for the chromophore. Reaction was allowed to continue until an EV of approximately 0.9 was reached, these times are given in table 7.10. The various amounts of starting materials are given in table 7.9. The EV of the chromophore was 5.06, i.e. 96% pure giving an effective molecular weight of 395g. However the EV of the dibenzalacetone derivative used in polymer A was 5.19. This had the effect of decreasing the amount added to the reaction mixture and thus the product was of lower density.

Table 7.9

Weights of constituents of polymers A-F

Polymer	Weight of benzalacetone	Weight of bisphenol A	Weight of hydantoin	Total
A	50g	-	15g	65.0g
B	50g	4.78g	16.22g	71.0g
C	50g	10.76g	18.60g	79.36g
D	50g	18.44g	20.90g	89.34g
E	40g	34.40g	23.50g	97.90g
F	40g	40.20g	19.30g	79.50g

Table 7.10

Reaction times of polymers A-F

A	12hrs.	D	18hrs.
B	18hrs.	E	22hrs.
C	18hrs.	F	18hrs.

The densities were measured as described in section 7.6 and are set out in table 7.11.

Table 7.11

Densities of and chromophore concentrations in polymers A-F.

Polymer	Density kg/m^3	Conc^{n} of dibenzalacetone derivative M/ℓ	Conc^{n} of hydantoin M/ℓ
A	1175	2.39	2.12
B	1260	2.35	2.24
C	1270	2.12	2.32
D	1196	1.77	2.19
E	1126	1.22	2.11
F	1146	0.76	2.18

Again a general decrease in density is observed after polymer A, see above, as the amount of bisphenol A diglycidyl ether is increased. Any divergence from the trend can be explained by experimental error.

A sample of polymer A was prepared without adding any tetramethyl ammonium chloride, this gave a polymer, after a great length of reaction time, that did not crosslink on irradiation. The density was about 1150 kg/m^3. This lack of photosensitivity has been attributed to a lack of branched chains: i.e. it has been suggested that the catalyst promotes a reaction between the hydroxyl groups formed by the reaction of the hydantoin with an epoxy group and a second epoxy group from a second molecule, in order to produce branched chains.

7.9.2 Gel Permeation Chromatography.

The samples were diluted to 4% of the original concentration the sensitivity of the detector was set at the least sensitive setting. All other conditions were kept the same as in section 7.8.4.

The traces show that polymers A-F have very similar molecular weight distribution. Again a drop in size can be observed caused by the decrease in concentration of chromophore. However in this case because the absorbance of the compound is extremely high, the sensitivity remains the same.

Figure 7.6a
A GPC of polymers A - C.

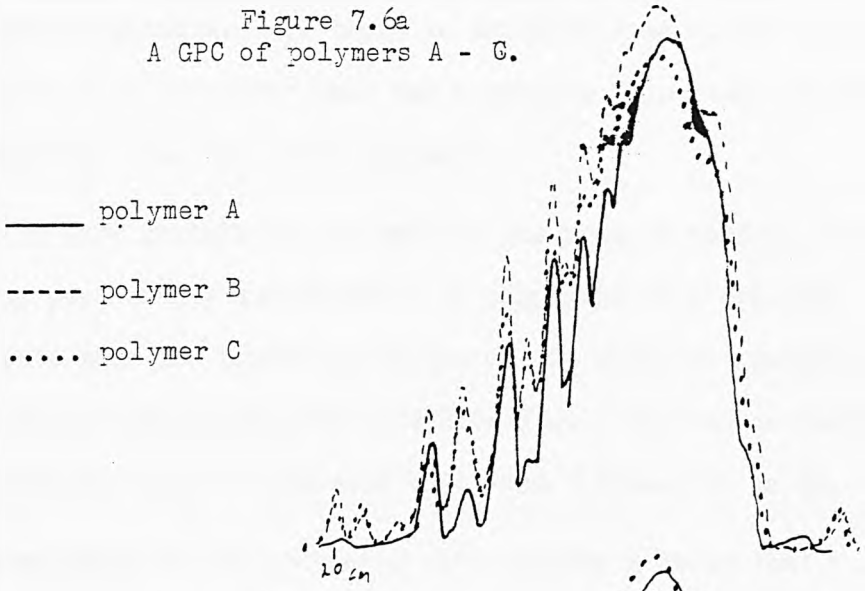

Figure 7.6b
A GPC of polymers D - F.

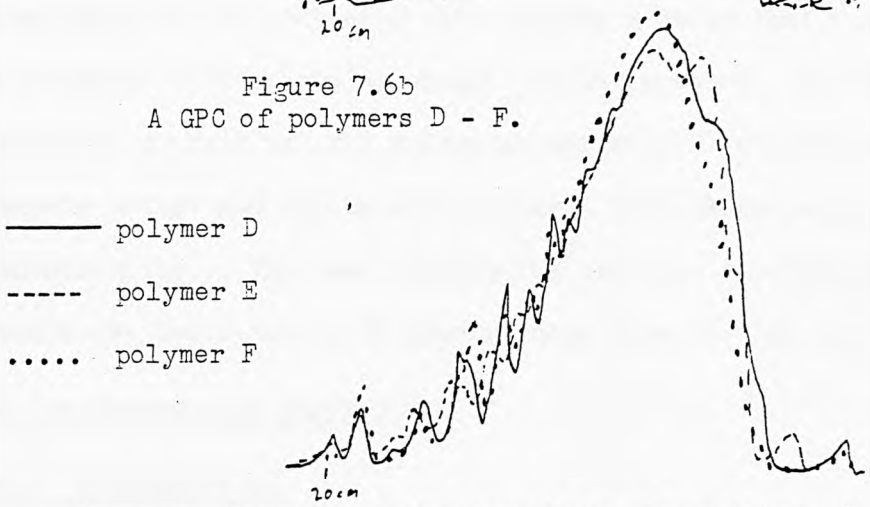

← Increasing distance from point of injection.

Figure 7.7
A GPC of polymers A and X.

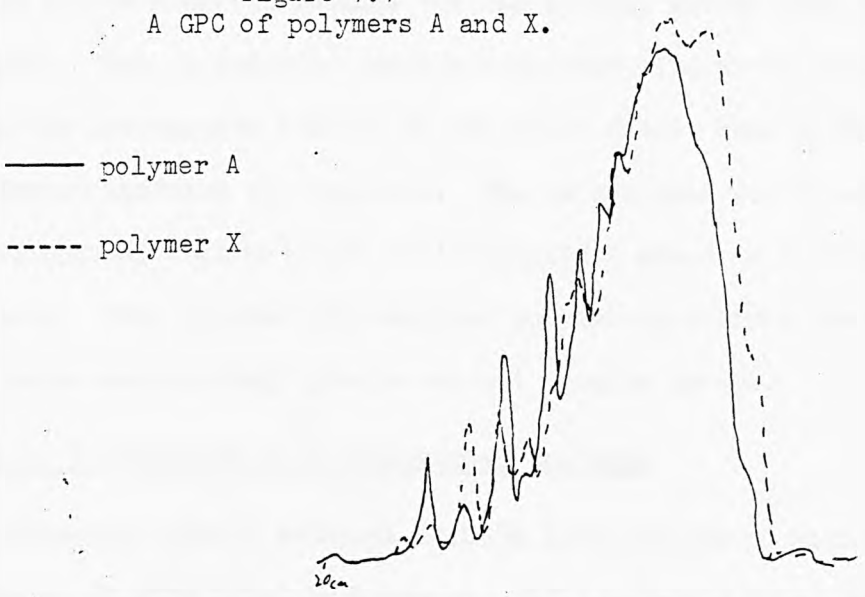

← Increasing distance from point of injection.

On closer inspection polymer A possesses a little less of the very low molecular weight component and a little less of the higher molecular weight components, i.e. those on the 10 cm side of the largest peak. Polymer E on the other hand has a greater proportion of these latter components than the other polymers.

If the same postulation is made as was made in section 7.8.4, i.e. that every peak can be attributed to a component of a specific molecular weight, then the molecular weight of the component present to the highest proportion in polymer A is 3164-3542. This again indicates that it is made up from 6-7 chalcone units and 7 hydantoin units.

A comparison of the polymer X with polymer A shows that a lot more of the component with molecular weight 3542 is present. In almost equal proportions to this are the molecular weight 3670 (7 chalcone units, 8 hydantoin units) and the molecular weight 4048 (8 chalcone units, 8 hydantoin units). This may account for the high concentration of chromophores indicated by IR spectroscopy (see section 4.6.3.2.).

7.10 Preparation of Polymer 9

7.10.1 Introduction.

Previous work had shown that the glycidylation of 3,4-dihydroxy chalcone could not be achieved because the two hydroxy groups were too close together. Thus in order to produce a polymer similar to polymer 1 but with the chromophore pendant to the chain rather than in the backbone a different approach was required. The method used was to advance 3,4-dihydroxy chalcone with N,N'-diglycidyl ether of 5,5-dimethyl hydantoin. This yielded the required polymer apart from the fact that the ends were hydroxyl groups and not epoxide groups.

7.10.2 Preparation of 3,4-Dihydroxy Chalcone

3,4-Dihydroxy phenyl methanal (0.833M 115g) was mixed with 1-phenyl ethanone (0.833M 100g) in methanol. HCl gas was bubbled through the mix-

ture for 5 hours in which time 227g were added. The mixture was stirred for one hour after the addition was complete. During the addition of HCl the temperature was kept below 10°C using an ice bath..

The product from this reaction was a black powder. When this was dissolved up in acetone and dropped into a large excess of water, an off-yellow coloured solution developed. However on further addition, only a dark green precipitate could be obtained. The colour of this crude product can be improved by recrystallising the aldehyde before the start of the preparation.

The N.M.R. of the crude product showed that the aldehyde and the ketone had disappeared.

m.p. 184°C Lit Value 204-205°C,

The dark green precipitate was dissolved up in ethanol and boiled for fifteen minutes with activated charcoal. The solution was filtered hot using filter aid and the product was allowed to crystallise out. This was a dark brown solid which was dissolved in boiling ethanol and this solution was dropped into vigorously stirred water. This yielded a bright yellow coloured product.

m.p. 203-204°C

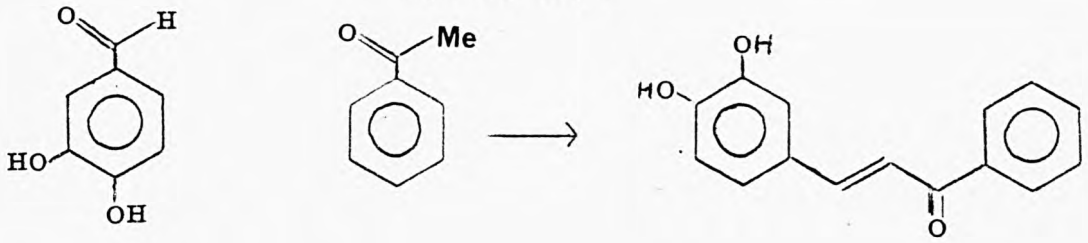

A mass spectrum was obtained and this showed a molecular ion at 240 m/e. The loss of hydroxyl group would lead to the ion at 223 m/e. The loss of a phenyl group gives rise to the ion at 163 m/e. However the most important peaks are those at 135 m/e and 105 m/e as they correspond to the following ions:-

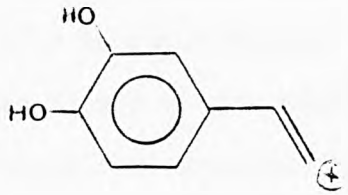

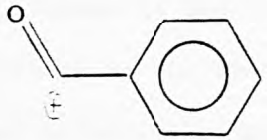

The absence of peaks at 137 m/e and 103 m/e confirms that the structure is:-

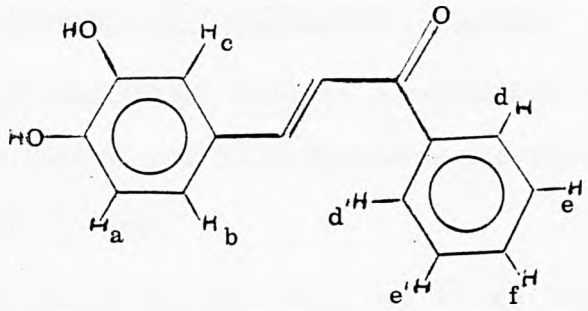

and not the 3'4'-dihydroxy compound.

A 220 Hz N.M.R. spectrum was expanded and the following data obtained.

6.88 (1H, d, J_{ab}= 8Hz, a), 7.25 (1H, $d_{of}d$, J_{ab}= 8Hz, J_{bc}= 2Hz, b)

7.35 (1H, d, J_{bc}= 2Hz, c), 7.61 (2H, m, e and e')

7.66 (2H, s, g and h), 7.71 (1H, m, f), 8.16 (2H, m, d and d')

Proton a is shifted up-field compared to protons in benzene by the electron donating and hence shielding effect of the hydroxyl group. It is split into a doublet by ortho coupling with b, the slope of the perturbation indicates that the first two peaks couple. The coupling constant is typical of ortho coupling.

Proton b has two effects acting upon it, i.e. the electron donating effect of the hydroxyl group and the electron withdrawing effect of the alkene. This leads to its position downfield of proton a. It is coupled to a and to c (meta coupling) hence it is a doublet of doublets. The coupling constant J_{bc} is typical of meta coupling.

Proton c is again subject to two effects, however it has been differentiated from b by its coupling pattern. Protons in the other ring will all be shifted downfield by the unsaturated ketone. Protons e and e' will be least affected as they are in the meta position. Proton f will be more affected due to its para position and proton d will be shifted further downfield.

The fact that the alkene protons give a singlet is pure coincidence. They could be split by using a different solvent system.

7.10.3 Advancement of 3,4-Dihydroxy Chalcone.

An EV of N,N'-diglycidyl ether of 5,6-dimethyl-hydantoin was obtained. This showed that it was 97.6% diepoxide and thus had an effective molecular weight of 246g.

Thus 3,4-dihydroxy chalcone (24g, 0.1 M) was placed in a 3-necked flask with N,N'-diglycidyl ether of 5,5-dimethyl hydantoin (22.14g, 0.09 M). 2-Ethoxy ethanol (69.21g) was used to make up a 40% solution and T.M.A.C. (0.2307g) was used as a catalyst. (The molar ratio of chalcone to hydantoin is 10:9. This is to ensure that the polymers will have chalcone and not hydantoin end groups.)

The mixture was heated to 115°C and vigorously stirred for 5 hours, after which time an EV of 0.57 was obtained. After 21 hours the EV was 0.3. Thus it was assumed that the reaction would go no further and it was stopped.

The polymer is a dark-brown liquid which yields a yellowy-brown film when the solvent has been stripped off.

The infra-red spectrum is very similar to that of polymer 1.

7.11 Preparation of Polymer G.

7.11.1 Introduction

In order to remove the carbonyl groups in the hydantoin, so as to mon-

itor the movement of the 1645cm^{-1} band (due to the conjugated carbonyl group) on irradiation, and to observe the change in properties by inserting a group more flexible than 5,5-dimethyl-hydantoin, 1,5-pentandiol was used to advance 4,4'-diglycidyl ether of 4,4'-dihydroxy-benzalacetone.

7.11.2 Experimental Method.

The conditions were exactly as before that is a 40% solution in 2-ethoxy-ethanol kept at 115°C in a three neck flask fitted with a condenser, a thermometer and a mechanical stirrer. Precautions were taken to prevent light entering the reaction vessel.

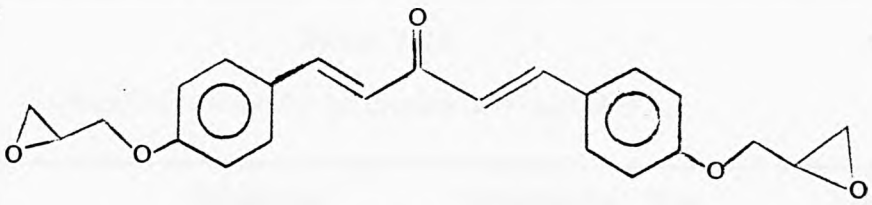

60g

$HO-CH_2-CH_2-CH_2-CH_2-CH_2-OH$

14.2g

100 hours

0.148g of tetramethyl ammonium chloride

Polymer G with an EV of 0.9

The long reaction time is due to the acidity of the hydroxyl protons. Phenolic hydroxyl groups and hydantoin have much more labile protons.

7.12 Sensitivity.

7.12.1 Experimental Method.

Sensitivity is another test for characterizing a photosensitive polymer. It was measured in this case using a step test which consists of a strip of plastic with a graduated decrease in the amount of light let through with one being completely clear and twenty-one being completely

black. A film of the polymer to be tested was spread on a copper board using a No.4 KBar. The solvent was evaporated in an oven at 80°C for 10 minutes. The thickness was measured using an elcometer 250N. The film was irradiated through the steptest for 5 minutes. The lamp used was an M033, spectral output from which is shown in figure 4.11b , the distance of the sample from the lamp 75cm. The films were developed for two minutes in cyclohexanone, and the number of steps remaining was recorded.. The greater the number of steps remaining the higher the sensitivity.

7.12.2 Results.

Table 7.12

Sensitivities of polymers 1-9 and A-F.

Polymer	Thickness $x10^{-6}$m	Irradiation Time minutes	Steps remaining.
1	10-14	5	11
2	10-12	5	9
3	10-12	5	6
4	10-12	5	3
5	8-12	15	5
6	8-12	15	2
7	8-12	20	1
8	8-12	20	0
9	8-10	5	5
A	8-12	5	14
B	8-12	5	12
C	8-10	5	10
D	7-9	5	7
E	9-12	5	4
F	9-12	5	0

* No steps remaining after 5 minutes.

7.12.3 Conclusion.

The sensitivity is greatly affected by the concentration of chromophore present. This is consistent with the model presented in chapter 3. As predicted by this model the second series of polymers has a greater sensitivity as more chromophores are in reactive sites. The results for polymers 5,6 and 7 indicate that longer irradiation times can improve sensitivity. Polymer 8 demonstrates unequivocably that it is the chal-

cone chromophore that gives the polymers their photo-sensitivity.

In order to test the effects of increased irradiation time polymers B, C and D were irradiated for various times. The results are presented below:-

Table 7.13

Effects of longer irradiation times on sensitivity of polymers A-D.

Polymer	Thickness $x10^{-6}m$	Irradiation Time minutes	Steps remaining.
A	8-12	5	14
B	10-12	3	11
B	8-12	5	12
B	10-13	7	14
C	8-10	5	10
C	10-12	10	13
C	10-12	15	13
D	8-9	5	6
D	10-13	5	7
D	10-12	10	10

This set of results shows that sensitivity can be increased by increasing irradiation time. However the results shown by polymer C indicate that there is a limit to the sensitivity that can be achieved. These results would be important if irradiation time were irrelevant, as cheaper polymers could be made by reducing the chromophore concentration.

CHAPTER EIGHT

FURTHER WORK

As in the previous work there are four main areas of further work i.e. photoacoustic experiments, infra-red experiments, FT-IR-PAS experiments and UV/Vis diffuse reflectance experiments.

8.1 Photoacoustic Experiments.

As the work has shown that the spectrometer used has considerable drawbacks for use with the polymers, a new spectrometer is required. This should have:- a 1000W source so that modulation frequencies of at least 2kHz could be attained, an optical bench which allows spectra to be obtained below 300nm, a cell with a capability of being flushed with helium, and a much improved X-Y recorder. Polymers with much lower extinction coefficients should also be used initially so that the concept of depth profiling could be investigated more thoroughly.

8.2 Transmission Infra-Red Experiments.

In this case films of less than 0.7μm should be investigated using signal averaging techniques to remove noise. This would give more information on the concentration gradient and thus help with the iterative solution of the rate equations.

More polymers need to be made in order to calibrate the nonlinear section of the calibration curves for the 1600,1572 and 984cm^{-1} bands. The 1572 and 984 bands require further calibration so that films thicker than 4×10^{-6}m can be studied and the indications that cure cannot reach deeper depths can be followed up.

8.3 FT-IR-PAS Experiments.

Standardization of sample size and calibration of spectra needs to be

carried out so that quantitative results can be obtained. Depth profiling should be followed up by using helium in the cell, and variation in the mirror velocity could again be attempted.

8.4 UV/Visible Diffuse Reflectance Experiment.

Further work is required to investigate the band occurring at 320nm (310nm for polymers 1-7) in order to discover the exact nature of the chromophore causing this band. An attempt could be made to calibrate the spectra using the polymers already made.

REFERENCES.

1. H.A.J.Carless and G.K.Fekarurhobo, J.C.S. Chem. Commun., 667 (1984).

2. G.E.Green, B.P.Stark and S.A.Zahir, J.Macro. Sci. Revs. Macrochem., C21, 187 (1981-1982).

3. American Can Co., U.S.Patent, 3,936,557, (1976).

4. R.J.Kiliam, Proc. Radiat. Curing, V, 421 (1980).

5. G.E.Green, B.P.Stark, Chem.Brit., 17, 228 (1981).

6. J.Franck, Trans. Faraday Soc., 21, 536 (1926).

7. A.Jablonski, Z.Physik, 94, 38 (1935) .

8. P.Sykes, "A Guide Book to Mechanisms in Organic Chemistry" P.221, 4th.Ed., Longman, (1975).

9. J.A.Baltrop and J.D.Coyle, "Excited States in Organic Chemistry" P.179, Wiley, (1975).

10. H.A.J.Carless, Tet. Letts., 3173 (1973).

11. J.C.Dalton, P.A.Wriede and N.J.Turro, J.Amer.Chem.Soc., 92, 1318 (1970).

12. Ref.9 page 177.

13. H.Stobbe and K.Bremer, J.Prakt.Chem., 3, 12 (1929).

14. M.D.Cohen and G.N.J.Schmidt, J. Chem. Soc., 1966 (1964).

15. M.D.Cohen and G.N.J.Schimdt, J. Chem. Soc., 2021 (1964).

16. H.G.Curme, C.C.Natalle and D.J.Kelly, J. Phys. Chem., 71, 767 (1967).

17. P.L.Egerton, E.M.Hyde, J.Trigg, A.Payne, P.Benyon, M.V.Mijovic and A.Reiser, J. Amer. Chem. Soc., 103, 3859 (1981).

18. Y.Shindo, K.Horie and I.Mila, Chem. Letts., 5, 639 (1983).

19. Ref.9 page 214.

20. C.S.Lam, D.Valentine and G.S.Hammond, J.Amer. Chem. Soc., 89, 3462 (1967).

21. P.J.Wagner and D.J.Bucket, J. Amer. Chem. Soc., 91, 5090 (1969).

22. C.Azuma, K.Sanui, N.Ogata, J. Appl. Polym. Sci., 27 2065 (1982).

23. M.Tsuda, Yugisoesi Kagaku, 30, 589 (1972).

24. R.A.Caldwell and M.Singh, J. Amer. Chem. Soc., 105, 5139 (1983).

25. S.A.Zahir, J. Appl. Polym. Sci., 23, 1355 (1979).

26. S.P.Panda, J. Polym. Sci., A-1 13, 1757 (1975).

27. G.Ciamician and P.Silber, Ber., 42, 1386 (1909).

28. P.Praetorius and F.Korn, Ber., 43, 7744 (1910)

29. C.W.Shopee, Y.Wang, S.Sternbell and G.C.Brophy, J.C.S.Perkin 1, 1880 (1976).

30. H.Stobbe and E.Färber, Ber., 58, 1548 (1925).

31. N.W.Alcock, N.Heron, J.Kemp and C.W.Shopee, J.C.S.Chem. Commun., 785 (1975).

32. R.T.Morrison and R.N.Boyd,"Organic Chemistry" P.562, 3rd Ed., Allyn and Bacon, (1973).

33. B.Dobinson, W.Hoffman and B.P.Stark, "Determination of Epoxide Groups", Pergamon Press, (1969).

34. G.A.Delzene, Makromol Chem. Supp., 2, 169 (1979).

35. G.A.Delzene, J. Radiation Curing, 6, 2 (1979).

36. G.Oster and N.L.Yang, Chem. Rev., 68, 125 (1968).

37. E.Trommsdorf, H.Kohle and P.Lagally, Makromol Chem., 1, 189 (1948).

38. R.J.Holman and H.Rubin, J. Oil Col. Chem. Assoc., 61, 189 (1978).

39. S.Clarke and R.H.Shanks, Polym. Photo. Chem., 1, 103 (1981).

40. G.Plews and R.Phillips, J. Coat. Technol., 51, 69 (1979).

41. Farbenfab Bayer, German Patenet, D.A.S., 694,149 (1966).

42. H.G.Heine, Tet. Letts., 47, 4755 (1972).

43. H.G.Heine and H.J.Traechner, Prog. Org. Coat., 3, 115 (1975).

44. H.G.Hagman, F.P.B. Van der Maeden and P.C.G.M. Janssen, Makromol Chem., 180, 2531 (1979).

45. S.P.Pappas and A.K.Chattopadhyoy, J. Polym. Sci. Polym. Letts. Ed., 13, 483 (1975).

46. S.P.Pappas, Radiat. Curing., 8, 28 (1981).

47. G.Berner, R.Kirchmayer and G.Rist, J. Oil Col. Chem. Assoc., 61, 105 (1978).

48. A.Bores, R.Kirchmayer and G.Rist, Helv. Chim. Acta., 61, 305 (1978).

49. R.F.Bartholomew and R.S.Davidson, J. Chem. Soc., C(12), 2342 (1971).

50. S.G.Cohen and H.M.Chao, J. Amer. Chem. Soc., 90, 165 (1968).

51. R.S.Davidson and P.F.Lambeth, Chem. Commun., 9, 511 (1968).

52. C.R.Morgan and A.D.Ketley, Amer. Chem. Soc. Div. Org. Coat. Plast. Chem., 33, 281 (1973).

53. C.R.Morgan, F.Magnolta and A.D.Ketley, J. Polym. Sci. Polym. Chem. Ed., 15, 627 (1977).

54. C.R.Morgan and A.D.Ketley, J. Radiat. Curing, 7, 10 (1980).

55. C.R.Morgan and A.D.Ketley, J. Polym. Sci. Polym. Letts. Ed., 16, 75 (1978).

56. S.Clarke and R.A.Shanks, J. Macromol Sci., A14, 69 (1980).

57. Inmont Corp., U.S.Patent, 3,673,140 (1972).

58. V.D.McGinniss, Photgr. Sci. Eng., 23, 124 (1979).

59. M.J.Davis, J.Doherty, A.A.Godfrey, P.N.Green,J.R.A.Young and M.A.Parrish, J. Oil Col. Chem. Assoc., 61, 256 (1978).

60. North American Aviation Inc., U.S.Patent, 3,205,157 (1965).

61. M.P.Dreyfuss and P.Dreyfuss, J. Polym. Sci., Part A1, 4, 2179 (1966).

62. S.I.Schlesinger, Photogr. Sci. Eng., 18, 387 (1974).

63. G.Baltz and G.Schiemann, Ber., 60, 1186 (1927).

64. Ref.2 Page 240 and the references therein.

65. J.W.Knapczyk and W.E.M^{c}Ewen, J. Org. Chem., 35, 2359 (1970).

66. J.W.Knapczyk, J.J.Lubinowski and W.E.M^{c}Ewen, Tet. Letts., 35, 3739 (1972).

67. J.V.Crivello and J.H.W.Lam, Macromolecules, 10, 1307 (1977).

68. J.V.Crivello and J.H.W.Lam, J. Polym. Sci. Polym. Chem. Ed., 17, 977 (1979).

69. 3M U.K.Patent, 2,014,144 (1979).

70. J.V.Crivello and J.H.W.Lam, J. Polym. Sci. Polym. Chem. Ed., 18, 2677 and 2697 (1980).

71. American Can Co., U.S.Patent, 4,197,174 (1980).

72. J.V.Crivello and J.H.W.Lam, J. Polym. Sci. Polym. Chem. Ed., 16, 2441 (1978).

73. S.P.Pappas and J.H.Jilek, Photogr. Sci. Eng., 23, 140 (1979).

74. J.V.Crivello and J.H.W.Lam, J. Polym. Sci. Polym. Chem. Ed., 17, 1059 (1979).

75. W.R.Watt, Amer. Chem. Soc. Div. Org. Coat. Plast. Chem., 38, 36 (1978).

76. E.M.Robertson, W.P.Van Deusen and C.M.Minsk, J. Appl. Polym. Sci., 2, 308 (1959).

77. J.Kosar, "Light Sensitive Systems", John Wileys, New York, (1965).

78. W.Harm, "Biological Effects of Ultra-Violet Radiation", Cambridge University Press, (1980).

79. Eastman Kodak Co., British Patent, 813,604, (1959).

80. C.C.Unruh, J. Polym. Sci., 45, 325 (1960).

81. S.Farid, P.A.Martic, R.C.Daly, D.R.Thompson, D.P.Specht, S.E. Hartman and J.L.R.Williams, Pure and Applied Chem., 51, 241 (1979).

82. A.Reiser and P.L.Egerton, Photogr. Sci. Eng., 23, 144 (1979).

83. See ref.2, page 224.

84. T.A.Shankoff and A.M.Trozzolo, Photogr. Sci. Eng., 19, 173 (1975).

85. J.K.Sugden, Synth. Commun., 6, 98 (1976).

86. A.Reiser and P.L.Egerton, Macromolecules, 12, 670 (1979).

87. S.Stinson, Chem. Eng. News, 61, (32) 7 (1983).

88. S.Stinson, Chem. Eng. News, 61, (39) 23 (1983).

89. A.G.Bell, Amer. J. Sci., 20, 305 (1880).

90. A.G.Bell, Philos. Mag., 11, 510 (1881).

91. J.Tyndall, Proc. R. Soc. Lond., 31, 307 (1881).

92. W.C.Roentgen, Philos. Mag., 11, 308 (1881).

93. M.C.Viengerov, Pokl Akund Nauk, S.S.S.R., 19, 687 (1938).

94. K.F.Luft, Z. Tech. Phys., 24, 97 (1943).

95. A.Rosencwaig, Opt. Commun., 7, 305 (1973).

96. A.Rosencwaig and A.Gersho, Science, 190, 556 (1975).

97. A.Rosencwaig and A.Gersho, J. Appl. Phys., 47, 64 (1976).

98. M.J.Adams, G.F.Kirkbright and K.R.Menon, Anal. Chem., 51, 508 (1979).

99. J.F.McClelland and R.W.Kniseley, Appl. Phys. Letts., 28, 467 (1976).

100. A.Rosencwaig, Rev. Sci. Instrum., 48, 1133 (1977).

101. R.A.Forman and H.S.Bennett, Appl. Opt., 15, 2405 (1976).

102. L.C.Aamodt, J.C.Murphy and J.G.Parker, J. Appl. Phys., 48, 927 (1977).

103. G.C.Wetsel Jr., F.A.McDonald, J. Appl. Phys., 49, 2313 (1978).

104. A.Rosencwaig, "Advances in Electronics and Electron Physics", Vol.46, (L.Marton Ed.), Academic Press New York (1978).

105. M.J.Adams, B.C.Beadle, A.A.King and G.F.Kirkbright, Analyst, 101, 553 (1976).

106. M.J.Adams, G.F.Kirkbright, Analyst, 102, 678 (1977).

107. A.Rosencwaig, "Photoacoustic Spectroscopy", P.273, J.Wiley and Sons, New York (1980).

108. A.Rosencwaig and G.Busse, Appl. Phys. Letts., 36, 725 (1980).

109. G.F.Kirkbright and R.M.Miller, Analyst,107, 798 (1982).

110. A.Rosencwaig and S.S.Hall, Anal. Chem., 47, 548 (1975).

111. S.L.Castleden, C.M.Elliott, G.F.Kirkbright and D.E.M.Spillane, Anal. Chem., 51, 2152 (1979).

112. C.M.Ashworth, S.L.Castleden and G.F.Kirkbright, J. Photoacoustics, 1, 152 (1982).

113. V.A.Fishman and A.J.Bard, Anal. Chem., 53, 102 (1981).

114. S.L.Castleden, G.F.Kirkbright and S.E.Long, Can. J. Spec., 27, 245 (1982).

115. G.F.Kirkbright and S.L.Castleden, Chem. in Brit., 16, 661 (1980).

116. R.S.Davidson, D.King, P.A.Duffield, D.M.Lewis, J. Soc. Dyes. Colour., 99, 123 (1983).

117. R.S.Davidson, D.King, J. Physique Third Conference of PAS, Paris April, (1983).

118. S.L.Castleden, G.F.Kirkbright and K.R.Menon, Analyst, 105, 1075 (1980).

119. O.Jin, G.F.Kirkbright and D.E.M.Spillane, Appl. Spec., 36, 120 (1982).

120. P.S.Belton and S.F.Tanner, Analyst, 108, 591 (1983).

121. J. Physique Third Conference on PAS, Paris, (1983).

122. M.E.Abuzied, E.E.Nofal, F.A.Abdul-Rasoul, M.A.Marafi, G.S.Mahmoud and A.Ledwith, J. Appl. Polym. Sci., 28, 2317 (1983).

123. W.Herschel, Phil. Trans. Roy. Soc., 90, 255 (1800).

124. H.A.Laitinen and G.W.Ewing, "A History of Analytical Chemistry", Division of Analytical Chemistry, Amer. Chem. Soc., New York, (1977).

125. H.H.Hausdorf, "Analysis of Polymers by Infra-red Spectroscopy", Pittsburgh Conference on Analytical and Applied Spectroscopy, March, (1951).

126. D.O.Hummel, "Atlas of Polymer and Plastic Analysis", vol.1, Verlag Chemie, Munich, (1978).

127. P.Ganns, "Vibrating Molecules", Chapman and Hall, (1971).

128. Z.Cihla, and J.Plyva, Coll. Czech. Chem. Commun., 26,(1903). (1961).

129. M.A.Golab, J.Shipman, J. Spectro. Chim. Acta., 20, 701 (1964).

130. T.Shimanouchi and M.Tasumi, Bull. Chem. Soc., Japan, 34, 359 (1961).

131. H.Nagui, J. Appl. Polym. Sci., 7, 1697 (1963).

132. T.Takenchi and S.Mori, Anal. Chem., 37, 589 (1965).

133. M.Takayanagi and K.Goto, J. Appl. Polym. Sci., 29, 2057 (1984).

134. J.P.Luongo, J. Polym. Sci., 42, 139 (1960).

135. J.N.Lomonte, Anal. Chem., 36, 192 (1964).

136. B.Ranby, "Polymer Surfaces", Editors D.T.Clark and W.J.Feast, (P.281) J.Wiley and Sons, (1978).

137. T.Bendaikha and C.Decker, J. Rad. Curing, 11, 6 (1984).

138. T.Nishikubo, M.Imaura, T.Mizuko and T.Takaoka, J. Appl. Polym. Sci., 18, 3445 (1974).

139. G.L.Collins, D.A.Young and J.R.Costanza, J. Coat. Technol., 48, 48 (1976).

140. A.Van Neerbos, J. Oil and Colour Chem. Assoc., 61, 241 (1978).

141. G.Plews and R.Phillips, J. Coat. Technol., 51, 69 (1979).

142. R.Phillips, J. Oil Colour Chem. Assoc., 61, 233 (1978).

143. C.Azuma, N.Hashizume, K.Sanui and N.Ogata, J. Appl. Polym. Sci., 28, 543 (1983).

144. El.H.Sabr Nal and G.Smets, Polym. Photo. Chem., 5, 93 (1984).

145. J.Fahrefort, Spectro. Chima. Acta., 17, 698 (1961).

146. N.J.Harrick, Phys. Rev. Letts., 4, 224 (1960).

147. H.A.Willis and V.J.I.Zichy, "Polymer Surfaces" Editors D.T.Clark and W.J.Feast, Page 287, J.Wiley and Sons, (1978).

148. D.Blais, M.Day and D.M.Wiles, J. Appl. Polym. Sci., 17, 1895 (1973).

149. J.Shimada and M.Hishino, J. Appl. Polym. Sci., 19, 1439 (1975).

150. P.Blais, D.J.Carlsson and D.M.Wiles. J. Polym. Sci., A1, 10, 1077 (1972).

151. J.Blear, J. Coating Technol. 53, 51 (1981).

152. G.P.Cunningham and C.M.Hansen, J.Coating Technol., 53, 39 (1981).

153. M.Palpacuer, O.Bernard, C.Deloupy, M.Rolland and M.J.M.Abudie, Polymer, 23, 1847 (1982).

154. G,W.C.Kaye and T.H.Laby, "Tables of Physical and Chemical Constants", P.251 14th Ed., Longman, (1973).

155. P.L.Egerton, E.Ditts and H.Reiser, Macromol., 14, 95 (1981).

156. A.H.Taylor, J.Opt. Soc. Am., 4, 9 (1919).

157. A.C.Hardy, J. Opt. Soc. Am., 18, 96 (1929).

158. G.Kortüm, "Reflectance Spectroscopy", Spronger Verlay, Berlin, (1969).

159. P.Bouguer, Traite d'Optique Sur La Gradation De La Lumiere, Paris, (1760).

160. L.Grabowski, J. Astrophys., 39, 299 (1914).

161. E.M.Berry, J. Opt. Soc. Am., 7, 627 (1923).

162. W.A.Rense, J. Opt. Soc. Am., 40, 55 (1950).

163. G.Kortum and R.Hamm, Ber. Bunsenhes, 72, 1182 (1968).

164. K.E.Torrance and E.M.Sparrow, J. Opt. Soc. Am., 57, 1105 (1967).

165. P.Kubelka and F.Munk, Z. Tech. Phys., 12, 593 (1931).

166. P.Kubelka, J. Opt. Soc. Am., 38, 448 (1948).

167. G.Kortüm, W.Braun and G.Herzoy, Angew. Chem. Int. Ed. Engl., 2, 333 (1963).

168. R.W.Frei and J.P.MacNeil, "Diffuse Reflectance Spectroscopy in Environmental Problem Solving", The Chemical Rubber Co.,Press, (1973).

169. A.C.Hardy, "Handbook of Colourimetry", M.I.T.Press, Cambridge, Mass., (1936).

170. A.Rosencwaig and S.S.Hall, Anal. Chem., 47, 548 (1975).

171. C.B.Ford and R.J.Hurtubise, Anal. Chem., 52, 656 (1980).

172. R.A.Dalterio and R.J.Hurtubise, Anal. Chem., 56, 773 (1984).

173. M.A.Kaiser and D.B.Chase, Anal. Chem., 52, 1849 (1980).

174. R.T.Graf, J.C.Koenig and H.Ishida, Anal.Chem., 56, 773 (1984).

175. W.B.White, Appl. Spectroscy., 21, 167 (1967).

176. R.Rohl, J.W.Childers and R.A.Palmer, Anal. Chem., 54, 1234 (1982).

177. R.S.Davidson and D,King, Anal. Chem., 56, 1409 (1984).

178. H.G.Hecht, Anal.Chem., 48, 1775 (1976).

179. H.G.Hecht, Appl. Spectroscy., 34, 161 (1980).

180. H.G.Hecht, Appl. Spectroscy., 37, 348 (1983).

181. A.A.Michelson, Phil. Mag., 31, 256 (1881).

182. P.B.Fellgett, Ph.D. Thesis., University of Cambridge, (1951).

183. J.W.Cooley and J.W.Tukey, Math., Comput., 19, 297 (1965).

184. M.L.Forman , J. Opt. Soc. Am., 56, 978 (1966).

185. P.R.Griffiths, "Chemical Infra-red Fourier Transform Spectroscopy" John Wiley and Sons, New York, (1975).

186. G.Busse and B.Bullemer, Infra-red Phys., 18, 225 (1978).

187. D.W.Vidrine, I.R.Spectral Lines, 1, 5 (1979).

188. R.G.Rockley, Chem. Phys. Lett., 68, 455 (1979).

189. D.W.Vidrine, Appl.Spectroscy., 34, 314 (1980)..

190. M.G.Rockley, Appl.Spectroscy., 34, 405 (1980).

191. S.M.Riseman and E.M.Eyring, Spectroscy. Lett., 14, 163 (1981).

192. M.G.Rockley, A.E.Ratcliffe, D.M.Davis and M.K.Woodard, Appl. Spectroscy., 38, 553 (1984).

193. Y.C.Teng and B.S.H.Royce, Appl. Opts., 21, 77 (1982).

194. K.Krishnan, Appl. Spectroscy., 35, 549 (1981).

195. J.F.McClelland and R.N.Kniseley, Appl. Phys. Letts., 28, 467 (1976).

196. M.G.Rockley and J.P.Devlin, Appl. Spectroscy., 34, 407 (1980).

197. S.R.Lowry, D.G.Mead and D.W.Vidrine, Anal. Chem., 54, 546 (1982).

198. L.B.Lloyd, R.C.Yeats and E.M.Eyring, Anal. Chem., 54, 549 (1982).

199. J.A.Gardella, D.Z.Jiang and E.M.Eyring, Appl. Spectroscy., 37, 131, (1983).

200. R.S.Davidson and G.V.Fraser, J. Soc. Dyers, Col. , 100, 167 (1984).

201. M.Rockley, M.Woodard, H.H.Richardson, R.M.Davis, W.Purdie and J.M.Bowen, Anal. Chem., 55, 32 (1983).

202. J.A.Gardella, G.L.Grobe, W.L.Hopson and E.M.Eyring, Anal. Chem., 56, 1169 (1984).